中央大学博士論文

A Study on Diffraction of Electromagnetic Wave by Dielectric Wedges

NGUYEN Minh Duc

博士（工学）

中央大学大学院

理工学研究科

電気·情報系専攻

令和 5 年度

2024 年 3 月

Contents

List of Figures

Chapter 1

Introduction

1.1 Research Background

From the nineteenth century, electromagnetic (EM) wave has been known since the work of J. Maxwell that describe how electric and magnetic fields are generated by charges, currents, and changes of the fields [1], [2]. After that, many topics for studying and applications of the electromagnetic wave have been conducted over a century [3]. Among the countless problems of electromagnetic, electromagnetic scattering wave always attractive and difficult topic. During the history of development, many outstanding physicists and mathematicians contributed to the theory of electromagnetic scattering wave [4]–[13]. Electromagnetic scattering is a general physical process, which describes and explains the field behavior when the electromagnetic waves are forced to deviate from a straight trajectory by one or more obstacles in the medium through which they pass. Knowledge about scattering properties at high frequencies of objects made of lossy material is paramount in radar applications, anti-radar designs, and high-frequency electronic device manufacture. It is also an important basis for understanding radio wave propagation conditions. From there, the optimal base station placement can be determined and compatible antenna models can be developed in wireless communication applications. Although topics on the scattering of electromagnetic waves have been widely studied with various shapes and models for several decades, finding reliable and efficient solutions always remains a challenging and unsolved problem. Nowadays, as high-speed and large-capacity mobile communications become more popular, to ensure stable communication between wireless communication base stations and small mobile wireless terminals, understanding radio wave propagation and scattering behavior becomes even more significant. On the other hand, the rapid development of urban areas leads to the increase of large obstacles such as buildings and vehicles. In there, the high-rise buildings always have the most strong influence on radio wave transmission. Because buildings come in so many different shapes, it would be extremely difficult to create a direct solution to each building's scattering problem. However, the common denominator is that most of the large buildings are block-shaped, with large polygonal surfaces that can be thought of as sets of wedges. Therefore, a more feasible solution is to find out the scattering behavior of each wedge separately. Then, by summing up the scattering problem of many wedges, one can easily evaluate and estimate the effect of the buildings on wave propagation.

Many solutions have been proposed for the scattering problems of electromagnetic waves, in which several available exact solutions [14], [15] and numerical methods [16]–[23] can be utilized for a limited number of simple shapes and small objects. Although these

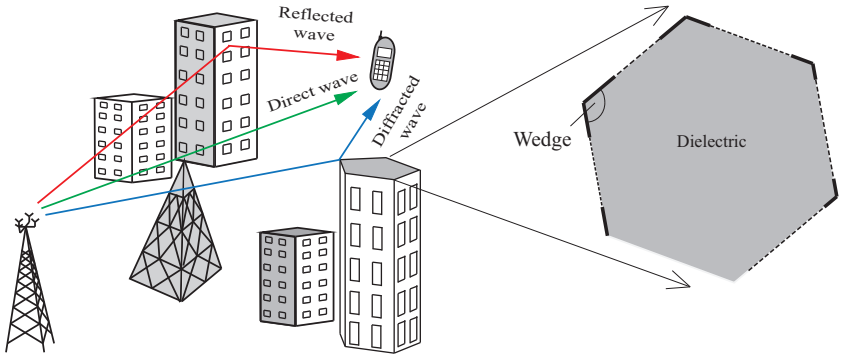

Figure 1.1: Scattering by a high building.

methods can provide highly reliable results, they consume a lot of time and memory due to the large number of calculations, and are not ideal solutions for large objects. Therefore, to calculate the scattering of large objects such as buildings, one needs to develop approximation approaches that can provide acceptably fast as well as highly accurate approximation solutions.

In the high-frequency domain, some classical approximation methods may be able to analyze the scattering problems by large conducting objects [24]–[27], such as geometrical optics (GO), physical optics (PO), geometrical theory of diffraction (GTD) and its extended uniform solutions. Here, GO is a ray-based method that describes the scattering phenomena of electromagnetic waves by an object [28]–[31]. The GO technique is based on the rule of optics ray, in which incident rays are assumed to be reflected by the scattering objects as if the surfaces of these objects are plane at the illuminated point. The GO scattering fields can be obtained simply by utilizing the usual reflection and transmission principles of rays at the interfaces of objects. However, the limitation of the GO method is that it does not provide information about the diffraction effect and the field behavior in the shadowed areas of the scattering objects.

An alternative model of diffraction named GTD was propounded first in 1802 to overcome the shortcomings of GO. The GTD can be known as an extension of GO, which can describe the diffraction behavior in shadowed regions that GO ignores [32]–[36]. It was found that in addition to the usual GO reflected and transmitted rays, there is the existence of diffracted rays that are excited when incident rays illuminate the vertices, edges, or corners of an obstacle, or when the incident rays graze the object's surface. In the above cases, GO does not provide a prescription to determine the subsequent path of scattered rays. The behavior of diffracted rays can be described by applying several laws of diffraction, similar to the laws of reflection and refraction. The diffracted field can be obtained by multiplying the field of the incident ray at the diffracted point with an appropriate diffraction coefficient using the Fresnel integral. The scattering field can then be represented as the sum of the GO field and diffracted fields. Despite solving the diffraction failure of GO, GTD and its extensions [37]–[41] may be only applicable to conductive objects. For penetrable objects, an extension of the uniform theory of diffraction (HUTD) [42] were proposed to solve the radiation field of the lossy dielectric objects adding the reflection and transmission coefficients into the UTD (uniform theory of diffraction) formulation. However, this solution only provides the field behaviors in the outside region of objects. This limitation requires us to look for a more potential solution as physical optics (PO) approximation.

The PO approximation was first introduced in 1882 by Kirchhoff. PO is well known

as a simple and very efficient method for many applications in radar, antenna, and other electromagnetic problems. The foundation of the PO method is developed based on the surface equivalence theorem [43]–[45]. In the high-frequency domain, this method can be efficiently utilized to solve scattering problems caused by the conducting objects [46]–[51]. Here, the scattering field can be calculated as the radiation from the induced PO currents excited on the illuminated surfaces of the scattered object. These PO currents can be easily determined from the magnetic field of the incident wave and the surface of the object. However, when the scattering objects are made of penetrable material, the problem becomes more complicated due to due to the appearance of scattering phenomena inside the object. In this case, the PO current based on the incident wave is not sufficient to construct an accurate solution as in the case of non-penetrable objects.

To solve complicated scattering problems of penetrable objects, several possible solutions based on the PO method have been proposed for both the internal and external fields. These solutions are also developed based on the surface equivalence theorem [52]–[54], in which equivalent electric and magnetic currents were proposed to replace the PO currents. These equivalent electric and magnetic currents need more informations then the PO currents. They can be constructed based on the magnetic and electric fields of the incident, reflected and transmitted GO rays. Then the scattering fields can be derived form the radiation integrations of these induced currents. For conducting objects, the solution from electric and magnetic currents was found to obtain the same results as the PO solution [55]. According to the above basis, uniform asymptotic solutions of PO have been proposed to solve the diffraction problem of dielectric wedges [56], [57]. In these investigations, the singularity behaviors of the diffraction coefficient near the shadow boundaries of the GO rays were mended by multiplying the transition functions with the non-uniform components. These transition functions can be obtained from the Fresnel integral. However, these investigations have not clearly shown the accuracy of the diffracted field of PO. In addition, it was found from the conducting case that the diffracted field of PO doesn't satisfy the boundary and edge conditions, and this may also continue to occur in the solutions for dielectric wedge cases [58], [59]. A solution named HRD (hidden rays of diffraction) has also been proposed to extend a concept of HUTD to the internal diffracted field [60], [61]. This solution is expected to correct the error of PO in terms of boundary condition by using additional hidden rays. These hidden rays were introduced to be easily traced by using the usual principle of GO in the non-physical domain, in which the free space domain and dielectric domain are exchanged for each other. It is also said that the HRD solution may satisfy the edge condition by modifying the angular period of the cotangent functions [62]. Although the above approximation solutions are efficient tools for solving the diffraction problems of the dielectric wedge in the high-frequency domain, their reliability has not been clearly verified yet. Therefore, we need to conduct more investigations to know the accuracy of these approximation solutions, as well as to find other reliable solutions for the edge diffraction problems of dielectric objects.

In this investigation, an extended PO (EPO) asymptotic solution has been presented for edge diffraction by a dielectric wedge for both TM and TE-polarized plane waves. This solution is constructed based on the equivalent currents method, in which the scattering field from a dielectric wedge may be formulated as the corresponding radiation from equivalent induced electric and magnetic currents on wedge surfaces. Unlike conventional PO, these equivalent currents are obtained from the electric and magnetic fields of GO rays. While the outer induced currents are determined by the incident and reflected GO

rays, the currents inside the wedge are constructed from the corresponding transmitted rays. The scattering fields can then be found by integrating the above equivalent electric and magnetic currents with the two-dimensional Green's function. The obtained radiation integrals can then be evaluated by using the saddle point technique. Then, uniform asymptotic solutions including transition functions have been obtained. Using the error function complement, these transition functions have mended the singularity behavior at the shadow boundaries of GO ryas. The edge diffracted fields were represented in terms of cotangent functions, which have one-to-one correspondences with the incident, reflected, and transmitted GO rays. General unified formulations have then been proposed to be applicable to any incident directions. The numerical results have been performed to compare our EPO solution with other reference methods such as HRD and FDTD (Finite-Difference Time-Domain) simulation. The observed comparison results show a correlation between the reliability of our solution and previous methods. In addition, a concept of lateral waves was proposed to enhance the accuracy of our current solutions.

1.2 Physical Optics Approximation

The physical optics approximation is constructed based on the surface equivalence theorem, which is known as a more rigorous reformulation of Huygens's principle [43], and was introduced by Schelkunoff in 1936 [44]. This theorem is also known as the field equivalence principle [45] or simply as the equivalence principle. According to the principle of the equivalence theorem, the actual radiation sources within a region can be replaced by equivalent fictitious sources that produce a similar field behavior as the actual sources within that region. Based on this principle, the radiation problems can be solved by considering the current densities on a fictitious closed surface surrounding the actual object. This is known as a more rigorous improvement of the Huygens-Fresnel principle, in which each point on the wavefront is considered as a spherical wave source. The equivalent currents on the imaginary surface are determined by the uniqueness theorem in electromagnetic.

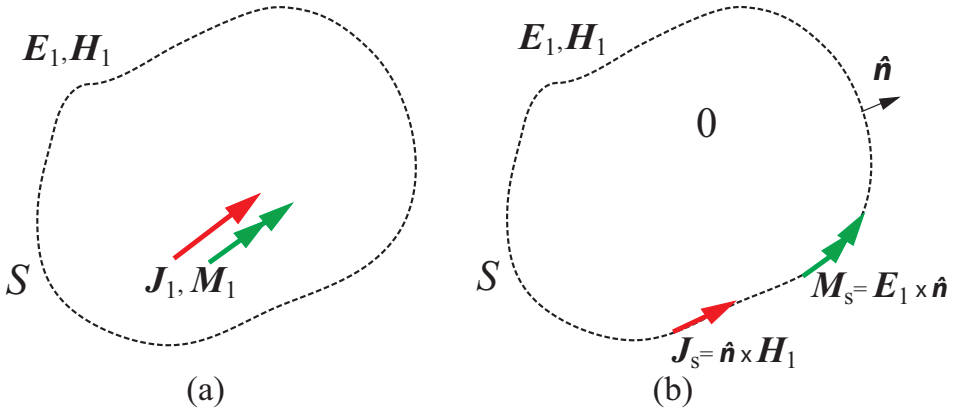

Figure 1.2: Field equivalence principle model. (a) Fields $\boldsymbol{E}_1$, $\boldsymbol{H}_1$ excited by original sources by $\boldsymbol{J}_1$, $\boldsymbol{M}_1$. (b) Fields $\boldsymbol{E}_1$, $\boldsymbol{H}_1$ excited by the equivalence surface currents $\boldsymbol{J}_s$, $\boldsymbol{M}_s$ on S.

Based on the surface equivalence theorem, the external radiation field of a closed surface can be obtained from the distribution of suitable imaginary electric and magnetic cur-

rents according to the boundary conditions. Accordingly, the density of these equivalent currents is chosen so that the external fields are the same as those excited by the actual radiation sources, while the internal fields of the closed surface are null. Thus, one can deduce the radiation fields in the outside and inside regions of the surface if the density of the equivalent current can be determined. This theorem is mathematically rigorous and the correctness of the derived field depends on the accuracy of the obtained equivalent current densities.

Let us now consider electromagnetic fields $\boldsymbol{E}_1$, $\boldsymbol{H}_1$, which are excited by actual electric and magnetic current sources ($\boldsymbol{J}_1$, $\boldsymbol{M}_1$) as in Fig. 1.2(a). Assuming that a closed surface S surrounds the sources $\boldsymbol{J}_1$, $\boldsymbol{M}_1$, then the radiation fields outside surface S can be found from equivalent electric and magnetic currents on surface S as shown in Fig. 1.2(b).

$$\boldsymbol{J}_s = \hat{\boldsymbol{n}} \times \boldsymbol{H}_1, \tag{1.1}$$

$$\boldsymbol{M}_s = \boldsymbol{E}_1 \times \hat{\boldsymbol{n}}. \tag{1.2}$$

where $\hat{\boldsymbol{n}}$ is a normal unit vector on surface S towards the outside. The reliability of this equivalence depends on the accuracy of the fields $\boldsymbol{E}_1$, $\boldsymbol{H}_1$ on the virtual surface S. However, the exact determination of the fields sometimes becomes difficult, then one may use the field approximation for evaluating the radiation problems.

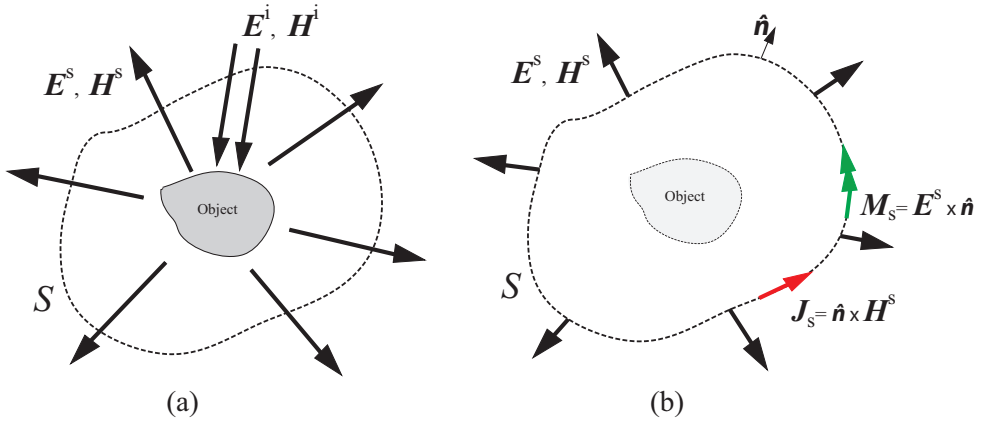

Figure 1.3: Field equivalence principle model. (a) Scattering fields $\boldsymbol{E}^s$, $\boldsymbol{H}^s$ by an object due to the incident wave $\boldsymbol{E}^i$, $\boldsymbol{H}^i$. (b) Scattering fields $\boldsymbol{E}^s$, $\boldsymbol{H}^s$ by the equivalence surface currents $\boldsymbol{J}_s$, $\boldsymbol{M}_s$ on S.

Now consider the case, in which the scattering fields $\boldsymbol{E}^s$, $\boldsymbol{H}^s$ are excited by an object illuminated by incident fields $\boldsymbol{E}^i$, $\boldsymbol{H}^i$ from the exterior region, as shown in Fig. 1.3(a). The total field outside the object may then be represented by the summation of the incident and scattering fields as

$$\boldsymbol{E} = \boldsymbol{E}^i + \boldsymbol{E}^s \tag{1.3}$$

$$\boldsymbol{H} = \boldsymbol{H}^i + \boldsymbol{H}^s. \tag{1.4}$$

If one assumes that the scattering fields $\boldsymbol{E}^s$, $\boldsymbol{H}^s$ are excited by the secondary radiation sources on the object, the external scattering fields can then be found from the equivalent current sources $\boldsymbol{J}_s$ and $\boldsymbol{M}_s$ on surface S as in Fig. 1.3(b). These surface currents can be defined as:

$$\boldsymbol{J}_s = \hat{\boldsymbol{n}} \times \boldsymbol{H}^s, \tag{1.5}$$

$$\boldsymbol{M}_s = \boldsymbol{E}^s \times \hat{\boldsymbol{n}}. \tag{1.6}$$

Then by integrating the above surface currents with Green's function along the surface, the radiation field at the observation point $\boldsymbol{r}$ can be expressed as

$$\boldsymbol{E}^s(\boldsymbol{r}) = -\int_S \left\{ j\omega\mu_0 \boldsymbol{J}_s(\boldsymbol{r}')G(\boldsymbol{r},\boldsymbol{r}') + \boldsymbol{M}_s(\boldsymbol{r}') \times \nabla' G(\boldsymbol{r},\boldsymbol{r}') - \frac{\boldsymbol{J}_s(\boldsymbol{r}')}{j\omega\varepsilon_0} \cdot \nabla'\nabla' G(\boldsymbol{r},\boldsymbol{r}') \right] dS', \tag{1.7}$$

$$\boldsymbol{H}^s(\boldsymbol{r}) = -\int_S \left\{ j\omega\varepsilon_0 \boldsymbol{M}_s(\boldsymbol{r}')G(\boldsymbol{r},\boldsymbol{r}') - \boldsymbol{J}_s(\boldsymbol{r}') \times \nabla' G(\boldsymbol{r},\boldsymbol{r}') - \frac{\boldsymbol{M}_s(\boldsymbol{r}')}{j\omega\mu_0} \cdot \nabla'\nabla' G(\boldsymbol{r},\boldsymbol{r}') \right\} dS', \tag{1.8}$$

where ω, ε_0 and μ_0 are the angular frequency, vacuum permittivity and vacuum permeability, respectively. ∇' indicates differentiation with respect to the prime source coordinates, and $G(\boldsymbol{r},\boldsymbol{r}')$ is Green's function. The above formulations are mathematically rigorous, and the obtained radiation fields are reliable as long as one can correctly determine the equivalent electric and magnetic currents $\boldsymbol{J}_s$ and $\boldsymbol{M}_s$. However, it is usually difficult to know the exact distribution of these equivalent currents.

Physical optics (PO) is a well-known high-frequency approximate technique that allows us to solve scattering problems for electrically large conducting objects. The advantage of PO solution is that it is able to describe the diffraction effect including the smooth transition between the lit and shadowed portions of space at the shadowed boundary. In this investigation, the PO approximation is constructed by determining the surface fields of the object from the geometrical optics rays and then the scattering field can be calculated by integrating these fields over the object's surface. It usually means that the current that can be found on a tangent plane of the object is taken as the same as the current at each point on the illuminated region of the scatterer. On the other hand, in the shadowed regions, the current is equal to zero. Then, the scattering field can be calculated approximately by an integral over these approximate currents. To ensure the accuracy of the PO approximation, one has to rigorously comply with several constraints before choosing this method to solve the electromagnetic scattering problems. First, the scattering objects must be electrically large, and their surfaces must vary smoothly. Second, it must be possible to distinguish between illuminated and non-illuminated regions of the scattering objects.

Now, if one considers a plane wave incident on a smooth surface of a large perfectly conducting object as in Fig. 1.4(a), the scattered fields ($\boldsymbol{E}^s$ $\boldsymbol{H}^s$) outside the object can be given by the reflected fields, while the fields inside the conducting object are null. According to the surface equivalent theorem, the closed surface is selected so that the surface S is outside the scattering object, so instead of choosing the arbitrary closed surface, one may choose most of it to coincide with the conducting parts of the physical structure of the object as in Fig. 1.4(b). By such a choice, the external scattering fields of the conducting object can be found from the surface characteristics of the object for the high-frequency domain, and the internal field of the object is null. The equivalent currents can then be determined from the tangential components of the total field at the surface of the object. For perfectly conducting objects, the equivalent magnetic current is equal to zero. In addition, the equivalent electric current in the shadowed region of the object is also zero. Thus, one only needs to determine the electric current $\boldsymbol{J}_s$ on the illuminated region from the sum of the incident and scattered fields. In addition, considering the characterization of the boundary S as a PEC plane, the PO approximation states that the incident and scattered magnetic fields at the boundary S are in phase and also have

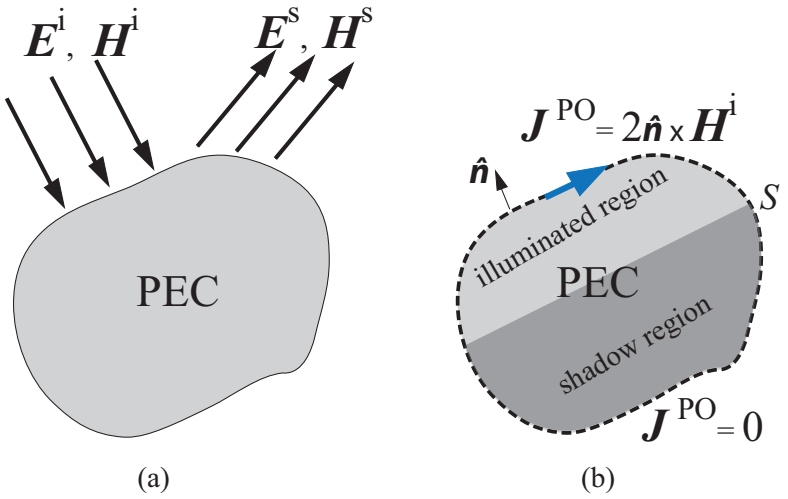

Figure 1.4: Physical optics approximation for conducting object: (a) Conducting object is illuminated by the incident wave $\boldsymbol{E}^i$, $\boldsymbol{H}^i$. (b) PO equivalent current on visual surface S.

the same amplitude. Thus, the tangential component of the magnetic field on the surface is exactly twice that of incident wave, and the electric current can then be expressed as:

$$\boldsymbol{J}_s = \hat{\boldsymbol{n}} \times (\boldsymbol{H}^{\mathrm{i}} + \boldsymbol{H}^{\mathrm{s}}) = 2\hat{\boldsymbol{n}} \times \boldsymbol{H}^{\mathrm{i}}. \tag{1.9}$$

The electric current $\boldsymbol{J}_s$ in Eq.(1.9) is called as physical optics (PO) equivalent current $\boldsymbol{J}^{\mathrm{PO}}$. Then, the complete PO formulation of the PO current density for the illuminated and shadowed regions can be written as:

$$\boldsymbol{J}^{\mathrm{PO}} = \begin{cases} 2\hat{\boldsymbol{n}} \times \boldsymbol{H}^i & \text{on illuminated surface,} \quad (1.10a) \\ 0 & \text{on shadowed surface,} \quad (1.10b) \end{cases}$$

This difference in the current density between the illuminated and shadowed regions of the object is one of the important caveats to using the PO approximation correctly, as mentioned before. The scattering field can then be determined by integrating the PO current $\boldsymbol{J}^{\mathrm{PO}}$ on the visual surface S with the Green's function G as Eqs.(1.7) and (1.8).

1.3 Contents of Thesis

This thesis includes six chapters.

In Chapter 2, a uniform solutions based on physical optics (PO) are represented for the scattering problem of conducting wedges for TM and TE-polarized electromagnetic plane waves. According to PO method, the electromagnetic scattering fields by a conducting wedge can be found from PO currents on illuminated surface of the wedge. This PO currents can easily determined from the information of the magnetic fields of the incident waves and the wedge surfaces. Then, the scattering fields excited from these PO currents are derived by integrating these currents with free-space Green's function. By using the saddle point technique to solve the scattering integrals, a uniform asymptotic solution including the cotangent functions and the error function complement of the edge diffracted field has been obtained. These cotangent functions correspond one-to-one with

the incident and reflected GO rays. Depending on the incident direction, one has different formulations of scattering fields corresponding to each illuminated surface. By combining the contributions from both surfaces and carefully rearranging, unified formulations were then proposed to be applicable to any direction of the incident wave.

In Chapter 3, an extended PO approximation for the scattering problem of dielectric wedges is proposed for both TM and TE polarizations based on previous results of the conducting wedge problem. Different from conducting case, when the incident wave illuminates the wedge surfaces, it excites not only the reflected wave in the outer region, but also the transmitted wave inside the wedge. These reflected and transmitted rays can be normally derived from the formulation of the incident wave by using Snell's law. Therefore, the PO current constructed from the incident wave is not enough to be utilized for calculating the scattering fields by the dielectric wedges. Instead, the radiation fields of dielectric wedges can be found from equivalent electric and magnetic currents on the dielectric wedge surfaces. Unlike conventional PO, these equivalent currents are obtained from electric and magnetic fields of the GO incident, reflected and transmitted rays outside and inside the wedge, respectively. The radiation integrals were then performed separately for each pair of electric and magnetic currents of the corresponding GO ray with Green's functions. By using the same saddle point technique as in the conducting case, corresponding uniform asymptotic solutions of scattering fields by dielectric wedges were then obtained from these integrations. Then, the total external and internal scattering fields can then be obtained by combining contributions from the incident and reflection waves on the outside and the transmitted waves on the inside, respectively. As same as conducting case, the diffracted fields of the dielectric wedge also can be represented in terms of cotangent functions with the corresponding reflection and transmission coefficients.

Chapter 4 presents other calculation methods for wedge diffraction of dielectric wedge as heuristic extension of UTD (HUTD) and hidden rays of diffraction (HRD). Here, HUTD is high frequency approximation methods, which is extended from the uniform theory of diffraction (UTD). By adding the reflection coefficients, the formulation of UTD for conducting wedge can then be applied to the scattering problem of lossy dielectric wedge. However, the HUTD solution only describes the field behavior outside the dielectric wedge and ignores the information of the internal field. To solve this limitation, the hidden rays of diffraction (HRD) is represented to extend a concept of HUTD to the internal diffracted field of the dielectric wedge. In this method, additional hidden rays are proposed in the non-physical imagined region to satisfy the boundary condition. The diffraction coefficients of HRD solution are also illustrated by cotangent functions with modified angular period based on the edge condition.

In Chapter 5, The numerical results are performed to discuss the accuracy of extended PO approximation method by comparison with those by other reference methods such as HRD and FDTD simulation. The comparisons are made for both conducting and dielectric wedge cases. Interesting precision variation between PO and HRD for conducting and dielectric wedges can be observed from comparison results. Furthermore, the observed difference of the internal field leads us to an important discovery about the missing contributions from the lateral wave concept.

Finally, Chapter 6 shows some conclusions on our research and future research plans. In the following discussion, the time-harmonic factor $e^{j\omega t}$ is assumed and suppressed throughout the thesis.

Chapter 2

Physical Optics Approximation for Conducting Wedge

In the previous Introduction, we have reviewed over the surface equivalence theorem and physical optics approximation method. In this chapter, a practical scattering problem of electromagnetic scattering of electromagnetic wave by a perfectly conducting wedge will be solved by applying PO approximation method. Based on PO approximation, the PO current is determined on the illuminated surface of the wedge. The radiation integrals obtained from the PO currents will be analyzed by the saddle point method. The obtained scattering field will include as the reflected and diffracted fields. Study on the electromagnetic scattering of the conducting wedge by PO approximation will be presented in both TM and TE polarizations in this chapter.

2.1 Formulation of PO Approximation

According to the physical optics (PO) method, when a PEC object is illuminated by an incident electromagnetic wave ($\boldsymbol{E}^{\mathrm{i}}$, $\boldsymbol{H}^{\mathrm{i}}$), the scattering field ($\boldsymbol{E}^{\mathrm{s}}$, $\boldsymbol{H}^{\mathrm{s}}$) outside the object may be considered as the field radiated from the induced PO currents on the illuminated surfaces. For the two-dimensional configuration ($\frac{\partial}{\partial z} \equiv 0$), the scattering field ($\boldsymbol{E}^{\mathrm{s}}$, $\boldsymbol{H}^{\mathrm{s}}$) can be calculated by integrating the PO current $\boldsymbol{J}^{\mathrm{PO}}$ on the boundary S of the object with the Green's function G as [15]

$$\boldsymbol{E}^{\mathrm{s}} = -\int_S j\omega\mu_0 \boldsymbol{J}^{\mathrm{PO}}(\boldsymbol{r'}) G(\boldsymbol{r}, \boldsymbol{r'}) dl', \tag{2.1}$$

$$\boldsymbol{H}^{\mathrm{s}} = \int_S \boldsymbol{J}^{\mathrm{PO}}(\boldsymbol{r'}) \times \nabla' G(\boldsymbol{r}, \boldsymbol{r'}) dl', \tag{2.2}$$

where ω and μ_0 are the angular frequency and permeability, respectively. ∇' indicates differentiation with respect to the prime source coordinates, and $G(\boldsymbol{r}, \boldsymbol{r'})$ is Green's function, which satisfies

$$(\nabla^2 + k^2) G(\boldsymbol{r}, \boldsymbol{r'}) = -\delta(\boldsymbol{r} - \boldsymbol{r'}), \tag{2.3}$$

where $k = \omega\sqrt{\varepsilon_0\mu_0}$ denotes the free space wave number. For two-dimensional problem, one gets [36]

$$G(\boldsymbol{r}, \boldsymbol{r'}) = \frac{1}{4j} H_0^{(2)}(k\sqrt{(x-x')^2 + (y-y')^2}), \tag{2.4}$$

where $H_0^{(2)}(k\sqrt{(x-x')^2+(y-y')^2})$ is the zero-th order Hankel function of the second kind and can be represented as [15]

$$H_0^{(2)}(k\sqrt{(x-x')^2+(y-y')^2}) = \frac{1}{\pi}\int_{-\infty}^{\infty} \frac{e^{-j\eta(x-x')-j\sqrt{k^2-\eta^2}|y-y'|}}{\sqrt{k^2-\eta^2}} d\eta. \tag{2.5}$$

If the scattering object is made by a large electric conductor, the PO current $\boldsymbol{J}^{\mathrm{PO}}$ can be approximated on the object's surface as

$$\boldsymbol{J}^{\mathrm{PO}} = \begin{cases} 2\hat{\boldsymbol{n}} \times \boldsymbol{H}^i & \text{on illuminated surface,} \quad (2.6a) \\ 0 & \text{on shadowed surface,} \quad (2.6b) \end{cases}$$

where $\hat{\boldsymbol{n}}$ is a unit normal vector on the object's surface to the exterior observation region, and $\boldsymbol{H}^i$ denotes the magnetic field of incident wave. This PO current $\boldsymbol{J}^{\mathrm{PO}}$ can be a good approximation as long as the scattering object is a flat perfectly electrical conducting object and very large compared with the wavelength.

Now one considers a perfectly electrical conducting wedge as in Fig. 2.1, in which the wedge angle is ϕ_{w}. Assuming that the wedge is illuminated by an electromagnetic incident plane wave with incident angle ϕ_0. Then, the scattering calculation may be separated into two polarizations.

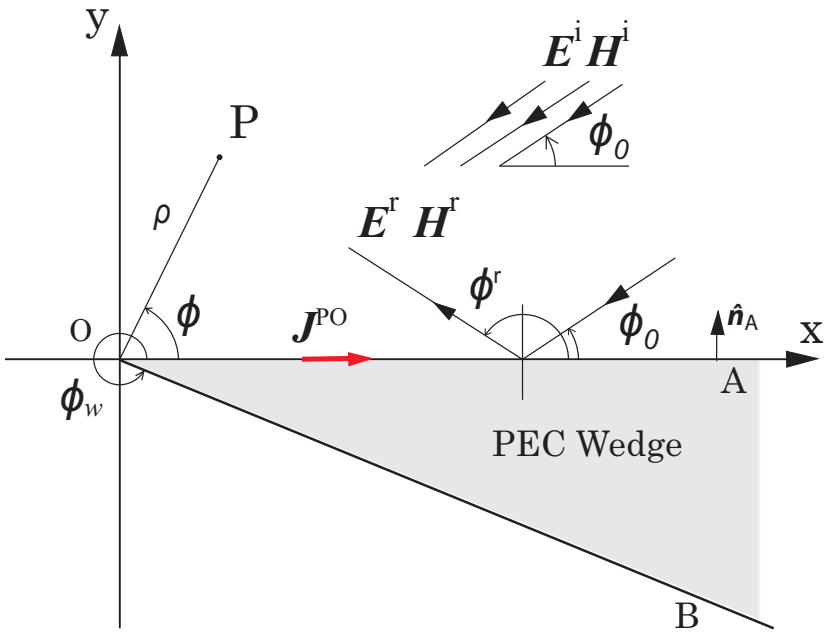

Figure 2.1: PEC wedge: one-side illumination.

2.2 TM-Polarized Plane Wave

A TM-polarized incident plane wave can be given by:

$$\boldsymbol{H}^{\mathrm{i}} = e^{jkx\cos\phi_0 + jky\sin\phi_0}\hat{\boldsymbol{z}}, \tag{2.7}$$

$$\boldsymbol{E}^{\mathrm{i}} = \sqrt{\frac{\mu_0}{\varepsilon_0}} e^{jkx\cos\phi_0 + jky\sin\phi_0}(\sin\phi_0\hat{\boldsymbol{x}} - \cos\phi_0\hat{\boldsymbol{y}}), \tag{2.8}$$

where $k = \omega\sqrt{\varepsilon_0\mu_0}$ is the wave number in free space. The illumination can be divided into three cases depending on the direction of the incident wave. When $\phi_0 < \phi_w - \pi$, only surface OA is illuminated, then the scattering field can be calculated from the current $\boldsymbol{J}_{\mathrm{A}}^{\mathrm{PO}}$ on surface OA. On the other hand, if only surface OB is illuminated ($\phi_0 > \pi$), the scattering field is found from the corresponding PO current $\boldsymbol{J}_{\mathrm{B}}^{\mathrm{PO}}$. When the incident wave illuminates both surfaces OA and OB ($\phi_w - \pi < \phi_0 < \pi$), one may need the combination of the two above currents. The PO current $\boldsymbol{J}_{\mathrm{A}}^{\mathrm{PO}}$ can be found from the magnetic field of the incident wave as:

$$\boldsymbol{J}_A^{\mathrm{PO}} = 2\hat{\boldsymbol{n}}_A \times \boldsymbol{H}^{\mathrm{i}}|_{y=0} = 2e^{jkx\cos\phi_0}\hat{\boldsymbol{x}}. \tag{2.9}$$

When surface OB is illuminated as in Fig. 2.2, the TM-polarized incident plane wave can

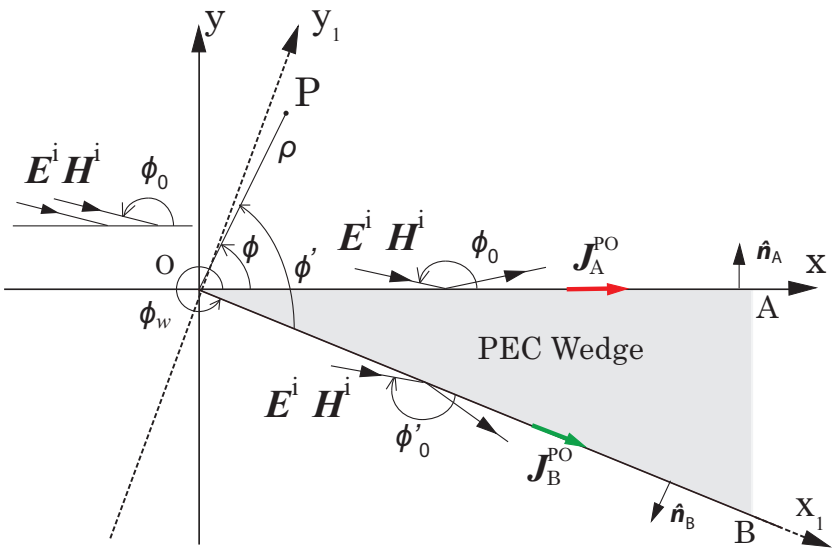

Figure 2.2: PEC wedge: two-side illumination.

be rewritten by using the coordinate Ox_1y_1 as

$$\boldsymbol{H}_B^{\mathrm{i}} = e^{jkx_1\cos(\phi_w-\phi_0)-jky_1\sin(\phi_w-\phi_0)}\hat{\boldsymbol{z}}, \tag{2.10}$$

$$\begin{aligned}\boldsymbol{E}_B^{\mathrm{i}} = &-\sqrt{\frac{\mu_0}{\varepsilon_0}}e^{jkx_1\cos(\phi_w-\phi_0)-jky_1\sin(\phi_w-\phi_0)} \\ &\cdot\left[\sin(\phi_w-\phi_0)\hat{\boldsymbol{x}}_{\mathbf{1}} + \cos(\phi_w-\phi_0)\hat{\boldsymbol{y}}_{\mathbf{1}}\right].\end{aligned} \tag{2.11}$$

Then the PO current $\boldsymbol{J}_B^{\mathrm{PO}}$ on surface OB can be found as:

$$\boldsymbol{J}_B^{\mathrm{PO}} = 2\hat{\boldsymbol{n}}_B \times \boldsymbol{H}_B^{\mathrm{i}}|_{y_1=0} = -2e^{jkx_1\cos(\phi_w-\phi_0)}\hat{\boldsymbol{x}}_{\mathbf{1}}. \tag{2.12}$$

Then the scattering magnetic fields can be obtained by integrating the PO currents $\boldsymbol{J}_A^{\mathrm{PO}}$ and $\boldsymbol{J}_B^{\mathrm{PO}}$ with Green's function G as

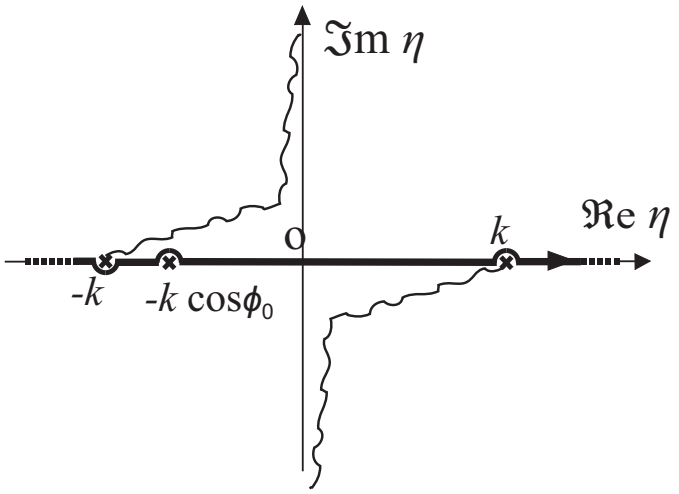

Figure 2.3: Integration contour for Eqs.(2.13) and (2.35) in the complex η plane.

$$
\begin{aligned}
H_A^s =& \frac{-j}{4}\int_S J_A^{\mathrm{PO}} \frac{\partial}{\partial y'} H_0^{(2)}(k\sqrt{(x-x')^2+(y-y')^2})dS|_{y'=0} \\
=& \frac{-j}{4}\int_0^\infty 2e^{jkx'\cos\phi_0}\left(\frac{\pm j}{\pi}\int_{-\infty}^\infty e^{-j\eta(x-x')-j\sqrt{k^2-\eta^2}|y|}d\eta\right)dx' \quad (y \gtrless 0) \\
=& \frac{\pm 1}{2\pi}\int_0^\infty\int_{-\infty}^\infty e^{jkx'\cos\phi_0}e^{-j\eta(x-x')-j\sqrt{k^2-\eta^2}|y|}d\eta dx' \quad (y \gtrless 0) \\
=& \frac{\pm 1}{2\pi}\int_{-\infty}^\infty\left(\int_0^\infty e^{jkx'\cos\phi_0+j\eta x'}dx'\right)e^{-j\eta x-j\sqrt{k^2-\eta^2}|y|}d\eta \quad (y \gtrless 0) \\
=& \frac{\pm j}{2\pi}\int_{-\infty}^\infty \frac{e^{-j\eta x-j\sqrt{k^2-\eta^2}|y|}}{k\cos\phi_0+\eta}d\eta, \quad (y \gtrless 0)
\end{aligned} \tag{2.13}
$$

and

$$
\begin{aligned}
H_B^s =& \frac{-j}{4}\int_S J_B^{\mathrm{PO}} \frac{\partial}{\partial y'} H_0^{(2)}(k\sqrt{(x_1-x_1')^2+(y_1-y_1')^2})dS|_{y_1'=0} \\
=& \frac{j}{4}\int_0^\infty 2e^{jkx_1'\cos(\phi_w-\phi_0)}\left(\frac{\pm j}{\pi}\int_{-\infty}^\infty e^{-j\eta(x_1-x_1')-j\sqrt{k^2-\eta^2}|y_1|}d\eta\right)dx_1' \quad (y_1 \gtrless 0) \\
=& \frac{\mp 1}{2\pi}\int_0^\infty\int_{-\infty}^\infty e^{jkx_1'\cos(\phi_w-\phi_0)}e^{-j\eta(x_1-x_1')-j\sqrt{k^2-\eta^2}|y_1|}d\eta dx_1' \quad (y_1 \gtrless 0) \\
=& \frac{\mp 1}{2\pi}\int_{-\infty}^\infty\left(\int_0^\infty e^{jkx_1'\cos(\phi_w-\phi_0)+j\eta x_1'}dx'\right)e^{-j\eta x_1-j\sqrt{k^2-\eta^2}|y_1|}d\eta \quad (y_1 \gtrless 0) \\
=& \frac{\mp j}{2\pi}\int_{-\infty}^\infty \frac{e^{-j\eta x_1-j\sqrt{k^2-\eta^2}|y_1|}}{k\cos(\phi_w-\phi_0)+\eta}d\eta, \quad (y_1 \gtrless 0)
\end{aligned} \tag{2.14}
$$

where the integration contour in η plane is given in Fig. 2.3 and Fig. 2.4. Convert to complex plane of angle w using the transformation $\eta = k\sin w$, with the cylindrical

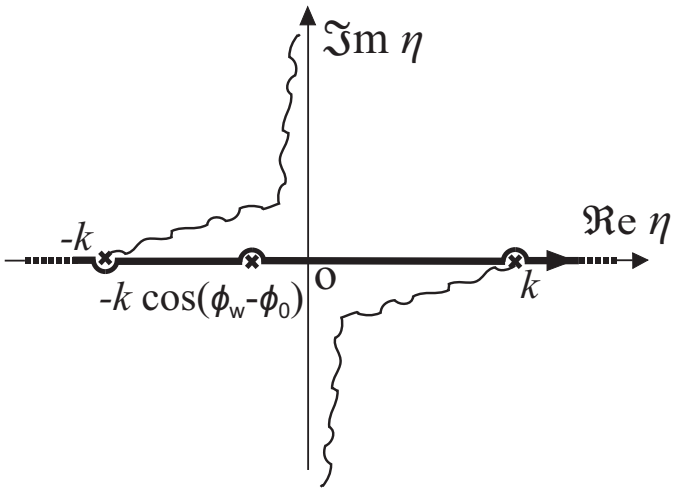

Figure 2.4: Integration contour for Eqs.(2.14) and (2.36) in the complex η plane.

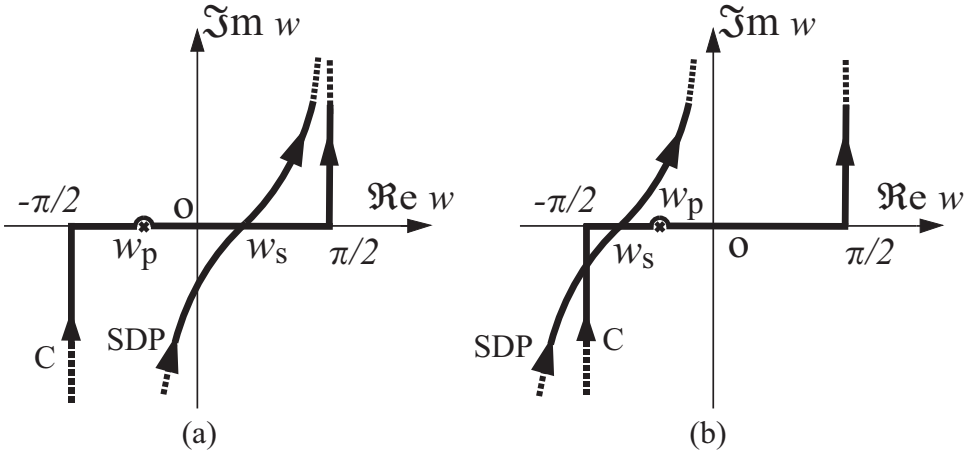

Figure 2.5: Integration contours C and SDP for Eqs.(2.15) and (2.16) in the complex angular w plane: (a) $w_s > w_p$. (b) $w_s < w_p$.

coordinate (ρ, ϕ), Eq.(2.13) can be obtained as

$$\begin{aligned} H_A^s =& \frac{\pm j}{2\pi} \int_{\mathrm{C}} \frac{e^{-jk\rho \sin w \cos\phi \mp jk\rho \cos w \sin\phi}}{k\cos\phi_0 + k\sin w} d(k\sin w) \quad (\phi \lessgtr \pi) \\ =& \frac{\pm j}{2\pi} \int_{\mathrm{C}} \frac{\cos w}{\cos\phi_0 + \sin\ w} e^{-jk\rho\sin(w\pm\phi)} dw, \quad (\phi \lessgtr \pi) \end{aligned} \tag{2.15}$$

where the integration contour C runs in the complex w plane as in Fig. 2.5. Similarly, by using the the cylindrical coordinate (ρ, ϕ') with $x_1 = \rho\cos\phi'$ and $y_1 = \rho\sin\phi'$, Eq.(2.14) can be obtained as

$$\begin{aligned} H_B^s =& \frac{\mp j}{2\pi} \int_{\mathrm{C}} \frac{e^{-jk\rho \sin w \cos\phi' \mp jk\rho \cos w \sin\phi'}}{k\cos(\phi_w - \phi_0) + k\sin w} d(k\sin w) \quad (\phi' \lessgtr \pi) \\ =& \frac{\mp j}{2\pi} \int_{\mathrm{C}} \frac{\cos w}{\cos(\phi_w - \phi_0) + \sin\ w} e^{-jk\rho\sin(w\pm\phi')} dw, \quad (\phi' \lessgtr \pi) \end{aligned} \tag{2.16}$$

where the contour C can be defined as in Fig. 2.5 with the different position of the pole w_p. Since the above integrals in Eq.(2.15) and Eq.(2.16) cannot be analytically evaluated, the

saddle point method and the uniform asymptotic solution may be used on the assumption for a large k with respect to w variable. The integrals have saddle points w_{s} and the poles w_{p}. By considering the location of these saddle pint and the pole, the z-component of the scattering fields H_A^s and H_B^s can then be obtained as

$$H_A^s = H_d^{\mathrm{A}} + H_p^{\mathrm{A}}, \tag{2.17}$$
$$H_B^s = H_d^{\mathrm{B}} + H_p^{\mathrm{B}}, \tag{2.18}$$

where H_p^{A} and H_p^{B} are the contributions from the poles, which exactly represent the magnetic fields of geometrical optics (GO) incident and reflected waves, and can be given by:

$$H_p^{\mathrm{A}} = \pm e^{jk\rho\cos(\phi_0-\pi-|\phi-\pi|)}U(|\phi-\pi|-\phi_0), \quad (\phi \lessgtr \pi), \tag{2.19}$$
$$H_p^{\mathrm{B}} = \mp e^{jk\rho\cos(\phi_{\mathrm{w}}-\phi_0-\pi-|\phi'-\pi|)}U(|\phi'-\pi|-\phi_{\mathrm{w}}+\phi_0). \quad (\phi' \lessgtr \pi) \tag{2.20}$$

H_d^{A} and H_d^{B} are diffracted fields, which can be obtained by evaluating the integrals on the SDP contour as:

$$H_d^{\mathrm{A}} = -C(k\rho)\left[S^-(\phi+\phi_0)U(\pi-\phi) + S^-(\phi-\phi_0)U(\phi-\pi) + \frac{2\sin\phi}{\cos\phi+\cos\phi_0}\right], \tag{2.21}$$

$$\begin{aligned} H_d^{\mathrm{B}} =& C(k\rho)\Bigg[S^-(\phi'+\phi_{\mathrm{w}}-\phi_0)U(\pi-\phi') + S^-(\phi'-\phi_{\mathrm{w}}+\phi_0)U(\phi'-\pi) \\ &+ \frac{2\sin\phi'}{\cos\phi'+\cos(\phi_{\mathrm{w}}-\phi_0)}\Bigg], \end{aligned} \tag{2.22}$$

where $C(\chi) = (8\pi\chi)^{-1/2}e^{-j(\chi+\pi/4)}$ represents the asymptotic formulation of the Green's function in free space for the two-dimensional problem when χ is large. $S^{\pm}(\alpha)$ is the transition function and is defined as

$$S^{\pm}(\alpha) = \frac{1}{\sqrt{\pi}C(k\rho)}e^{jk\rho\cos\alpha}\,\mathrm{sgn}(\pi\pm\alpha)Q\left[(1+j)\left|\cos\frac{\alpha}{2}\right|\sqrt{k\rho}\right] - \frac{1}{\cos(\alpha/2)}, \tag{2.23}$$

where $Q(y) = \int_y^\infty e^{-x^2}dx$ and $\mathrm{sgn}(x)$ are error function complement and sign function, respectively. On the other hand, one has transformations:

$$\begin{aligned} \frac{2\sin\phi}{\cos\phi+\cos\phi_0} =& \frac{\sin\phi_0+\sin\phi}{\cos\phi_0+\cos\phi} + \frac{\sin\phi-\sin\phi_0}{\cos\phi+\cos\phi_0} \\ =& \frac{2\sin\frac{\phi+\phi_0}{2}\cos\frac{\phi-\phi_0}{2}}{2\cos\frac{\phi+\phi_0}{2}\cos\frac{\phi-\phi_0}{2}} + \frac{2\cos\frac{\phi+\phi_0}{2}\sin\frac{\phi-\phi_0}{2}}{2\cos\frac{\phi+\phi_0}{2}\cos\frac{\phi-\phi_0}{2}} \\ =& \frac{\sin\frac{\phi+\phi_0}{2}}{\cos\frac{\phi+\phi_0}{2}} + \frac{\sin\frac{\phi-\phi_0}{2}}{\cos\frac{\phi-\phi_0}{2}} \\ =& \frac{\cos\frac{\pi-(\phi+\phi_0)}{2}}{\sin\frac{\pi-(\phi+\phi_0)}{2}} + \frac{\cos\frac{\pi-(\phi-\phi_0)}{2}}{\sin\frac{\pi-(\phi-\phi_0)}{2}} \\ =& \cot\frac{\pi-(\phi+\phi_0)}{2} + \cot\frac{\pi-(\phi-\phi_0)}{2}, \end{aligned} \tag{2.24}$$

$$
\begin{aligned}
\frac{2\sin\phi'}{\cos\phi'+\cos(\phi_{\rm w}-\phi_0)} =& \frac{\sin(\phi_{\rm w}-\phi_0)+\sin\phi'}{\cos(\phi_{\rm w}-\phi_0)+\cos\phi'} + \frac{\sin\phi'-\sin(\phi_{\rm w}-\phi_0)}{\cos\phi'+\cos(\phi_{\rm w}-\phi_0)} \\
=& \frac{2\sin\frac{\phi'+(\phi_{\rm w}-\phi_0)}{2}\cos\frac{\phi'-(\phi_{\rm w}-\phi_0)}{2}}{2\cos\frac{\phi'+(\phi_{\rm w}-\phi_0)}{2}\cos\frac{\phi'-(\phi_{\rm w}-\phi_0)}{2}} + \frac{2\cos\frac{\phi'+(\phi_{\rm w}-\phi_0)}{2}\sin\frac{\phi'-\phi_0}{2}}{2\cos\frac{\phi'+\phi_0}{2}\cos\frac{\phi'-(\phi_{\rm w}-\phi_0)}{2}} \\
=& \frac{\sin\frac{\phi'+(\phi_{\rm w}-\phi_0)}{2}}{\cos\frac{\phi'+(\phi_{\rm w}-\phi_0)}{2}} + \frac{\sin\frac{\phi'-(\phi_{\rm w}-\phi_0)}{2}}{\cos\frac{\phi'-(\phi_{\rm w}-\phi_0)}{2}} \\
=& \frac{\cos\frac{\pi-(\phi'+\phi_{\rm w}-\phi_0)}{2}}{\sin\frac{\pi-(\phi'+\phi_{\rm w}-\phi_0)}{2}} + \frac{\cos\frac{\pi-(\phi'-\phi_{\rm w}+\phi_0)}{2}}{\sin\frac{\pi-(\phi'-\phi_{\rm w}+\phi_0)}{2}} \\
=& \cot\frac{\pi-(\phi'+\phi_{\rm w}-\phi_0)}{2} + \cot\frac{\pi-(\phi'-\phi_{\rm w}+\phi_0)}{2}. \qquad (2.25)
\end{aligned}
$$

By using above transformations and converting $\phi' = \phi + 2\pi - \phi_{\rm w}$, the diffracted fields $H_d^{\rm A}$ and $H_d^{\rm B}$ can be rewritten as:

$$
\begin{aligned}
H_d^{\rm A} =& -C(k\rho)\Bigg[\cot\frac{\pi-(\phi-\phi_0)}{2} + S^-(\phi-\phi_0)U(\phi-\pi) \\
&+ \cot\frac{\pi-(\phi+\phi_0)}{2} + S^-(\phi+\phi_0)U(\pi-\phi)\Bigg], \qquad (2.26) \\
H_d^{\rm B} =& -C(k\rho)\Bigg[\cot\frac{\pi+(\phi-\phi_0)}{2} + S^+(\phi+\phi_0)U(\phi_{\rm w}-\pi-\phi) \\
&+ \cot\frac{\pi+(\phi+\phi_0-2\phi_{\rm w})}{2} + S^+(\phi+\phi_0-2\phi_{\rm w})U(\phi+\pi-\phi_{\rm w})\Bigg]. \qquad (2.27)
\end{aligned}
$$

The cotangent functions in Eqs.(2.26) and (2.27) have singularities, which have one-to-one correspondences with the shadow boundaries of the incident and reflected GO rays on surface OA and OB, respectively. One notes that Eqs.(2.26) and (2.27) exist depending on the incident direction. When the incident wave illuminates surface OA or OB only, the diffracted given by only Eq.(2.26) or Eq.(2.27), respectively. On the other hand, when both sides of wedge are illuminated, the diffraction can be calculated by the sum of two second components in Eqs.(2.26) and (2.27). This means one need three equations to describe exactly the behavior of diffracted field depending on incident direction. When the incident direction changes, only suitable one of the three equations has to be selected to describe the corresponding diffracted field behavior. This can sometimes be bothersome for the calculation. Thus, by decomposing the contributions due to the PO currents $\boldsymbol{J}_{\rm A}^{\rm PO}$ and $\boldsymbol{J}_{\rm B}^{\rm PO}$, and by carefully rearranging the terms, a unified expression containing four cotangent functions for the diffracted field can be obtained. This unified expression provides valid field behavior for any incident direction and observation angle $0 < (\phi, \phi_0) < \phi_{\rm w}$, and can be written as

$$
\begin{aligned}
H_{\mathrm{d}} = -C(k\rho)\Bigg[& \cot\frac{\pi+(\phi-\phi_0)}{2}+S^{+}(\phi-\phi_0)U(\phi_{\mathrm{w}}-\pi-\phi)U(\phi_0+\pi-\phi_{\mathrm{w}}) \\
& + \cot\frac{\pi-(\phi-\phi_0)}{2}+S^{-}(\phi-\phi_0)U(\phi-\pi)U(\pi-\phi_0) \\
& + \cot\frac{|\pi-\phi_0|-\phi}{2}\,\mathrm{sgn}(\pi-\phi_0)+S^{-}(\phi+\phi_0)U(\pi-\phi)U(\pi-\phi_0) \\
& + \cot\frac{|\pi+\phi_0-\phi_{\mathrm{w}}|+\phi-\phi_{\mathrm{w}}}{2}\,\mathrm{sgn}(\pi+\phi_0-\phi_w) \\
& + S^{+}(\phi_0+\phi-2\phi_{\mathrm{w}})U(\phi+\pi-\phi_{\mathrm{w}})U(\phi_0+\pi-\phi_{\mathrm{w}})\Bigg]. \qquad (2.28)
\end{aligned}
$$

When the direction of incident wave ϕ_0 changes, two of four cotangent functions in Eq.(2.28) correspond to the non-physical rays and cancel out each other to show exact behavior of the diffracted fields. For example, when only surface OA is illuminated, the first and fourth cotangent functions with their uniform expression are canceled. Then, the remainder equations give us the contribution of diffracted due to incident and reflected waves from surface OA only. Same behavior also occur when only surface OB or both sides of wedge are illuminated.

Similarly, the GO contributions in Eqs.(2.19) and (2.20) also can be rewritten with transformation $\phi' = \phi + 2\pi - \phi_{\mathrm{w}}$ and combined as:

$$
\begin{aligned}
H_z^{\mathrm{p}} = & e^{jk\rho\cos(\phi+\phi_0)}U(\pi-\phi-\phi_0)U(\pi-\phi_0) - e^{jk\rho\cos(\phi-\phi_0)}U(\phi-\pi-\phi_0)U(\pi-\phi_0) \\
& + e^{jk\rho\cos(\phi+\phi_0-2\phi_{\mathrm{w}})}U(\phi+\pi-2\phi_{\mathrm{w}}+\phi_0)U(\phi_0+\pi-\phi_{\mathrm{w}}) \\
& - e^{jk\rho\cos(\phi-\phi_0)}U(\phi_0-\pi-\phi)U(\phi_0+\pi-\phi_{\mathrm{w}}). \qquad (2.29)
\end{aligned}
$$

2.3 TE-Polarized Plane Wave

For TE-polarization, the incident plane wave can be given by:

$$
\boldsymbol{E}^{\mathrm{i}} = e^{jkx\cos\phi_0+jky\sin\phi_0}\hat{\boldsymbol{z}}, \qquad (2.30)
$$

$$
\boldsymbol{H}^{\mathrm{i}} = \sqrt{\frac{\varepsilon_0}{\mu_0}}e^{jkx\cos\phi_0+jky\sin\phi_0}(-\sin\phi_0\hat{\boldsymbol{x}}+\cos\phi_0\hat{\boldsymbol{y}}). \qquad (2.31)
$$

The TE-polarized incident wave also can be rewritten by using the coordinate Ox_1y_1 for surface OB illumination as:

$$
\boldsymbol{E}_B^{\mathrm{i}} = e^{jkx_1\cos(\phi_w-\phi_0)-jky_1\sin(\phi_w-\phi_0)}\hat{\boldsymbol{z}}, \qquad (2.32)
$$

$$
\begin{aligned}
\boldsymbol{H}_B^{\mathrm{i}} = & \sqrt{\frac{\varepsilon_0}{\mu_0}}e^{jkx_1\cos(\phi_w-\phi_0)-jky_1\sin(\phi_w-\phi_0)} \\
& \cdot\left[\sin(\phi_w-\phi_0)\hat{\boldsymbol{x_1}}+\cos(\phi_w-\phi_0)\hat{\boldsymbol{y_1}}\right]. \qquad (2.33)
\end{aligned}
$$

Then the corresponding PO currents $\boldsymbol{J}_A^{\mathrm{PO}}$ and $\boldsymbol{J}_B^{\mathrm{PO}}$ can be obtained as

$$
\begin{aligned}
\boldsymbol{J}_A^{\mathrm{PO}} = & 2\hat{\boldsymbol{n}}_B\times\boldsymbol{H}_A^{\mathrm{i}}|_{y_1=0} = 2\sqrt{\frac{\varepsilon_0}{\mu_0}}e^{jkx\cos\phi_0}\sin\phi_0\hat{\boldsymbol{z}}, \\
\boldsymbol{J}_B^{\mathrm{PO}} = & 2\hat{\boldsymbol{n}}_B\times\boldsymbol{H}_B^{\mathrm{i}}|_{y_1=0} = 2\sqrt{\frac{\varepsilon_0}{\mu_0}}e^{jkx_1\cos(\phi_w-\phi_0)}\sin(\phi_w-\phi_0)\hat{\boldsymbol{z}}. \qquad (2.34)
\end{aligned}
$$

Then the scattering electric fields can be obtained by integrating the PO currents $\boldsymbol{J}_A^{\mathrm{PO}}$ and $\boldsymbol{J}_B^{\mathrm{PO}}$ with Green's function G as

$$\begin{aligned}
E_A^s =& \frac{-\omega\mu_0}{4}\int_S J_A^{\mathrm{PO}} H_0^{(2)}(k\sqrt{(x-x')^2+(y-y')^2})dS|_{y'=0} \\
=& \frac{-\omega\mu_0}{4}\int_0^\infty \left[2\sqrt{\frac{\varepsilon_0}{\mu_0}}e^{jkx'\cos\phi_0}\sin\phi_0 \frac{1}{\pi}\int_{-\infty}^{\infty}\frac{e^{-j\eta(x-x')-j\sqrt{k^2-\eta^2}|y-y'|}}{\sqrt{k^2-\eta^2}}d\eta\right]_{y'=0} dx' \\
=& -\frac{k}{2\pi}\sin\phi_0\int_0^\infty\int_{-\infty}^{\infty} e^{jkx'\cos\phi_0}\frac{e^{-j\eta(x-x')-j\sqrt{k^2-\eta^2}|y|}}{\sqrt{k^2-\eta^2}}d\eta dx' \\
=& -\frac{k}{2\pi}\sin\phi_0\int_{-\infty}^{\infty}\left(\int_0^\infty e^{jkx'\cos\phi_0+j\eta x'}dx'\right)\frac{e^{-j\eta x-j\sqrt{k^2-\eta^2}|y|}}{\sqrt{k^2-\eta^2}}d\eta \\
=& -\frac{jk}{2\pi}\sin\phi_0\int_{-\infty}^{\infty}\frac{e^{-j\eta x-j\sqrt{k^2-\eta^2}|y|}}{(k\cos\phi_0+\eta)\sqrt{k^2-\eta^2}}d\eta, \qquad (2.35)
\end{aligned}$$

$$\begin{aligned}
E_B^s =& \frac{-\omega\mu_0}{4}\int_S J_B^{\mathrm{PO}} H_0^{(2)}(k\sqrt{(x_1-x_1')^2+(y_1-y_1')^2})dS|_{y_1'=0} \\
=& \frac{-\omega\mu_0}{4}\int_0^\infty \left[2\sqrt{\frac{\varepsilon_0}{\mu_0}}e^{jkx_1'\cos(\phi_w-\phi_0)}\sin(\phi_w-\phi_0)\right. \\
& \left.\cdot\frac{1}{\pi}\int_{-\infty}^{\infty}\frac{e^{-j\eta(x_1-x_1')-j\sqrt{k^2-\eta^2}|y_1-y_1'|}}{\sqrt{k^2-\eta^2}}d\eta\right]_{y_1'=0} dx_1' \\
=& -\frac{k}{2\pi}\sin(\phi_w-\phi_0)\int_0^\infty\int_{-\infty}^{\infty} e^{jkx_1'\cos(\phi_\omega-\phi_0)}\frac{e^{-j\eta(x_1-x_1')-j\sqrt{k^2-\eta^2}|y_1|}}{\sqrt{k^2-\eta^2}}d\eta dx_1' \\
=& -\frac{k}{2\pi}\sin(\phi_w-\phi_0)\int_{-\infty}^{\infty}\left(\int_0^\infty e^{jkx_1'\cos(\phi_\omega-\phi_0)+j\eta x_1'}dx_1'\right)\frac{e^{-j\eta x_1-j\sqrt{k^2-\eta^2}|y_1|}}{\sqrt{k^2-\eta^2}}d\eta \\
=& -\frac{jk}{2\pi}\sin(\phi_w-\phi_0)\int_{-\infty}^{\infty}\frac{e^{-j\eta x_1-j\sqrt{k^2-\eta^2}|y_1|}}{\{k\cos(\phi_w-\phi_0)+\eta\}\sqrt{k^2-\eta^2}}d\eta. \qquad (2.36)
\end{aligned}$$

Converting to plane of complex angle w with the transformation $\eta = k\sin w$, and using the cylindrical coordinates $(\rho,\ \phi)$ and $(\rho,\ \phi')$, Eqs.(2.35) and (2.36) can be rewritten as

$$\begin{aligned}
E_A^s =& -\frac{j}{2\pi}\sin\phi_0\int_{\mathrm{C}}\frac{e^{-jk\rho\sin w\cos\phi\mp jk\rho\cos w\sin\phi}}{\cos\phi_0+\sin w}dw \\
=& -\frac{j}{2\pi}\sin\phi_0\int_{\mathrm{C}}\frac{e^{-jk\rho\sin(w\pm\phi)}}{\cos\phi_0+\sin w}dw. \qquad (2.37) \\
E_B^s =& -\frac{j}{2\pi}\sin(\phi_w-\phi_0)\int_{\mathrm{C}}\frac{e^{-jk\rho\sin w\cos\phi'\mp jk\rho\cos w\sin\phi'}}{\cos(\phi_w-\phi_0)+\sin w}dw \\
=& -\frac{j}{2\pi}\sin(\phi_w-\phi_0)\int_{\mathrm{C}}\frac{e^{-jk\rho\sin(w\pm\phi')}}{\cos(\phi_w-\phi_0)+\sin w}dw, \qquad (2.38)
\end{aligned}$$

where the contour C can be defined as in Fig. 2.5. By the same manner as TM polarization, the integrals in Eq.(2.37) and Eq.(2.38) can be solved by using the saddle point

technique with respect to w variable. Then, the uniform asymptotic solutions of the scattering electric fields E_A^s and E_B^s can be obtained as

$$E_A^s = E_d^{\mathrm{A}} + E_p^{\mathrm{A}}, \tag{2.39}$$

$$E_B^s = E_d^{\mathrm{B}} + E_p^{\mathrm{B}}, \tag{2.40}$$

where E_p^{A} and E_p^{B} also represents the contribution of geometrical optics (GO) incident and reflected rays as:

$$\begin{aligned} E_p^{\mathrm{A}} =& - e^{jk\rho\cos(\phi_0-\pi-|\phi-\pi|)}U(|\phi-\pi|-\phi_0) \\ =& - e^{jk\rho\cos(\phi+\phi_0)}U(\pi-\phi-\phi_0) - -E_0 e^{jk\rho\cos(\phi-\phi_0)}U(\phi-\pi-\phi_0), \end{aligned} \tag{2.41}$$

$$\begin{aligned} E_p^{\mathrm{B}} =& - e^{jk\rho\cos(\phi_{\mathrm{w}}-\phi_0-\pi-|\phi'-\pi|)}U(|\phi'-\pi|-\phi_{\mathrm{w}}+\phi_0) \\ =& -e^{jk\rho\cos(\phi-\phi_0|)}U(\phi_0-\pi-\phi) - E_0 e^{jk\rho\cos(\phi+\phi_0-2\phi_{\mathrm{w}})}U(\phi+\phi_0+\pi-2\phi_{\mathrm{w}}), \end{aligned} \tag{2.42}$$

and E_d^{A} and E_d^{B} are diffracted fields, which can be written as:

$$E_d^{\mathrm{A}} = - C(k\rho)\left[S^-(\phi-\phi_0)U(\phi-\pi) - S^-(\phi+\phi_0)U(\pi-\phi) - \frac{2\sin\phi_0}{\cos\phi+\cos\phi_0}\right], \tag{2.43}$$

$$\begin{aligned} E_d^{\mathrm{B}} =& C(k\rho)\Bigg[S^-(\phi'+\phi_{\mathrm{w}}-\phi_0)U(\pi-\phi') - S^-(\phi'-\phi_{\mathrm{w}}+\phi_0)U(\phi'-\pi) \\ &+ \frac{2\sin(\phi_{\mathrm{w}}-\phi_0)}{\cos\phi'+\cos(\phi_{\mathrm{w}}-\phi_0)}\Bigg], \end{aligned} \tag{2.44}$$

One then has the following transformations:

$$\begin{aligned} \frac{-2\sin\phi_0}{\cos\phi+\cos\phi_0} =& \frac{-\sin\phi_0+\sin\phi}{\cos\phi_0+\cos\phi} - \frac{\sin\phi_0+\sin\phi}{\cos\phi+\cos\phi_0} \\ =& \frac{2\cos\frac{\phi+\phi_0}{2}\sin\frac{\phi-\phi_0}{2}}{2\cos\frac{\phi+\phi_0}{2}\cos\frac{\phi-\phi_0}{2}} - \frac{2\sin\frac{\phi+\phi_0}{2}\cos\frac{\phi-\phi_0}{2}}{2\cos\frac{\phi+\phi_0}{2}\cos\frac{\phi-\phi_0}{2}} \\ =& \frac{\sin\frac{\phi-\phi_0}{2}}{\cos\frac{\phi-\phi_0}{2}} - \frac{\sin\frac{\phi+\phi_0}{2}}{\cos\frac{\phi+\phi_0}{2}} \\ =& \frac{\cos\frac{\pi-(\phi-\phi_0)}{2}}{\sin\frac{\pi-(\phi-\phi_0)}{2}} - \frac{\cos\frac{\pi-(\phi+\phi_0)}{2}}{\sin\frac{\pi-(\phi+\phi_0)}{2}} \\ =& \cot\frac{\pi-(\phi-\phi_0)}{2} - \cot\frac{\pi-(\phi+\phi_0)}{2}, \end{aligned} \tag{2.45}$$

$$\begin{aligned} \frac{2\sin(\phi_{\mathrm{w}}-\phi_0)}{\cos\phi'+\cos(\phi_{\mathrm{w}}-\phi_0)} =& \frac{\sin\phi'+\sin(\phi_{\mathrm{w}}-\phi_0)}{\cos\phi'+\cos(\phi_{\mathrm{w}}-\phi_0)} - \frac{\sin\phi'-\sin(\phi_{\mathrm{w}}-\phi_0)}{\cos\phi'+\cos(\phi_{\mathrm{w}}-\phi_0)} \\ =& \frac{2\sin\frac{\phi'+(\phi_{\mathrm{w}}-\phi_0)}{2}\cos\frac{\phi'-(\phi_{\mathrm{w}}-\phi_0)}{2}}{2\cos\frac{\phi'+(\phi_{\mathrm{w}}-\phi_0)}{2}\cos\frac{\phi'-(\phi_{\mathrm{w}}-\phi_0)}{2}} - \frac{2\cos\frac{\phi'+(\phi_{\mathrm{w}}-\phi_0)}{2}\sin\frac{\phi'-\phi_0}{2}}{2\cos\frac{\phi'+\phi_0}{2}\cos\frac{\phi'-(\phi_{\mathrm{w}}-\phi_0)}{2}} \\ =& \frac{\sin\frac{\phi'+(\phi_{\mathrm{w}}-\phi_0)}{2}}{\cos\frac{\phi'+(\phi_{\mathrm{w}}-\phi_0)}{2}} - \frac{\sin\frac{\phi'-(\phi_{\mathrm{w}}-\phi_0)}{2}}{\cos\frac{\phi'-(\phi_{\mathrm{w}}-\phi_0)}{2}} \\ =& \frac{\cos\frac{\pi-(\phi'+\phi_{\mathrm{w}}-\phi_0)}{2}}{\sin\frac{\pi-(\phi'+\phi_{\mathrm{w}}-\phi_0)}{2}} - \frac{\cos\frac{\pi-(\phi'-\phi_{\mathrm{w}}+\phi_0)}{2}}{\sin\frac{\pi-(\phi'-\phi_{\mathrm{w}}+\phi_0)}{2}} \\ =& \cot\frac{\pi-(\phi'+\phi_{\mathrm{w}}-\phi_0)}{2} - \cot\frac{\pi-(\phi'-\phi_{\mathrm{w}}+\phi_0)}{2}. \end{aligned} \tag{2.46}$$

By using above transformations and converting $\phi' = \phi + 2\pi - \phi_{\rm w}$, the diffracted fields $E_d^{\rm A}$ and $E_d^{\rm B}$ can be rewritten as:

$$\begin{aligned} E_d^{\rm A} = &- C(k\rho)\Bigg[\cot\frac{\pi-(\phi-\phi_0)}{2} + S^-(\phi-\phi_0)U(\phi-\pi) \\ &\qquad - \cot\frac{\pi-(\phi+\phi_0)}{2} - S^-(\phi+\phi_0)U(\pi-\phi)\Bigg], \qquad (2.47) \\ E_d^{\rm B} = &- C(k\rho)\Bigg[\cot\frac{\pi+(\phi-\phi_0)}{2} + S^+(\phi+\phi_0)U(\phi_{\rm w}-\pi-\phi) \\ &\qquad - \cot\frac{\pi+(\phi+\phi_0-2\phi_{\rm w})}{2} - S^+(\phi+\phi_0-2\phi_{\rm w})U(\phi+\pi-\phi_{\rm w})\Bigg]. \qquad (2.48) \end{aligned}$$

As same as TM polarization case, the singularities of the cotangent functions in Eqs.(2.47) and (2.48) correspond to the shadow boundaries of the incident and reflected GO rays on surface OA and OB, respectively. One also can see that the diffracted field of TE polarization need three separate equation to describe the field behavior when the incident direction changes. Then, by decomposing the contributions due to the PO currents $\boldsymbol{J}_{\rm A}^{\rm PO}$ and $\boldsymbol{J}_{\rm B}^{\rm PO}$, by carefully rearranging the terms, a unified expression for the diffracted field can be obtained as

$$\begin{aligned} E_{\rm d} = -C(k\rho)\Bigg[&\cot\frac{\pi+(\phi-\phi_0)}{2} + S^+(\phi-\phi_0)U(\phi_{\rm w}-\pi-\phi)U(\phi_0+\pi-\phi_{\rm w}) \\ &+ \cot\frac{\pi-(\phi-\phi_0)}{2} + S^-(\phi-\phi_0)U(\phi-\pi)U(\pi-\phi_0) \\ &- \cot\frac{|\pi-\phi_0|-\phi}{2} - S^-(\phi+\phi_0)U(\pi-\phi)U(\pi-\phi_0) \\ &- \cot\frac{|\pi+\phi_0-\phi_{\rm w}|+\phi-\phi_{\rm w}}{2} \\ &- S^+(\phi_0+\phi-2\phi_{\rm w})U(\phi+\pi-\phi_{\rm w})U(\phi_0+\pi-\phi_{\rm w})\Bigg]. \qquad (2.49) \end{aligned}$$

When the incident angle ϕ_0 changes, the cancellation between two of four cotangent functions also occurs to create exact behavior of diffracted field as TM polarization in previous section. However, one can see that Eq.(2.49) doesn't need the sign functions to have this cancellation as the formulation of TM-polarization. This is due to the difference of phase between two polarizations. Similarly, the GO contributions also can then be combined as:

$$\begin{aligned} \hat{E}_z^{\rm p} = &- e^{jk\rho\cos(\phi+\phi_0)}U(\pi-\phi-\phi_0)U(\pi-\phi_0) - e^{jk\rho\cos(\phi-\phi_0)}U(\phi-\pi-\phi_0)U(\pi-\phi_0) \\ &- e^{jk\rho\cos(\phi+\phi_0-2\phi_{\rm w})}U(\phi+\pi-2\phi_{\rm w}+\phi_0)U(\phi_0+\pi-\phi_{\rm w}) \\ &- e^{jk\rho\cos(\phi-\phi_0)}U(\phi_0-\pi-\phi)U(\phi_0+\pi-\phi_{\rm w}). \qquad (2.50) \end{aligned}$$

Four terms in Eq.(2.50) are exactly equal to the electric field of the incident and reflected GO waves on surfaces OA and OB, respectively.

Chapter 3

Extended Physical Optics Approximation for Dielectric Wedge

In previous chapter, uniform asymptotic solution based on PO method have been presented for scattering problem of conducting wedge. Based on results of the conducting wedge problem, an extended PO approximation for the scattering problem of dielectric wedges is proposed in this chapter. In this dielectric wedge case, a rather flat-angle wedge is selected to avoid the multiple internal reflections of the transmitted. The radiation fields of dielectric wedges can be found from equivalent electric and magnetic currents, which are found from electric and magnetic fields of the GO incident, reflected and transmitted waves. Uniform asymptotic solutions of scattering fields by dielectric wedges were then obtained from the integrations for both TM and TE polarizations.

3.1 Extended PO Based on Equivalent Currents

As mentioned before, when the incident wave illuminates a dielectric wedge, it excites the reflected in the outside and transmitted waves in the inside. Accordingly, the PO currents determined by the incident wave are not enough to solve scattering problem of penetrable objects. In this case, the equivalent electric and magnetic currents can be utilized to calculate the scattering field. These induced currents can be found from the total of GO fields as:

$$\boldsymbol{J} = \hat{\boldsymbol{n}} \times \boldsymbol{H}, \tag{3.1}$$

$$\boldsymbol{M} = \boldsymbol{E} \times \hat{\boldsymbol{n}}. \tag{3.2}$$

where $\boldsymbol{H}$ and $\boldsymbol{E}$ denote the magnetic and electric fields, respectively. For the outside region of wedge, the total field may be given by the sum of incident and reflected waves, while the internal field is determined by the transmitted wave. For two-dimensional objects, the current density is distributed along the boundary length C of the object. Then, the integrals of the scattering fields ($\boldsymbol{E}^{\mathrm{s}}$, $\boldsymbol{H}^{\mathrm{s}}$) in Eq.(1.7) and (1.8) can be rewritten by integral along the length of the object as

$$\boldsymbol{E}^{\mathrm{s}} = -\int_C \left[j\omega\mu \boldsymbol{J}(\boldsymbol{r'}) G(\boldsymbol{r}, \boldsymbol{r'}) + \boldsymbol{M}(\boldsymbol{r'}) \times \nabla' G(\boldsymbol{r}, \boldsymbol{r'}) \right] dl', \tag{3.3}$$

$$\boldsymbol{H}^{\mathrm{s}} = -\int_C \left[j\omega\varepsilon \boldsymbol{M}(\boldsymbol{r'}) G(\boldsymbol{r}, \boldsymbol{r'}) - \boldsymbol{J}(\boldsymbol{r'}) \times \nabla' G(\boldsymbol{r}, \boldsymbol{r'}) \right] dl', \tag{3.4}$$

where ω, ε and μ are the angular frequency, permittivity and permeability, respectively. And two-dimensional Green's function $G(\boldsymbol{r}, \boldsymbol{r}')$ can be found in Eq.(2.4).

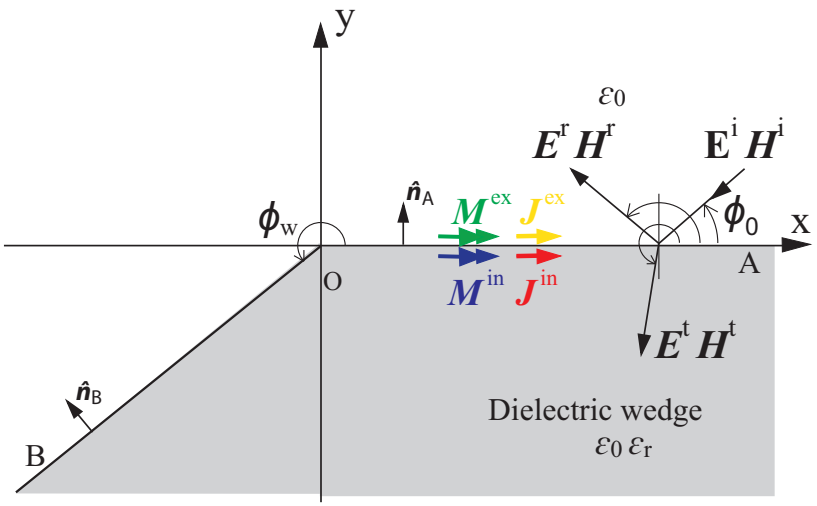

Figure 3.1: Dielectric wedge.

Now, one considers a dielectric wedge of the dielectric constant ε_r and the wedge angle is ϕ_w as in Fig. 3.1. Assuming that the dielectric wedge is illuminated by an incident plane wave. Then, the equivalent electric and magnetic currents outside wedge can be expressed as:

$$\boldsymbol{J}^{ex} = \hat{\boldsymbol{n}}_A \times (\boldsymbol{H}^i + \boldsymbol{H}^r), \tag{3.5}$$

$$\boldsymbol{M}^{ex} = (\boldsymbol{E}^i + \boldsymbol{E}^r) \times \hat{\boldsymbol{n}}_A. \tag{3.6}$$

Inside the wedge, the electric and magnetic currents may be given by:

$$\boldsymbol{J}^{in} = -\hat{\boldsymbol{n}}_A \times \boldsymbol{H}^t \tag{3.7}$$

$$\boldsymbol{M}^{in} = \boldsymbol{E}^t \times (-\hat{\boldsymbol{n}}_A). \tag{3.8}$$

From these equivalent currents, the scattering field can then be calculated separately in two polarization cases as follows:

3.2 TM-Polarized Plane Wave

As represented before, a TM-polarized incident plane wave is given by:

$$\boldsymbol{H}^i = e^{jkx\cos\phi_0 + jky\sin\phi_0}\hat{\boldsymbol{z}}, \tag{3.9}$$

$$\boldsymbol{E}^i = \sqrt{\frac{\mu_0}{\varepsilon_0}} e^{jkx\cos\phi_0 + jky\sin\phi_0}(\sin\phi_0\hat{\boldsymbol{x}} - \cos\phi_0\hat{\boldsymbol{y}}), \tag{3.10}$$

When the incident illuminates surface OA of the dielectric wedge, it excites the scattering fields in both exterior and interior regions of the dielectric wedge. Therefore, The calculations can be performed sequentially as follows: the reflected wave ($\boldsymbol{H}_A^r$, $\boldsymbol{E}_A^r$) in the outside region and transmitted wave ($\boldsymbol{H}_A^t$, $\boldsymbol{E}_A^t$) in the inside region. Accordingly, the external and internal fields can be calculated sequentially as follows.

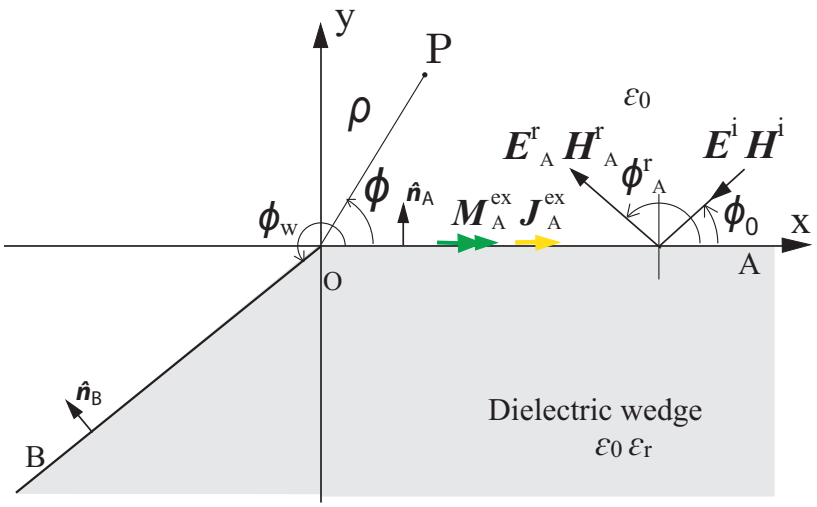

Figure 3.2: Outside dielectric wedge: surface OA is illuminated.

3.2.1 Exterior Field

Outside the wedge, the incident wave excites the reflected wave ($\boldsymbol{H}^{\mathrm{r}}_{\mathrm{A}}$, $\boldsymbol{E}^{\mathrm{r}}_{\mathrm{A}}$) as:

$$\boldsymbol{H}^{\mathrm{r}}_{\mathrm{A}} = \Gamma_{\mathrm{A}} e^{jkx\cos\phi_0 - jky\sin\phi_0}\hat{\boldsymbol{z}}, \tag{3.11}$$

$$\boldsymbol{E}^{\mathrm{r}}_{\mathrm{A}} = -\Gamma_{\mathrm{A}}\sqrt{\frac{\mu_0}{\varepsilon_0}} e^{jkx\cos\phi_0 - jky\sin\phi_0}(\sin\phi_0\hat{\boldsymbol{x}} + \cos\phi_0\hat{\boldsymbol{y}}), \tag{3.12}$$

where Γ_{A} is the corresponding reflection coefficient on surface OA and can be written as:

$$\Gamma_{\mathrm{A}} = \frac{\varepsilon_{\mathrm{r}}\sin\phi_0 - \sqrt{\varepsilon_{\mathrm{r}} - \cos^2\phi_0}}{\varepsilon_{\mathrm{r}}\sin\phi_0 + \sqrt{\varepsilon_{\mathrm{r}} - \cos^2\phi_0}}. \tag{3.13}$$

Then, the external equivalent currents $\boldsymbol{J}^{\mathrm{ex}}_{\mathrm{A}}$ and $\boldsymbol{M}^{\mathrm{ex}}_{\mathrm{A}}$ can be found from the magnetic and electric fields of above GO rays. Accordingly, one may obtain the corresponding equivalent electric and magnetic currents on surface OA from the formulations of the incident and reflected waves, respectively as:

$$\boldsymbol{J}^{\mathrm{iA}} = \hat{\boldsymbol{n}}_{\mathrm{A}} \times \boldsymbol{H}^{\mathrm{i}}|_{y=0} = e^{jkx\cos\phi_0}\hat{\boldsymbol{x}} \tag{3.14}$$

$$\boldsymbol{M}^{\mathrm{iA}} = \boldsymbol{E}^{\mathrm{i}} \times \hat{\boldsymbol{n}}_{\mathrm{A}}|_{y=0} = \sqrt{\frac{\mu_0}{\varepsilon_0}} e^{jkx\cos\phi_0}\sin\phi_0\hat{\boldsymbol{z}} \tag{3.15}$$

$$\boldsymbol{J}^{\mathrm{rA}} = \hat{\boldsymbol{n}}_{\mathrm{A}} \times \boldsymbol{H}^{\mathrm{r}}_{\mathrm{A}}|_{y=0} = \Gamma_{\mathrm{A}} e^{jkx\cos\phi_0}\hat{\boldsymbol{x}} \tag{3.16}$$

$$\boldsymbol{M}^{\mathrm{rA}} = \boldsymbol{E}^{\mathrm{r}}_{\mathrm{A}} \times \hat{\boldsymbol{n}}_{\mathrm{A}}||_{y=0} = -\Gamma_{\mathrm{A}}\sqrt{\frac{\mu_0}{\varepsilon_0}} e^{jkx\cos\phi_0}\sin\phi_0\hat{\boldsymbol{z}}. \tag{3.17}$$

By substituting above equivalent currents into Eq.(3.4), the z-component of the scattering

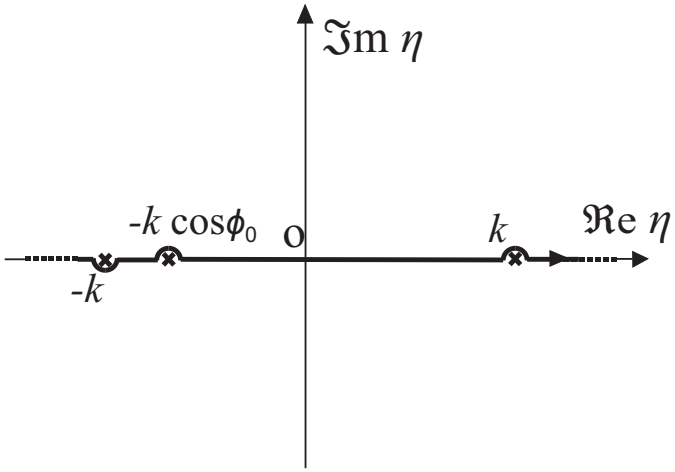

Figure 3.3: Integration contour for Eqs.(3.18) and (3.19) in the complex η plane.

fields due to incident and reflected waves on surface OA can be obtained as:

$$
\begin{aligned}
H_{\mathrm{s}}^{\mathrm{iA}} &= -\int_C \left[j\omega\varepsilon_0 \boldsymbol{M}^{\mathrm{iA}}(\boldsymbol{r'})G - \boldsymbol{J}^{\mathrm{iA}} \times \nabla' G \right] dl' \\
&= \int_0^\infty e^{jkx'\cos\phi_0} \left(-jk\sin\phi_0 G + \frac{\partial G}{\partial y'} \right)_{y'=0} dx' \\
&= \int_0^\infty e^{jkx'\cos\phi_0} \left(\frac{-k\sin\phi_0}{\sqrt{k^2-\eta^2}} \pm 1 \right) \frac{1}{4\pi} \left(\int_{-\infty}^\infty e^{-j\eta(x-x')-j\sqrt{k^2-\eta^2}|y|} d\eta \right) dx' \quad (y \gtrless 0) \\
&= \int_0^\infty \int_{-\infty}^\infty e^{-j\eta(x-x')-j\sqrt{k^2-\eta^2}|y|} e^{jkx'\cos\phi_0} \left(\frac{-k\sin\phi_0}{\sqrt{k^2-\eta^2}} \pm 1 \right) \frac{1}{4\pi} d\eta dx' \quad (y \gtrless 0) \\
&= \frac{1}{4\pi} \int_{-\infty}^\infty \left(\int_0^\infty e^{jkx'\cos\phi_0 + j\eta x'} dx' \right) \left(\frac{-k\sin\phi_0}{\sqrt{k^2-\eta^2}} \pm 1 \right) e^{-j\eta x - j\sqrt{k^2-\eta^2}|y|} d\eta \quad (y \gtrless 0) \\
&= \frac{j}{4\pi} \int_{-\infty}^\infty \left(\frac{-k\sin\phi_0}{\sqrt{k^2-\eta^2}} \pm 1 \right) \frac{e^{-j\eta x - j\sqrt{k^2-\eta^2}|y|}}{(k\cos\phi_0 + \eta)} d\eta, \quad (y \gtrless 0)
\end{aligned} \tag{3.18}
$$

$$
\begin{aligned}
H_{\mathrm{s}}^{\mathrm{rA}} &= -\int_C \left[j\omega\varepsilon_0 \boldsymbol{M}^{\mathrm{rA}}(\boldsymbol{r'})G - \boldsymbol{J}^{\mathrm{rA}} \times \nabla' G \right] dl' \\
&= \int_0^\infty \Gamma_{\mathrm{A}} e^{jkx'\cos\phi_0} \left(jk\sin\phi_0 G + \frac{\partial G}{\partial y'} \right)_{y'=0} dx' \\
&= \int_0^\infty \Gamma_{\mathrm{A}} e^{jkx'\cos\phi_0} \left(\frac{k\sin\phi_0}{\sqrt{k^2-\eta^2}} \pm 1 \right) \frac{1}{4\pi} \left(\int_{-\infty}^\infty e^{-j\eta(x-x')-j\sqrt{k^2-\eta^2}|y|} d\eta \right) dx' \quad (y \gtrless 0) \\
&= \int_0^\infty \int_{-\infty}^\infty \Gamma_{\mathrm{A}} e^{-j\eta(x-x')-j\sqrt{k^2-\eta^2}|y|} e^{jkx'\cos\phi_0} \left(\frac{k\sin\phi_0}{\sqrt{k^2-\eta^2}} \pm 1 \right) \frac{1}{4\pi} d\eta dx' \quad (y \gtrless 0) \\
&= \frac{\Gamma_{\mathrm{A}}}{4\pi} \int_{-\infty}^\infty \left(\int_0^\infty e^{jkx'\cos\phi_0 + j\eta x'} dx' \right) \left(\frac{k\sin\phi_0}{\sqrt{k^2-\eta^2}} \pm 1 \right) e^{-j\eta x - j\sqrt{k^2-\eta^2}|y|} d\eta \quad (y \gtrless 0) \\
&= \frac{j\Gamma_{\mathrm{A}}}{4\pi} \int_{-\infty}^\infty \left(\frac{k\sin\phi_0}{\sqrt{k^2-\eta^2}} \pm 1 \right) \frac{e^{-j\eta x - j\sqrt{k^2-\eta^2}|y|}}{(k\cos\phi_0 + \eta)} d\eta \quad (y \gtrless 0)
\end{aligned} \tag{3.19}
$$

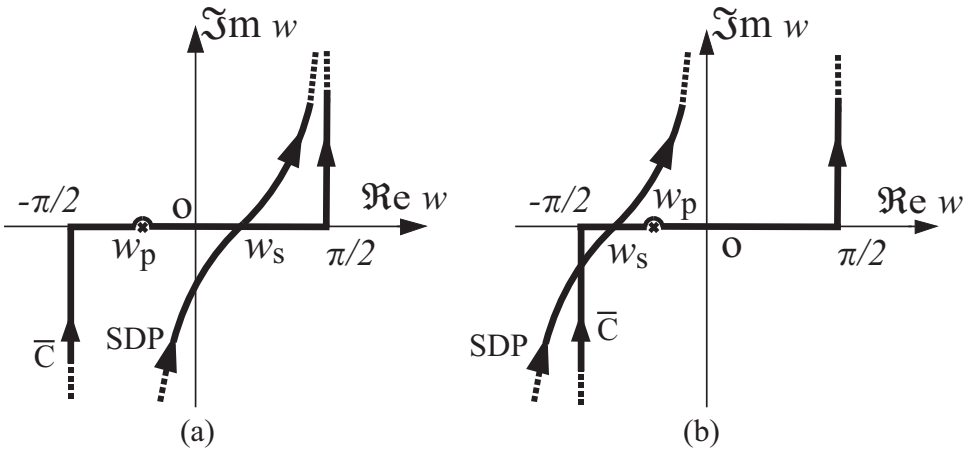

Figure 3.4: Integration contours $\overline{\mathrm{C}}$ and SDP for Eqs.(3.20) and (3.21) in the complex angular w plane: (a) $w_s > w_p$. (b) $w_s < w_p$.

Convert to complex plane of angle w using the transformation $\eta = k\sin w$, with the cylindrical coordinate (ρ, ϕ), Eqs.(3.18) and (3.19) can be rewritten as:

$$\begin{aligned}
H_{\mathrm{s}}^{\mathrm{iA}} =& \frac{j}{4\pi}\int_{\overline{\mathrm{C}}} \frac{k(-\sin\phi_0 \pm \cos w)}{k\cos w} \frac{e^{-jk\rho\sin w\cos\phi \mp jk\rho\cos w\sin\phi}}{k(\cos\phi_0+\sin w)} k\cos w dw \quad (\phi \lessgtr \pi) \\
=& \frac{j}{4\pi}\int_{\overline{\mathrm{C}}} \frac{-\sin\phi_0 \pm \cos w}{\cos\phi_0+\sin w} e^{-jk\rho(\sin w\cos\phi \pm \cos w\sin\phi)} dw \quad (\phi \lessgtr \pi) \\
=& \frac{\pm j}{4\pi}\int_{\overline{\mathrm{C}}} \cot\frac{\pi/2+w\pm\phi_0}{2} e^{-jk\rho\sin(w\pm\phi)} dw, \quad (\phi \lessgtr \pi) \qquad (3.20) \\
H_{\mathrm{s}}^{\mathrm{rA}} =& \frac{j\Gamma_{\mathrm{A}}}{4\pi}\int_{\overline{\mathrm{C}}} \frac{k(\sin\phi_0 \pm \cos w)}{k\cos w} \frac{e^{-jk\rho\sin w\cos\phi \mp jk\rho\cos w\sin\phi}}{k(\cos\phi_0+\sin w)} k\cos w dw \quad (\phi \lessgtr \pi) \\
=& \frac{j\Gamma_{\mathrm{A}}}{4\pi}\int_{\overline{\mathrm{C}}} \frac{\sin\phi_0 \pm \cos w}{\cos\phi_0+\sin w} e^{-jk\rho(\sin w\cos\phi \pm \cos w\sin\phi)} dw \quad (\phi \lessgtr \pi) \\
=& \frac{\pm j\Gamma_{\mathrm{A}}}{4\pi}\int_{\overline{\mathrm{C}}} \cot\frac{\pi/2+w\mp\phi_0}{2} e^{-jk\rho\sin(w\pm\phi)} dw, \quad (\phi \lessgtr \pi) \qquad (3.21)
\end{aligned}$$

where the contour $\overline{\mathrm{C}}$ can be defined as in Fig. 3.4. By using saddle point technique in the same manner of the PEC wedge case, uniform asymptotic solutions for $H_{\mathrm{s}}^{\mathrm{iA}}$ and $H_{\mathrm{s}}^{\mathrm{rA}}$ can be obtained as:

$$\begin{aligned}
H_{\mathrm{s}}^{\mathrm{iA}} =& H_{\mathrm{d}}^{\mathrm{iA}} + H_{\mathrm{p}}^{\mathrm{iA}} && (3.22) \\
H_{\mathrm{p}}^{\mathrm{iA}} =& -e^{jk\rho\cos(\phi-\phi_0)} U(\phi-\pi-\phi_0) && (3.23) \\
H_{\mathrm{s}}^{\mathrm{rA}} =& H_{\mathrm{d}}^{\mathrm{rA}} + H_{\mathrm{p}}^{\mathrm{rA}} && (3.24) \\
H_{\mathrm{p}}^{\mathrm{rA}} =& \Gamma_{\mathrm{A}} e^{jk\rho\cos(\phi+\phi_0)} U(\pi-\phi_0-\phi), && (3.25)
\end{aligned}$$

where $H_{\mathrm{d}}^{\mathrm{iA}}$ and $H_{\mathrm{d}}^{\mathrm{rA}}$ present the diffracted field contributions and can be given by:

$$H_{\mathrm{d}}^{\mathrm{iA}} = -C(k\rho)\left[\cot\frac{\pi-(\phi-\phi_0)}{2} + S^{-}(\phi-\phi_0)U(\phi-\pi)\right] \qquad (3.26)$$

$$H_{\mathrm{d}}^{\mathrm{rA}} = -C(k\rho)\left[\Gamma_A\cot\frac{\pi-(\phi+\phi_0)}{2} + \Gamma_A S^{-}(\phi+\phi_0)U(\pi-\phi)\right] \qquad (3.27)$$

When surface OB is illuminated, the corresponding reflected wave ($\boldsymbol{H}_{\mathrm{B}}^{\mathrm{r}}$, $\boldsymbol{E}_{\mathrm{B}}^{\mathrm{r}}$) can be

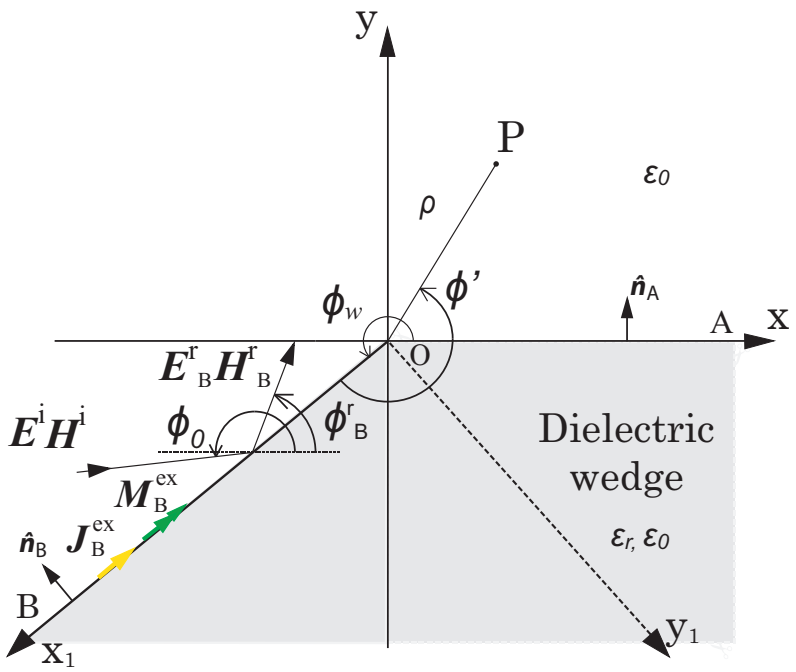

Figure 3.5: Outside dielectric wedge: surface OB is illuminated.

written in the coordinate Ox_1y_1 as:

$$\boldsymbol{H}_{\mathrm{B}}^{\mathrm{r}} = \Gamma_{\mathrm{B}} e^{jkx_1\cos(\phi_{\mathrm{w}}-\phi_0)+jky_1(\phi_{\mathrm{w}}-\sin\phi_0)}\hat{\boldsymbol{z}}, \tag{3.28}$$

$$\boldsymbol{E}_{\mathrm{B}}^{\mathrm{r}} = \Gamma_{\mathrm{B}}\sqrt{\frac{\mu_0}{\varepsilon_0}} e^{jkx_1\cos(\phi_{\mathrm{w}}-\phi_0)+jk_1y\sin(\phi_{\mathrm{w}}-\phi_0)}[\sin(\phi_{\mathrm{w}}-\phi_0)\hat{\boldsymbol{x}}-\cos(\phi_{\mathrm{w}}-\phi_0)\hat{\boldsymbol{y}}], \tag{3.29}$$

where the reflection coefficient Γ_{B} from surface OB is defined as:

$$\Gamma_{\mathrm{B}} = \frac{\varepsilon_{\mathrm{r}}\sin(\pi+\phi_0-\phi_{\mathrm{w}}) - \sqrt{\varepsilon_{\mathrm{r}}-\cos^2(\pi+\phi_0-\phi_{\mathrm{w}})}}{\varepsilon_{\mathrm{r}}\sin(\pi+\phi_0-\phi_{\mathrm{w}}) + \sqrt{\varepsilon_{\mathrm{r}}-\cos^2(\pi+\phi_0-\phi_{\mathrm{w}})}}, \tag{3.30}$$

From the GO incident and reflected rays on surface OB, one can define external currents $\boldsymbol{J}_{\mathrm{B}}^{\mathrm{ex}}$ and $\boldsymbol{M}_{\mathrm{B}}^{\mathrm{ex}}$. The electric and magnetic currents due to the incident and reflected waves on surface OB then can be obtained separately as:

$$\boldsymbol{J}^{\mathrm{iB}} = \hat{\boldsymbol{n}}_{\mathrm{B}} \times \boldsymbol{H}_{\mathrm{B}}^{\mathrm{i}}|_{y_1=0} = -e^{jkx_1\cos(\phi_w-\phi_0)}\hat{\boldsymbol{x_1}}, \tag{3.31}$$

$$\boldsymbol{M}^{\mathrm{iB}} = \boldsymbol{E}^{\mathrm{i}} \times \hat{\boldsymbol{n}}_{\mathrm{B}}|_{y_1=0} = \sqrt{\frac{\mu_0}{\varepsilon_0}} e^{jkx_1\cos(\phi_w-\phi_0)}\sin(\phi_w-\phi_0)\hat{\boldsymbol{z}}, \tag{3.32}$$

$$\boldsymbol{J}^{\mathrm{rB}} = \hat{\boldsymbol{n}}_{\mathrm{B}} \times \boldsymbol{H}_{\mathrm{B}}^{\mathrm{r}}|_{y_1=0} = -\Gamma_{\mathrm{B}} e^{jkx_1\cos(\phi_w-\phi_0)}\hat{\boldsymbol{x_1}}, \tag{3.33}$$

$$\boldsymbol{M}^{\mathrm{rB}} = \boldsymbol{E}_{\mathrm{B}}^{\mathrm{r}} \times \hat{\boldsymbol{n}}_{\mathrm{B}}||_{y_1=0} = -\Gamma_{\mathrm{B}}\sqrt{\frac{\mu_0}{\varepsilon_0}} e^{jkx_1\cos(\phi_w-\phi_0)}\sin(\phi_w-\phi_0)\hat{\boldsymbol{z}}. \tag{3.34}$$

Then, the z-component of the scattering fields due to incident and reflected waves on

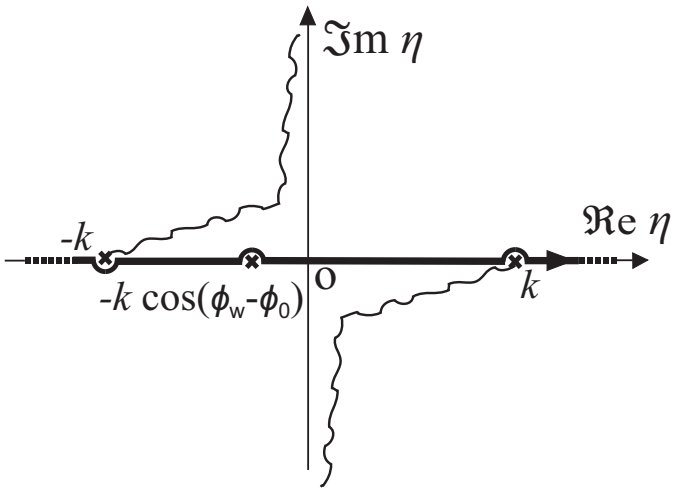

Figure 3.6: Integration contour for Eqs.(3.35) and (3.36) in the complex η plane.

surface OB can also be obtained as:

$$
\begin{aligned}
H_{\mathrm{s}}^{\mathrm{iB}} &= -\int_C \left[j\omega\varepsilon_0 \boldsymbol{M}^{\mathrm{iB}}(\boldsymbol{r'})G - \boldsymbol{J}^{\mathrm{iB}} \times \nabla' G \right] dl' \\
&= \int_0^\infty e^{jkx_1' \cos(\phi_{\mathrm{w}}-\phi_0)} \left(-jk\sin(\phi_{\mathrm{w}}-\phi_0)G - \frac{\partial G}{\partial y_1'} \right)_{y_1'=0} dx_1' \\
&= \int_0^\infty e^{jkx_1' \cos(\phi_{\mathrm{w}}-\phi_0)} \left(\frac{-k\sin(\phi_{\mathrm{w}}-\phi_0)}{\sqrt{k^2-\eta^2}} \mp 1 \right) \frac{1}{4\pi} \left(\int_{-\infty}^\infty e^{-j\eta(x_1-x_1')-j\sqrt{k^2-\eta^2}|y_1|} d\eta \right) dx_1' \quad (y_1 \gtrless 0) \\
&= \int_0^\infty \int_{-\infty}^\infty e^{-j\eta(x_1-x_1')-j\sqrt{k^2-\eta^2}|y_1|} e^{jkx_1' \cos(\phi_{\mathrm{w}}-\phi_0)} \left(\frac{-k\sin(\phi_{\mathrm{w}}-\phi_0)}{\sqrt{k^2-\eta^2}} \mp 1 \right) \frac{1}{4\pi} d\eta dx_1' \quad (y_1 \gtrless 0) \\
&= \frac{1}{4\pi} \int_{-\infty}^\infty \left(\int_0^\infty e^{jkx_1' \cos(\phi_{\mathrm{w}}-\phi_0)+j\eta x_1'} dx_1' \right) \left(\frac{-k\sin(\phi_{\mathrm{w}}-\phi_0)}{\sqrt{k^2-\eta^2}} \mp 1 \right) e^{-j\eta x_1 - j\sqrt{k^2-\eta^2}|y_1|} d\eta \quad (y_1 \gtrless 0) \\
&= \frac{j}{4\pi} \int_{-\infty}^\infty \left(\frac{-k\sin(\phi_{\mathrm{w}}-\phi_0)}{\sqrt{k^2-\eta^2}} \mp 1 \right) \frac{e^{-j\eta x_1 - j\sqrt{k^2-\eta^2}|y_1|}}{k\cos(\phi_{\mathrm{w}}-\phi_0)+\eta} d\eta \quad (y_1 \gtrless 0) \qquad (3.35)
\end{aligned}
$$

$$
\begin{aligned}
H_{\mathrm{s}}^{\mathrm{rB}} &= -\int_C \left[j\omega\varepsilon_0 \boldsymbol{M}^{\mathrm{rB}}(\boldsymbol{r'})G - \boldsymbol{J}^{\mathrm{rB}} \times \nabla' G \right] dl' \\
&= \int_0^\infty \Gamma_{\mathrm{B}} e^{jkx_1' \cos(\phi_{\mathrm{w}}-\phi_0)} \left(jk\sin(\phi_{\mathrm{w}}-\phi_0)G - \frac{\partial G}{\partial y_1'} \right)_{y_1'=0} dx_1' \\
&= \int_0^\infty \Gamma_{\mathrm{B}} e^{jkx_1' \cos(\phi_{\mathrm{w}}-\phi_0)} \left(\frac{k\sin(\phi_{\mathrm{w}}-\phi_0)}{\sqrt{k^2-\eta^2}} \mp 1 \right) \frac{1}{4\pi} \left(\int_{-\infty}^\infty e^{-j\eta(x_1-x_1')-j\sqrt{k^2-\eta^2}|y_1|} d\eta \right) dx_1' \quad (y_1 \gtrless 0) \\
&= \int_0^\infty \int_{-\infty}^\infty \Gamma_{\mathrm{B}} e^{-j\eta(x_1-x_1')-j\sqrt{k^2-\eta^2}|y_1|} e^{jkx_1' \cos(\phi_{\mathrm{w}}-\phi_0)} \left(\frac{k\sin(\phi_{\mathrm{w}}-\phi_0)}{\sqrt{k^2-\eta^2}} \mp 1 \right) \frac{1}{4\pi} d\eta dx_1' \quad (y_1 \gtrless 0) \\
&= \frac{\Gamma_{\mathrm{B}}}{4\pi} \int_{-\infty}^\infty \left(\int_0^\infty e^{jkx_1' \cos(\phi_{\mathrm{w}}-\phi_0)+j\eta x_1'} dx_1' \right) \left(\frac{k\sin(\phi_{\mathrm{w}}-\phi_0)}{\sqrt{k^2-\eta^2}} \mp 1 \right) e^{-j\eta x_1 - j\sqrt{k^2-\eta^2}|y_1|} d\eta \quad (y_1 \gtrless 0) \\
&= \frac{j\Gamma_{\mathrm{B}}}{4\pi} \int_{-\infty}^\infty \left(\frac{k\sin(\phi_{\mathrm{w}}-\phi_0)}{\sqrt{k^2-\eta^2}} \mp 1 \right) \frac{e^{-j\eta x_1 - j\sqrt{k^2-\eta^2}|y_1|}}{k\cos(\phi_{\mathrm{w}}-\phi_0)+\eta} d\eta \quad (y_1 \gtrless 0) \qquad (3.36)
\end{aligned}
$$

Convert to complex plane of angle w using the transformation $\eta = k\sin w$, with the cylindrical coordinate (ρ, ϕ'), Eqs.(3.35) and (3.36) can be rewritten as:

$$\begin{aligned}
H_{\rm s}^{\rm iB} =& \frac{j}{4\pi}\int_{\overline{\rm C}} \frac{k(-\sin(\phi_{\rm w}-\phi_0)\mp\cos w)}{k\cos w}\frac{e^{-jk\rho\sin w\cos\phi'\mp jk\rho\cos w\sin\phi'}}{k(\cos(\phi_{\rm w}-\phi_0)+\sin w)}k\cos w dw \quad (\phi' \lessgtr \pi)\\
=& \frac{j}{4\pi}\int_{\overline{\rm C}} \frac{-\sin(\phi_{\rm w}-\phi_0)\mp\cos w}{\cos(\phi_{\rm w}-\phi_0)+\sin w}e^{-jk\rho(\sin w\cos\phi'\pm\cos w\sin\phi')}dw \quad (\phi' \lessgtr \pi)\\
=& \frac{\mp j}{4\pi}\int_{\overline{\rm C}} \cot\frac{\pi/2+w\mp(\phi_{\rm w}-\phi_0)}{2}e^{-jk\rho\sin(w\pm\phi')}dw, \quad (\phi' \lessgtr \pi) \qquad (3.37)\\
H_{\rm s}^{\rm rB} =& \frac{j\Gamma_{\rm B}}{4\pi}\int_{\overline{\rm C}} \frac{k(\sin(\phi_{\rm w}-\phi_0)\mp\cos w)}{k\cos w}\frac{e^{-jk\rho\sin w\cos\phi'\mp jk\rho\cos w\sin\phi'}}{k(\cos(\phi_{\rm w}-\phi_0)+\sin w)}k\cos w dw \quad (\phi' \lessgtr \pi)\\
=& \frac{j\Gamma_{\rm B}}{4\pi}\int_{\overline{\rm C}} \frac{\sin(\phi_{\rm w}-\phi_0)\mp\cos w}{\cos(\phi_{\rm w}-\phi_0)+\sin w}e^{-jk\rho(\sin w\cos\phi'\pm\cos w\sin\phi')}dw \quad (\phi' \lessgtr \pi)\\
=& \frac{\mp j\Gamma_{\rm B}}{4\pi}\int_{\overline{\rm C}} \cot\frac{\pi/2+w\pm(\phi_{\rm w}-\phi_0)}{2}e^{-jk\rho\sin(w\pm\phi')}dw, \quad (\phi' \lessgtr \pi) \qquad (3.38)
\end{aligned}$$

where the contour $\overline{\rm C}$ can be defined similarly as in Fig. 3.4 with the different position of the pole w_p. By using saddle point technique, uniform asymptotic solutions for $H_{\rm s}^{\rm iB}$ and $H_{\rm s}^{\rm rB}$ can be obtained as:

$$\begin{aligned}
H_{\rm s}^{\rm iB} =& H_{\rm d}^{\rm iB} + H_{\rm p}^{\rm iB} \qquad (3.39)\\
H_{\rm p}^{\rm iB} =& -e^{jk\rho\cos(\phi'+\phi_{\rm w}-\phi_0)}U(\pi-\phi_{\rm w}+\phi_0-\phi')\\
=& -e^{jk\rho\cos(\phi-\phi_0)}U\phi_0-\pi-\phi), \qquad (3.40)\\
H_{\rm s}^{\rm rB} =& H_{\rm d}^{\rm rB} + H_{\rm p}^{\rm rB} \qquad (3.41)\\
H_{\rm p}^{\rm rB} =& \Gamma_{\rm B}e^{jk\rho\cos(\phi'-\phi_{\rm w}+\phi_0)}U(\phi'-\pi-\phi_{\rm w}+\phi_0)\\
=& \Gamma_{\rm B}e^{jk\rho\cos(\phi+\phi_0-2\phi_{\rm w})}U(\phi+\phi_0+\pi-2\phi_{\rm w}). \qquad (3.42)
\end{aligned}$$

where the diffracted fields $H_{\rm d}^{\rm iB}$ and $H_{\rm d}^{\rm rB}$ can be given by:

$$\begin{aligned}
H_{\rm d}^{\rm iB} =& -C(k\rho)\left[-\cot\frac{\pi-(\phi'+\phi_{\rm w}-\phi_0)}{2} - S^-(\phi'+\phi_{\rm w}-\phi_0)U(\pi-\phi')\right]\\
=& -C(k\rho)\left[\cot\frac{\pi+(\phi-\phi_0)}{2} + S^+(\phi-\phi_0)U(\phi_{\rm w}-\pi-\phi)\right] \qquad (3.43)\\
H_{\rm d}^{\rm rB} =& -C(k\rho)\left[-\Gamma_{\rm B}\cot\frac{\pi-(\phi'-\phi_{\rm w}+\phi_0)}{2} - \Gamma_{\rm B}S^-(\phi'-\phi_{\rm w}+\phi_0)U(\phi'-\pi)\right]\\
=& -C(k\rho)\left[\Gamma_{\rm B}\cot\frac{\pi+(\phi_0+\phi-2\phi_{\rm w})}{2} + \Gamma_{\rm B}S^+(\phi_0+\phi-2\phi_{\rm w})U(\pi+\phi-\phi_{\rm w})\right]. \qquad (3.44)
\end{aligned}$$

by considering the incident direction, one has the unified formulation of diffracted field outside the wedge as:

$$
\begin{aligned}
H_{\mathrm{d}}^{\mathrm{Out}} = -C(k\rho)\Bigg[& \cot\frac{\pi-(\phi-\phi_0)}{2}U(\phi_{\mathrm{w}}-\pi-\phi_0)+S^{-}(\phi-\phi_0)U(\phi-\pi)U(\phi_{\mathrm{w}}-\pi-\phi_0) \\
& +\cot\frac{\pi+(\phi-\phi_0)}{2}U(\phi_0-\pi)+S^{+}(\phi-\phi_0)U(\phi_{\mathrm{w}}-\pi-\phi)U(\phi_0-\pi) \\
& +\Gamma_A\cot\frac{\pi-(\phi+\phi_0)}{2}U(\pi-\phi_0)+\Gamma_{\mathrm{A}}S^{-}(\phi+\phi_0)U(\pi-\phi)U(\pi-\phi_0) \\
& +\Gamma_{\mathrm{B}}\cot\frac{\pi+(\phi_0+\phi-2\phi_{\mathrm{w}})}{2}U(\pi+\phi_0-\phi_{\mathrm{w}})+\Gamma_{\mathrm{B}}S^{+}(\phi_0+\phi-2\phi_{\mathrm{w}}) \\
& \cdot U(\pi+\phi-\phi_{\mathrm{w}})U(\pi+\phi_0-\phi_{\mathrm{w}})\Bigg]. \qquad (3.45)
\end{aligned}
$$

Similarly, one can also obtain unified formulation for GO contribution as:

$$
\begin{aligned}
H_{\mathrm{p}}^{\mathrm{Out}} = & -e^{jk\rho\cos(\phi-\phi_0)}U(\phi-\pi-\phi_0)U(\phi_{\mathrm{w}}-\pi-\phi_0) \\
& -e^{jk\rho\cos(\phi-\phi_0)}U\phi_0-\pi-\phi)U(\phi_0-\pi) \\
& +\Gamma_{\mathrm{A}}e^{jk\rho\cos(\phi+\phi_0)}U(\pi-\phi_0-\phi)U(\pi-\phi_0) \\
& +\Gamma_{\mathrm{B}}e^{jk\rho\cos(\phi+\phi_0-2\phi_{\mathrm{w}})}U(\phi+\phi_0+\pi-2\phi_{\mathrm{w}})U(\phi_0+\pi-\phi_{\mathrm{w}}). \qquad (3.46)
\end{aligned}
$$

When the dielectric constant ε_{r} tends to infinity (the dielectric wedge become a PEC wedge), the reflection coefficients Γ_{A} and Γ_{B} become a unit. Accordingly, the resulting diffracted field $H_{\mathrm{d}}^{\mathrm{Out}}$ in Eqs.(3.45) becomes exactly the same as the one formulated by the PO formulation.

3.2.2 Interior Field

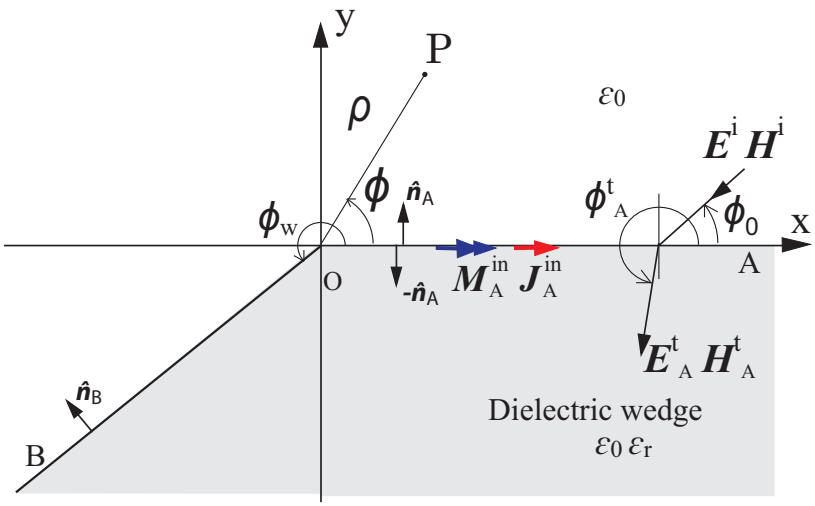

Figure 3.7: Inside dielectric wedge: surface OA is illuminated.

Inside the dielectric wedge, the transmitted wave ($\boldsymbol{H}_{\mathrm{A}}^{\mathrm{t}}$, $\boldsymbol{E}_{\mathrm{A}}^{\mathrm{t}}$) excited by the incident

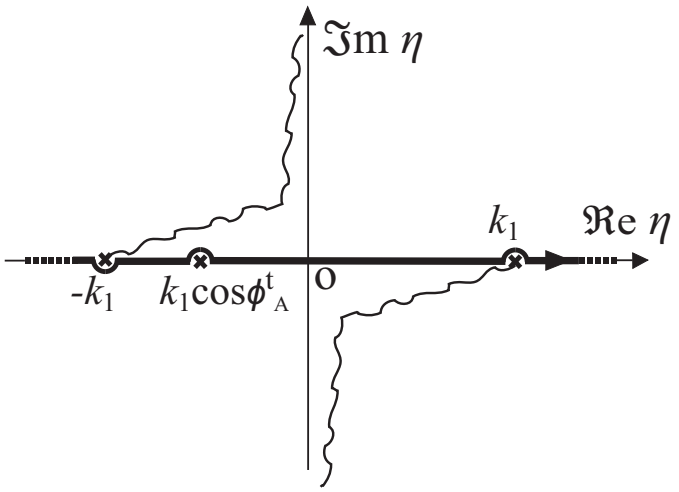

Figure 3.8: Integration contour for Eq.(3.53) in the complex η plane.

wave from surface OA can be given by:

$$\boldsymbol{H}_{\mathrm{A}}^{\mathrm{t}} = \mathrm{T}_{\mathrm{A}} e^{-jk_1 x\cos\phi_{\mathrm{A}}^{\mathrm{t}} - jk_1 y\sin\phi_{\mathrm{A}}^{\mathrm{t}}}\hat{\boldsymbol{z}}, \tag{3.47}$$

$$\boldsymbol{E}_{\mathrm{A}}^{\mathrm{t}} = \mathrm{T}_{\mathrm{A}}\sqrt{\frac{\mu_0}{\varepsilon_{\mathrm{r}}\varepsilon_0}} e^{-jk_1 x\cos\phi_{\mathrm{A}}^{\mathrm{t}} - jk_1 y\sin\phi_{\mathrm{A}}^{\mathrm{t}}}(-\sin\phi_{\mathrm{A}}^{\mathrm{t}}\hat{\boldsymbol{x}} + \cos\phi_{\mathrm{A}}^{\mathrm{t}}\hat{\boldsymbol{y}}), \tag{3.48}$$

with k_1 $(= \omega\sqrt{\varepsilon_{\mathrm{r}}\varepsilon_0\mu_0})$ is the wave number inside dielectric wedge. $\phi_{\mathrm{A}}^{\mathrm{t}}$ $(\geqslant \pi)$ is the transmitted angle and is defined as:

$$\phi_{\mathrm{A}}^{\mathrm{t}} = \pi + \arccos(\frac{\cos\phi_0}{\sqrt{\varepsilon_{\mathrm{r}}}}) \tag{3.49}$$

T_{A} is the transmission coefficient from surface OA and given by:

$$\mathrm{T}_{\mathrm{A}} = 1 + \Gamma_{\mathrm{A}} = \frac{2\varepsilon_{\mathrm{r}}\sin\phi_0}{\varepsilon_{\mathrm{r}}\sin\phi_0 + \sqrt{\varepsilon_{\mathrm{r}} - \cos^2\phi_0}}. \tag{3.50}$$

Then the corresponding internal magnetic and electric currents due to transmitted wave $(\boldsymbol{H}_{\mathrm{A}}^{\mathrm{t}}, \boldsymbol{E}_{\mathrm{A}}^{\mathrm{t}})$ can be obtained as:

$$\boldsymbol{J}_{\mathrm{A}}^{\mathrm{in}} = \boldsymbol{J}^{\mathrm{tA}} = (-\hat{\boldsymbol{n}}_{\mathrm{A}}) \times \boldsymbol{H}_{\mathrm{A}}^{\mathrm{t}}|_{y=0} = -\mathrm{T}_{\mathrm{A}} e^{-jk_1 x\cos\phi_{\mathrm{A}}^{\mathrm{t}}}\hat{\boldsymbol{x}} \tag{3.51}$$

$$\boldsymbol{M}_{\mathrm{A}}^{\mathrm{in}} = \boldsymbol{M}^{\mathrm{tA}} = \boldsymbol{E}_{\mathrm{A}}^{\mathrm{t}} \times (-\hat{\boldsymbol{n}}_{\mathrm{A}})||_{y=0} = \mathrm{T}_{\mathrm{A}}\sqrt{\frac{\mu_0}{\varepsilon_{\mathrm{r}}\varepsilon_0}} e^{-jk_1 x\cos\phi_{\mathrm{A}}^{\mathrm{t}}}\sin\phi_{\mathrm{A}}^{\mathrm{t}}\hat{\boldsymbol{z}}. \tag{3.52}$$

Then, the scattering magnetic field excited by the transmitted wave $(\boldsymbol{H}_{\mathrm{A}}^{\mathrm{t}}, \boldsymbol{E}_{\mathrm{A}}^{\mathrm{t}})$ can be

represented as:

$$
\begin{aligned}
H_{\mathrm{s}}^{\mathrm{tA}} =& -\int_C \left[j\omega\varepsilon_{\mathrm{r}}\varepsilon_0 \boldsymbol{M}^{\mathrm{tA}}(\boldsymbol{r'})G - \boldsymbol{J}^{\mathrm{tA}} \times \nabla' G \right] dl' \\
=& \int_0^{\infty} -\mathrm{T_A} e^{-jk_1 x' \cos\phi_{\mathrm{A}}^{\mathrm{t}}} \left(jk_1 \sin\phi_{\mathrm{A}}^{\mathrm{t}} G + \frac{\partial G}{\partial y'} \right)_{y'=0} dx' \\
=& \int_0^{\infty} -\mathrm{T_A} e^{-jk_1 x' \cos\phi_{\mathrm{A}}^{\mathrm{t}}} \left(\frac{k_1 \sin\phi_{\mathrm{A}}^{\mathrm{t}}}{\sqrt{k_1^2 - \eta^2}} - 1 \right) \frac{1}{4\pi} \left(\int_{-\infty}^{\infty} e^{-j\eta(x-x') - j\sqrt{k_1^2-\eta^2}|y|} d\eta \right) dx' \\
=& \int_0^{\infty} \int_{-\infty}^{\infty} -\mathrm{T_A} e^{-j\eta(x-x') - j\sqrt{k_1^2-\eta^2}|y|} e^{-jk_1 x' \cos\phi_{\mathrm{A}}^{\mathrm{t}}} \left(\frac{k_1 \sin\phi_{\mathrm{A}}^{\mathrm{t}}}{\sqrt{k_1^2 - \eta^2}} - 1 \right) \frac{1}{4\pi} d\eta dx' \\
=& \frac{-\mathrm{T_A}}{4\pi} \int_{-\infty}^{\infty} \left(\int_0^{\infty} e^{-jk_1 x' \cos\phi_{\mathrm{A}}^{\mathrm{t}} + j\eta x'} dx' \right) \left(\frac{k_1 \sin\phi_{\mathrm{A}}^{\mathrm{t}}}{\sqrt{k_1^2 - \eta^2}} - 1 \right) e^{-j\eta x - j\sqrt{k_1^2-\eta^2}|y|} d\eta \\
=& \frac{-j\mathrm{T_A}}{4\pi} \int_{-\infty}^{\infty} \left(\frac{k_1 \sin\phi_{\mathrm{A}}^{\mathrm{t}}}{\sqrt{k_1^2 - \eta^2}} - 1 \right) \frac{e^{-j\eta x - j\sqrt{k_1^2-\eta^2}|y|}}{-k_1 \cos\phi_{\mathrm{A}}^{\mathrm{t}} + \eta} d\eta. \qquad (3.53)
\end{aligned}
$$

Convert to complex plane of angle w using the transformation $\eta = k_1 \sin w$, with the cylindrical coordinate (ρ, ϕ), Eq.(3.53) can be rewritten as:

$$
\begin{aligned}
H_{\mathrm{s}}^{\mathrm{tA}} =& \frac{-j\mathrm{T_A}}{4\pi} \int_{\overline{\mathrm{C}}} \frac{k_1(\sin\phi_{\mathrm{A}}^{\mathrm{t}} - \cos w)}{k_1 \cos w} \frac{e^{-jk_1\rho \sin w \cos\phi + jk_1\rho \cos w \sin\phi}}{k_1(-\cos\phi_{\mathrm{A}}^{\mathrm{t}} + \sin w)} k_1 \cos w dw \\
=& \frac{-j\mathrm{T_A}}{4\pi} \int_{\overline{\mathrm{C}}} \frac{\sin\phi_{\mathrm{A}}^{\mathrm{t}} - \cos w}{-\cos\phi_{\mathrm{A}}^{\mathrm{t}} + \sin w} e^{-jk_1\rho(\sin w \cos\phi - \cos w \sin\phi)} dw \\
=& \frac{-j\Gamma_{\mathrm{A}}}{4\pi} \int_{\overline{\mathrm{C}}} \cot\frac{\phi_{\mathrm{A}}^{\mathrm{t}} - w + \pi/2}{2} e^{-jk_1\rho\sin(w-\phi)} dw. \qquad (3.54)
\end{aligned}
$$

The contour $\overline{\mathrm{C}}$ can be defined similarly as in Fig. 3.4, where the position of the pole w_p changes depending on the transmitted angle $\phi_{\mathrm{A}}^{\mathrm{t}}$. By using saddle point technique, uniform asymptotic solution for $H_{\mathrm{s}}^{\mathrm{tA}}$ can be obtained as:

$$
\begin{aligned}
H_{\mathrm{s}}^{\mathrm{tA}} =& H_{\mathrm{d}}^{\mathrm{tA}} + H_{\mathrm{p}}^{\mathrm{tA}} \qquad (3.55) \\
H_{\mathrm{p}}^{\mathrm{tA}} =& \mathrm{T_A} e^{-jk_1\rho\cos(\phi - \phi_{\mathrm{A}}^{\mathrm{t}})} U(\phi - \phi_{\mathrm{A}}^{\mathrm{t}}), \qquad (3.56)
\end{aligned}
$$

where $H_{\mathrm{d}}^{\mathrm{tA}}$ represents the diffracted field contributions, and can be given by:

$$
H_{\mathrm{d}}^{\mathrm{tA}} = -C(k_1\rho) \left[\mathrm{T_A} \cot\frac{\phi - \phi_{\mathrm{A}}^{\mathrm{t}}}{2} - \mathrm{T_A} S^{-}(\pi - \phi_{\mathrm{A}}^{\mathrm{t}} + \phi) U(\phi - \phi_{\mathrm{w}}) \right]. \qquad (3.57)
$$

The contribution from $H_{\mathrm{p}}^{\mathrm{tA}}$ is exactly equal to the magnetic field of transmitted wave from surface OA.

When surface OB is illuminated, one may also have transmitted wave ($\boldsymbol{H}_{\mathrm{B}}^{\mathrm{t}}$, $\boldsymbol{E}_{\mathrm{B}}^{\mathrm{t}}$) from surface OB, which can be written in the coordinate system Ox_1y_1 as:

$$
\begin{aligned}
\boldsymbol{H}_{\mathrm{B}}^{\mathrm{t}} =& \mathrm{T_B} e^{-jk_1 x_1 \cos(\phi_{\mathrm{B}}^{\mathrm{t}} - \phi_{\mathrm{w}}) - jk_1 y_1 \sin\phi_{\mathrm{A}}^{\mathrm{t}}} \hat{\boldsymbol{z}}, \qquad (3.58) \\
\boldsymbol{E}_{\mathrm{B}}^{\mathrm{t}} =& \mathrm{T_B} \sqrt{\frac{\mu_0}{\varepsilon_{\mathrm{r}}\varepsilon_0}} e^{-jk_1 x_1 \cos(\phi_{\mathrm{B}}^{\mathrm{t}} - \phi_{\mathrm{w}}) - jk_1 y_1 \sin(\phi_{\mathrm{B}}^{\mathrm{t}} - \phi_{\mathrm{w}})} [-\sin(\phi_{\mathrm{B}}^{\mathrm{t}} - \phi_{\mathrm{w}}) \hat{\boldsymbol{x_1}} + \cos(\phi_{\mathrm{B}}^{\mathrm{t}} - \phi_{\mathrm{w}}) \hat{\boldsymbol{y_1}}], \qquad (3.59)
\end{aligned}
$$

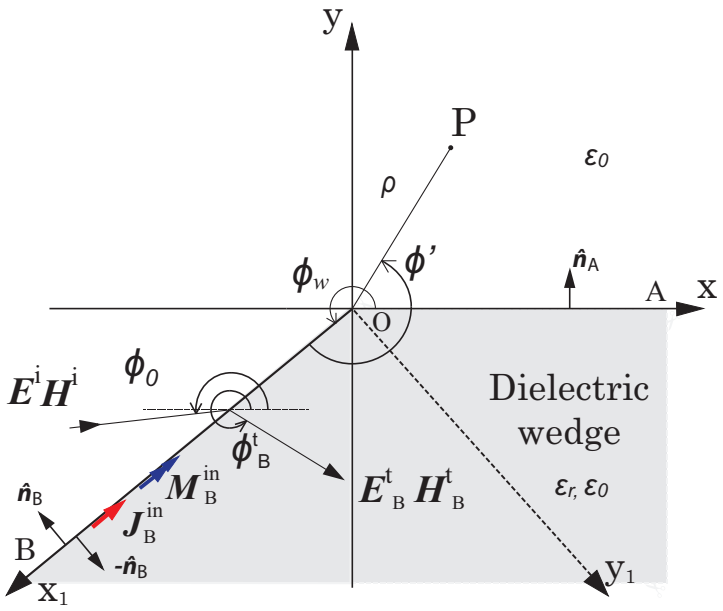

Figure 3.9: Inside dielectric wedge: surface OB is illuminated.

where the transmitted angle $\phi_{\mathrm{B}}^{\mathrm{t}}$ and the transmission coefficient $\mathrm{T_B}$ are defined as:

$$\phi_{\mathrm{B}}^{\mathrm{t}} = \phi_{\mathrm{w}} + \arccos\frac{\cos(\pi+\phi_0-\phi_{\mathrm{w}})}{\sqrt{\varepsilon_{\mathrm{r}}}} \tag{3.60}$$

$$\mathrm{T_B} = 1+\Gamma_{\mathrm{B}} = \frac{2\varepsilon_{\mathrm{r}}\sin(\pi+\phi_0-\phi_{\mathrm{w}})}{\varepsilon_{\mathrm{r}}\sin(\pi+\phi_0-\phi_{\mathrm{w}})+\sqrt{\varepsilon_{\mathrm{r}}-\cos^2(\pi+\phi_0-\phi_{\mathrm{w}})}}. \tag{3.61}$$

Then, the internal equivalent currents $\boldsymbol{J}_{\mathrm{B}}^{\mathrm{in}}$ and $\boldsymbol{M}_{\mathrm{B}}^{\mathrm{in}}$ can be derived as:

$$\boldsymbol{J}_{\mathrm{B}}^{\mathrm{in}} = \boldsymbol{J}^{\mathrm{tB}} = (-\hat{\boldsymbol{n}}_{\mathrm{B}})\times\boldsymbol{H}_{\mathrm{B}}^{\mathrm{t}}|_{y_1=0} = \mathrm{T_B}e^{-jk_1x_1\cos(\phi_{\mathrm{B}}^{\mathrm{t}}-\phi_{\mathrm{w}})}\hat{\boldsymbol{x}}_{\mathbf{1}} \tag{3.62}$$

$$\boldsymbol{M}_{\mathrm{B}}^{\mathrm{in}} = \boldsymbol{M}^{\mathrm{tB}} = \boldsymbol{E}_{\mathrm{B}}^{\mathrm{t}}\times(-\hat{\boldsymbol{n}}_{\mathrm{B}})||_{y_1=0} = -\mathrm{T_B}\sqrt{\frac{\mu_0}{\varepsilon_{\mathrm{r}}\varepsilon_0}}e^{-jk_1x_1\cos(\phi_{\mathrm{B}}^{\mathrm{t}}-\phi_{\mathrm{w}})}\sin(\phi_{\mathrm{B}}^{\mathrm{t}}-\phi_{\mathrm{w}})\hat{\boldsymbol{z}}. \tag{3.63}$$

Then, one has the z-component of the scattering fields due to the transmitted wave on surface OB as:

$$\begin{aligned}
H_{\mathrm{s}}^{\mathrm{tB}} &= -\int_C\left[j\omega\varepsilon_{\mathrm{r}}\varepsilon_0\boldsymbol{M}^{\mathrm{tB}}(\boldsymbol{r'})G-\boldsymbol{J}^{\mathrm{tB}}\times\nabla'G\right]dl' \\
&= \int_0^\infty \mathrm{T_B}e^{-jk_1x_1'\cos(\phi_{\mathrm{B}}^{\mathrm{t}}-\phi_{\mathrm{w}})}\left(jk_1\sin(\phi_{\mathrm{B}}^{\mathrm{t}}-\phi_{\mathrm{w}})G+\frac{\partial G}{\partial y_1'}\right)_{y_1'=0}dx_1' \\
&= \int_0^\infty \mathrm{T_B}e^{-jk_1x_1'\cos(\phi_{\mathrm{B}}^{\mathrm{t}}-\phi_{\mathrm{w}})}\left(\frac{k_1\sin(\phi_{\mathrm{B}}^{\mathrm{t}}-\phi_{\mathrm{w}})}{\sqrt{k_1^2-\eta^2}}+1\right)\frac{1}{4\pi}\left(\int_{-\infty}^\infty e^{-j\eta(x_1-x_1')-j\sqrt{k_1^2-\eta^2}|y_1|}d\eta\right)dx_1' \\
&= \int_0^\infty\int_{-\infty}^\infty \mathrm{T_B}e^{-j\eta(x_1-x_1')-j\sqrt{k_1^2-\eta^2}y_1}e^{-jk_1x_1'\cos(\phi_{\mathrm{B}}^{\mathrm{t}}-\phi_{\mathrm{w}})}\left(\frac{k_1\sin(\phi_{\mathrm{B}}^{\mathrm{t}}-\phi_{\mathrm{w}})}{\sqrt{k_1^2-\eta^2}}+1\right)\frac{1}{4\pi}d\eta dx_1' \\
&= \frac{\mathrm{T_B}}{4\pi}\int_{-\infty}^\infty\left(\int_0^\infty e^{-jk_1x_1'\cos(\phi_{\mathrm{B}}^{\mathrm{t}}-\phi_{\mathrm{w}})+j\eta x_1'}dx_1'\right)\left(\frac{k_1\sin(\phi_{\mathrm{B}}^{\mathrm{t}}-\phi_{\mathrm{w}})}{\sqrt{k_1^2-\eta^2}}+1\right)e^{-j\eta x_1-j\sqrt{k_1^2-\eta^2}y_1}d\eta \\
&= \frac{j\mathrm{T_B}}{4\pi}\int_{-\infty}^\infty\left(\frac{k_1\sin(\phi_{\mathrm{B}}^{\mathrm{t}}-\phi_{\mathrm{w}})}{\sqrt{k_1^2-\eta^2}}+1\right)\frac{e^{-j\eta x_1-j\sqrt{k_1^2-\eta^2}y_1}}{-k_1\cos(\phi_{\mathrm{B}}^{\mathrm{t}}-\phi_{\mathrm{w}})+\eta}d\eta.
\end{aligned} \tag{3.64}$$

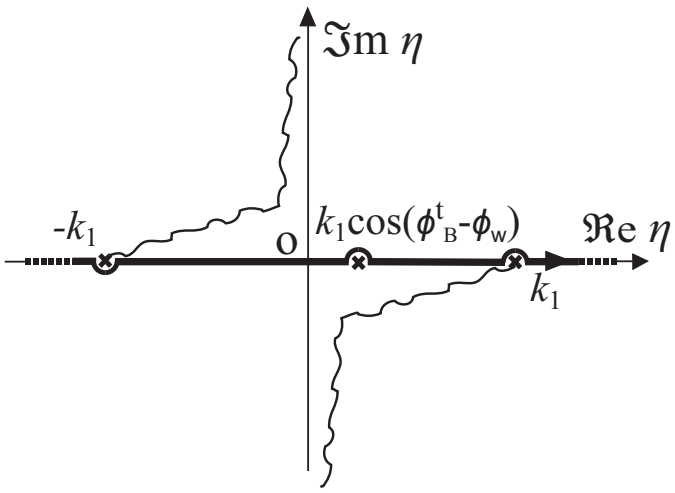

Figure 3.10: Integration contour for Eq.(3.64) in the complex η plane.

Convert to complex plane of angle w using the transformation $\eta = k_1 \sin w$, with the cylindrical coordinate (ρ, ϕ'), Eq.(3.64) can be rewritten as:

$$\begin{aligned} H_{\rm s}^{\rm tB} =& \frac{j{\rm T_B}}{4\pi}\int_{\overline{\rm C}} \frac{k_1(\sin(\phi_{\rm B}^{\rm t}-\phi_{\rm w})+\cos w)}{k_1\cos w}\frac{e^{-jk_1\rho\sin w\cos\phi'-jk_1\rho\cos w\sin\phi'}}{k_1(-\cos(\phi_{\rm B}^{\rm t}-\phi_{\rm w})+\sin w)}k_1\cos w dw \\ =& \frac{j{\rm T_B}}{4\pi}\int_{\overline{\rm C}} \frac{\sin(\phi_{\rm B}^{\rm t}-\phi_{\rm w})+\cos w}{-\cos(\phi_{\rm B}^{\rm t}-\phi_{\rm w})+\sin w}e^{-jk_1\rho(\sin w\cos\phi'+\cos w\sin\phi')}dw \\ =& \frac{j\Gamma_{\rm B}}{4\pi}\int_{\overline{\rm C}} \cot\frac{\phi_{\rm B}^{\rm t}-\phi_{\rm w}+w-\pi/2}{2}e^{-jk_1\rho\sin(w+\phi')}dw, \end{aligned} \tag{3.65}$$

where the contour $\overline{\rm C}$ can be defined similarly as in Fig. 3.4, and the position of the pole w_p depends on the transmitted angle $\phi_{\rm B}^{\rm t}$. By using saddle point technique, uniform asymptotic solution for $H_{\rm s}^{\rm tB}$ can be obtained as:

$$H_{\rm s}^{\rm tB} = H_{\rm d}^{\rm tB} + H_{\rm p}^{\rm tB} \tag{3.66}$$

$$H_{\rm p}^{\rm tB} = {\rm T_B}e^{-jk_1\rho\cos(\phi'-\phi_{\rm B}^{\rm t}+\phi_{\rm w})}U(\phi_{\rm B}^{\rm t}-\phi_{\rm w}-\phi'), \tag{3.67}$$

where $H_{\rm d}^{\rm tB}$ represents the diffracted field contributions, and can be given by:

$$H_{\rm d}^{\rm tB} = -C(k_1\rho)\left[-{\rm T_B}\cot\frac{\phi'-\phi_{\rm B}^{\rm t}+\phi_{\rm w}}{2}+{\rm T_B}S^-(\pi-\phi_{\rm B}^{\rm t}+\phi_{\rm w}+\phi')U(2\pi-\phi_{\rm w}-\phi')U(\phi')\right]. \tag{3.68}$$

By converting $\phi' = \phi - \phi_{\rm w}$, $H_{\rm p}^{\rm tB}$ and $H_{\rm d}^{\rm tB}$ can be rewritten as:

$$H_{\rm p}^{\rm tB} = {\rm T_B}e^{-jk_1\rho\cos(\phi-\phi_{\rm B}^{\rm t})}U(\phi_{\rm B}^{\rm t}-\phi), \tag{3.69}$$

$$H_{\rm d}^{\rm tB} = -C(k_1\rho)\left[-{\rm T_B}\cot\frac{\phi-\phi_{\rm B}^{\rm t}}{2}+{\rm T_B}S^-(\pi-\phi_{\rm B}^{\rm t}+\phi)U(\phi-\phi_{\rm w})\right]. \tag{3.70}$$

The contribution from $H_{\rm p}^{\rm tB}$ in Eq.(3.69) is exactly equal to the magnetic field of transmitted wave from surface OB. By combining the contributions from surfaces OA and OB

with considering the incident direction, a general unified formulation of the internal fields can be obtained as:

$$\begin{aligned} H_{\mathrm{p}}^{\mathrm{in}} =& \mathrm{T_A} e^{-jk_1\rho\cos(\phi-\phi_{\mathrm{A}}^{\mathrm{t}})} U(\phi-\phi_{\mathrm{A}}^{\mathrm{t}}) U(\pi-\phi_0) \\ &+ \mathrm{T_B} e^{-jk_1\rho\cos(\phi-\phi_{\mathrm{B}}^{\mathrm{t}})} U(\phi_{\mathrm{B}}^{\mathrm{t}}-\phi) U(\phi_0+\pi-\phi_{\mathrm{w}}), \end{aligned} \tag{3.71}$$

$$\begin{aligned} H_{\mathrm{d}}^{\mathrm{in}} =& -C(k_1\rho)\Bigg[\mathrm{T_A}\cot\frac{\phi-\phi_{\mathrm{A}}^{\mathrm{t}}}{2} U(\pi-\phi_0) - \mathrm{T_A} S^-(\pi-\phi_{\mathrm{A}}^{\mathrm{t}}+\phi) U(\phi-\phi_{\mathrm{w}}) U(\pi-\phi_0) \\ &- \mathrm{T_B}\cot\frac{\phi-\phi_{\mathrm{B}}^{\mathrm{t}}}{2} U(\phi_0+\pi-\phi_{\mathrm{w}}) + \mathrm{T_B} S^-(\pi-\phi_{\mathrm{B}}^{\mathrm{t}}+\phi) U(\phi-\phi_{\mathrm{w}}) \\ &\cdot U(\phi_0+\pi-\phi_{\mathrm{w}})\Bigg]. \end{aligned} \tag{3.72}$$

3.3 TE-Polarized Plane Wave

For TE-polarization, the incident plane wave can be given by:

$$\boldsymbol{E}^{\mathrm{i}} = e^{jkx\cos\phi_0 + jky\sin\phi_0}\hat{\boldsymbol{z}}, \tag{3.73}$$

$$\boldsymbol{H}^{\mathrm{i}} = \sqrt{\frac{\varepsilon_0}{\mu_0}} e^{jkx\cos\phi_0 + jky\sin\phi_0}(-\sin\phi_0\hat{\boldsymbol{x}} + \cos\phi_0\hat{\boldsymbol{y}}). \tag{3.74}$$

The TE-polarized incident wave also can be rewritten by using the coordinate Ox_1y_1 for surface OB illumination as:

$$\boldsymbol{E}_B^{\mathrm{i}} = e^{jkx_1\cos(\phi_w-\phi_0) - jky_1\sin(\phi_w-\phi_0)}\hat{\boldsymbol{z}}, \tag{3.75}$$

$$\boldsymbol{H}_B^{\mathrm{i}} = \sqrt{\frac{\varepsilon_0}{\mu_0}} e^{jkx_1\cos(\phi_w-\phi_0) - jky_1\sin(\phi_w-\phi_0)} \left[\sin(\phi_w-\phi_0)\hat{\boldsymbol{x_1}} + \cos(\phi_w-\phi_0)\hat{\boldsymbol{y_1}}\right]. \tag{3.76}$$

As same as the TM-polarization, the TE-polarized incident wave excites the reflected and transmitted waves outside and inside the dielectric wedge, respectively. Then, the scattering problem can be solved in each region as follows:

3.3.1 Exterior Field

Outside the wedge, the reflected field excited from surface OA can be written as:

$$\boldsymbol{E}_{\mathrm{A}}^{\mathrm{r}} = \bar{\Gamma}_{\mathrm{A}} e^{jkx\cos\phi_0 - jky\sin\phi_0}\hat{\boldsymbol{z}}, \tag{3.77}$$

$$\boldsymbol{H}_{\mathrm{A}}^{\mathrm{r}} = \bar{\Gamma}_{\mathrm{A}}\sqrt{\frac{\varepsilon_0}{\mu_0}} e^{jkx\cos\phi_0 + jky\sin\phi_0}(\sin\phi_0\hat{\boldsymbol{x}} + \cos\phi_0\hat{\boldsymbol{y}}). \tag{3.78}$$

where $\bar{\Gamma}_{\mathrm{A}}$ is the corresponding reflection coefficient on surface OA and can be written as:

$$\bar{\Gamma}_{\mathrm{A}} = \frac{\sin\phi_0 - \sqrt{\varepsilon_{\mathrm{r}} - \cos^2\phi_0}}{\sin\phi_0 + \sqrt{\varepsilon_{\mathrm{r}} - \cos^2\phi_0}}. \tag{3.79}$$

When surface OB is illuminated, the corresponding reflected wave ($\boldsymbol{E}_{\mathrm{B}}^{\mathrm{r}}$, $\boldsymbol{H}_{\mathrm{B}}^{\mathrm{r}}$) can be written in the coordinate Ox_1y_1 as:

$$\boldsymbol{E}_B^{\mathrm{r}} = \bar{\Gamma}_{\mathrm{B}} e^{jkx_1\cos(\phi_{\mathrm{w}}-\phi_0) + jky_1(\phi_{\mathrm{w}}-\sin\phi_0)}\hat{\boldsymbol{z}}, \tag{3.80}$$

$$\boldsymbol{H}_B^{\mathrm{r}} = \bar{\Gamma}_{\mathrm{B}}\sqrt{\frac{\varepsilon_0}{\mu_0}} e^{jkx_1\cos(\phi_w-\phi_0) + jky_1\sin(\phi_w-\phi_0)} \left[-\sin(\phi_w-\phi_0)\hat{\boldsymbol{x_1}} + \cos(\phi_w-\phi_0)\hat{\boldsymbol{y_1}}\right], \tag{3.81}$$

where the reflection coefficient $\bar{\Gamma}_{\mathrm{B}}$ from surface OB is defined as:

$$\bar{\Gamma}_{\mathrm{B}} = \frac{\sin(\phi_0+\pi-\phi_{\mathrm{w}}) - \sqrt{\varepsilon_{\mathrm{r}} - \cos^2(\phi_0+\pi-\phi_{\mathrm{w}})}}{\sin(\phi_0+\pi-\phi_{\mathrm{w}}) + \sqrt{\varepsilon_{\mathrm{r}} - \cos^2(\phi_0+\pi-\phi_{\mathrm{w}})}}, \tag{3.82}$$

From the formulations of the incident and reflected waves, one may obtain the corresponding equivalent electric and magnetic currents on surface OA as:

$$\boldsymbol{J}^{\mathrm{iA}} = \hat{\boldsymbol{n}}_{\mathrm{A}} \times \boldsymbol{H}^{\mathrm{i}}|_{y=0} = \sqrt{\frac{\varepsilon_0}{\mu_0}} e^{jkx\cos\phi_0} \sin\phi_0 \hat{\boldsymbol{z}} \tag{3.83}$$

$$\boldsymbol{M}^{\mathrm{iA}} = \boldsymbol{E}^{\mathrm{i}} \times \hat{\boldsymbol{n}}_{\mathrm{A}}|_{y=0} = -e^{jkx\cos\phi_0} \hat{\boldsymbol{x}} \tag{3.84}$$

$$\boldsymbol{J}^{\mathrm{rA}} = \hat{\boldsymbol{n}}_{\mathrm{A}} \times \boldsymbol{H}^{\mathrm{r}}_{\mathrm{A}}|_{y=0} = -\bar{\Gamma}_{\mathrm{A}} \sqrt{\frac{\varepsilon_0}{\mu_0}} e^{jkx\cos\phi_0} \sin\phi_0 \hat{\boldsymbol{z}} \tag{3.85}$$

$$\boldsymbol{M}^{\mathrm{rA}} = \boldsymbol{E}^{\mathrm{r}}_{\mathrm{A}} \times \hat{\boldsymbol{n}}_{\mathrm{A}}||_{y=0} = -\bar{\Gamma}_{\mathrm{A}} e^{jkx\cos\phi_0} \hat{\boldsymbol{x}}. \tag{3.86}$$

By substituting above equivalent currents into Eq.(3.3), the z-component of the scattering fields due to incident and reflected waves on surface OA can be obtained as:

$$\begin{aligned}
E_{\mathrm{s}}^{\mathrm{iA}} &= -\int_C \left[j\omega\mu_0 \boldsymbol{J}^{\mathrm{iA}} G + \boldsymbol{M}^{\mathrm{iA}} \times \nabla' G \right] dl' \\
&= \int_0^\infty e^{jkx'\cos\phi_0} \left(-jk\sin\phi_0 G + \frac{\partial G}{\partial y'} \right)_{y'=0} dx' \\
&= \int_0^\infty e^{jkx'\cos\phi_0} \left(\frac{-k\sin\phi_0}{\sqrt{k^2-\eta^2}} \pm 1 \right) \frac{1}{4\pi} \left(\int_{-\infty}^\infty e^{-j\eta(x-x')-j\sqrt{k^2-\eta^2}|y|} d\eta \right) dx' \quad (y \gtrless 0) \\
&= \int_0^\infty \int_{-\infty}^\infty e^{-j\eta(x-x')-j\sqrt{k^2-\eta^2}|y|} e^{jkx'\cos\phi_0} \left(\frac{-k\sin\phi_0}{\sqrt{k^2-\eta^2}} \pm 1 \right) \frac{1}{4\pi} d\eta dx' \quad (y \gtrless 0) \\
&= \frac{1}{4\pi} \int_{-\infty}^\infty \left(\int_0^\infty e^{jkx'\cos\phi_0 + j\eta x'} dx' \right) \left(\frac{-k\sin\phi_0}{\sqrt{k^2-\eta^2}} \pm 1 \right) e^{-j\eta x - j\sqrt{k^2-\eta^2}|y|} d\eta \quad (y \gtrless 0) \\
&= \frac{j}{4\pi} \int_{-\infty}^\infty \left(\frac{-k\sin\phi_0}{\sqrt{k^2-\eta^2}} \pm 1 \right) \frac{e^{-j\eta x - j\sqrt{k^2-\eta^2}|y|}}{(k\cos\phi_0 + \eta)} d\eta \quad (y \gtrless 0)
\end{aligned} \tag{3.87}$$

$$\begin{aligned}
E_{\mathrm{s}}^{\mathrm{rA}} &= -\int_C \left[j\omega\varepsilon_0 \boldsymbol{J}^{\mathrm{rA}}(\boldsymbol{r'}) G + \boldsymbol{M}^{\mathrm{rA}} \times \nabla' G \right] dl' \\
&= \int_0^\infty \bar{\Gamma}_{\mathrm{A}} e^{jkx'\cos\phi_0} \left(jk\sin\phi_0 G + \frac{\partial G}{\partial y'} \right)_{y'=0} dx' \\
&= \int_0^\infty \bar{\Gamma}_{\mathrm{A}} e^{jkx'\cos\phi_0} \left(\frac{k\sin\phi_0}{\sqrt{k^2-\eta^2}} \pm 1 \right) \frac{1}{4\pi} \left(\int_{-\infty}^\infty e^{-j\eta(x-x')-j\sqrt{k^2-\eta^2}|y|} d\eta \right) dx' \quad (y \gtrless 0) \\
&= \int_0^\infty \int_{-\infty}^\infty \bar{\Gamma}_{\mathrm{A}} e^{-j\eta(x-x')-j\sqrt{k^2-\eta^2}|y|} e^{jkx'\cos\phi_0} \left(\frac{k\sin\phi_0}{\sqrt{k^2-\eta^2}} \pm 1 \right) \frac{1}{4\pi} d\eta dx' \quad (y \gtrless 0) \\
&= \frac{\bar{\Gamma}_{\mathrm{A}}}{4\pi} \int_{-\infty}^\infty \left(\int_0^\infty e^{jkx'\cos\phi_0 + j\eta x'} dx' \right) \left(\frac{k\sin\phi_0}{\sqrt{k^2-\eta^2}} \pm 1 \right) e^{-j\eta x - j\sqrt{k^2-\eta^2}|y|} d\eta \quad (y \gtrless 0) \\
&= \frac{j\bar{\Gamma}_{\mathrm{A}}}{4\pi} \int_{-\infty}^\infty \left(\frac{k\sin\phi_0}{\sqrt{k^2-\eta^2}} \pm 1 \right) \frac{e^{-j\eta x - j\sqrt{k^2-\eta^2}|y|}}{(k\cos\phi_0 + \eta)} d\eta \quad (y \gtrless 0)
\end{aligned} \tag{3.88}$$

Convert to complex plane of angle w using the transformation $\eta = k\sin w$, with the cylindrical coordinate $(\rho,\ \phi)$, Eqs.(3.87) and (3.88) can be rewritten as:

$$\begin{aligned}
E_{\mathrm{s}}^{\mathrm{iA}} =& \frac{j}{4\pi}\int_{\overline{\mathrm{C}}} \frac{k(-\sin\phi_0 \pm \cos w)}{k\cos w} \frac{e^{-jk\rho\sin w\cos\phi \mp jk\rho\cos w\sin\phi}}{k(\cos\phi_0+\sin w)} k\cos w dw \quad (\phi \lessgtr \pi) \\
=& \frac{j}{4\pi}\int_{\overline{\mathrm{C}}} \frac{-\sin\phi_0 \pm \cos w}{\cos\phi_0+\sin w} e^{-jk\rho(\sin w\cos\phi \pm \cos w\sin\phi)} dw \quad (\phi \lessgtr \pi) \\
=& \frac{\pm j}{4\pi}\int_{\overline{\mathrm{C}}} \cot\frac{\pi/2+w\pm\phi_0}{2} e^{-jk\rho\sin(w\pm\phi)} dw, \quad (\phi \lessgtr \pi) \qquad (3.89)
\end{aligned}$$

$$\begin{aligned}
E_{\mathrm{s}}^{\mathrm{rA}} =& \frac{j\bar{\Gamma}_{\mathrm{A}}}{4\pi}\int_{\overline{\mathrm{C}}} \frac{k(\sin\phi_0 \pm \cos w)}{k\cos w} \frac{e^{-jk\rho\sin w\cos\phi \mp jk\rho\cos w\sin\phi}}{k(\cos\phi_0+\sin w)} k\cos w dw \quad (\phi \lessgtr \pi) \\
=& \frac{j\bar{\Gamma}_{\mathrm{A}}}{4\pi}\int_{\overline{\mathrm{C}}} \frac{\sin\phi_0 \pm \cos w}{\cos\phi_0+\sin w} e^{-jk\rho(\sin w\cos\phi \pm \cos w\sin\phi)} dw \quad (\phi \lessgtr \pi) \\
=& \frac{\pm j\bar{\Gamma}_{\mathrm{A}}}{4\pi}\int_{\overline{\mathrm{C}}} \cot\frac{\pi/2+w\mp\phi_0}{2} e^{-jk\rho\sin(w\pm\phi)} dw, \quad (\phi \lessgtr \pi) \qquad (3.90)
\end{aligned}$$

where the contour $\overline{\mathrm{C}}$ can be defined as in Fig. 3.4. By using saddle point technique, uniform asymptotic solutions for $E_{\mathrm{s}}^{\mathrm{iA}}$ and $E_{\mathrm{s}}^{\mathrm{rA}}$ can be obtained as:

$$E_{\mathrm{s}}^{\mathrm{iA}} = E_{\mathrm{d}}^{\mathrm{iA}} + E_{\mathrm{p}}^{\mathrm{iA}} \qquad (3.91)$$

$$E_{\mathrm{p}}^{\mathrm{iA}} = -\, e^{jk\rho\cos(\phi-\phi_0)} U(\phi-\pi-\phi_0) \qquad (3.92)$$

$$E_{\mathrm{s}}^{\mathrm{rA}} = E_{\mathrm{d}}^{\mathrm{rA}} + E_{\mathrm{p}}^{\mathrm{rA}} \qquad (3.93)$$

$$E_{\mathrm{p}}^{\mathrm{rA}} = \bar{\Gamma}_{\mathrm{A}} e^{jk\rho\cos(\phi+\phi_0)} U(\pi-\phi_0-\phi), \qquad (3.94)$$

where $E_{\mathrm{d}}^{\mathrm{iA}}$ and $E_{\mathrm{d}}^{\mathrm{rA}}$ present the diffracted field contributions and can be given by:

$$E_{\mathrm{d}}^{\mathrm{iA}} = -\, C(k\rho)\left[\cot\frac{\pi-(\phi-\phi_0)}{2} + S^{-}(\phi-\phi_0)U(\phi-\pi)\right] \qquad (3.95)$$

$$E_{\mathrm{d}}^{\mathrm{rA}} = -\, C(k\rho)\left[\bar{\Gamma}_{\mathrm{A}}\cot\frac{\pi-(\phi+\phi_0)}{2} + \bar{\Gamma}_{\mathrm{A}} S^{-}(\phi+\phi_0)U(\pi-\phi)\right] \qquad (3.96)$$

Similarly, one can obtain the electric and magnetic currents due to the incident and reflected waves on surface OB as:

$$\boldsymbol{J}^{\mathrm{iB}} = \hat{\boldsymbol{n}}_{\mathrm{B}} \times \boldsymbol{H}_{\mathrm{B}}^{\mathrm{i}}|_{y_1=0} = \sqrt{\frac{\varepsilon_0}{\mu_0}} e^{jkx_1\cos(\phi_w-\phi_0)} \sin(\phi_w-\phi_0)\hat{\boldsymbol{z}}, \qquad (3.97)$$

$$\boldsymbol{M}^{\mathrm{iB}} = \boldsymbol{E}^{\mathrm{i}} \times \hat{\boldsymbol{n}}_{\mathrm{B}}|_{y_1=0} = e^{jkx_1\cos(\phi_w-\phi_0)} \hat{\boldsymbol{x}}_{\boldsymbol{1}}, \qquad (3.98)$$

$$\boldsymbol{J}^{\mathrm{rB}} = \hat{\boldsymbol{n}}_{\mathrm{B}} \times \boldsymbol{H}_{\mathrm{B}}^{\mathrm{r}}|_{y_1=0} = -\bar{\Gamma}_{\mathrm{B}}\sqrt{\frac{\varepsilon_0}{\mu_0}} e^{jkx_1\cos(\phi_w-\phi_0)} \sin(\phi_w-\phi_0)\hat{\boldsymbol{z}}, \qquad (3.99)$$

$$\boldsymbol{M}^{\mathrm{rB}} = \boldsymbol{E}_{\mathrm{B}}^{\mathrm{r}} \times \hat{\boldsymbol{n}}_{\mathrm{B}}||_{y_1=0} = \bar{\Gamma}_{\mathrm{B}} e^{jkx_1\cos(\phi_w-\phi_0)} \hat{\boldsymbol{x}}_{\boldsymbol{1}}. \qquad (3.100)$$

Then, the z-component of the scattering fields due to incident and reflected waves on surface OB can also be obtained as:

$$
\begin{aligned}
E_{\mathrm{s}}^{\mathrm{iB}} =& -\int_C \left[j\omega\mu_0 \boldsymbol{J}^{\mathrm{iB}} G + \boldsymbol{M}^{\mathrm{iB}} \times \nabla' G \right] dl' \\
=& \int_0^{\infty} e^{jkx_1' \cos(\phi_{\mathrm{w}} - \phi_0)} \left(-jk \sin(\phi_{\mathrm{w}} - \phi_0) G - \frac{\partial G}{\partial y_1'} \right)_{y_1'=0} dx_1' \\
=& \int_0^{\infty} e^{jkx_1' \cos(\phi_{\mathrm{w}} - \phi_0)} \left(\frac{-k \sin(\phi_{\mathrm{w}} - \phi_0)}{\sqrt{k^2 - \eta^2}} \mp 1 \right) \frac{1}{4\pi} \left(\int_{-\infty}^{\infty} e^{-j\eta(x_1 - x_1') - j\sqrt{k^2-\eta^2}|y_1|} d\eta \right) dx_1' \quad (y_1 \gtrless 0) \\
=& \int_0^{\infty} \int_{-\infty}^{\infty} e^{-j\eta(x_1 - x_1') - j\sqrt{k^2-\eta^2}|y_1|} e^{jkx_1' \cos(\phi_{\mathrm{w}} - \phi_0)} \left(\frac{-k \sin(\phi_{\mathrm{w}} - \phi_0)}{\sqrt{k^2 - \eta^2}} \mp 1 \right) \frac{1}{4\pi} d\eta dx_1' \quad (y_1 \gtrless 0) \\
=& \frac{1}{4\pi} \int_{-\infty}^{\infty} \left(\int_0^{\infty} e^{jkx_1' \cos(\phi_{\mathrm{w}} - \phi_0) + j\eta x_1'} dx_1' \right) \left(\frac{-k \sin(\phi_{\mathrm{w}} - \phi_0)}{\sqrt{k^2 - \eta^2}} \mp 1 \right) e^{-j\eta x_1 - j\sqrt{k^2-\eta^2}|y_1|} d\eta \quad (y_1 \gtrless 0) \\
=& \frac{j}{4\pi} \int_{-\infty}^{\infty} \left(\frac{-k \sin(\phi_{\mathrm{w}} - \phi_0)}{\sqrt{k^2 - \eta^2}} \mp 1 \right) \frac{e^{-j\eta x_1 - j\sqrt{k^2-\eta^2}|y_1|}}{k \cos(\phi_{\mathrm{w}} - \phi_0) + \eta} d\eta, \quad (y_1 \gtrless 0)
\end{aligned} \tag{3.101}
$$

$$
\begin{aligned}
E_{\mathrm{s}}^{\mathrm{rB}} =& -\int_C \left[j\omega\varepsilon_0 \boldsymbol{J}^{\mathrm{rB}} G + \boldsymbol{M}^{\mathrm{rB}} \times \nabla' G \right] dl' \\
=& \int_0^{\infty} \bar{\Gamma}_{\mathrm{B}} e^{jkx_1' \cos(\phi_{\mathrm{w}} - \phi_0)} \left(jk \sin(\phi_{\mathrm{w}} - \phi_0) G - \frac{\partial G}{\partial y_1'} \right)_{y_1'=0} dx_1' \\
=& \int_0^{\infty} \bar{\Gamma}_{\mathrm{B}} e^{jkx_1' \cos(\phi_{\mathrm{w}} - \phi_0)} \left(\frac{k \sin(\phi_{\mathrm{w}} - \phi_0)}{\sqrt{k^2 - \eta^2}} \mp 1 \right) \frac{1}{4\pi} \left(\int_{-\infty}^{\infty} e^{-j\eta(x_1 - x_1') - j\sqrt{k^2-\eta^2}|y_1|} d\eta \right) dx_1' \quad (y_1 \gtrless 0) \\
=& \int_0^{\infty} \int_{-\infty}^{\infty} \bar{\Gamma}_{\mathrm{B}} e^{-j\eta(x_1 - x_1') - j\sqrt{k^2-\eta^2}|y_1|} e^{jkx_1' \cos(\phi_{\mathrm{w}} - \phi_0)} \left(\frac{k \sin(\phi_{\mathrm{w}} - \phi_0)}{\sqrt{k^2 - \eta^2}} \mp 1 \right) \frac{1}{4\pi} d\eta dx_1' \quad (y_1 \gtrless 0) \\
=& \frac{\bar{\Gamma}_{\mathrm{B}}}{4\pi} \int_{-\infty}^{\infty} \left(\int_0^{\infty} e^{jkx_1' \cos(\phi_{\mathrm{w}} - \phi_0) + j\eta x_1'} dx_1' \right) \left(\frac{k \sin(\phi_{\mathrm{w}} - \phi_0)}{\sqrt{k^2 - \eta^2}} \mp 1 \right) e^{-j\eta x_1 - j\sqrt{k^2-\eta^2}|y_1|} d\eta \quad (y_1 \gtrless 0) \\
=& \frac{j\bar{\Gamma}_{\mathrm{B}}}{4\pi} \int_{-\infty}^{\infty} \left(\frac{k \sin(\phi_{\mathrm{w}} - \phi_0)}{\sqrt{k^2 - \eta^2}} \mp 1 \right) \frac{e^{-j\eta x_1 - j\sqrt{k^2-\eta^2}|y_1|}}{k \cos(\phi_{\mathrm{w}} - \phi_0) + \eta} d\eta. \quad (y_1 \gtrless 0)
\end{aligned} \tag{3.102}
$$

Convert to complex plane of angle w using the transformation $\eta = k \sin w$, with the cylindrical coordinate (ρ, ϕ'), Eqs.(3.101) and (3.102) can be rewritten as:

$$
\begin{aligned}
E_{\mathrm{s}}^{\mathrm{iB}} =& \frac{j}{4\pi} \int_{\overline{\mathrm{C}}} \frac{k(-\sin(\phi_{\mathrm{w}} - \phi_0) \mp \cos w)}{k \cos w} \frac{e^{-jk\rho \sin w \cos \phi' \mp jk\rho \cos w \sin \phi'}}{k(\cos(\phi_{\mathrm{w}} - \phi_0) + \sin w)} k \cos w dw \quad (\phi' \lesseqgtr \pi) \\
=& \frac{j}{4\pi} \int_{\overline{\mathrm{C}}} \frac{-\sin(\phi_{\mathrm{w}} - \phi_0) \mp \cos w}{\cos(\phi_{\mathrm{w}} - \phi_0) + \sin w} e^{-jk\rho(\sin w \cos \phi' \pm \cos w \sin \phi')} dw \quad (\phi' \lesseqgtr \pi) \\
=& \frac{\mp j}{4\pi} \int_{\overline{\mathrm{C}}} \cot \frac{\pi/2 + w \mp (\phi_{\mathrm{w}} - \phi_0)}{2} e^{-jk\rho \sin(w \pm \phi')} dw, \quad (\phi' \lesseqgtr \pi)
\end{aligned} \tag{3.103}
$$

$$
\begin{aligned}
E_{\mathrm{s}}^{\mathrm{rB}} =& \frac{j\bar{\Gamma}_{\mathrm{B}}}{4\pi} \int_{\overline{\mathrm{C}}} \frac{k(\sin(\phi_{\mathrm{w}} - \phi_0) \mp \cos w)}{k \cos w} \frac{e^{-jk\rho \sin w \cos \phi' \mp jk\rho \cos w \sin \phi'}}{k(\cos(\phi_{\mathrm{w}} - \phi_0) + \sin w)} k \cos w dw \quad (\phi' \lesseqgtr \pi) \\
=& \frac{j\bar{\Gamma}_{\mathrm{B}}}{4\pi} \int_{\overline{\mathrm{C}}} \frac{\sin(\phi_{\mathrm{w}} - \phi_0) \mp \cos w}{\cos(\phi_{\mathrm{w}} - \phi_0) + \sin w} e^{-jk\rho(\sin w \cos \phi' \pm \cos w \sin \phi')} dw \quad (\phi' \lesseqgtr \pi) \\
=& \frac{\mp j\bar{\Gamma}_{\mathrm{B}}}{4\pi} \int_{\overline{\mathrm{C}}} \cot \frac{\pi/2 + w \pm (\phi_{\mathrm{w}} - \phi_0)}{2} e^{-jk\rho \sin(w \pm \phi')} dw, \quad (\phi' \lesseqgtr \pi)
\end{aligned} \tag{3.104}
$$

where the contour $\overline{\mathrm{C}}$ can be defined similarly as in Fig. 3.4. By using saddle point technique, uniform asymptotic solutions for $E_{\mathrm{s}}^{\mathrm{iB}}$ and $E_{\mathrm{s}}^{\mathrm{rB}}$ can be obtained as:

$$\begin{aligned}
E_{\mathrm{s}}^{\mathrm{iB}} =& E_{\mathrm{d}}^{\mathrm{iB}} + E_{\mathrm{p}}^{\mathrm{iB}} && (3.105)\\
E_{\mathrm{p}}^{\mathrm{iB}} =& - e^{jk\rho\cos(\phi'+\phi_{\mathrm{w}}-\phi_0)}U(\pi-\phi_{\mathrm{w}}+\phi_0-\phi')\\
=& - e^{jk\rho\cos(\phi-\phi_0)}U\phi_0-\pi-\phi), && (3.106)\\
E_{\mathrm{s}}^{\mathrm{rB}} =& E_{\mathrm{d}}^{\mathrm{rB}} + E_{\mathrm{p}}^{\mathrm{rB}} && (3.107)\\
E_{\mathrm{p}}^{\mathrm{rB}} =& \bar{\Gamma}_{\mathrm{B}} e^{jk\rho\cos(\phi'-\phi_{\mathrm{w}}+\phi_0)}U(\phi'-\pi-\phi_{\mathrm{w}}+\phi_0)\\
=& \bar{\Gamma}_{\mathrm{B}} e^{jk\rho\cos(\phi+\phi_0-2\phi_{\mathrm{w}})}U(\phi+\phi_0+\pi-2\phi_{\mathrm{w}}). && (3.108)
\end{aligned}$$

The diffracted fields $E_{\mathrm{d}}^{\mathrm{iB}}$ and $E_{\mathrm{d}}^{\mathrm{rB}}$ can be written as:

$$\begin{aligned}
E_{\mathrm{d}}^{\mathrm{iB}} =& - C(k\rho)\Bigg[- \cot\frac{\pi-(\phi'+\phi_{\mathrm{w}}-\phi_0)}{2} - S^{-}(\phi'+\phi_{\mathrm{w}}-\phi_0)U(\pi-\phi')\Bigg]\\
=& - C(k\rho)\Bigg[\cot\frac{\pi+(\phi-\phi_0)}{2} + S^{+}(\phi-\phi_0)U(\phi_{\mathrm{w}}-\pi-\phi)\Bigg] && (3.109)\\
E_{\mathrm{d}}^{\mathrm{rB}} =& - C(k\rho)\Bigg[- \bar{\Gamma}_{\mathrm{B}}\cot\frac{\pi-(\phi'-\phi_{\mathrm{w}}+\phi_0)}{2} - \bar{\Gamma}_{\mathrm{B}} S^{-}(\phi'-\phi_{\mathrm{w}}+\phi_0)U(\phi'-\pi)\Bigg]\\
=& - C(k\rho)\Bigg[\bar{\Gamma}_{\mathrm{B}}\cot\frac{\pi+(\phi_0+\phi-2\phi_{\mathrm{w}})}{2} + \bar{\Gamma}_{\mathrm{B}} S^{+}(\phi_0+\phi-2\phi_{\mathrm{w}})U(\pi+\phi-\phi_{\mathrm{w}})\Bigg]. && (3.110)
\end{aligned}$$

By considering the incident direction, one has the unified formulation of diffracted field outside the wedge as:

$$\begin{aligned}
E_{\mathrm{d}}^{\mathrm{Out}} = -C(k\rho)\Bigg[& \cot\frac{\pi-(\phi-\phi_0)}{2}U(\phi_{\mathrm{w}}-\pi-\phi_0) + S^{-}(\phi-\phi_0)U(\phi-\pi)U(\phi_{\mathrm{w}}-\pi-\phi_0)\\
& + \cot\frac{\pi+(\phi-\phi_0)}{2}U(\phi_0-\pi) + S^{+}(\phi-\phi_0)U(\phi_{\mathrm{w}}-\pi-\phi)U(\phi_0-\pi)\\
& + \bar{\Gamma}_{\mathrm{A}}\cot\frac{\pi-(\phi+\phi_0)}{2}U(\pi-\phi_0) + \bar{\Gamma}_{\mathrm{A}} S^{-}(\phi+\phi_0)U(\pi-\phi)U(\pi-\phi_0)\\
& + \bar{\Gamma}_{\mathrm{B}}\cot\frac{\pi+(\phi_0+\phi-2\phi_{\mathrm{w}})}{2}U(\pi+\phi_0-\phi_{\mathrm{w}}) + \bar{\Gamma}_{\mathrm{B}} S^{+}(\phi_0+\phi-2\phi_{\mathrm{w}})\\
& \cdot U(\pi+\phi-\phi_{\mathrm{w}})U(\pi+\phi_0-\phi_{\mathrm{w}})\Bigg]. \qquad (3.111)
\end{aligned}$$

Similarly, one can also obtain unified formulation for GO contribution as:

$$\begin{aligned}
E_{\mathrm{p}}^{\mathrm{Out}} =& - e^{jk\rho\cos(\phi-\phi_0)}U(\phi-\pi-\phi_0)U(\phi_{\mathrm{w}}-\pi-\phi_0)\\
& - e^{jk\rho\cos(\phi-\phi_0)}U\phi_0-\pi-\phi)U(\phi_0-\pi)\\
& + \bar{\Gamma}_{\mathrm{A}} e^{jk\rho\cos(\phi+\phi_0)}U(\pi-\phi_0-\phi)U(\pi-\phi_0)\\
& + \bar{\Gamma}_{\mathrm{B}} e^{jk\rho\cos(\phi+\phi_0-2\phi_{\mathrm{w}})}U(\phi+\phi_0+\pi-2\phi_{\mathrm{w}})U(\phi_0+\pi-\phi_{\mathrm{w}}). \qquad (3.112)
\end{aligned}$$

3.3.2 Interior Field

Inside the dielectric wedge, the transmitted wave ($\boldsymbol{E}_{\mathrm{A}}^{\mathrm{t}}$, $\boldsymbol{H}_{\mathrm{A}}^{\mathrm{t}}$) excited by TE-polarized incident wave from surface OA can be written as:

$$\boldsymbol{E}_{\mathrm{A}}^{\mathrm{t}} = \bar{\mathrm{T}}_{\mathrm{A}} e^{-jk_1 x\cos\phi_{\mathrm{A}}^{\mathrm{t}} - jk_1 y\sin\phi_{\mathrm{A}}^{\mathrm{t}}}\hat{\boldsymbol{z}}, \tag{3.113}$$

$$\boldsymbol{H}_{\mathrm{A}}^{\mathrm{t}} = \bar{\mathrm{T}}_{\mathrm{A}}\sqrt{\frac{\varepsilon_{\mathrm{r}}\varepsilon_0}{\mu_0}} e^{-jk_1 x\cos\phi_{\mathrm{A}}^{\mathrm{t}} - jk_1 y\sin\phi_{\mathrm{A}}^{\mathrm{t}}}(\sin\phi_{\mathrm{A}}^{\mathrm{t}}\hat{\boldsymbol{x}} - \cos\phi_{\mathrm{A}}^{\mathrm{t}}\hat{\boldsymbol{y}}), \tag{3.114}$$

where the transmission coefficient $\bar{\mathrm{T}}_{\mathrm{A}}$ is given by:

$$\bar{\mathrm{T}}_{\mathrm{A}} = 1 + \bar{\Gamma}_{\mathrm{A}} = \frac{2\sin\phi_0}{\sin\phi_0 + \sqrt{\varepsilon_{\mathrm{r}} - \cos^2\phi_0}}. \tag{3.115}$$

Then the corresponding magnetic and electric currents due to transmitted wave ($\boldsymbol{E}_{\mathrm{A}}^{\mathrm{t}}$, $\boldsymbol{H}_{\mathrm{A}}^{\mathrm{t}}$) can be obtained as:

$$\boldsymbol{J}^{\mathrm{tA}} = (-\hat{\boldsymbol{n}}_{\mathrm{A}}) \times \boldsymbol{H}_{\mathrm{A}}^{\mathrm{t}}|_{y=0} = \bar{\mathrm{T}}_{\mathrm{A}}\sqrt{\frac{\varepsilon_{\mathrm{r}}\varepsilon_0}{\mu_0}} e^{-jk_1 x\cos\phi_{\mathrm{A}}^{\mathrm{t}}}\sin\phi_{\mathrm{A}}^{\mathrm{t}}\hat{\boldsymbol{z}}, \tag{3.116}$$

$$\boldsymbol{M}^{\mathrm{tA}} = \boldsymbol{E}_{\mathrm{A}}^{\mathrm{t}} \times (-\hat{\boldsymbol{n}}_{\mathrm{A}})||_{y=0} = \bar{\mathrm{T}}_{\mathrm{A}} e^{-jk_1 x\cos\phi_{\mathrm{A}}^{\mathrm{t}}}\hat{\boldsymbol{x}}. \tag{3.117}$$

Then, the scattering electric field excited by the transmitted wave ($\boldsymbol{H}_{\mathrm{A}}^{\mathrm{t}}$, $\boldsymbol{E}_{\mathrm{A}}^{\mathrm{t}}$)) can be represented as:

$$\begin{aligned}
E_{\mathrm{s}}^{\mathrm{tA}} &= -\int_C \left[j\omega\mu_0 \boldsymbol{J}^{\mathrm{tA}} G + \boldsymbol{M}^{\mathrm{tA}} \times \nabla' G\right] dl' \\
&= \int_0^\infty -\bar{\mathrm{T}}_{\mathrm{A}} e^{-jk_1 x'\cos\phi_{\mathrm{A}}^{\mathrm{t}}} \left(jk_1\sin\phi_{\mathrm{A}}^{\mathrm{t}} G + \frac{\partial G}{\partial y'}\right)_{y'=0} dx' \\
&= \int_0^\infty -\bar{\mathrm{T}}_{\mathrm{A}} e^{-jk_1 x'\cos\phi_{\mathrm{A}}^{\mathrm{t}}} \left(\frac{k_1\sin\phi_{\mathrm{A}}^{\mathrm{t}}}{\sqrt{k_1^2 - \eta^2}} - 1\right) \frac{1}{4\pi} \left(\int_{-\infty}^\infty e^{-j\eta(x-x') - j\sqrt{k_1^2-\eta^2}|y|} d\eta\right) dx' \\
&= \int_0^\infty \int_{-\infty}^\infty -\bar{\mathrm{T}}_{\mathrm{A}} e^{-j\eta(x-x') - j\sqrt{k_1^2-\eta^2}|y|} e^{-jk_1 x'\cos\phi_{\mathrm{A}}^{\mathrm{t}}} \left(\frac{k_1\sin\phi_{\mathrm{A}}^{\mathrm{t}}}{\sqrt{k_1^2 - \eta^2}} - 1\right) \frac{1}{4\pi} d\eta dx' \\
&= \frac{-\bar{\mathrm{T}}_{\mathrm{A}}}{4\pi} \int_{-\infty}^\infty \left(\int_0^\infty e^{-jk_1 x'\cos\phi_{\mathrm{A}}^{\mathrm{t}} + j\eta x'} dx'\right) \left(\frac{k_1\sin\phi_{\mathrm{A}}^{\mathrm{t}}}{\sqrt{k_1^2 - \eta^2}} - 1\right) e^{-j\eta x - j\sqrt{k_1^2-\eta^2}|y|} d\eta \\
&= \frac{-j\bar{\mathrm{T}}_{\mathrm{A}}}{4\pi} \int_{-\infty}^\infty \left(\frac{k_1\sin\phi_{\mathrm{A}}^{\mathrm{t}}}{\sqrt{k_1^2 - \eta^2}} - 1\right) \frac{e^{-j\eta x - j\sqrt{k_1^2-\eta^2}|y|}}{-k_1\cos\phi_{\mathrm{A}}^{\mathrm{t}} + \eta} d\eta.
\end{aligned} \tag{3.118}$$

Convert to complex plane of angle w using the transformation $\eta = k_1\sin w$, with the cylindrical coordinate (ρ, ϕ), Eq.(3.118) can be rewritten as:

$$\begin{aligned}
E_{\mathrm{s}}^{\mathrm{tA}} &= \frac{-j\bar{\mathrm{T}}_{\mathrm{A}}}{4\pi} \int_{\overline{\mathrm{C}}} \frac{k_1(\sin\phi_{\mathrm{A}}^{\mathrm{t}} - \cos w)}{k_1\cos w} \frac{e^{-jk_1\rho\sin w\cos\phi + jk_1\rho\cos w\sin\phi}}{k_1(-\cos\phi_{\mathrm{A}}^{\mathrm{t}} + \sin w)} k_1\cos w dw \\
&= \frac{-j\bar{\mathrm{T}}_{\mathrm{A}}}{4\pi} \int_{\overline{\mathrm{C}}} \frac{\sin\phi_{\mathrm{A}}^{\mathrm{t}} - \cos w}{-\cos\phi_{\mathrm{A}}^{\mathrm{t}} + \sin w} e^{-jk_1\rho(\sin w\cos\phi - \cos w\sin\phi)} dw \\
&= \frac{-j\bar{\mathrm{T}}_{\mathrm{A}}}{4\pi} \int_{\overline{\mathrm{C}}} \cot\frac{\phi_{\mathrm{A}}^{\mathrm{t}} - w + \pi/2}{2} e^{-jk_1\rho\sin(w-\phi)} dw,
\end{aligned} \tag{3.119}$$

where the contour $\overline{\mathrm{C}}$ can be defined similarly as in Fig. 3.4. By using saddle point technique, uniform asymptotic solution for $E_{\mathrm{s}}^{\mathrm{tA}}$ can be obtained as:

$$E_{\mathrm{s}}^{\mathrm{tA}} = E_{\mathrm{d}}^{\mathrm{tA}} + E_{\mathrm{p}}^{\mathrm{tA}} \tag{3.120}$$

$$E_{\mathrm{p}}^{\mathrm{tA}} = \bar{\mathrm{T}}_{\mathrm{A}} e^{-jk_1\rho\cos(\phi-\phi_{\mathrm{A}}^{\mathrm{t}})} U(\phi-\phi_{\mathrm{A}}^{\mathrm{t}}), \tag{3.121}$$

where $E_{\mathrm{d}}^{\mathrm{tA}}$ represents the diffracted field contributions, and can be given by:

$$E_{\mathrm{d}}^{\mathrm{tA}} = -C(k_1\rho)\left[\bar{\mathrm{T}}_{\mathrm{A}}\cot\frac{\phi-\phi_{\mathrm{A}}^{\mathrm{t}}}{2} - \bar{\mathrm{T}}_{\mathrm{A}} S^{-}(\pi-\phi_{\mathrm{A}}^{\mathrm{t}}+\phi)U(\phi-\phi_{\mathrm{w}})\right]. \tag{3.122}$$

The contribution from $E_{\mathrm{p}}^{\mathrm{tA}}$ is exactly equal to the magnetic field of transmitted wave from surface OA. When surface OB is illuminated, one may also have transmitted wave ($\boldsymbol{E}_{\mathrm{B}}^{\mathrm{t}}$, $\boldsymbol{H}_{\mathrm{B}}^{\mathrm{t}}$) from surface OB, which can be written in coordinate system Ox_1y_1 as:

$$\boldsymbol{E}_{\mathrm{B}}^{\mathrm{t}} = \bar{\mathrm{T}}_{\mathrm{B}} e^{-jk_1x_1\cos(\phi_{\mathrm{B}}^{\mathrm{t}}-\phi_{\mathrm{w}})-jk_1y_1\sin\phi_{\mathrm{A}}^{\mathrm{t}}}\hat{\boldsymbol{z}}, \tag{3.123}$$

$$\boldsymbol{H}_{\mathrm{B}}^{\mathrm{t}} = \bar{\mathrm{T}}_{\mathrm{B}}\sqrt{\frac{\varepsilon_{\mathrm{r}}\varepsilon_0}{\mu_0}} e^{-jk_1x_1\cos(\phi_{\mathrm{B}}^{\mathrm{t}}-\phi_{\mathrm{w}})-jk_1y_1\sin(\phi_{\mathrm{B}}^{\mathrm{t}}-\phi_{\mathrm{w}})}[\sin(\phi_{\mathrm{B}}^{\mathrm{t}}-\phi_{\mathrm{w}})\hat{\boldsymbol{x}}_{\mathbf{1}} - \cos(\phi_{\mathrm{B}}^{\mathrm{t}}-\phi_{\mathrm{w}})\hat{\boldsymbol{y}}_{\mathbf{1}}], \tag{3.124}$$

where the transmission coefficient $\bar{\mathrm{T}}_{\mathrm{B}}$ is defined as:

$$\bar{\mathrm{T}}_{\mathrm{B}} = 1 + \bar{\Gamma}_{\mathrm{B}} = \frac{2\sin(\pi+\phi_0-\phi_{\mathrm{w}})}{\sin(\pi+\phi_0-\phi_{\mathrm{w}}) + \sqrt{\varepsilon_{\mathrm{r}} - \cos^2(\pi+\phi_0-\phi_{\mathrm{w}})}}. \tag{3.125}$$

Then, the corresponding equivalent currents $\boldsymbol{J}^{\mathrm{tB}}$ and $\boldsymbol{M}^{\mathrm{tB}}$ can be derived as:

$$\boldsymbol{J}^{\mathrm{tB}} = (-\hat{\boldsymbol{n}}_{\mathrm{B}}) \times \boldsymbol{H}_{\mathrm{B}}^{\mathrm{t}}|_{y_1=0} = -\mathrm{T}_{\mathrm{B}}\sqrt{\frac{\varepsilon_{\mathrm{r}}\varepsilon_0}{\mu_0}} e^{-jk_1x_1\cos(\phi_{\mathrm{B}}^{\mathrm{t}}-\phi_{\mathrm{w}})}\sin(\phi_{\mathrm{B}}^{\mathrm{t}}-\phi_{\mathrm{w}})\hat{\boldsymbol{z}}, \tag{3.126}$$

$$\boldsymbol{M}^{\mathrm{tB}} = \boldsymbol{E}_{\mathrm{B}}^{\mathrm{t}} \times (-\hat{\boldsymbol{n}}_{\mathrm{B}})||_{y_1=0} = -\mathrm{T}_{\mathrm{B}} e^{-jk_1x_1\cos(\phi_{\mathrm{B}}^{\mathrm{t}}-\phi_{\mathrm{w}})}\hat{\boldsymbol{x}}_{\mathbf{1}}. \tag{3.127}$$

Then, one has the z-component of the scattering fields due to the transmitted wave on surface OB as:

$$\begin{aligned}
E_{\mathrm{s}}^{\mathrm{tB}} &= -\int_C \left[j\omega\varepsilon_{\mathrm{r}}\varepsilon_0 \boldsymbol{J}^{\mathrm{tB}} G + \boldsymbol{M}^{\mathrm{tB}} \times \nabla' G\right] dl' \\
&= \int_0^\infty \bar{\mathrm{T}}_{\mathrm{B}} e^{-jk_1x_1'\cos(\phi_{\mathrm{B}}^{\mathrm{t}}-\phi_{\mathrm{w}})}\left(jk_1\sin(\phi_{\mathrm{B}}^{\mathrm{t}}-\phi_{\mathrm{w}})G + \frac{\partial G}{\partial y_1'}\right)_{y_1'=0} dx_1' \\
&= \int_0^\infty \bar{\mathrm{T}}_{\mathrm{B}} e^{-jk_1x_1'\cos(\phi_{\mathrm{B}}^{\mathrm{t}}-\phi_{\mathrm{w}})}\left(\frac{k_1\sin(\phi_{\mathrm{B}}^{\mathrm{t}}-\phi_{\mathrm{w}})}{\sqrt{k_1^2-\eta^2}}+1\right)\frac{1}{4\pi}\left(\int_{-\infty}^\infty e^{-j\eta(x_1-x_1')-j\sqrt{k_1^2-\eta^2}|y_1|}d\eta\right)dx_1' \\
&= \int_0^\infty\int_{-\infty}^\infty \bar{\mathrm{T}}_{\mathrm{B}} e^{-j\eta(x_1-x_1')-j\sqrt{k_1^2-\eta^2}y_1} e^{-jk_1x_1'\cos(\phi_{\mathrm{B}}^{\mathrm{t}}-\phi_{\mathrm{w}})}\left(\frac{k_1\sin(\phi_{\mathrm{B}}^{\mathrm{t}}-\phi_{\mathrm{w}})}{\sqrt{k_1^2-\eta^2}}+1\right)\frac{1}{4\pi}d\eta dx_1' \\
&= \frac{\bar{\mathrm{T}}_{\mathrm{B}}}{4\pi}\int_{-\infty}^\infty\left(\int_0^\infty e^{-jk_1x_1'\cos(\phi_{\mathrm{B}}^{\mathrm{t}}-\phi_{\mathrm{w}})+j\eta x_1'}dx_1'\right)\left(\frac{k_1\sin(\phi_{\mathrm{B}}^{\mathrm{t}}-\phi_{\mathrm{w}})}{\sqrt{k_1^2-\eta^2}}+1\right)e^{-j\eta x_1-j\sqrt{k_1^2-\eta^2}y_1}d\eta \\
&= \frac{j\bar{\mathrm{T}}_{\mathrm{B}}}{4\pi}\int_{-\infty}^\infty\left(\frac{k_1\sin(\phi_{\mathrm{B}}^{\mathrm{t}}-\phi_{\mathrm{w}})}{\sqrt{k_1^2-\eta^2}}+1\right)\frac{e^{-j\eta x_1-j\sqrt{k_1^2-\eta^2}y_1}}{-k_1\cos(\phi_{\mathrm{B}}^{\mathrm{t}}-\phi_{\mathrm{w}})+\eta}d\eta.
\end{aligned} \tag{3.128}$$

Convert to complex plane of angle w using the transformation $\eta = k_1 \sin w$, with the cylindrical coordinate (ρ, ϕ'), Eq.(3.128) can be rewritten as:

$$\begin{aligned} E_{\mathrm{s}}^{\mathrm{tB}} =& \frac{j\bar{\mathrm{T}}_{\mathrm{B}}}{4\pi}\int_{\overline{\mathrm{C}}} \frac{k_1(\sin(\phi_{\mathrm{B}}^{\mathrm{t}}-\phi_{\mathrm{w}})+\cos w)}{k_1\cos w}\frac{e^{-jk_1\rho\sin w\cos\phi' - jk_1\rho\cos w\sin\phi'}}{k_1(-\cos(\phi_{\mathrm{B}}^{\mathrm{t}}-\phi_{\mathrm{w}})+\sin w)}k_1\cos w dw \\ =& \frac{j\bar{\mathrm{T}}_{\mathrm{B}}}{4\pi}\int_{\overline{\mathrm{C}}} \frac{\sin(\phi_{\mathrm{B}}^{\mathrm{t}}-\phi_{\mathrm{w}})+\cos w}{-\cos(\phi_{\mathrm{B}}^{\mathrm{t}}-\phi_{\mathrm{w}})+\sin w}e^{-jk_1\rho(\sin w\cos\phi'+\cos w\sin\phi')}dw \\ =& \frac{j\bar{\mathrm{T}}_{\mathrm{B}}}{4\pi}\int_{\overline{\mathrm{C}}} \cot\frac{\phi_{\mathrm{B}}^{\mathrm{t}}-\phi_{\mathrm{w}}+w-\pi/2}{2}e^{-jk_1\rho\sin(w+\phi')}dw, \end{aligned} \tag{3.129}$$

where the contour $\overline{\mathrm{C}}$ can be defined similarly as in Fig. 3.4. By using saddle point technique, uniform asymptotic solution for $E_{\mathrm{s}}^{\mathrm{tB}}$ can be obtained as:

$$E_{\mathrm{s}}^{\mathrm{tB}} = E_{\mathrm{d}}^{\mathrm{tB}} + E_{\mathrm{p}}^{\mathrm{tB}} \tag{3.130}$$

$$E_{\mathrm{p}}^{\mathrm{tB}} = \bar{\mathrm{T}}_{\mathrm{B}} e^{-jk_1\rho\cos(\phi'-\phi_{\mathrm{B}}^{\mathrm{t}}+\phi_{\mathrm{w}})}U(\phi_{\mathrm{B}}^{\mathrm{t}}-\phi_{\mathrm{w}}-\phi'), \tag{3.131}$$

where $E_{\mathrm{d}}^{\mathrm{tB}}$ represents the diffracted field contributions, and can be given by:

$$E_{\mathrm{d}}^{\mathrm{tB}} = -C(k_1\rho)\bigg[-\bar{\mathrm{T}}_{\mathrm{B}}\cot\frac{\phi'-\phi_{\mathrm{B}}^{\mathrm{t}}+\phi_{\mathrm{w}}}{2} + \bar{\mathrm{T}}_{\mathrm{B}}S^{-}(\pi-\phi_{\mathrm{B}}^{\mathrm{t}}+\phi_{\mathrm{w}}+\phi')U(2\pi-\phi_{\mathrm{w}}-\phi')U(\phi')\bigg]. \tag{3.132}$$

By converting $\phi' = \phi - \phi_{\mathrm{w}}$, $E_{\mathrm{p}}^{\mathrm{tB}}$ and $E_{\mathrm{d}}^{\mathrm{tB}}$ can be rewritten as:

$$E_{\mathrm{p}}^{\mathrm{tB}} = \bar{\mathrm{T}}_{\mathrm{B}} e^{-jk_1\rho\cos(\phi-\phi_{\mathrm{B}}^{\mathrm{t}})}U(\phi_{\mathrm{B}}^{\mathrm{t}}-\phi), \tag{3.133}$$

$$E_{\mathrm{d}}^{\mathrm{tB}} = -C(k_1\rho)\bigg[-\bar{\mathrm{T}}_{\mathrm{B}}\cot\frac{\phi-\phi_{\mathrm{B}}^{\mathrm{t}}}{2} + \mathrm{T}_{\mathrm{B}}S^{-}(\pi-\phi_{\mathrm{B}}^{\mathrm{t}}+\phi)U(\phi-\phi_{\mathrm{w}})\bigg]. \tag{3.134}$$

The contribution from $E_{\mathrm{p}}^{\mathrm{tB}}$ in Eq.(3.133) is exactly equal to the magnetic field of transmitted wave from surface OB. By combining the contributions from surfaces OA and OB with considering the incident direction, a general unified formulation of the internal fields can be obtained as:

$$\begin{aligned} E_{\mathrm{p}}^{\mathrm{in}} =& \bar{\mathrm{T}}_{\mathrm{A}} e^{-jk_1\rho\cos(\phi-\phi_{\mathrm{A}}^{\mathrm{t}})}U(\phi-\phi_{\mathrm{A}}^{\mathrm{t}})U(\pi-\phi_0) \\ &+ \bar{\mathrm{T}}_{\mathrm{B}} e^{-jk_1\rho\cos(\phi-\phi_{\mathrm{B}}^{\mathrm{t}})}U(\phi_{\mathrm{B}}^{\mathrm{t}}-\phi)U(\phi_0+\pi-\phi_{\mathrm{w}}), \end{aligned} \tag{3.135}$$

$$\begin{aligned} E_{\mathrm{d}}^{\mathrm{in}} =& -C(k_1\rho)\bigg[\bar{\mathrm{T}}_{\mathrm{A}}\cot\frac{\phi-\phi_{\mathrm{A}}^{\mathrm{t}}}{2}U(\pi-\phi_0) - \bar{\mathrm{T}}_{\mathrm{A}}S^{-}(\pi-\phi_{\mathrm{A}}^{\mathrm{t}}+\phi)U(\phi-\phi_{\mathrm{w}})U(\pi-\phi_0) \\ &- \bar{\mathrm{T}}_{\mathrm{B}}\cot\frac{\phi-\phi_{\mathrm{B}}^{\mathrm{t}}}{2}U(\phi_0+\pi-\phi_{\mathrm{w}}) + \bar{\mathrm{T}}_{\mathrm{B}}S^{-}(\pi-\phi_{\mathrm{B}}^{\mathrm{t}}+\phi)U(\phi-\phi_{\mathrm{w}}) \\ &\cdot U(\phi_0+\pi-\phi_{\mathrm{w}})\bigg]. \end{aligned} \tag{3.136}$$

Chapter 4

Numerical Results Comparison and Discussion

In this chapter, the accuracy of extended PO (EPO) is evaluated by comparing the numerical results with those obtained from reference methods such as HRD (hidden ray of diffraction) and FDTD simulation. As mentioned in Chapter 1, the scattering problem of wedges may also be calculated using the UAPO solution. However, UAPO doesn't provide significant differences, which are created by the contribution of hidden rays as in the HRD solution. Thus, the results of UAPO are not shown in this chapter for comparison with our EPO. While the results EPO are derived from formulations in Chapter 2 and Chapter 3, those by HRD can be found from formulations in Appendix A. On the other hand, the field patterns of FDTD are obtained by linear interpolation of the field distribution, which can be directly obtained from the simulation. The computational processing of the FDTD method is relatively simple, but it consumes a lot of time and memory. The execution time and memory consumption of FDTD are many times larger than those of the EPO and HRD approximation methods. If the object size exceeds a certain value, the computer memory may not be enough to handle the calculation processing of FDTD. In addition, the size of the simulated objects in FDTD is limited, while the wedge body currently analyzed is infinite. Therefore, a suitable wave propagation time must be carefully selected to avoid the unexpected diffraction effect caused by the absorbing boundaries. The numerical comparisons can then be represented separately for PEC and dielectric cases as follows.

4.1 PEC wedge

In this section, the numerical results comparison is made for the PEC wedge case. In this case, one notes that the results of EPO are equal to the conventional PO. Thus, the EPO formulation can be applied to calculate numerical results for the PEC wedge case by setting corresponding reflection and transmission coefficients. In addition, to obtain reliable FDTD simulation results, the simulation parameters are selected for PEC wedges as in Table. 4.1. As shown in Fig. 4.1, when the incident wave illuminates wedge surfaces, it excites the GO reflected fields and edge diffracted field. Therefore, the scattering field can be considered as the sum of these contributions. Figure 4.2(a) shows the map of the total field contribution, which can be obtained directly from the FDTD simulation. In this case, the incident wave illuminates both surfaces of the wedge with incident angle

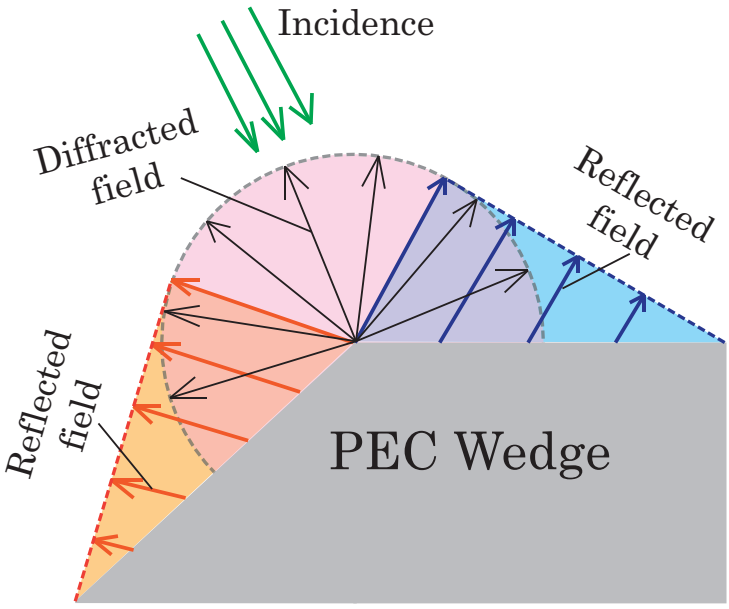

Figure 4.1: GO and diffracted rays by PEC wedge.

$\phi_0 = 115°$. and the wedge angle is selected as $\phi_w = 225°$. Then, the incident wave excites the GO reflected fields and edge diffracted fields from both surfaces OA and OB. Accordingly, the total field outside the PEC wedge is the sum of the incident, reflected and diffracted fields, while the internal is equal to zero. Then by subtracting GO reflected fields, one can obtain the distribution of diffracted fields as in Fig. 4.2(b). It can be seen that the diffracted distributes mainly near the areas, which correspond to the direction of reflected GO rays. From the above field distributions, the circular graph of the total and diffracted field can be obtained by linear interpolation technique to compare with EPO and HRD solutions.

Figure 4.3 shows the comparison of the total fields of the PEC wedge among three solutions: EPO, HRD, and FDTD. The numerical results were shown for both TM and TE-polarization cases. The field patterns are taken at the observation distance $\rho = 3\lambda$ from the total field distribution in Fig. 4.2(a). As shown in Figs. 4.3(a) and 4.3(b), the field patterns of the three solutions match pretty well in all directions for both TM and TE-polarization. One can also see the different behaviors of the total fields between two polarizations, in which the total fields of TE tend to zero near the interface while the other of TM doesn't. This is due to the difference in boundary conditions of two polarizations.

Figure 4.4 shows the comparison of diffracted fields of three solutions for TM and TE-polarizations. While the diffracted fields of EPO and HRD can be obtained by evaluating the radiation integrals on the SDP contour, those of FDTD simulation are the results of subtracting the GO fields from the total field. One can see that all patterns of the three solutions have two peaks, which correspond to the shadow boundary direction of reflected waves from surfaces OA and OB. One also observes that the diffracted field is very small compared with the GO fields, and distributes mainly in the regions that are near the shadow boundaries SB^r of the GO reflected fields. The contribution of the diffracted fields can compensate for the abrupt transitional behavior of the GO fields at the shadow boundaries. From the comparison, one also can observe that the HRD and FDTD results are almost identical, and have some differences from the EPO result. The differences become more apparent when the observation point approaches the wedge

Table 4.1: Parameters of FDTD simulation for PEC wedge.

Parameter	**Incident angle** $\phi_0 = 115°$	**Incident angle** $\phi_0 = 30°$
Frequency	6 GHz	6 GHz
Wave length	50 mm	50 mm
Max iteration number	45000	50000
Convergence	10^{-6}	10^{-6}
Time step	10^{-13}	10^{-13}
Calculation region	600 mm × 600 mm	700 mm × 700 mm
Yee cell size	0.25 mm × 0.25 mm	0.25 mm × 0.25 mm

surface. As mentioned above, the diffracted field is small compared with the GO rays, so one may not see the difference between HRD and EPO in the comparison of the total field. The differences can be explained by the fact that the diffracted field of the PO approximation doesn't satisfy the boundary and edge conditions. On the other hand, the HRD solution can satisfy the boundary condition thanks to the additional contribution of hidden diffracted rays in the non-physical region, which can be explained by the behavior of the cotangent functions. In addition, the angular period of the cotangent functions of HRD are modified based on the edge condition. Accordingly, the results of the HRD solution are exactly the same as those of the UTD solution in the perfectly conducting wedge case.

Figure 4.5 shows the cotangent functions of EPO and HRD solutions for TE-polarization in the two-side illumination case. These cotangent functions have singularity behaviors at the shadow boundaries of GO incident and reflected rays. When both surfaces are illuminated, one only has two shadow boundaries of GO reflected waves in the physical domain. Accordingly, the shadow boundaries of incident waves exist in the non-physical domain. As mentioned in Chapter 2, two of four cotangent functions in EPO formulation correspond to hidden incident rays and cancel out each other. Therefore, the EPO formulation only has two cotangent functions corresponding to GO rays in the physical domain as shown in Fig. 4.5(a). These two remainder cotangent functions can not cancel when $\phi = 0$ or ϕ_{w}, and this leads to the electric field of EPO not equal to zero at the interface of the wedge. On the other hand, the formulation of HRD always has four cotangent functions for any incident direction. And two cotangent functions of hidden incident rays in the non-physical domain can cancel two cotangent functions of reflected rays when $\phi = 0$ or ϕ_{w} as shown in Fig. 4.5(b). Accordingly, the electric field of HRD tends to zero at the interface to satisfy the boundary condition. A similar difference in cotangent functions between EPO and HRD can also observed for TM-polarization as shown in Fig. 4.6. However, in the TM-polarization case, four cotangent functions of HRD don't cancel out each other to give us zero magnetic fields at the wedge interface. Instead, the angular derivative of cotangent functions has cancellation at the interfaces, and this gives us the correct behavior of the diffracted field by HRD: the angular derivative of the diffracted field (H_{z}) becomes zero at the PEC boundary.

When the incident angle is selected as 30°, one has the comparisons of total and diffracted fields as in Fig. 4.7 and Fig. 4.8, respectively. In this case, the incident only illuminated the upper surface of the wedge. One can see that the differences of EPO compared with HRD and FDTD become bigger than those in the two-side illumination case. The difference can be observed more clearly when the observation point moves to the shadow regions. This shows that the error of EPO is more significant for the shadow region of the one-side illumination.

In Fig. 4.9 and Fig. 4.10, one has the comparisons among three solutions when the wedge is sharper ($\phi_{\mathrm{w}} = 315°$), and the incident wave illuminates both surfaces of the wedge. Compared to the case of wedge angle $\phi_{\mathrm{w}} = 225°$, the differences from EPO also become more apparent. On the other hand, unlike the flat-angle wedge, these differences are improved when the incident angle is selected as 30°. These behaviors show that the error of EPO in terms of boundary condition depends on the wedge angle and incident direction.

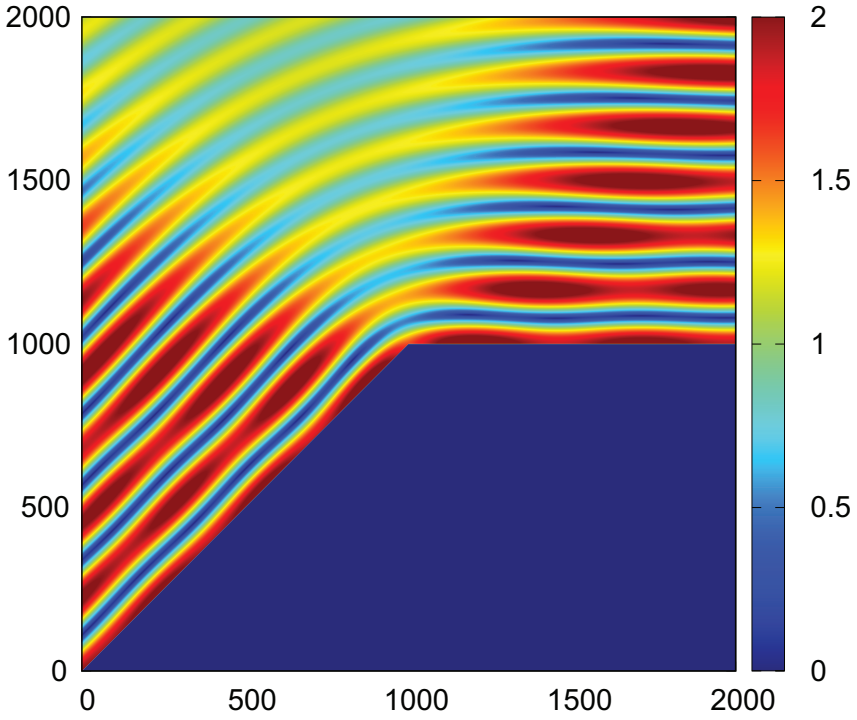

(a)

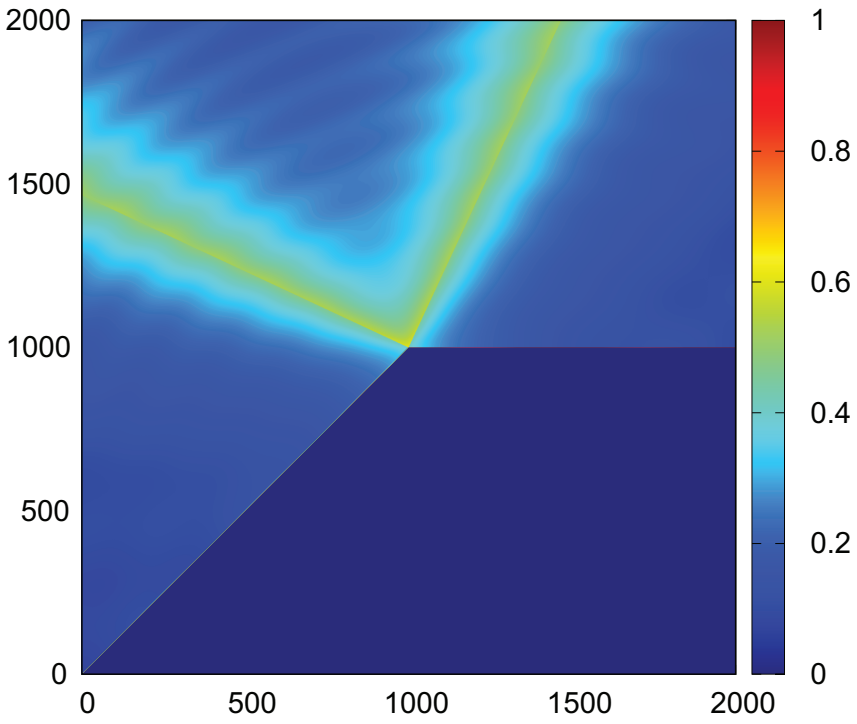

(b)

Figure 4.2: Field distribution of PEC wedge (FDTD calculation): $\phi_{\mathrm{w}} = 225°$, $\phi_0 = 115°$. (a) Total field. (b) Diffracted field.

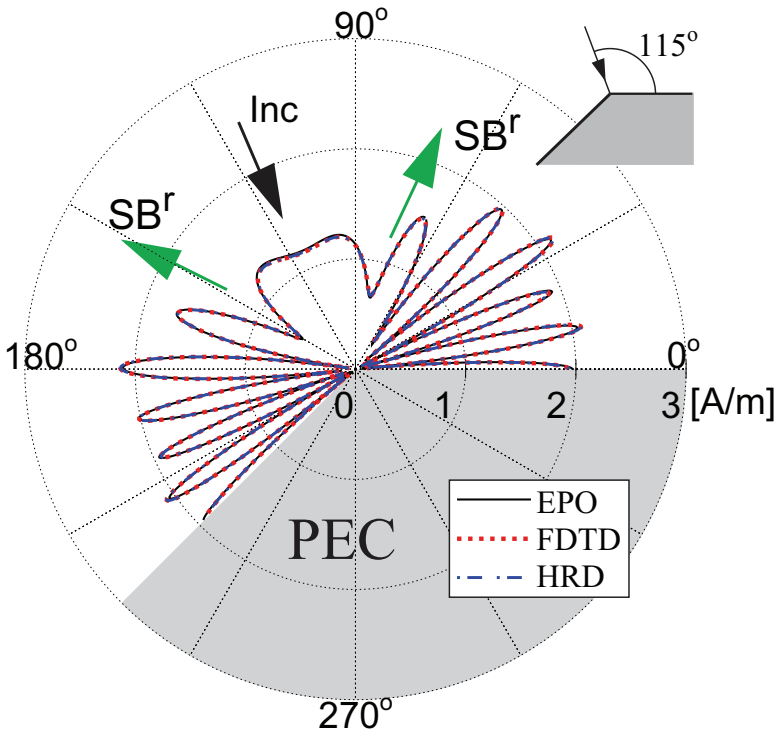

(a)

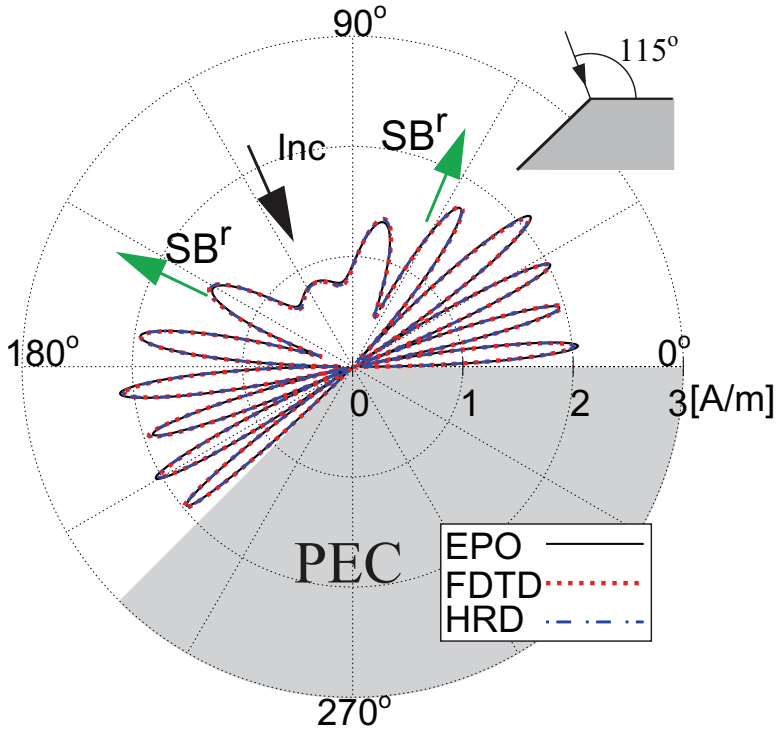

(b)

Figure 4.3: Total field of PEC wedge: $\phi_w = 225°$, $\phi_0 = 115°$ and $\rho = 3\lambda$. (a) TM polarization. (b) TE polarization.

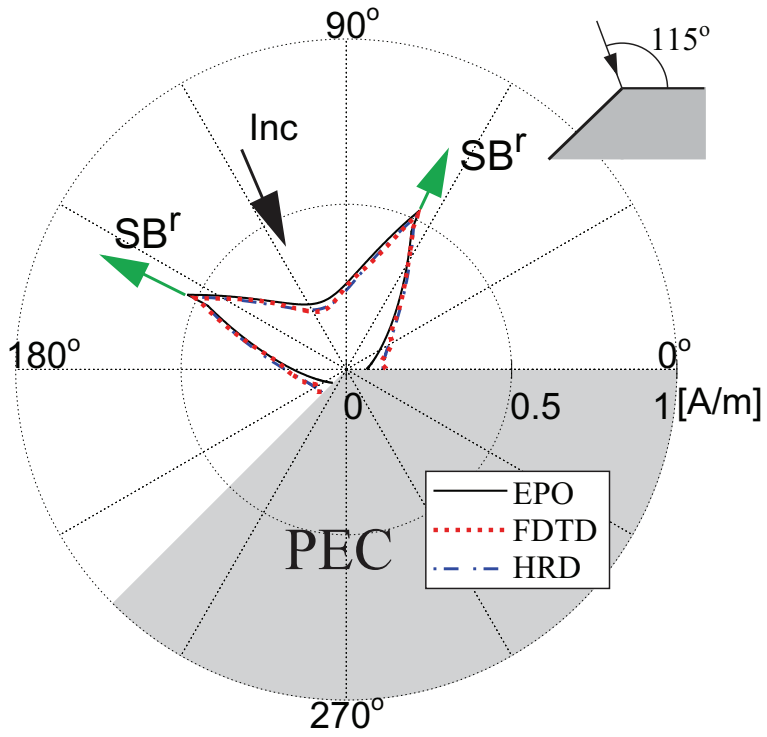

(a)

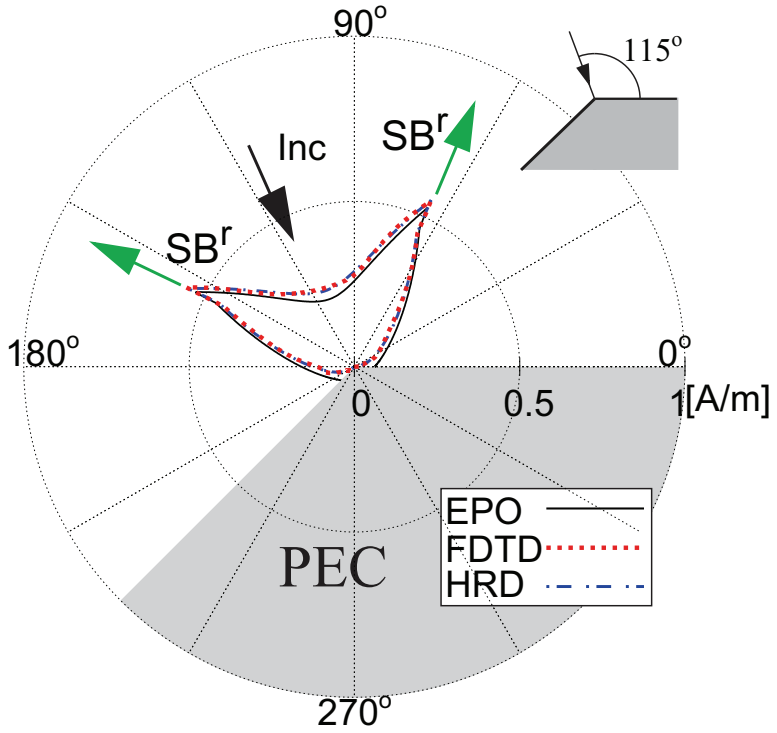

(b)

Figure 4.4: Diffracted field of PEC wedge: $\phi_w = 225°$, $\phi_0 = 115°$ and $\rho = 3\lambda$. (a) TM polarization. (b) TE polarization.

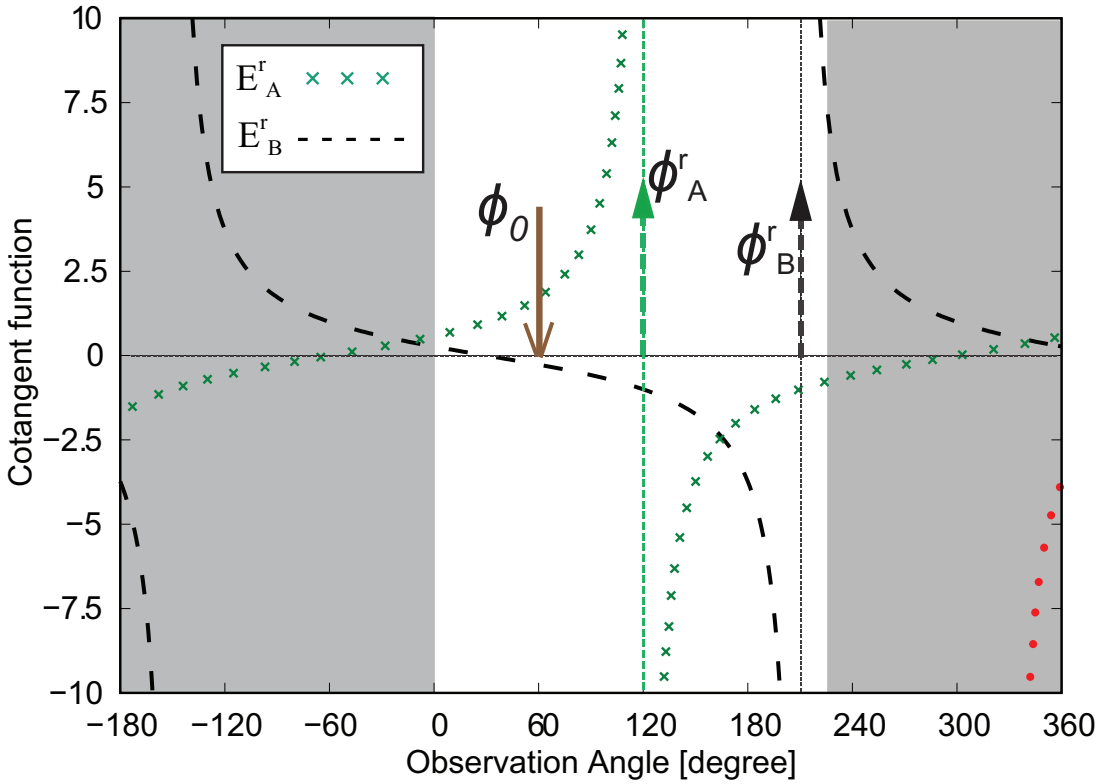

(a)

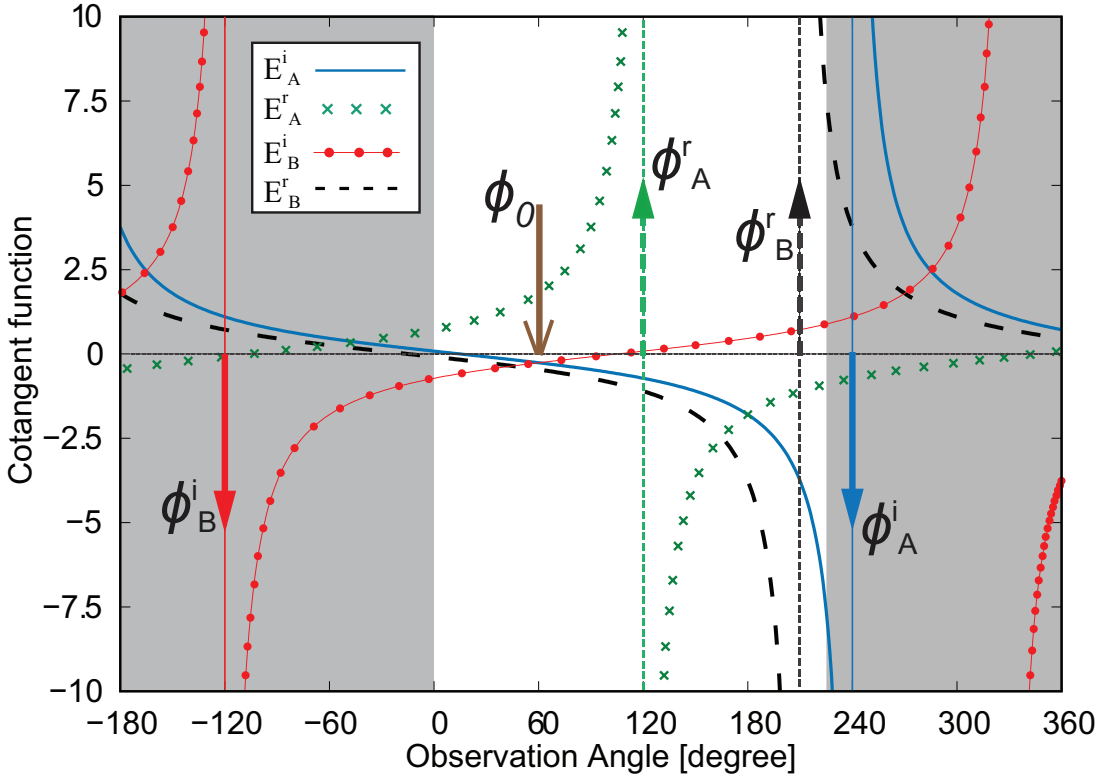

(b)

Figure 4.5: Cotangent functions of EPO and HRD (TE polarization): $\phi_{\mathrm{w}} = 225°$ and $\phi_0 = 60°$. (a) EPO. (b) HRD.

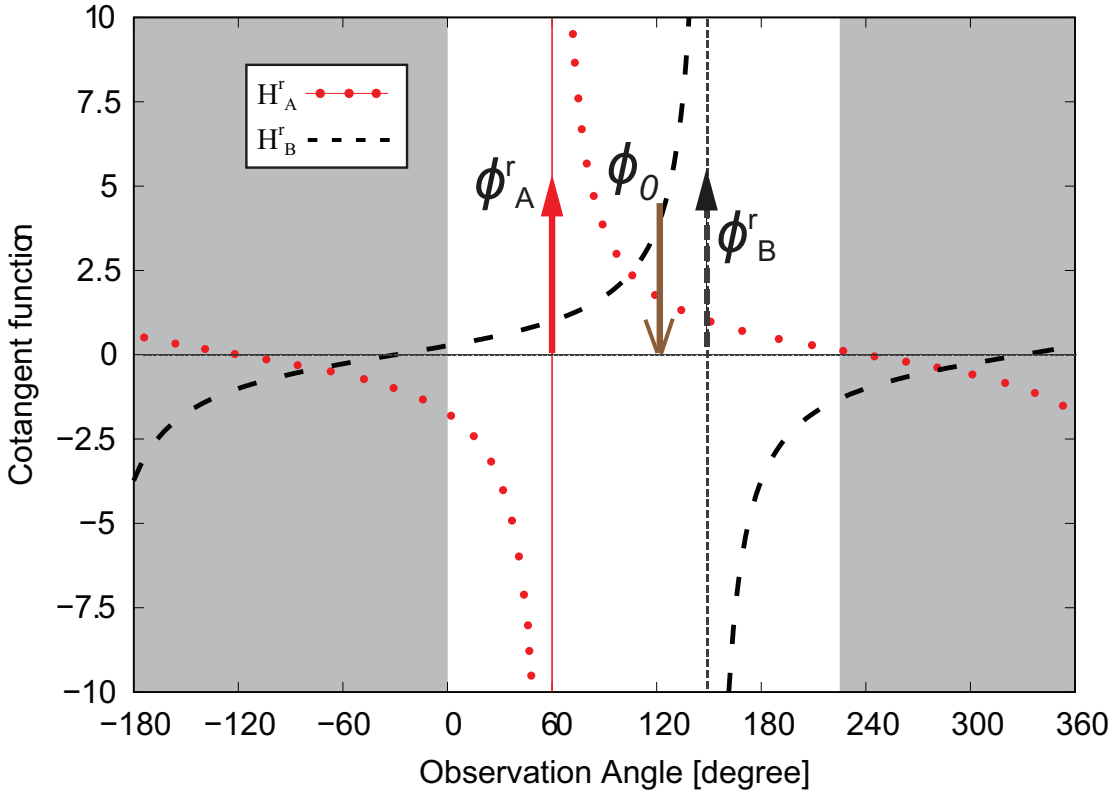

(a)

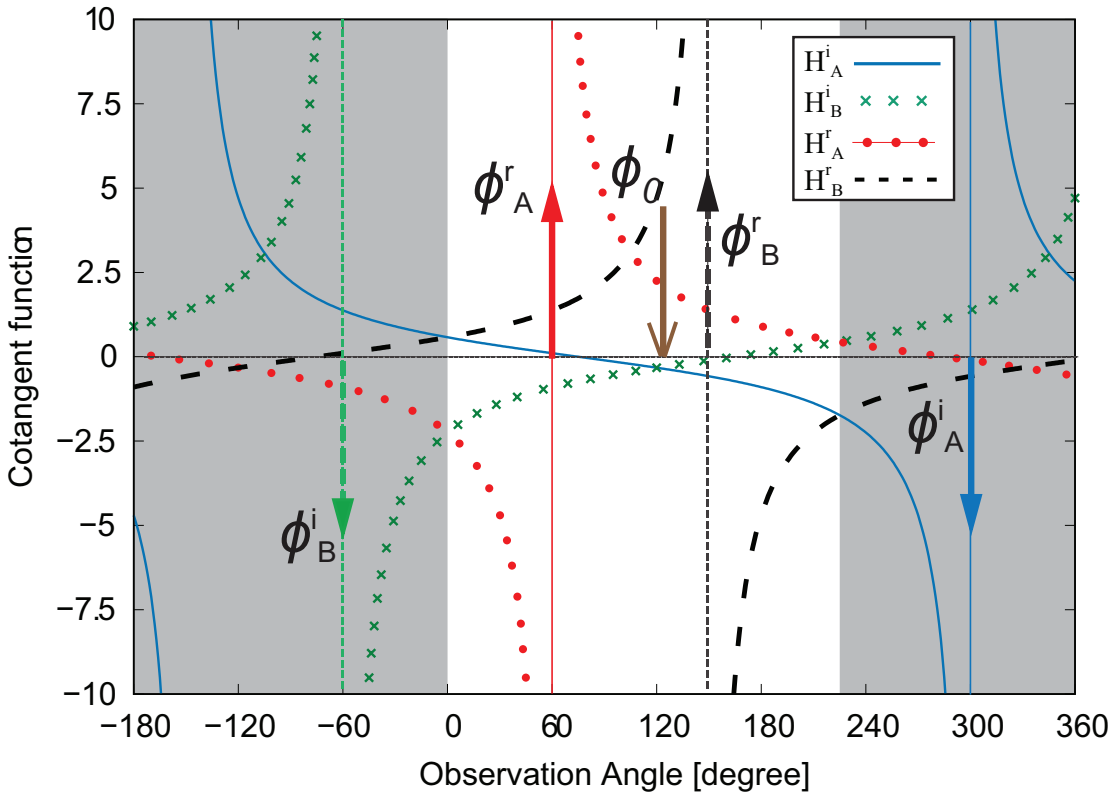

(b)

Figure 4.6: Cotangent functions of EPO and HRD (TM polarization): $\phi_w = 225°$ and $\phi_0 = 120°$. (a) EPO. (b) HRD.

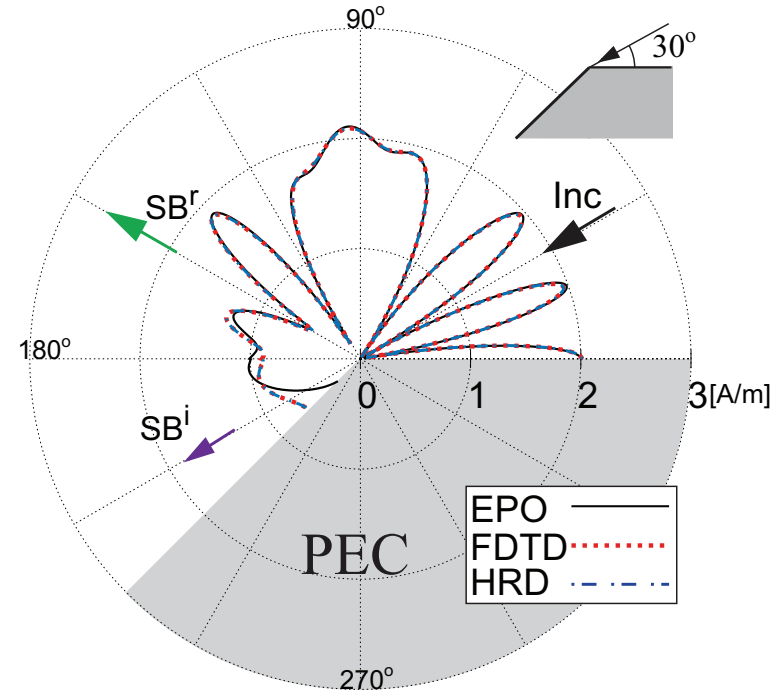

(a)

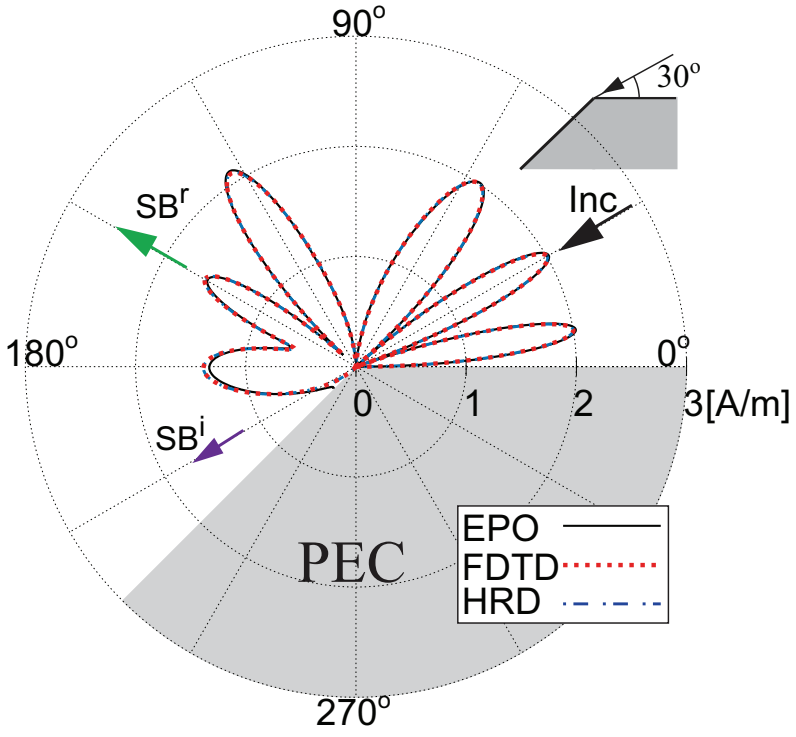

(b)

Figure 4.7: Total field of PEC wedge: $\phi_w = 225°$, $\phi_0 = 30°$ and $\rho = 3\lambda$. (a) TM polarization. (b) TE polarization.

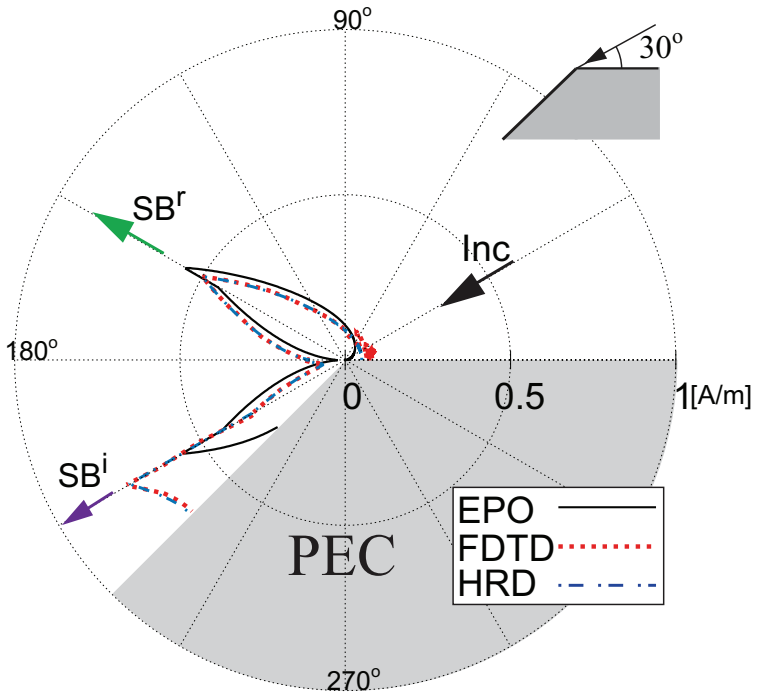

(a)

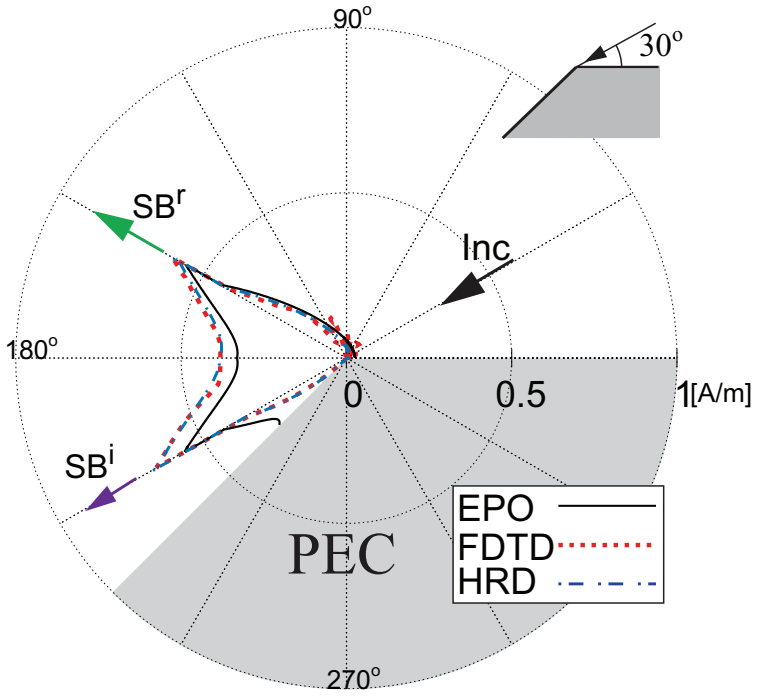

(b)

Figure 4.8: Diffracted field of PEC wedge: $\phi_{\mathrm{w}} = 225°$, $\phi_0 = 30°$ and $\rho = 3\lambda$. (a) TM polarization. (b) TE polarization.

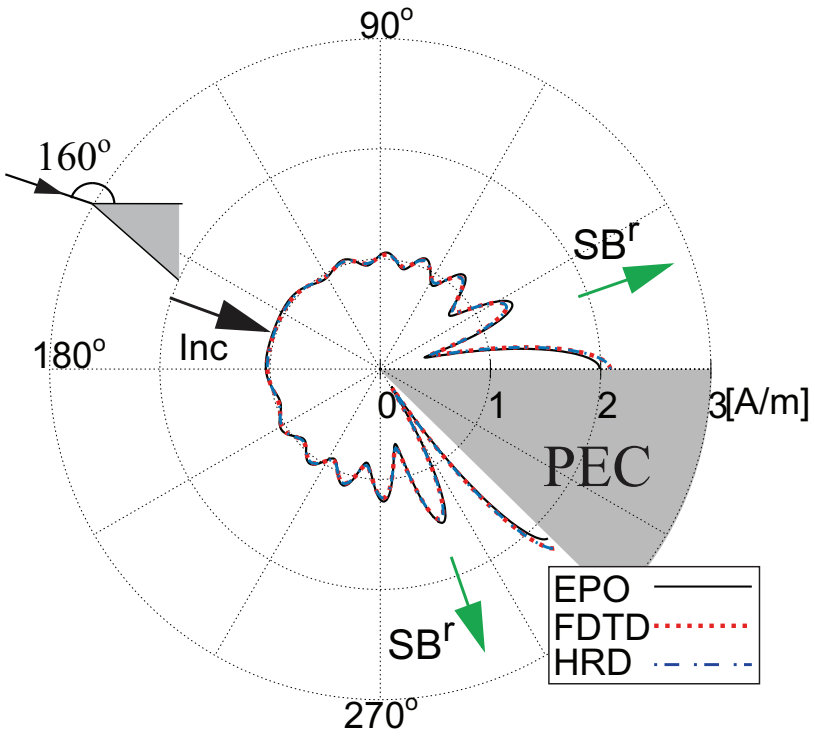

(a)

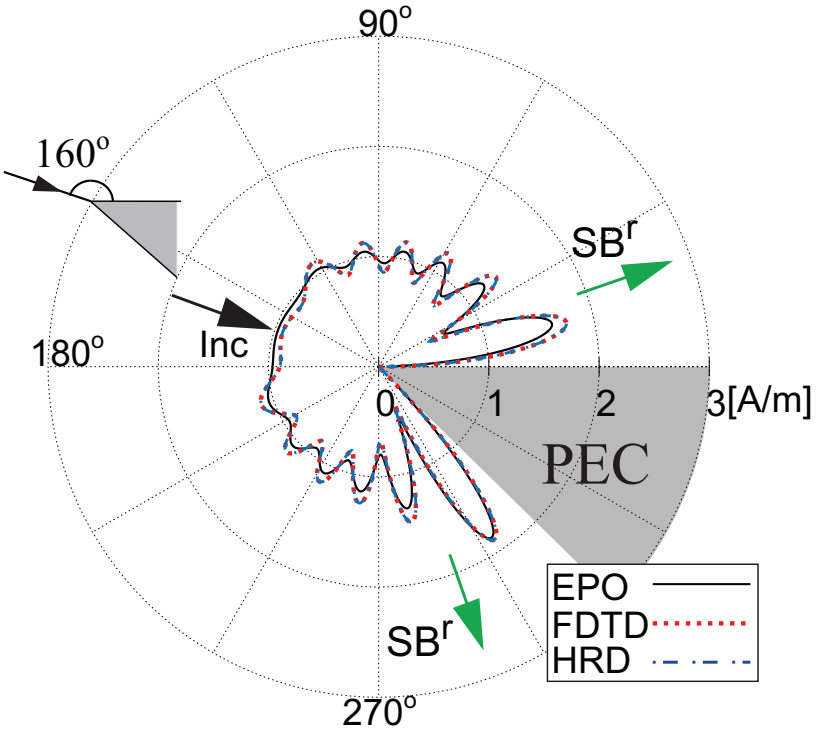

(b)

Figure 4.9: Total field of PEC wedge: $\phi_w = 315°$, $\phi_0 = 160°$ and $\rho = 3\lambda$. (a) TM polarization. (b) TE polarization.

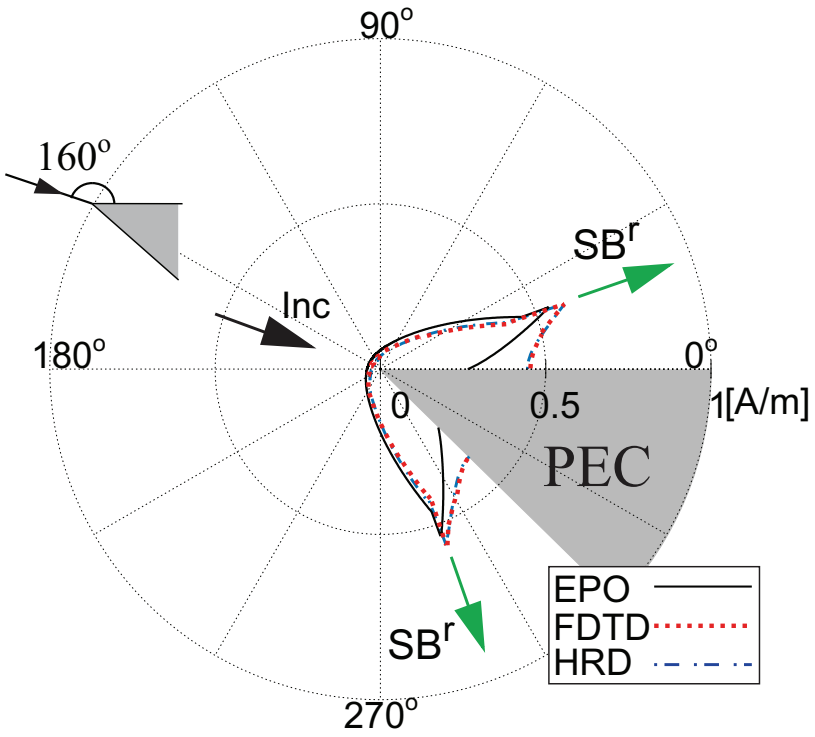

(a)

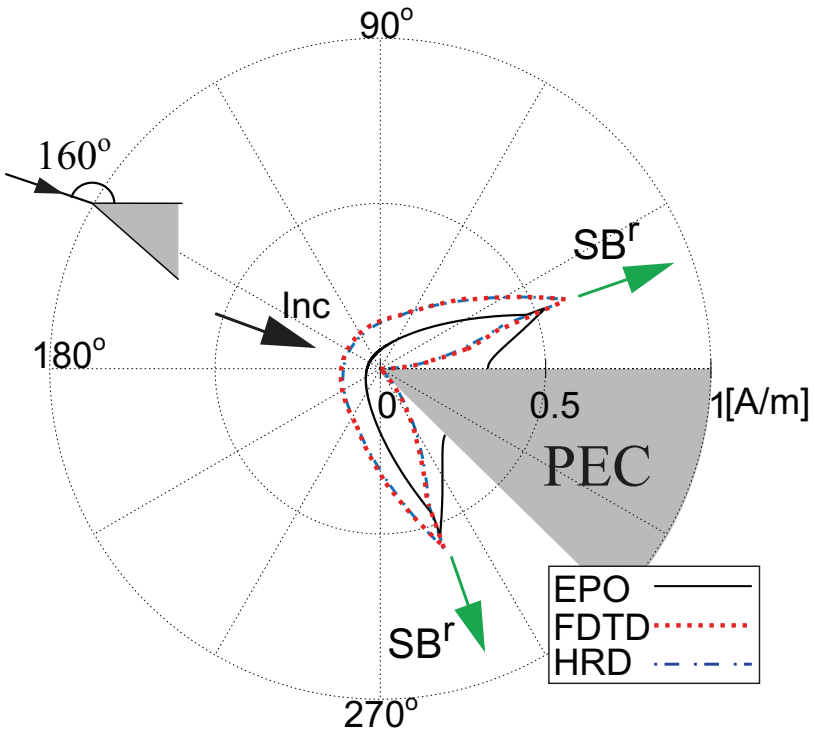

(b)

Figure 4.10: Diffracted field of PEC wedge: $\phi_w = 315°$, $\phi_0 = 160°$ and $\rho = 3\lambda$. (a) TM polarization. (b) TE polarization.

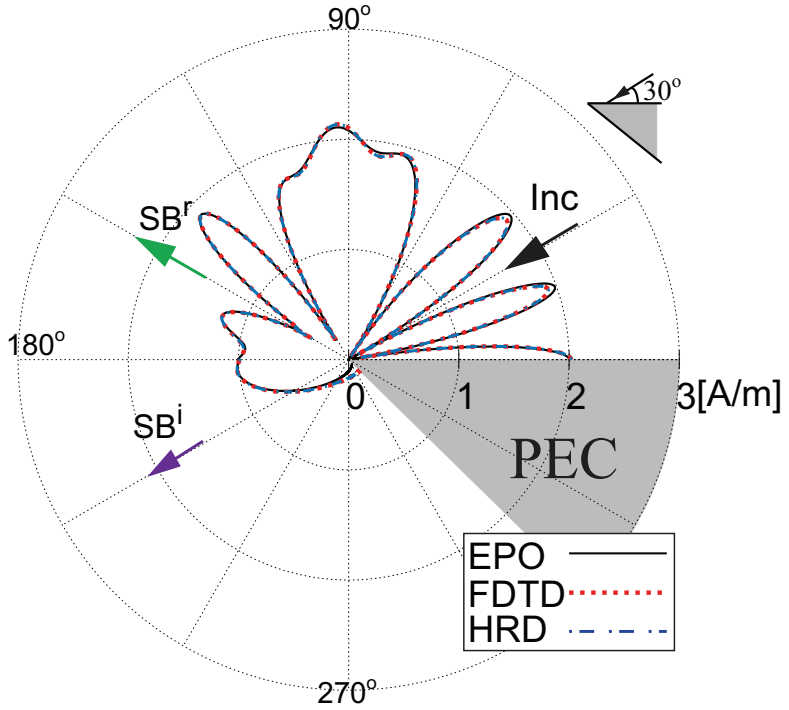

(a)

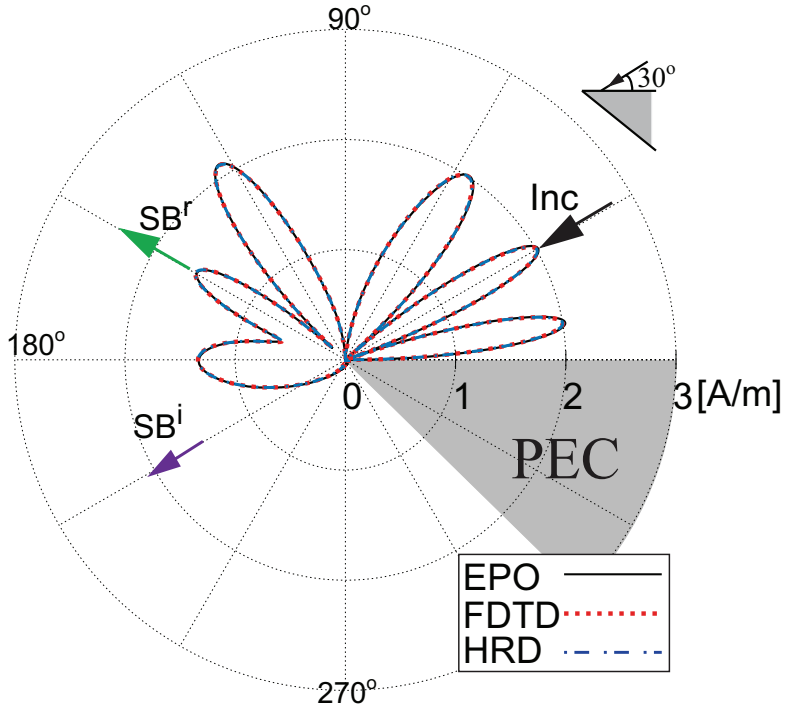

(b)

Figure 4.11: Total field of PEC wedge: $\phi_w = 315°$, $\phi_0 = 30°$ and $\rho = 3\lambda$. (a) TM polarization. (b) TE polarization.

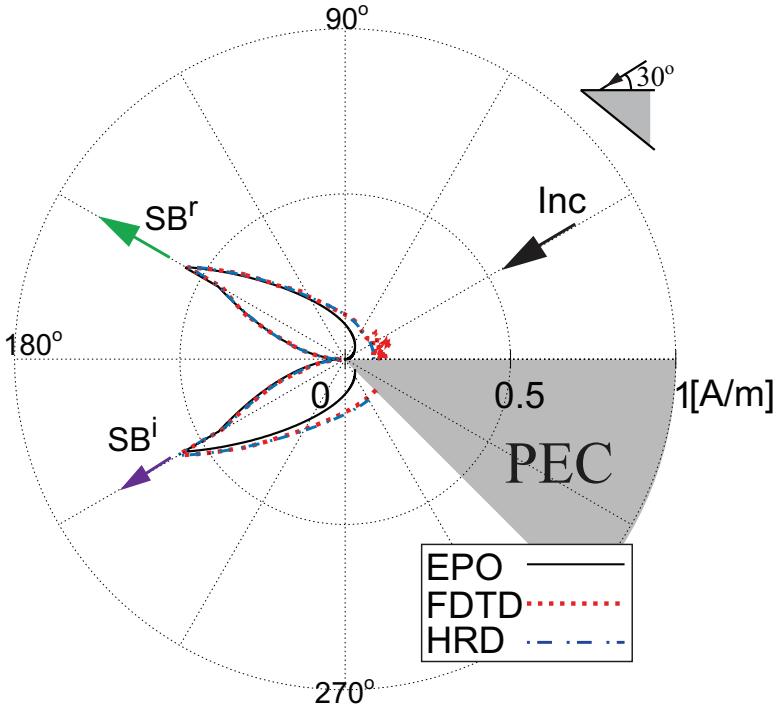

(a)

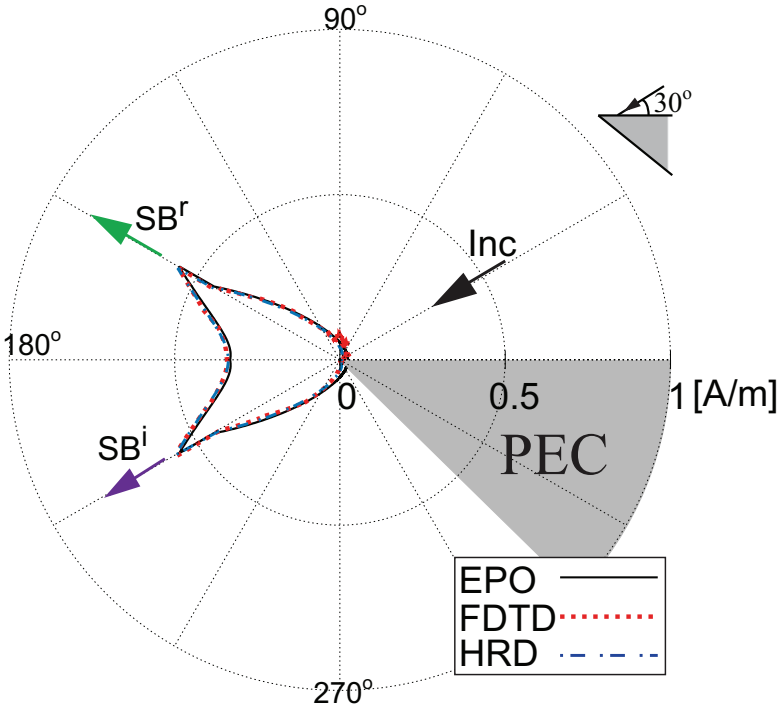

(b)

Figure 4.12: Diffracted field of PEC wedge: $\phi_w = 315°$, $\phi_0 = 30°$ and $\rho = 3\lambda$. (a) TM polarization. (b) TE polarization.

4.2 Dielectric wedge

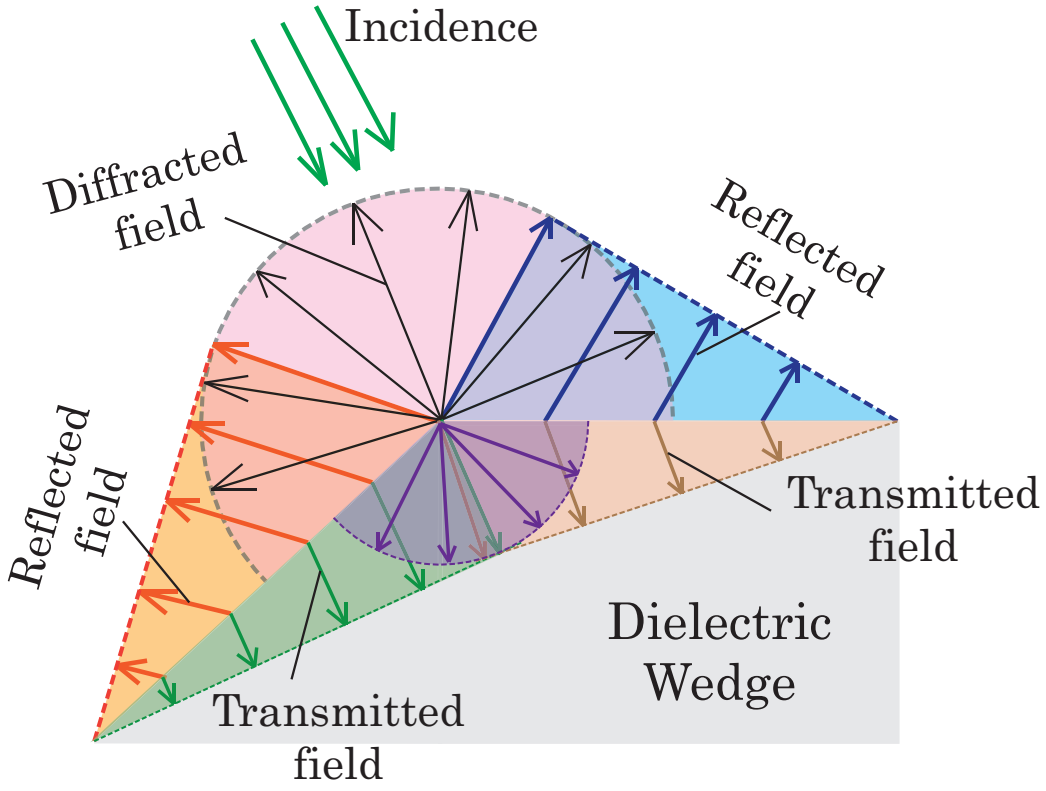

Figure 4.13: GO and diffracted rays by dielectric wedge.

When the PEC wedge is replaced by a dielectric wedge, one may have more transmitted waves from surfaces OA and OB. Therefore, the external scattering fields include the GO reflected and diffracted fields, while the internal fields are the sum of GO transmitted and diffracted fields as shown in Fig. 4.13. As same as the PEC wedge case, the FDTD simulation results of the dielectric wedge also have the spurious diffraction effect from the absorbing boundaries. In addition, unexpected multiple reflections may occur inside the finite dielectric wedge of FDTD. Thus, to avoid the multiple internal reflections of the transmitted rays inside the dielectric wedge, only a flat-angle wedge is selected for the numerical example in this dielectric case. This requires us to select an appropriate transient time carefully. In the following numerical comparisons, the numerical results are calculated for the wedge of wedge angle $\phi_{\mathrm{w}} = 225°$ and dielectric constant $\varepsilon_{\mathrm{r}} = 6$. The simulation parameters of FDTD for dielectric wedges are shown in Table. 4.2.

Figure 4.14 shows the total field distribution of the dielectric wedge for both TM and TE polarizations. It can be see that the total field of the TM polarization is stronger than that of the TE polarization. One also notes that an appropriate transient time has been selected so that the transmitted field doesn't excite the multiple reflections inside the wedge. By subtracting the GO reflected and transmitted fields based on the wavefronts, one obtains the diffracted field distribution as shown in Fig. 4.15. A difference in the magnitude of the internal diffracted field between TM and TE polarizations can also be observed. For more detailed comparisons, the field patterns were then derived from the field distribution at the observation distance $\rho = 3\lambda$.

Table 4.2: Parameters of FDTD simulation for dielectric wedge.

Parameter	**Incident angle** $\phi_0 = 115°$	**Incident angle** $\phi_0 = 30°$
Frequency	6 GHz	6 GHz
Wave length	50 mm	50 mm
Max iteration number	50000	55000
Convergence	10^{-6}	10^{-6}
Time step	10^{-13}	10^{-13}
Calculation region	600 mm $\times$ 600 mm	750 mm $\times$ 750 mm
Yee cell size	0.25 mm $\times$ 0.25 mm	0.25 mm $\times$ 0.25 mm
Dielectric constant	$\varepsilon_r = 6$	$\varepsilon_r = 6$

Figure 4.16 shows the comparison of the total fields when the incident wave illuminates the dielectric wedge with incident angle $\phi_0 = 115°$ for both TE and TM polarizations. In this case, the incident wave illuminates both sides of the dielectric wedge and excites the reflected and transmitted waves in the outside and inside regions, respectively. As shown in Figs. 4.16(a) and 4.16(b), the total fields of the three solutions match well for both TE and TM polarizations. It can be seen that the scattering field in the outside region has quite similar behavior to those of the PEC wedge case in Fig. 4.3. Inside the dielectric wedge, one can observe a main scattering lobe near the direction of the incident wave. The two biggest sidelobes correspond to the direction of the two transmitted waves from surfaces OA and OB. These field behaviors are nearly similar between TM and TE polarizations with different amplitudes due to the differences in reflection and diffracted coefficients.

Figure 4.17 shows the comparison of the diffracted fields of three solutions. In the outside region, one can see that the diffracted fields of EPO and FDTD have a good agreement, and have some differences with those of the HRD solution. This is different from the above PEC wedge case, in which HRD has better agreement with the FDTD simulation than EPO. So far, we have not been able to explain exactly why the EPO solution becomes better than the HRD solution when applied to the dielectric wedge. This change in the accuracy of EPO and HRD between PEC and dielectric cases may be due to the edge condition. Inside the dielectric wedge, all three solutions yield twin peaks at the shadow boundaries SB^t of the transmitted waves. While the diffracted fields of EPO and HRD in Fig. 4.17 exhibit the same behavior, those of the FDTD simulation show some differences. These differences are apparent in the areas near the shadow boundary directions of two transmitted waves from surfaces OA and OB. It can be observed that, in the wedge dielectric case, the diffracted fields of both EPO and HRD don't satisfy the boundary condition. This reminds us that some significant contributions at the boundary of two media may be missed, and need to be considered.

When one selects the incident angle ϕ_0 as 30°, the incident wave only illuminates surface OA and the comparison of the corresponding total fields is shown in Fig. 4.18. In this

case, the incident wave excites only one reflected wave and one transmitted wave from the illuminated surface OB. One observes that all three results match well in the exterior region for both TM and TE polarizations, while there are some differences in the interior region. To know what causes these differences, a comparison of the diffracted fields has been made and shown in Fig. 4.19 for both TM and TE polarizations. Similar to the one-side illumination case, the outer field of EPO and FDTD have a good agreement and have some differences with the HRD solution. However, the diffracted field has two large peaks corresponding to the shadow boundaries of the incident and transmitted wave compared with the direction of the reflected wave. Inside the wedge, the difference has been found in the diffracted field, in which additional field constituent seems to radiate in the interior region. One can see that the significant differences in the internal diffracted fields are the main reason for the difference in the field inside the wedge. These differences are bigger than those of the two-side illumination case in Fig. 4.17.

Figure 4.20 shows the behavior of cotangent functions corresponding to the outside region of the wedge for the one-side illumination. As the same as the PEC case, two cotangent functions have singularity behaviors in the physical domain, while two remainder functions have singularities in the non-physical domain. However, these cotangent functions of the dielectric case don't have any cancellation behavior at the interface of the wedge as PEC case. This is due to the change of reflection coefficients, which relates to the dielectric constant ε_{r}. Similarly, one has a cotangent function corresponding to transmitted waves inside the wedge as in Fig. 4.21. Here, one also sees that two cotangent functions have two corresponding singularity behaviors in physical and non-physical domains, respectively. The location of these behaviors corresponds to the shadow boundaries of transmitted rays.

In Fig. 4.22, one can see the remainder field of FDTD, which was obtained by subtracting the diffracted field of EPO from the diffracted field of FDTD in Fig. 4.19(a). The corresponding result for $\phi_0 = 40^\circ$ is also plotted in Fig. 4.22. It can be seen that the remainder field is distributed mainly in the areas near shadowed surface OB, where the surface diffracted wave is bigger than one on surface OA. When the incident angle changes to 40°, the remainder field becomes bigger, but keeps the same oscillation behavior as in the case of $\phi_0 = 30^\circ$. These observation results remind us of the concept of lateral wave, which relates to the boundary condition of edge diffracted field. One knows that the GO fields satisfy the boundary condition, in which the sum of the external incident and reflected field is equal to the internal transmitted field at the boundary of two media. On the other hand, the edge diffracted field excited by the incident wave at the wedge tip doesn't satisfy this boundary condition. This is due to the difference in the wave propagation speed of the edge diffracted field between the exterior and interior regions of the dielectric wedge. To compensate for this difference, one needs to consider the contribution of the lateral waves that are excited in the dielectric medium inside the wedge. The model of the lateral wave may be outlined sketch as in Figure 4.23. Here, the lateral waves are considered as the radiation field excited by a line source that is located at the boundary between two media. The wavefronts of these lateral waves create an angle of $\theta_{\mathrm{c}} = 1/\sqrt{\varepsilon_{\mathrm{r}}}$ with the surfaces of the wedge. One notices that the excitation of the lateral waves depends on the surface fields. As shown in Fig. 4.19, it can be observed that the diffracted field at the surface of $\phi = 225^\circ$ is stronger than the one at the surface of $\phi = 0^\circ$. Accordingly, the lateral waves in the vicinity of surface OB are also stronger than those of surface OA.

The contribution of these lateral waves may be found from the two-media problem, in

which the radiation due to a current source in the denser medium can be derived from free-space Green's function and a static Green's function G_s. This Green's function G_s has saddle points and branch points. Then the contribution from the branch points may describe the behavior of the lateral wave. The formulation of these branch points can be found in Appendix A. Figure 4.24 shows the total field distribution of FDTD for both TM and TE polarizations in the one-side illumination case ($\phi_0 = 30°$). One can see that the total fields of TM polarization are mainly distributed in the interior region, while those of TE polarization are almost distributed in the exterior region. Subtracting the incident field and the GO reflected field from surface OA in the outside, one then has the corresponding diffracted field distribution of TM and TE polarization as in Fig. 4.25. As mentioned before, the diffracted field is mainly distributed in the region around the direction of the GO reflected and transmitted waves. Figures 4.26 and 4.27 show the distribution of the remainder field of FDTD and possible lateral wave excited inside the dielectric wedge, in which the FDTD remainder field is obtained by subtracting the diffracted field from Fig. 4.25. One can see the same behavior between the remainder field of FDTD and the lateral waves. However, the amplitudes of the two results are different, and the lateral wave tends to infinity near the shadow boundary. This is due to the singularity behavior of the non-uniform solution when the branch point is near the saddle point. One also can observe the same behaviors of the wavefront of the FDTD remainder field and possible lateral wave inside the wedge as shown in Fig. 4.28. So far, it is still being investigated to apply the contribution of the lateral waves to our EPO solution.

Figure 4.29 and Figure 4.30 show the field behaviors of the dielectric wedge for wedge angle ϕ_w is selected as 330°. In Fig. 4.29, one can see a big difference between TM and TE polarization for both total and diffracted fields. While the internal fields of TM polarization are very small compared with those of TE polarization, an opposite phenomenon can be seen for the external region. One can see that the differences between TM and TE occur in the region containing the GO reflected and transmitted rays. This is due to the difference in the reflection and transmission coefficients between TM and TE polarizations. For the two-side illumination as in Fig. 4.29(a), the difference in the outer region is more apparent in small areas near two surfaces that are occupied by the reflected waves. A similar behavior can also be observed when the incident wave illuminates one side of the wedge with wedge angle $\phi_0 = 30°$ as in Fig. 4.30(a), in which the external total field of TE has weaker oscillation than TM polarization. In this one-side illumination, the difference in the reflected waves between TM and TE is bigger and occurs over a larger area than in the case of two-side illumination. Inside the wedge, the total field of TE behaves stronger than TM polarization. This change also occurs for the diffracted fields in the direction of reflected and transmitted waves as in Fig. 4.30(b).

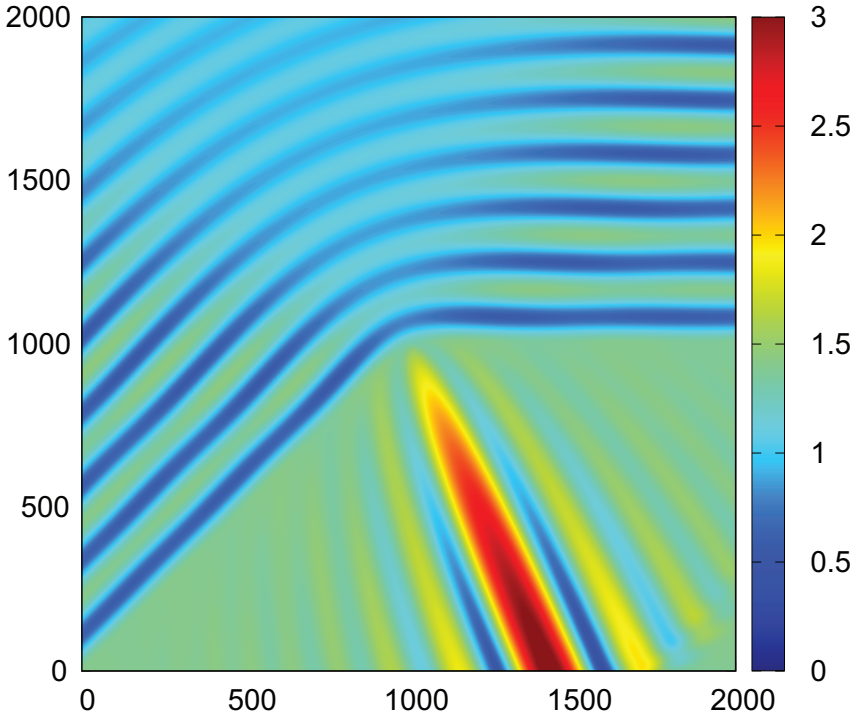

(a)

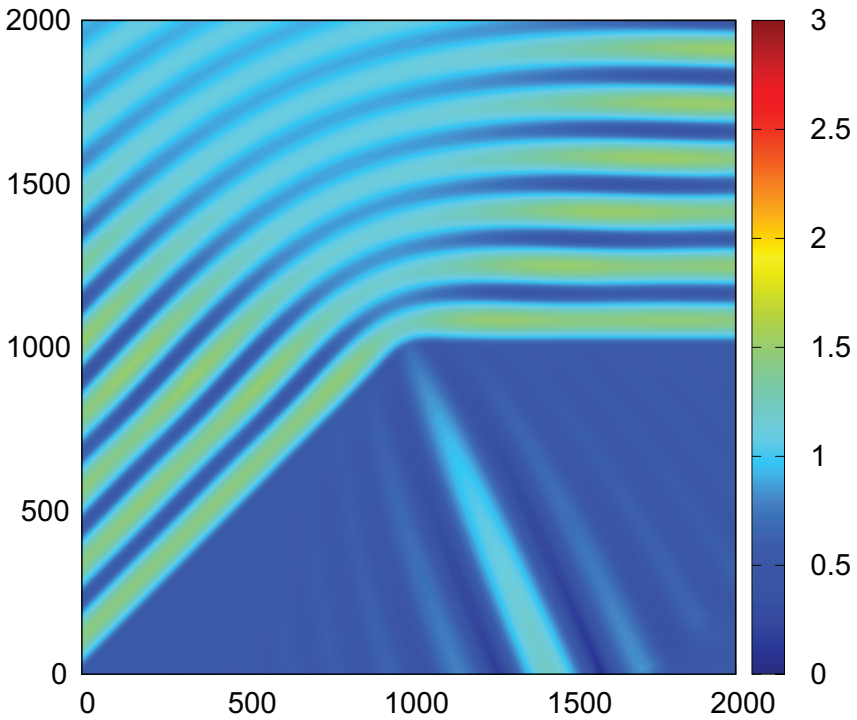

(b)

Figure 4.14: Total field distribution of dielectric wedge: $\phi_{\mathrm{w}} = 225°$, $\phi_0 = 115°$, $\varepsilon_{\mathrm{r}} = 6$. (a) TM polarization. (b) TE polarization.

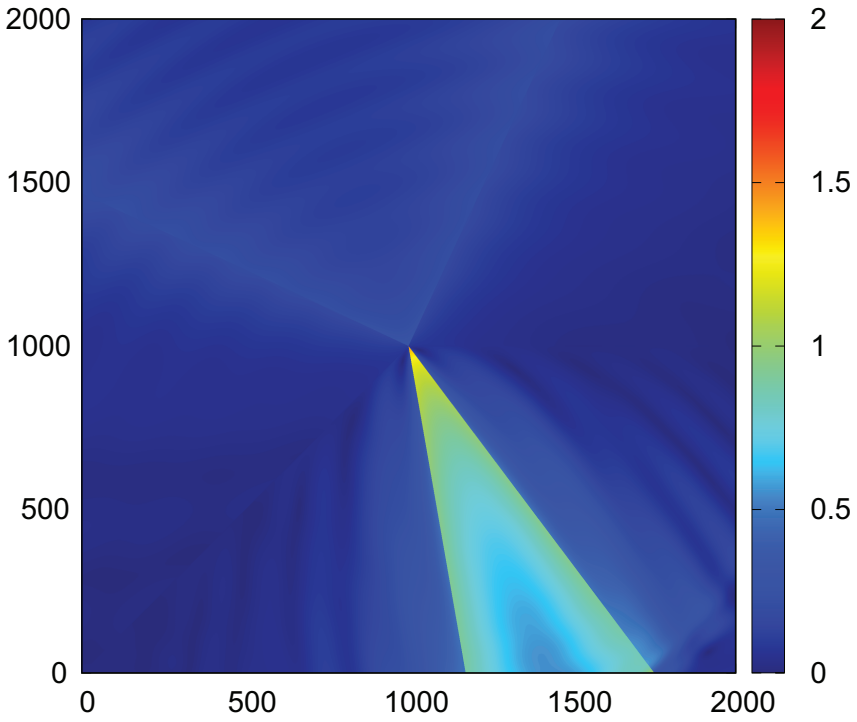

(a)

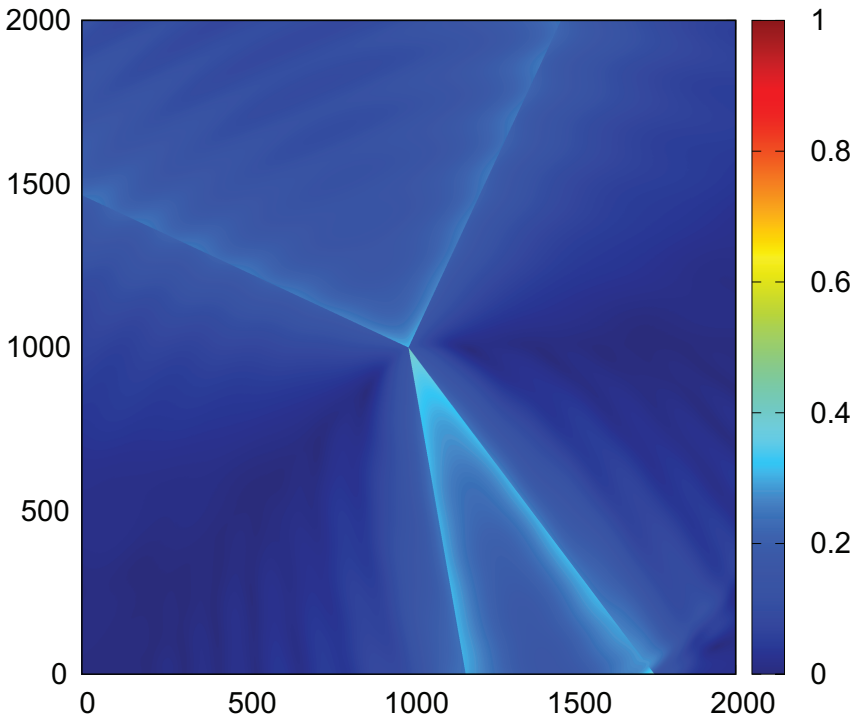

(b)

Figure 4.15: Diffracted field distribution of dielectric wedge: $\phi_{\mathrm{w}} = 225°$, $\phi_0 = 115°$, $\varepsilon_{\mathrm{r}} = 6$. (a) TM polarization. (b) TE polarization.

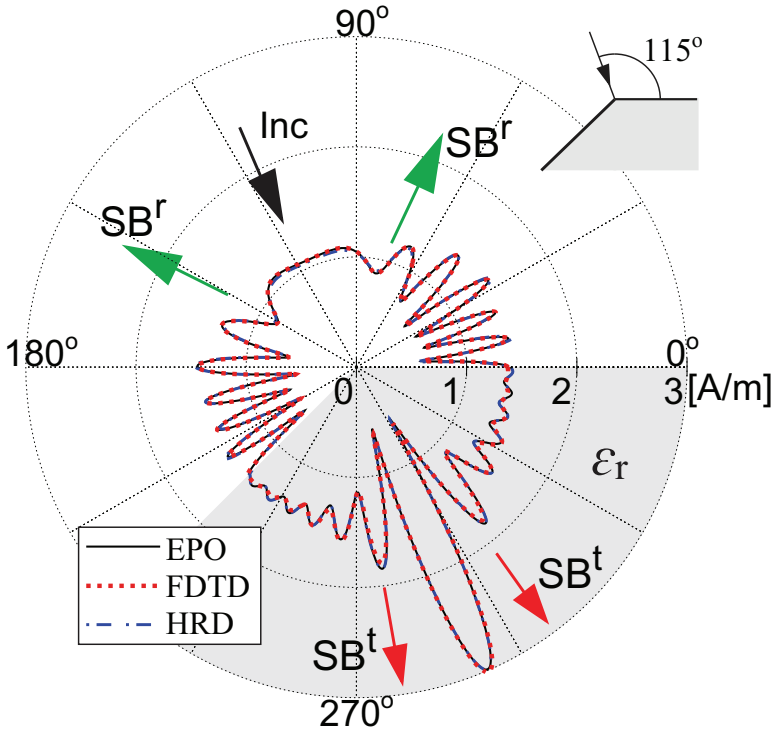

(a)

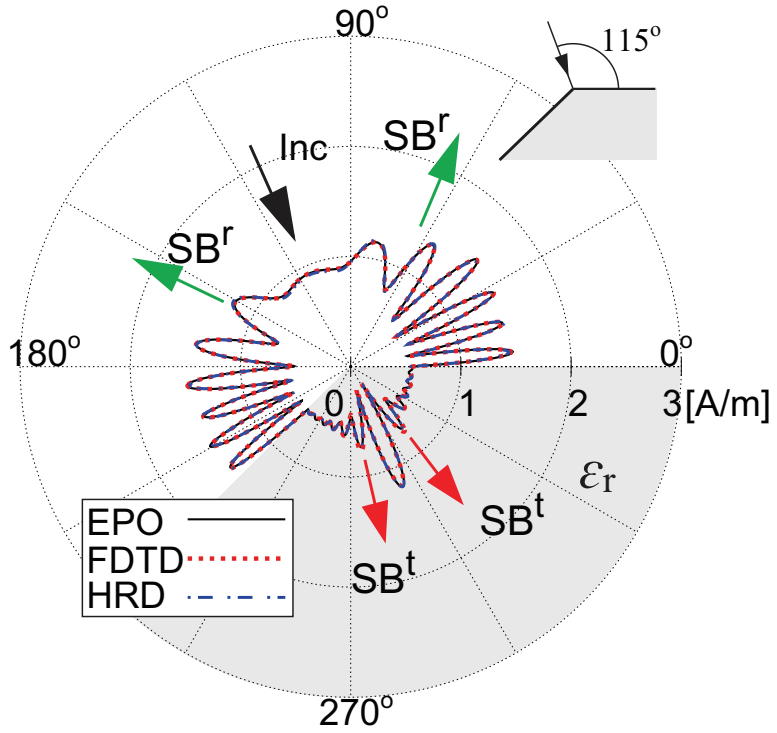

(b)

Figure 4.16: Total field of dielectric wedge: $\phi_w = 225°$, $\phi_0 = 115°$, $\varepsilon_r = 6$ and $\rho = 3\lambda$. (a) TM polarization. (b) TE polarization.

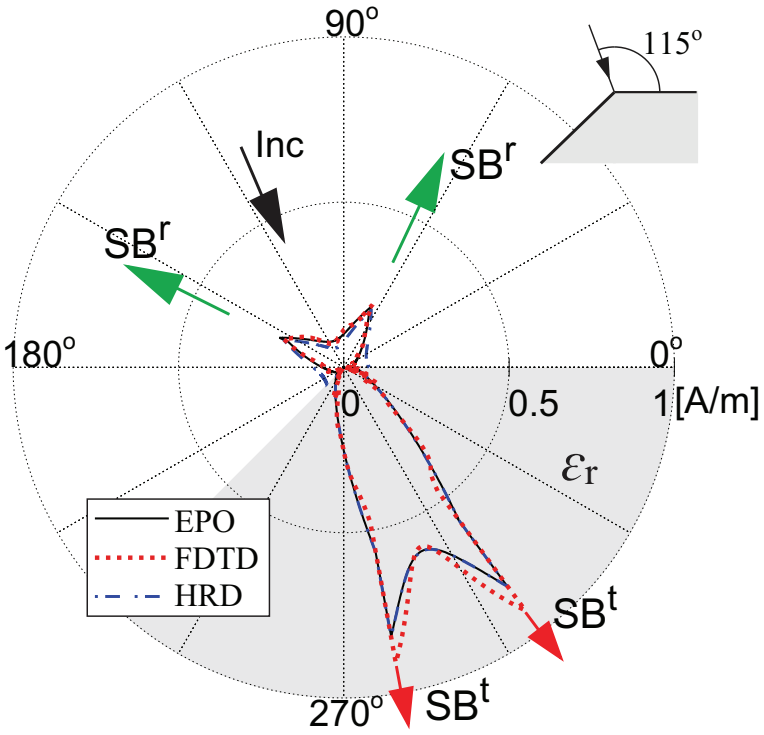

(a)

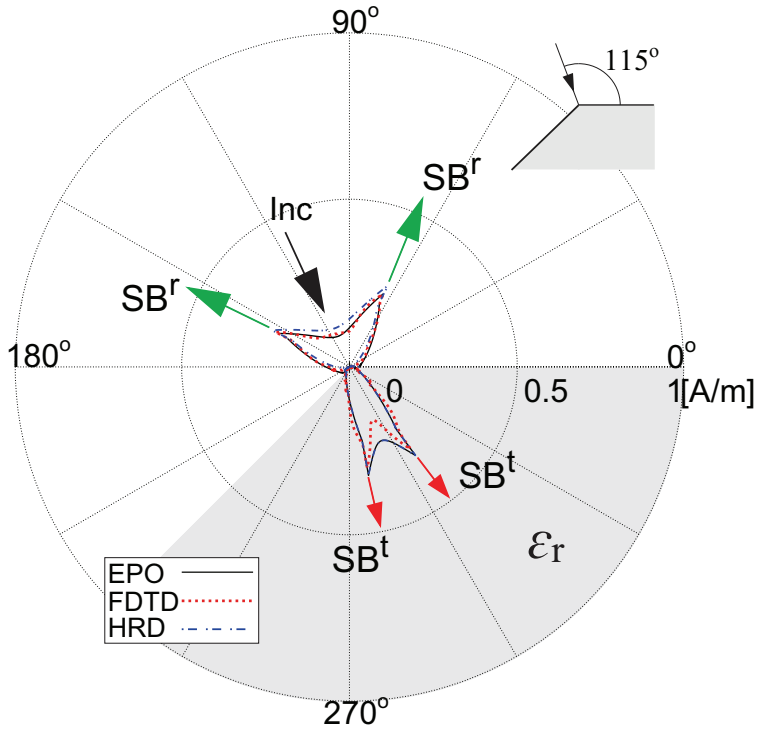

(b)

Figure 4.17: Diffracted field of dielectric wedge: $\phi_w = 225°$, $\phi_0 = 115°$, $\varepsilon_r = 6$ and $\rho = 3\lambda$. (a) TM polarization. (b) TE polarization.

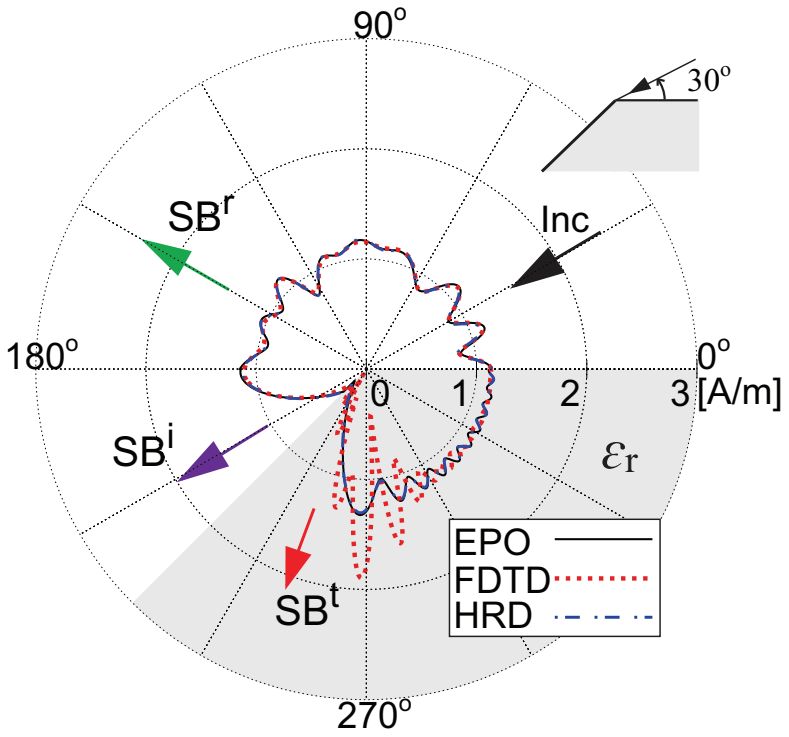

(a)

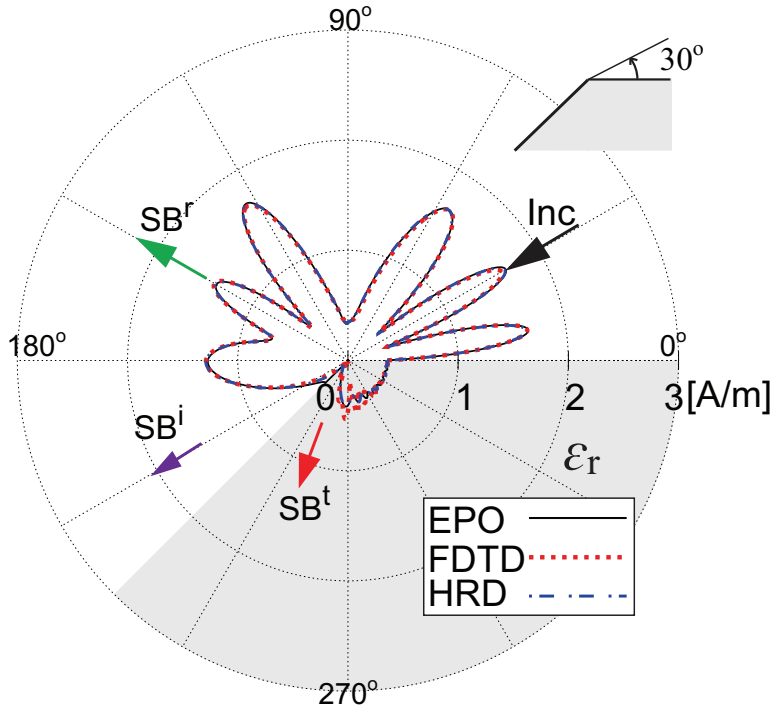

(b)

Figure 4.18: Total field of dielectric wedge: $\phi_w = 225°$, $\phi_0 = 30°$, $\varepsilon_r = 6$ and $\rho = 3\lambda$. (a) TM polarization. (b) TE polarization.

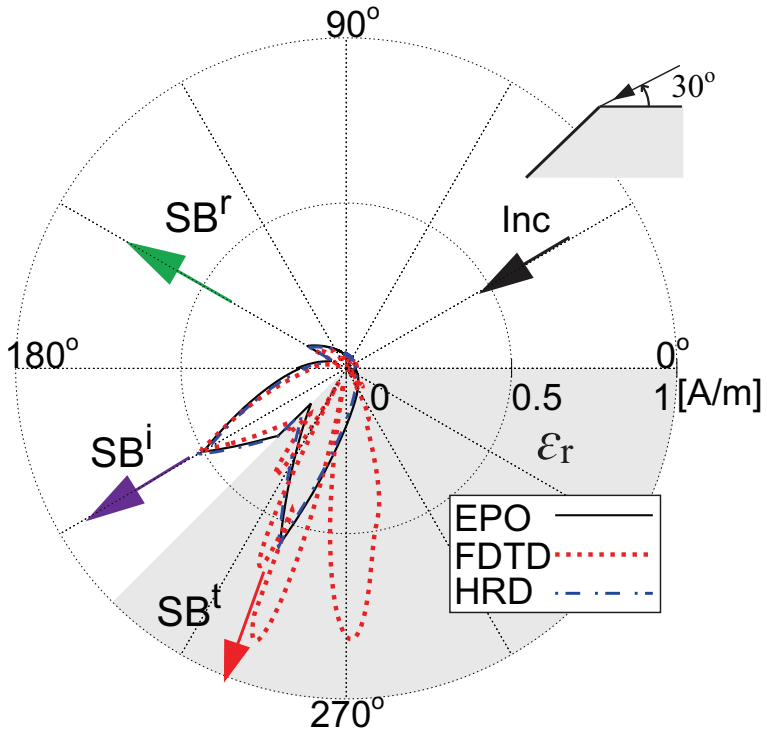

(a)

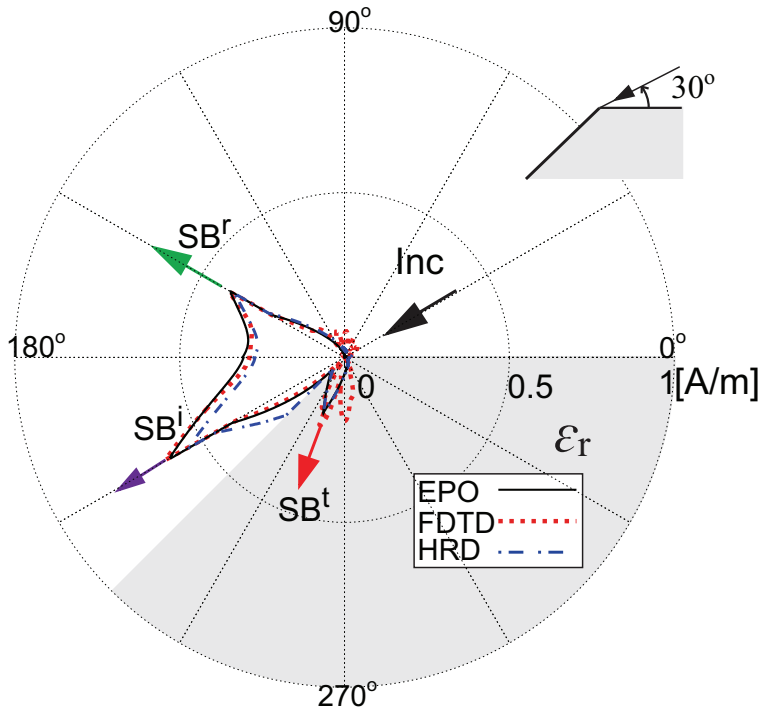

(b)

Figure 4.19: Diffracted field of dielectric wedge: $\phi_w = 225°$, $\phi_0 = 30°$, $\varepsilon_r = 6$ and $\rho = 3\lambda$. (a) TM polarization. (b) TE polarization.

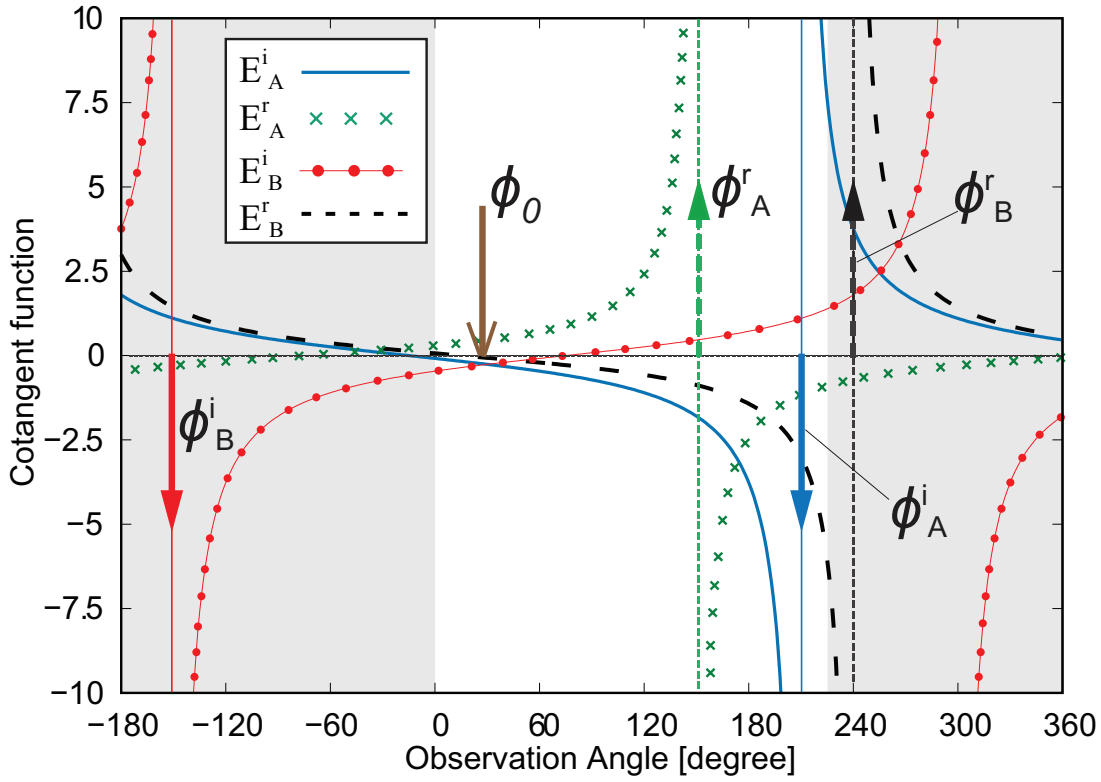

(a)

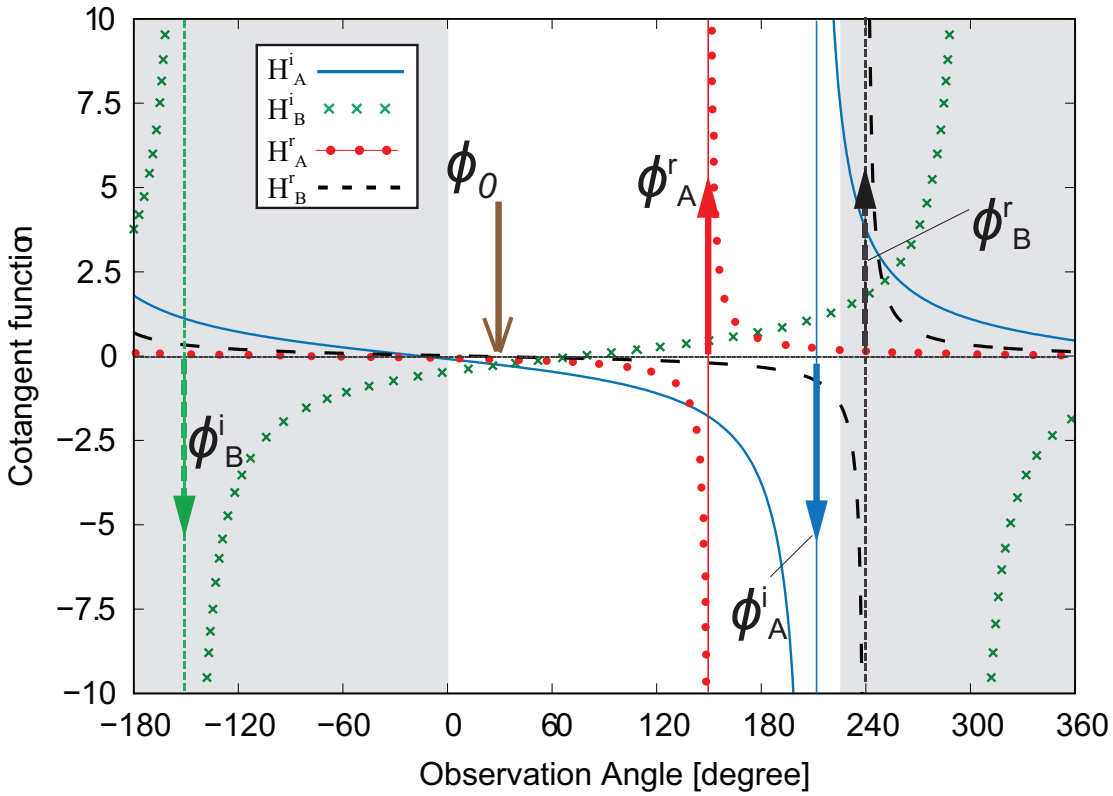

(b)

Figure 4.20: Cotangent functions outside dielectric wedge: $\phi_w = 225°$, $\phi_0 = 30°$ and $\varepsilon_r = 6$. (a) TE polarization. (b) TM polarization.

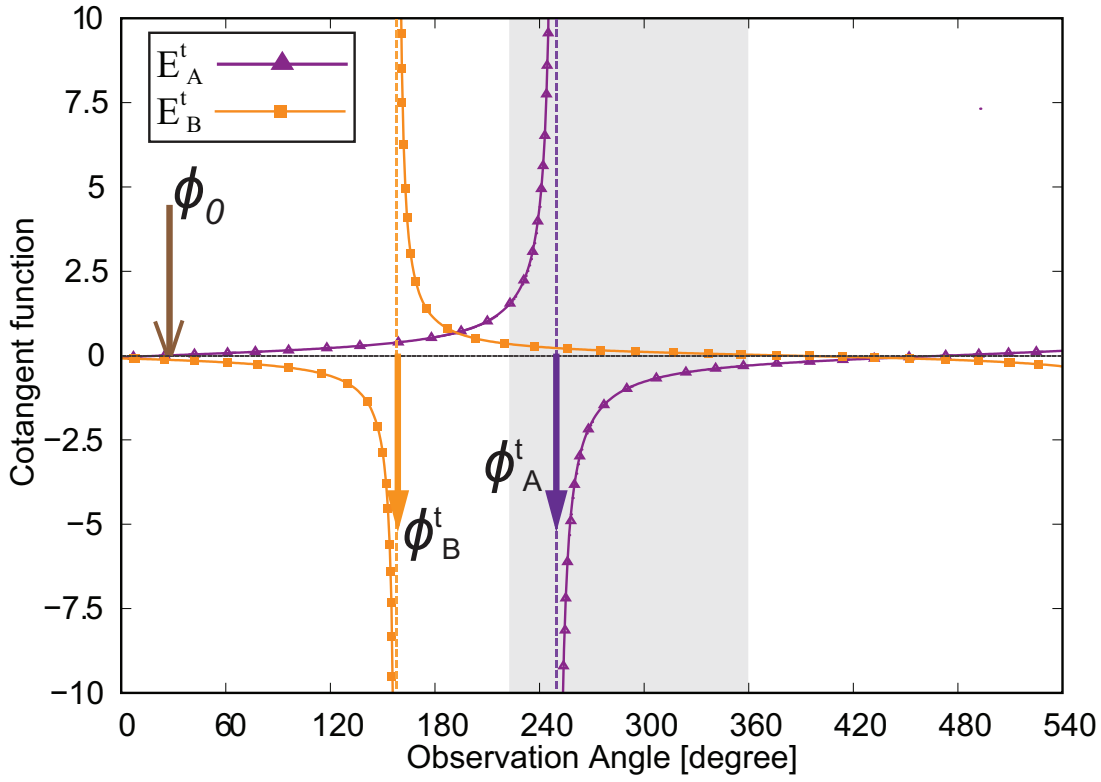

(a)

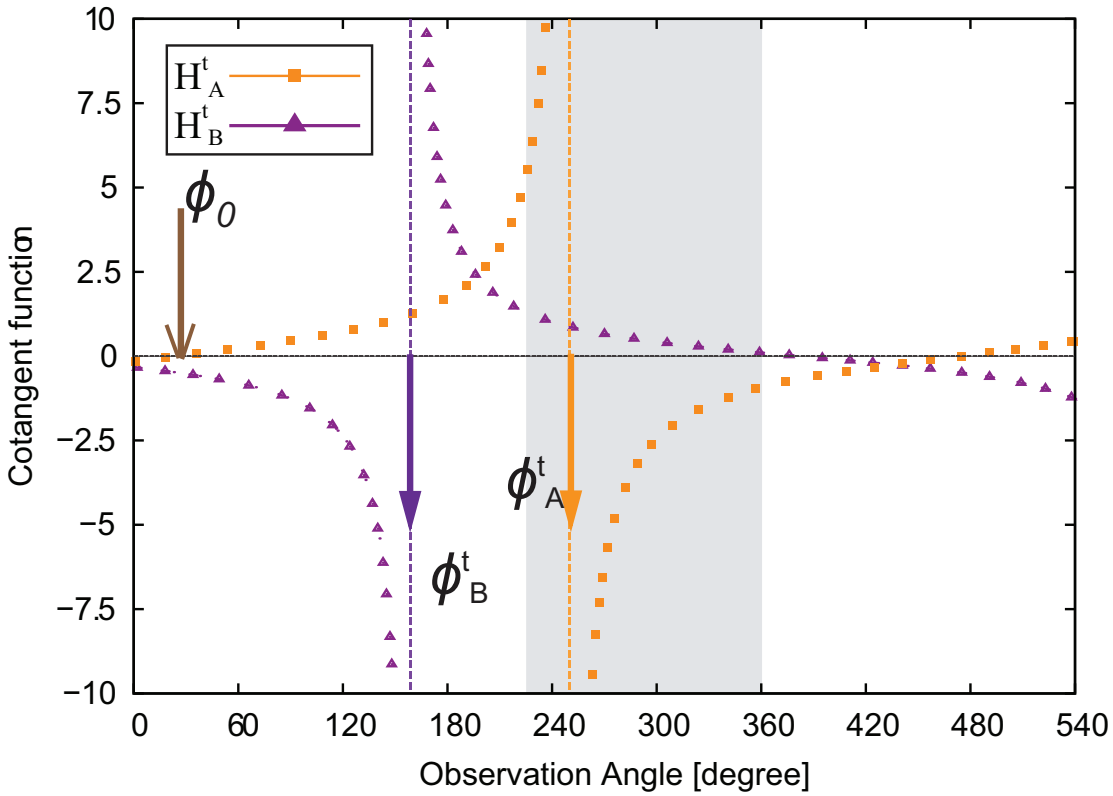

(b)

Figure 4.21: Cotangent functions inside dielectric wedge: $\phi_{\mathrm{w}} = 225°$, $\phi_0 = 30°$ and $\varepsilon_{\mathrm{r}} = 6$. (a) TE polarization. (b) TM polarization.

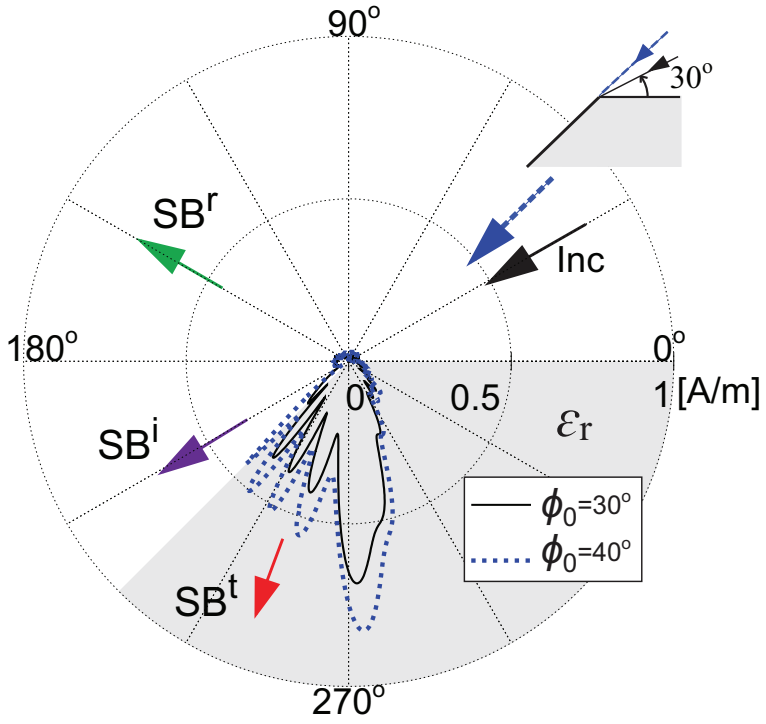

Figure 4.22: Remainder field of FDTD (TM polarization): $\phi_w = 225°$, $\varepsilon_r = 6$ and $\rho = 3\lambda$.

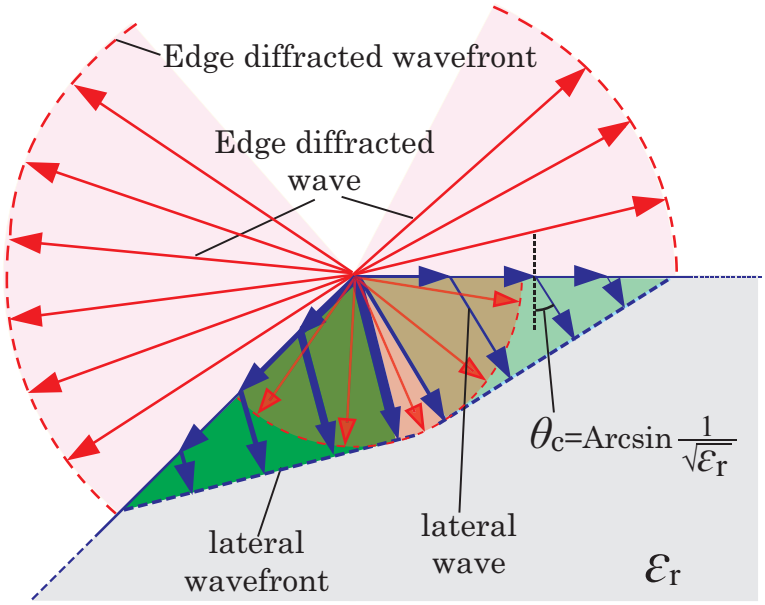

Figure 4.23: Possible lateral waves excited by edge diffracted surface waves.

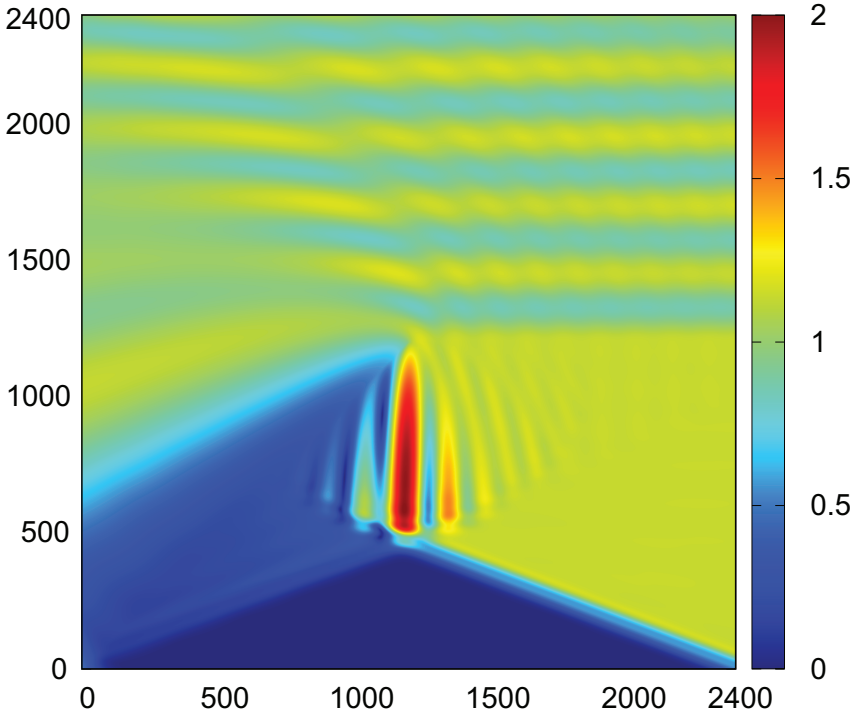

(a)

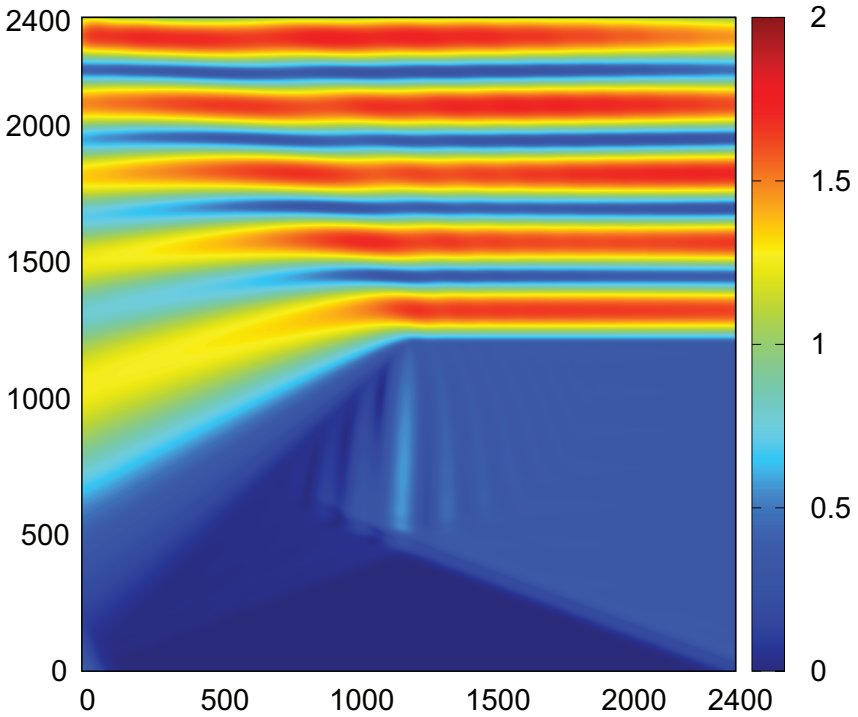

(b)

Figure 4.24: Total field distribution of dielectric wedge (FDTD): $\phi_{\mathrm{w}} = 225°$, $\phi_0 = 30°$ and $\varepsilon_{\mathrm{r}} = 6$. (a) TM polarization. (b) TE polarization.

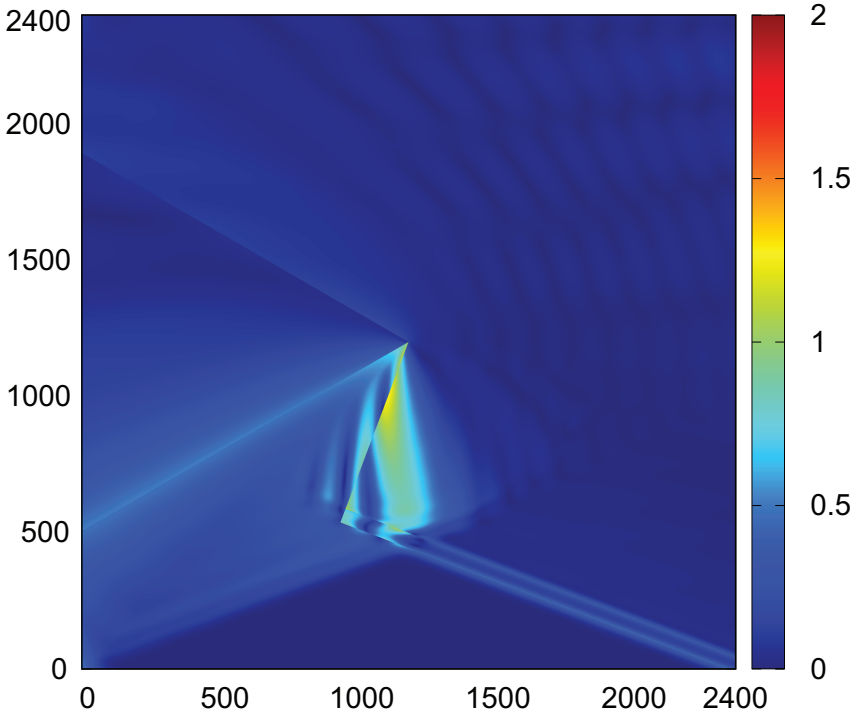

(a)

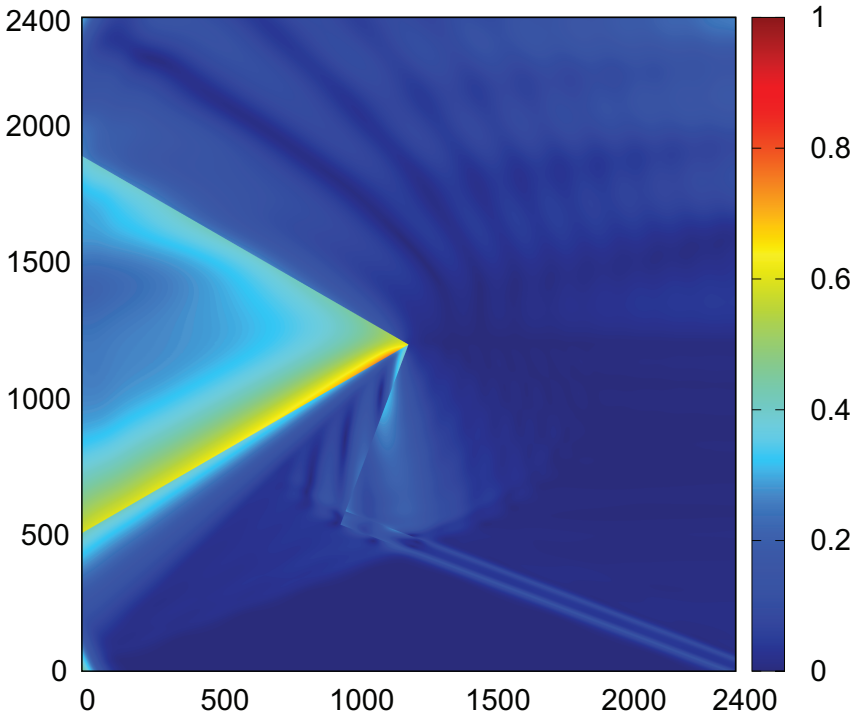

(b)

Figure 4.25: Diffracted field distribution of dielectric wedge (FDTD): $\phi_{\mathrm{w}} = 225°$, $\phi_0 = 30°$ and $\varepsilon_{\mathrm{r}} = 6$. (a) TM polarization. (b) TE polarization.

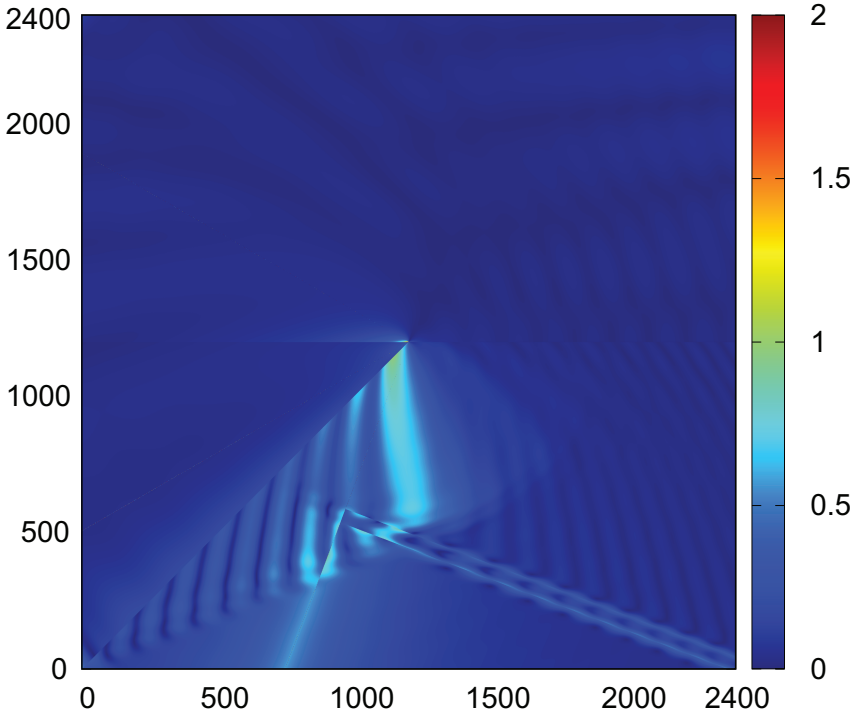

(a)

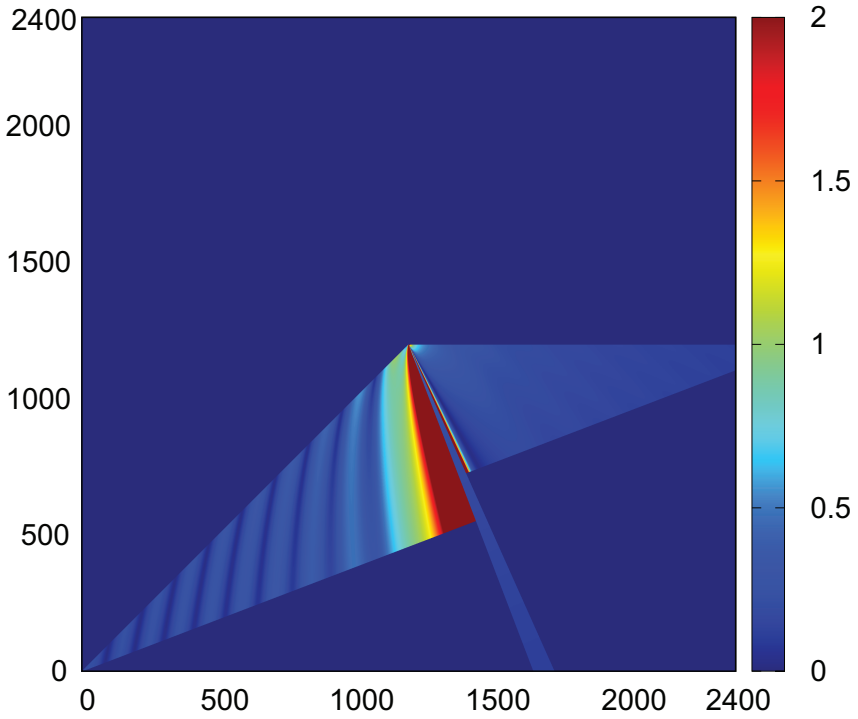

(b)

Figure 4.26: Distribution of FDTD remainder field and possible lateral wave (TM polarization): $\phi_{\mathrm{w}} = 225°$, $\phi_0 = 30°$, $\varepsilon_{\mathrm{r}} = 6$. (a) FDTD remainder field. (b) Lateral wave.

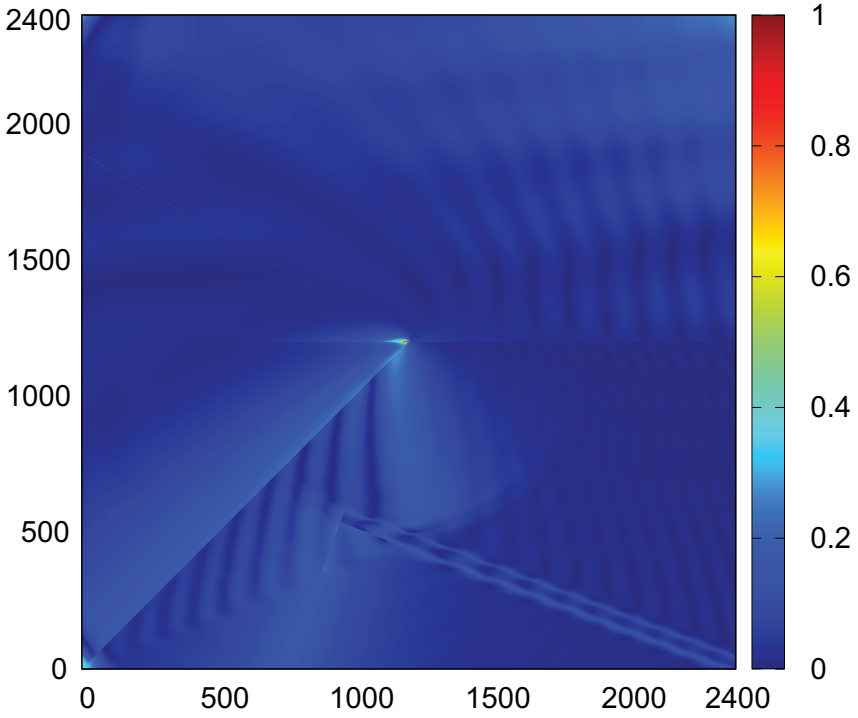

(a)

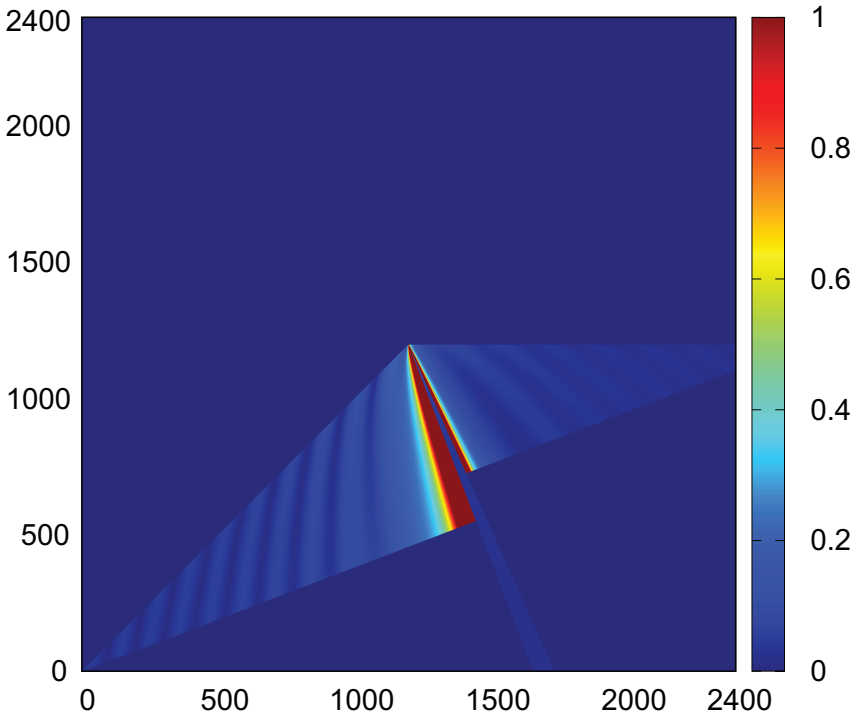

(b)

Figure 4.27: Distribution of FDTD remainder field and possible lateral wave (TE polarization): $\phi_{\mathrm{w}} = 225°$, $\phi_0 = 30°$, $\varepsilon_{\mathrm{r}} = 6$. (a) FDTD remainder field. (b) Lateral wave.

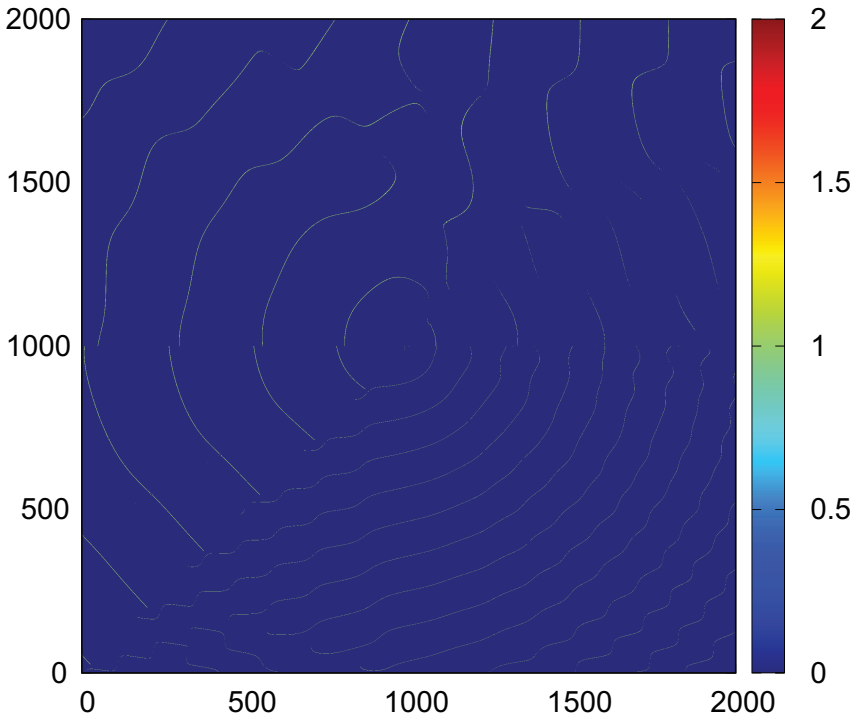

(a)

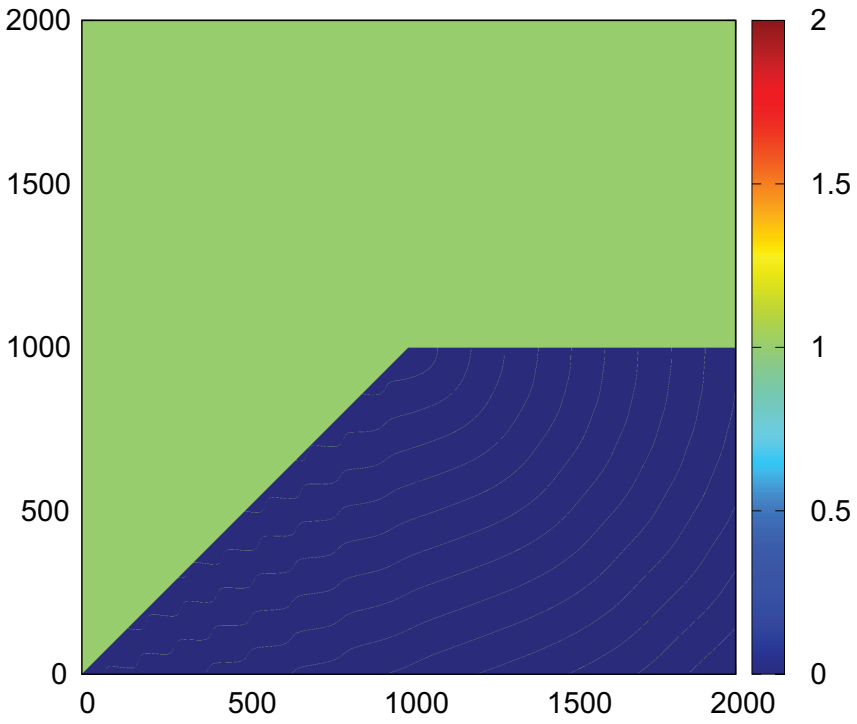

(b)

Figure 4.28: Wavefront of FDTD remainder field and possible lateral wave: $\phi_{\mathrm{w}} = 225°$, $\phi_0 = 30°$, $\varepsilon_{\mathrm{r}} = 6$. (a) FDTD remainder field. (b) Lateral wave.

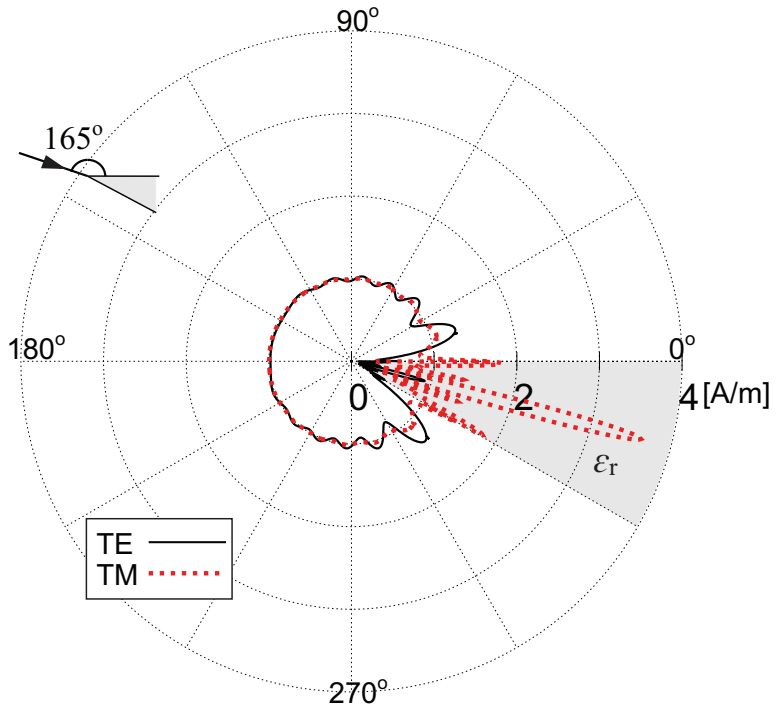

(a)

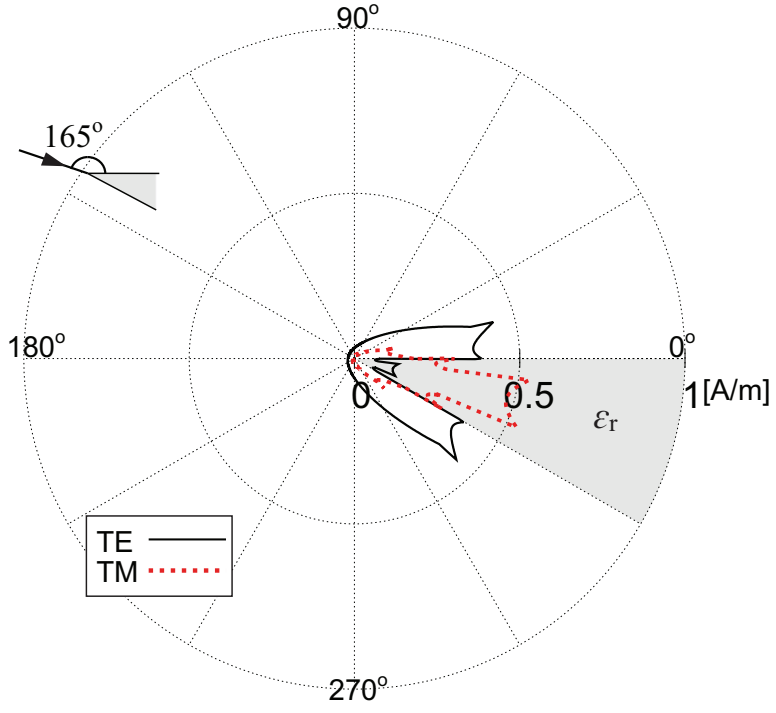

(b)

Figure 4.29: Total and diffracted fields of dielectric wedge: $\phi_w = 330°$, $\phi_0 = 165°$, $\varepsilon_r = 6$ and $\rho = 3\lambda$. (a) Total field. (b) Diffracted field.

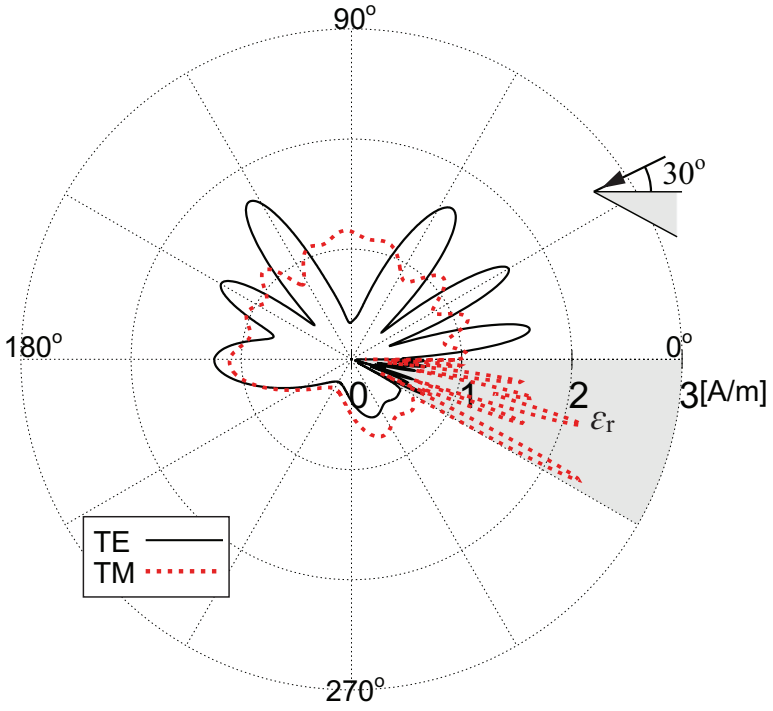

(a)

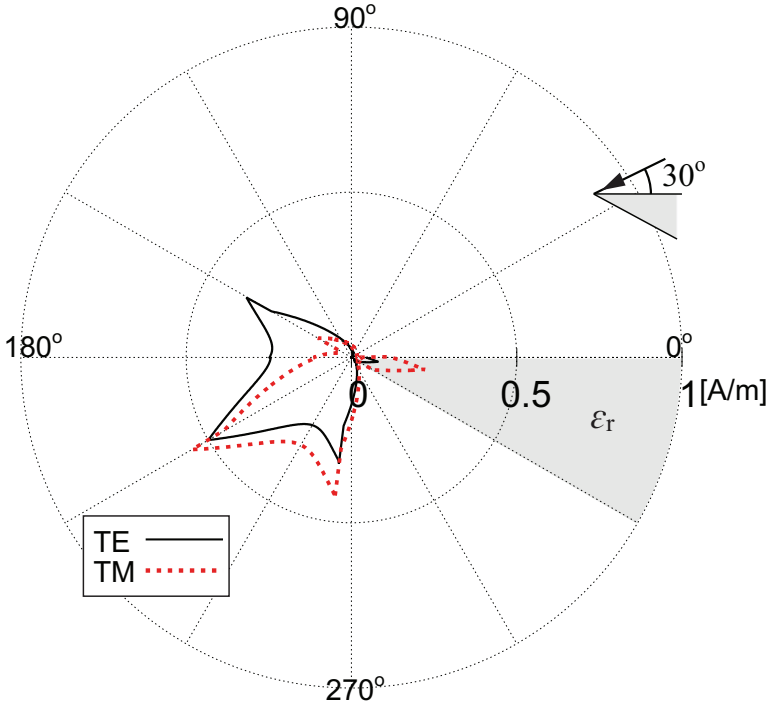

(b)

Figure 4.30: Total and diffracted fields of dielectric wedge: $\phi_w = 330°$, $\phi_0 = 30°$, $\varepsilon_r = 6$ and $\rho = 3\lambda$. (a) Total field. (b) Diffracted field.

Chapter 5

Conclusion and Future Work

5.1 Conclusion

In this thesis, the approximation solutions have been constructed based on the surface equivalence theorem for the scattering problem of the electromagnetic waves by wedges. The scattering fields by wedges can be calculated as the field radiated from the induced currents on the surfaces of the wedges.

For the PEC wedge cases, the induced currents can be approximated by the PO approximation method. Then the scattering fields can be obtained by integrating the PO currents on the illuminated surface with the two-dimensional Green's function. The obtained radiation integrals can then be solved by using the saddle point technique. The uniform asymptotic solution of the diffracted field was then expressed by different equations depending on the incident direction. To solve this calculation complication, a unified expression including four cotangent functions has been proposed. This solution is valid for all incident and observation angles.

For the scattering problem of dielectric wedge cases, an extended PO solution has been proposed by utilizing the equivalent electric and magnetic currents on the wedge's surface. These currents can be simply determined from the GO incident, reflected, and transmitted rays. The uniform asymptotic solutions were then found and represented in terms of cotangent functions.

The accuracy of EPO was then evaluated by comparing the numerical results with other reference methods. EPO has a better comparison with FDTD than HRD in the outer region of the dielectric wedge. In the inside region of the wedge, the diffracted fields of EPO and HRD yield almost the same behavior. Accordingly, EPO may be suitable for the scattering problem of the dielectric wedge without the nonphysical additional terms of HRD, and requires significantly less computational resources than FDTD. From the difference with FDTD, the lateral wave needs to be considered to enhance the accuracy of EPO and HRD inside the wedge. The accuracy change of the EPO and HRD solutions between the PEC and dielectric cases also reminds an additional consideration for the edge condition. These aspects are motivations for the next research in the future.

5.2 Future work

In order to improve the research, there are various things to do in the coming year.

- Firstly, it is necessary to find out the exact contribution of lateral wave to improve the accuracy of EPO solution for the internal field of dielectric wedge.
- On the other hand, the current calculations are performed for the lossless dielectric wedge. Thus, we need to extend the investigation for lossy materials following the same calculation process, but more complicated.
- Finally, I will extend the analytical calculation result for the other geometric shapes and the 3D scattering problems.

Appendix

A.1 Uniform Asymptotic Evaluation for Radiation Integral

A.1.1 TM polarization

In this section, the uniform asymptotic evaluation of the integral on SDP contour for TM polarization case is derived for example. As presented in Chapter 2, the diffracted magnetic field due to surface OA can be represented as integral on the SDP contour as

$$H_d^{\mathrm{A}} = \frac{\pm j}{2\pi} \int_{\mathrm{SDP}} \frac{\cos w}{\cos\phi_0 + \sin w} e^{-jk\rho\sin(w\pm\phi)} dw, \quad (\phi \lessgtr \pi). \tag{A–1}$$

Now, consider the integral $U(k\rho)$ on the SDP contour:

$$U(k\rho) = \int_{\mathrm{SDP}} p(w) e^{\Omega g(w)} dw, \tag{A–2}$$

where

$$g(w) = -j\sin(w \pm \phi), \tag{A–3}$$

$$p(w) = \frac{\cos w}{\cos\phi_0 + \sin w}, \tag{A–4}$$

$$\Omega = k\rho. \tag{A–5}$$

.

The function $p(w)$ has a simple pole singularity at $w = w_0$. In can be found from

$$\begin{aligned} & \cos\phi_0 + \sin w_0 = 0 \\ \text{as} \quad & w_0 = \phi_0 - \frac{\pi}{2} \pm 2n\pi \quad (n \in \mathbb{N}). \end{aligned} \tag{A–6}$$

Then $w_0 = \phi_0 - \pi/2$ is the pole singularity of function $p(w)$ which satisfies the condition $-\pi/2 < w_0 < \pi/2$. The function $g(w)$ has the first order saddle point w_s so that

$$\begin{aligned} & g'(w_s) = 0 \\ \text{as} \quad & -j\cos(w_s \pm \phi) = 0, \quad (\phi \lessgtr \pi) \\ \text{as} \quad & w_s = |\phi - \pi| - \frac{\pi}{2} \pm 2n\pi \quad (n \in \mathbb{N}). \end{aligned} \tag{A–7}$$

Then $w_s = |\phi - \pi| - \pi/2$ is the saddle point which satisfies the condition $-\pi/2 < w_s < \pi/2$. If the pole w_0 is near the saddle point w_s, the asymptotic approximation of the integral

$U(k\rho)$, valid uniformly as $w_0 \to w_s$, is given by

$$U(k\rho) \sim e^{\Omega g(w_s)} \left\{ \pm j2c\sqrt{\pi} e^{-\Omega d^2} Q(\mp jd\sqrt{\Omega}) + \sqrt{\frac{\pi}{\Omega}} R(0) \right\}, \quad Im(d) \gtrless 0, \tag{A–8}$$

where

$$R(0) = vf(w_s) + \frac{c}{d}, \tag{A–9}$$

$$Q(y) = \int_y^\infty e^{-x^2} dx, \tag{A–10}$$

and

$$\begin{aligned} c = &\lim_{w \to w_0} [(w - w_0) f(w)] = \lim_{w \to w_0} \frac{\cos w(w - w_0)}{\cos \phi_0 + \sin w} \\ = &\lim_{w \to w_0} \frac{\cos w(w - w_0)}{\sin w - \sin w_0} = \frac{\cos w_0}{\lim\limits_{w \to w_0} \dfrac{\sin w - \sin w_0}{w - w_0}} \\ = &\frac{\cos w_0}{\cos w_0} = 1. \end{aligned} \tag{A–11}$$

one also has

$$\begin{aligned} d = &\sqrt{g(w_s) - g(w_0)} = \sqrt{-j + j \sin(\phi_0 - \pi/2 \pm \phi)} \\ = &\sqrt{-j - j \cos(|\phi| + \phi_0)} = \sqrt{-j2 \cos^2 \{(\phi_0 \pm \phi)/2\}} \\ = &\pm \sqrt{2} \left| \cos \frac{\phi_0 \pm \phi}{2} \right| e^{-j\pi/4}, \quad (\phi \lessgtr \pi) \end{aligned} \tag{A–12}$$

and

$$v = \sqrt{\frac{-2}{g''(w_s)}} = \sqrt{\frac{-2}{j}} = \sqrt{2} e^{j\pi/4}. \tag{A–13}$$

The $\mathrm{Arg}(d)$ is defined so that $d \to (w_0 - w_s)/v$ as $w_0 \to w_s$. Then, one has two cases:
When $w_0 - w_s \gtrless 0$ or $\phi_0 \gtrless |\phi - \pi|$,

$$\begin{aligned} & & \cos \frac{\phi_0 \pm \phi}{2} \lessgtr 0 \\ \text{as} & & d = -\sqrt{2} \cos \left\{ \frac{\phi_0 \pm \phi}{2} \right\} e^{-j\pi/4}, \end{aligned} \tag{A–14}$$

and when $w_0 - w_s < 0$ or $\phi_0 < |\phi - \pi|$,

$$\begin{aligned} & & \cos \frac{\phi_0 \pm \phi}{2} > 0 \\ \text{as} & & d = -\sqrt{2} \cos \left\{ \frac{\phi_0 \pm \phi}{2} \right\} e^{-j\pi/4}. \end{aligned} \tag{A–15}$$

Finally, one gets

$$\begin{aligned} d = &- \sqrt{2} \cos \left\{ \frac{\phi_0 \pm \phi}{2} \right\} e^{-j\pi/4} \quad (\phi_0 \gtrless |\phi - \pi|) \\ = &(-1 + j) \cos \left\{ \frac{\phi_0 \pm \phi}{2} \right\}. \quad (\phi \lessgtr \pi) \end{aligned} \tag{A–16}$$

From Eq.(A–16), $\Im\mathrm{m}(d) \gtrless 0 \Leftrightarrow \phi_0 \lesseqgtr |\phi - \pi|$. Then the function $Q(\mp jb\sqrt{\Omega})$ can be represented as

$$\begin{aligned} Q(\mp jd\sqrt{\Omega}) =& Q\left[\mp j(-1+j)\cos\left\{\frac{\phi_0 \pm \phi}{2}\right\}\sqrt{\Omega}\right], \quad (\phi_0 \lesseqgtr |\phi - \pi|) \\ =& Q\left[\pm(1+j)\cos\left\{\frac{\phi_0 \pm \phi}{2}\right\}\sqrt{\Omega}\right], \quad (\phi_0 \lesseqgtr |\phi - \pi|) \\ =& Q\left[(1+j)\left|\cos\left\{\frac{\phi_0 \pm \phi}{2}\right\}\right|\sqrt{\Omega}\right], \quad (\phi_0 \lesseqgtr |\phi - \pi|). \end{aligned} \tag{A–17}$$

From Eqs.(A–11), (A–13), (A–16) and (A–17), the asymptotic approximation of the integral $U(k\rho)$ can be derived as

$$\begin{aligned} U(k\rho) \sim& \pm e^{-jk\rho} j2\sqrt{\pi} e^{jk\rho + jk\rho\cos(\phi_0 \pm \phi)} Q\left[(1+j)\left|\cos\left\{\frac{\phi_0 \pm \phi}{2}\right\}\right|\sqrt{k\rho}\right] \\ &+ e^{-jk\rho}\sqrt{\frac{\pi}{k\rho}}\left(\frac{\sqrt{2}e^{j\pi/4}\sin|\phi-\pi|}{\cos\phi_0 + \cos\phi} - \frac{e^{j\pi/4}}{\sqrt{2}\cos\{(\phi_0 \pm \phi)/2\}}\right), \quad (\phi_0 \lesseqgtr |\phi - \pi|), \\ =& \mathrm{sgn}(\pi - \phi_0 \mp \phi) 2j\sqrt{\pi} e^{jk\rho\cos(\phi_0 \pm \phi)} Q\left[(1+j)\left|\cos\left\{\frac{\phi_0 \pm \phi}{2}\right\}\right|\sqrt{k\rho}\right] \\ &+ e^{-jk\rho + j\pi/4}\sqrt{\frac{2\pi}{k\rho}}\left(\frac{\sin|\phi-\pi|}{\cos\phi_0 + \cos\phi} - \frac{1}{2\cos\{(\phi_0 \pm \phi)/2\}}\right). \end{aligned} \tag{A–18}$$

Then from Eq.(A–18) and Eq.(A–1), one obtains

$$\begin{aligned} H_d =& \frac{\pm j}{2\pi} U(k\rho), \quad (\phi \lesseqgtr \pi) \\ \sim& \mp \frac{1}{\sqrt{\pi}} e^{jk\rho\cos(\phi_0 \pm \phi)} \mathrm{sgn}(\pi - \phi_0 \mp \phi) Q\left[(1+j)\left|\cos\{\frac{\phi_0 \pm \phi}{2}\}\right|\sqrt{k\rho}\right] \\ &\mp e^{-jk\rho - j\pi/4}\sqrt{\frac{1}{8\pi k\rho}}\left(\frac{2\sin|\phi-\pi|}{\cos\phi + \cos\phi_0} - \frac{1}{\cos\{(\phi_0 \pm \phi)/2\}}\right), \quad (\phi \lesseqgtr \pi) \\ =& \mp \frac{1}{\sqrt{\pi}} e^{jk\rho\cos(\phi_0 \pm \phi)} \mathrm{sgn}(\pi - \phi_0 \mp \phi) Q\left[(1+j)\left|\cos\{\frac{\phi_0 \pm \phi}{2}\}\right|\sqrt{k\rho}\right] \\ &- C(k\rho)\left(\frac{2\sin\phi}{\cos\phi + \cos\phi_0} \mp \frac{1}{\cos\{(\phi_0 \pm \phi)/2\}}\right), \quad (\phi \lesseqgtr \pi). \end{aligned} \tag{A–19}$$

The complementary error-function Q in Eq.(A–19) can be expressed in term of the well-tabulated Fresnel integrals $C(x)$ ans $S(x)$ as

$$Q[(1+j)\xi] = \frac{\sqrt{\pi}}{2} - \sqrt{\frac{\pi}{2}}\left[C\left(\frac{2\xi}{\sqrt{\pi}}\right) - jS\left(\frac{2\xi}{\sqrt{\pi}}\right)\right], \tag{A–20}$$

where

$$C(x) = \int_0^x \cos\left(\frac{\pi}{2}t^2\right) dt, \quad S(x) = \int_0^x \sin\left(\frac{\pi}{2}t^2\right) dt. \tag{A–21}$$

A.2 TE polarization

For TE polarization, the diffracted electric field can be represented as

$$E_d^{\mathrm{A}} = -\frac{j}{2\pi}\sin\phi_0 \int_{\mathrm{SDP}} \frac{e^{-jk\rho\sin(w\pm\phi)}}{\cos\phi_0+\sin w}dw, \tag{A–22}$$

Now, consider the integral $I(k\rho)$ on the SDP contour:

$$I(k\rho) = \int_{\mathrm{SDP}} f(w)e^{\Omega q(w)}dw, \tag{A–23}$$

where

$$q(w) = -j\sin(w\pm\phi), \tag{A–24}$$

$$f(w) = \frac{1}{\cos\phi_0+\sin w}, \tag{A–25}$$

$$\Omega = k\rho. \tag{A–26}$$

.

The function $f(w)$ has a simple pole singularity at $w = w_0$. It can be found from

$$\begin{aligned} &\cos\phi_0+\sin w_0 = 0 \\ \text{as}\qquad &w_0 = \phi_0 - \frac{\pi}{2} \pm 2n\pi \quad (n\in\mathbb{N}). \end{aligned} \tag{A–27}$$

Then $w_0 = \phi_0 - \pi/2$ is the pole singularity of function $f(w)$ which satisfies the condition $-\pi/2 < w_0 < \pi/2$. The function $q(w)$ has the first order saddle point w_s so that

$$\begin{aligned} &q'(w_s) = 0 \\ \text{as}\qquad &-j\cos(w_s\pm\phi) = 0 \\ \text{as}\qquad &w_s = |\phi-\pi| - \frac{\pi}{2} \pm 2n\pi \quad (n\in\mathbb{N}). \end{aligned} \tag{A–28}$$

Then $w_s = |\phi-\pi|-\pi/2$ is the saddle point which satisfies the condition $-\pi/2 < w_s < \pi/2$. If the pole w_0 is near the saddle point w_s, the asymptotic approximation of the integral $I(k\rho)$, valid uniformly as $w_0 \to w_s$, is given by

$$I(k\rho) \sim e^{\Omega q(w_s)}\left\{\pm j2a\sqrt{\pi}e^{-\Omega b^2}Q(\mp jb\sqrt{\Omega}) + \sqrt{\frac{\pi}{\Omega}}T(0)\right\}, \quad Im(b) \gtrless 0, \tag{A–29}$$

where

$$T(0) = hf(w_s) + \frac{a}{b}, \tag{A–30}$$

$$Q(y) = \int_y^\infty e^{-x^2}dx, \tag{A–31}$$

and

$$\begin{aligned} a &= \lim_{w\to w_0}[(w-w_0)f(w)] = \lim_{w\to w_0}\frac{w-w_0}{\cos\phi_0+\sin w} \\ &= \lim_{w\to w_0}\frac{w-w_0}{\sin w-\sin w_0} = \frac{1}{\lim\limits_{w\to w_0}\dfrac{\sin w-\sin w_0}{w-w_0}} \\ &= \frac{1}{\cos w_0} = \frac{1}{\sin\phi_0}. \end{aligned} \tag{A–32}$$

One also has

$$\begin{aligned} b =& \sqrt{q(w_s) - q(w_0)} = \sqrt{-j + j\sin(\phi_0 - \pi/2 \pm \phi)} \\ =& \sqrt{-j - j\cos(|\phi| + \phi_0)} = \sqrt{-j2\cos^2\{(\phi_0 \pm \phi)/2\}} \\ =& \pm\sqrt{2}\left|\cos\frac{\phi_0 \pm \phi}{2}\right| e^{-j\pi/4}, \quad (\phi \lessgtr \pi) \end{aligned} \tag{A–33}$$

and

$$h = \sqrt{\frac{-2}{q''(w_s)}} = \sqrt{\frac{-2}{j}} = \sqrt{2}e^{j\pi/4}. \tag{A–34}$$

The $\mathrm{Arg}(b)$ is defined so that $b \to (w_0 - w_s)/h$ as $w_0 \to w_s$. Then one has two cases:
When $w_0 - w_s \geqslant 0$ or $\phi_0 \geqslant |\phi - \pi|$,

$$\begin{aligned} & \cos\frac{\phi_0 \pm \phi}{2} \leqslant 0 \\ \text{as} \qquad & d = -\sqrt{2}\cos\left\{\frac{\phi_0 \pm \phi}{2}\right\} e^{-j\pi/4}, \end{aligned} \tag{A–35}$$

and when $w_0 - w_s < 0$ or $\phi_0 < |\phi - \pi|$,

$$\begin{aligned} & \cos\frac{\phi_0 \pm \phi}{2} > 0 \\ \text{as} \qquad & d = -\sqrt{2}\cos\left\{\frac{\phi_0 \pm \phi}{2}\right\} e^{-j\pi/4}. \end{aligned} \tag{A–36}$$

Finally, one gets

$$\begin{aligned} b =& -\sqrt{2}\cos\left\{\frac{\phi_0 \pm \phi}{2}\right\} e^{-j\pi/4} \quad (\phi_0 \gtrless |\phi - \pi|) \\ =& (-1 + j)\cos\left\{\frac{\phi_0 \pm \phi}{2}\right\}. \quad (\phi \lessgtr \pi) \end{aligned} \tag{A–37}$$

From Eq.(A–37), $\Im\mathrm{m}(d) \gtrless 0 \Leftrightarrow \phi_0 \lessgtr |\phi - \pi|$. Then the function $Q(\mp jb\sqrt{\Omega})$ can be represented as

$$\begin{aligned} Q(\mp jb\sqrt{\Omega}) =& Q\left[\mp j(-1 + j)\cos\left\{\frac{\phi_0 \pm \phi}{2}\right\}\sqrt{\Omega}\right], \quad (\phi_0 \lessgtr |\phi - \pi|) \\ =& Q\left[\pm(1 + j)\cos\left\{\frac{\phi_0 \pm \phi}{2}\right\}\sqrt{\Omega}\right], \quad (\phi_0 \lessgtr |\phi - \pi|) \\ =& Q\left[(1 + j)\left|\cos\left\{\frac{\phi_0 \pm \phi}{2}\right\}\right|\sqrt{\Omega}\right], \quad (\phi_0 \lessgtr |\phi - \pi|). \end{aligned} \tag{A–38}$$

From Eqs.(A–32), (A–34), (A–37) and (A–38), the asymptotic approximation of the in-

tegral $I(k\rho)$ can be derived as

$$
\begin{aligned}
I(k\rho) \sim & \pm e^{-jk\rho} j \frac{2\sqrt{\pi}}{\sin\phi_0} e^{jk\rho + jk\rho\cos(\phi_0 \pm \phi)} Q\left[(1+j)\left|\cos\left\{\frac{\phi_0 \pm \phi}{2}\right\}\right|\sqrt{k\rho}\right] \\
& + e^{-jk\rho}\sqrt{\frac{\pi}{k\rho}}\left(\frac{\sqrt{2}e^{j\pi/4}}{\cos\phi_0 + \cos\phi} - \frac{e^{j\pi/4}}{\sqrt{2}\sin\phi_0\cos\{(\phi_0 \pm \phi)/2\}}\right), \quad (\phi_0 \lessgtr |\phi - \pi|), \\
= & \operatorname{sgn}(\pi - \phi_0 \mp \phi)\frac{2j\sqrt{\pi}}{\sin\phi_0} e^{jk\rho\cos(\phi_0 \pm \phi)} Q\left[(1+j)\left|\cos\left\{\frac{\phi_0 \pm \phi}{2}\right\}\right|\sqrt{k\rho}\right] \\
& + e^{-jk\rho + j\pi/4}\sqrt{\frac{2\pi}{k\rho}}\left(\frac{1}{\cos\phi_0 + \cos\phi} - \frac{1}{2\sin\phi_0\cos\{(\phi_0 \pm \phi)/2\}}\right). \qquad \text{(A–39)}
\end{aligned}
$$

Then from Eq.(A–39) and Eq.(A–22), one obtains

$$
\begin{aligned}
E_d = & -\frac{j}{2\pi}\sin\phi_0 I(k\rho) \\
\sim & \frac{1}{\sqrt{\pi}} e^{jk\rho\cos(\phi_0 \pm \phi)} \operatorname{sgn}(\pi - \phi_0 \mp \phi) Q\left[(1+j)\left|\cos\{\frac{\phi_0 \pm \phi}{2}\}\right|\sqrt{k\rho}\right] \\
& + e^{-jk\rho - j\pi/4}\sqrt{\frac{1}{8\pi k\rho}}\left(\frac{2\sin\phi_0}{\cos\phi + \cos\phi_0} - \frac{1}{\cos\{(\phi_0 \pm \phi)/2\}}\right) \quad (\phi \lessgtr \pi) \\
= & \frac{1}{\sqrt{\pi}} e^{jk\rho\cos(\phi_0 \pm \phi)} \operatorname{sgn}(\pi - \phi_0 \mp \phi) Q\left[(1+j)\left|\cos\{\frac{\phi_0 \pm \phi}{2}\}\right|\sqrt{k\rho}\right] \\
& + C(k\rho)\left(\frac{2\sin\phi_0}{\cos\phi + \cos\phi_0} - \frac{1}{\cos\{(\phi_0 \pm \phi)/2\}}\right). \quad (\phi \lessgtr \pi) \qquad \text{(A–40)}
\end{aligned}
$$

A.3 Hidden Rays of Diffraction

It is well known that the diffracted field of the PO approximation method doesn't satisfy the boundary and edge conditions. To correct the error of PO, the HRD solution was then proposed to satisfy the boundary and edge conditions for the PEC wedge cases. In this solution, additional hidden diffracted rays have been traced in the non-physical domain. The contribution of these rays can compensate for the shortcoming of PO at the boundary of the wedge. For TM polarization, the HRD solution of diffracted fields in the outer and inner regions of a two-dimensional dielectric wedge can be represented as:

$$
\begin{aligned}
\bar{H}^+ = & -C(k\rho) \\
& \cdot \Bigg[\frac{1}{n}\cot\frac{\pi - (\phi - \phi_0)}{2n} + S^-(\phi - \phi_0)U(\phi - \pi) \\
& + \frac{1}{n}\cot\frac{\pi + (\phi - \phi_0)}{2n} + S^+(\phi - \phi_0)U(\phi_{\mathrm{w}} - \pi - \phi) \\
& + \frac{\Gamma'_{\mathrm{A}}}{n}\cot\frac{\pi - (\phi + \phi_0)}{2n} + \Gamma'_{\mathrm{A}} S^-(\phi + \phi_0)U(\pi - \phi) \\
& + \frac{\Gamma'_{\mathrm{B}}}{n}\cot\frac{\pi + (\phi + \phi_0 - 2\phi_{\mathrm{w}})}{2n} + \Gamma'_{\mathrm{B}} S^+(\phi_0 + \phi - 2\phi_{\mathrm{w}}) \\
& \cdot U(\phi + \pi - \phi_{\mathrm{w}})\Bigg], \qquad \text{(A–41)}
\end{aligned}
$$

$$\bar{H}^{-} = -C(k_1\rho) \cdot \left[\frac{\mathrm{T}'_{\mathrm{A}}}{n} \cot \frac{\phi - \phi^{\mathrm{t}}_{\mathrm{A}}}{2n} - \mathrm{T}'_{\mathrm{A}} S^{-}(\pi - \phi^{\mathrm{t}}_{\mathrm{A}} + \phi) U(\phi - \phi_{\mathrm{w}}) - \frac{\mathrm{T}'_{\mathrm{B}}}{n} \cot \frac{\phi - \phi^{\mathrm{t}}_{\mathrm{B}}}{2n} - \mathrm{T}'_{\mathrm{B}} S^{-}(\phi^{\mathrm{t}}_{\mathrm{B}} + \pi - \phi) U(\phi - \phi_{\mathrm{w}}) \right], \tag{A–42}$$

where the corresponding reflection coefficients Γ'_{A} and Γ'_{B} of surfaces OA and OB are given by

$$\Gamma'_{\mathrm{A}} = \frac{\varepsilon_{\mathrm{r}} |\sin\phi_0| - \sqrt{\varepsilon_{\mathrm{r}} - \cos^2\phi_0}}{\varepsilon_{\mathrm{r}} |\sin\phi_0| + \sqrt{\varepsilon_{\mathrm{r}} - \cos^2\phi_0}} \tag{A–43}$$

$$\Gamma'_{\mathrm{B}} = \frac{\varepsilon_{\mathrm{r}} |\sin(\phi_0 + \pi - \phi_{\mathrm{w}})| - \sqrt{\varepsilon_{\mathrm{r}} - \cos^2(\phi_0 + \pi - \phi_{\mathrm{w}})}}{\varepsilon_{\mathrm{r}} |\sin(\phi_0 + \pi - \phi_{\mathrm{w}})| + \sqrt{\varepsilon_{\mathrm{r}} - \cos^2(\phi_0 + \pi - \phi_{\mathrm{w}})}}. \tag{A–44}$$

$\mathrm{T}'_{\mathrm{A}} = 1 + \Gamma'_{\mathrm{A}}$ and $\mathrm{T}'_{\mathrm{B}} = 1 + \Gamma'_{\mathrm{B}}$ are corresponding transmission coefficients from surfaces OA and OB, respectively. Based on the edge condition, the angular period of cotangent functions has been modified, in which the parameter n is selected as the minimum positive value that satisfies:

$$\varepsilon_{\mathrm{r}} \tan\frac{-\phi_{\mathrm{w}}}{n} = \tan\frac{2\pi - \phi_{\mathrm{w}}}{n}. \tag{A–45}$$

For the PO solution, modifying the angular period based on the edge condition does not provide a significant correction to the field behavior as HRD. The formulations of HRD solution in Eqs.(A–41) and (A–42) are applicable for all directions of the incident wave. One may also need the contribution of the additional multiple diffracted fields depending on the particular cases of the wedge and incident angles.

For TE-polarized plane incident wave, the external and internal diffracted fields can also be found from Eqs.(A–41) and (A–42), in which the reflection and transmission coefficients of the TM polarization are replaced by the corresponding coefficients as:

$$\bar{\Gamma}'_{\mathrm{A}} = \frac{|\sin\phi_0| - \sqrt{\varepsilon_{\mathrm{r}} - \cos^2\phi_0}}{|\sin\phi_0| + \sqrt{\varepsilon_{\mathrm{r}} - \cos^2\phi_0}} \tag{A–46}$$

$$\bar{\Gamma}'_{\mathrm{B}} = \frac{|\sin(\phi_0 + \pi - \phi_{\mathrm{w}})| - \sqrt{\varepsilon_{\mathrm{r}} - \cos^2(\phi_0 + \pi - \phi_{\mathrm{w}})}}{|\sin(\phi_0 + \pi - \phi_{\mathrm{w}})| + \sqrt{\varepsilon_{\mathrm{r}} - \cos^2(\phi_0 + \pi - \phi_{\mathrm{w}})}} \tag{A–47}$$

$$\bar{\mathrm{T}}'_{\mathrm{A}} = 1 + \Gamma'_{\mathrm{A}} \tag{A–48}$$

$$\bar{\mathrm{T}}'_{\mathrm{B}} = 1 + \Gamma'_{\mathrm{B}}. \tag{A–49}$$

A.4 Possible Lateral Wave

Consider two-media problem with a current source located in denser media 1 as in Fig. A–1. The radiation fields excited by the current source can be derived from the two-dimensional Green's functions. The problem can then be considered in two case polarizations as follows [15].

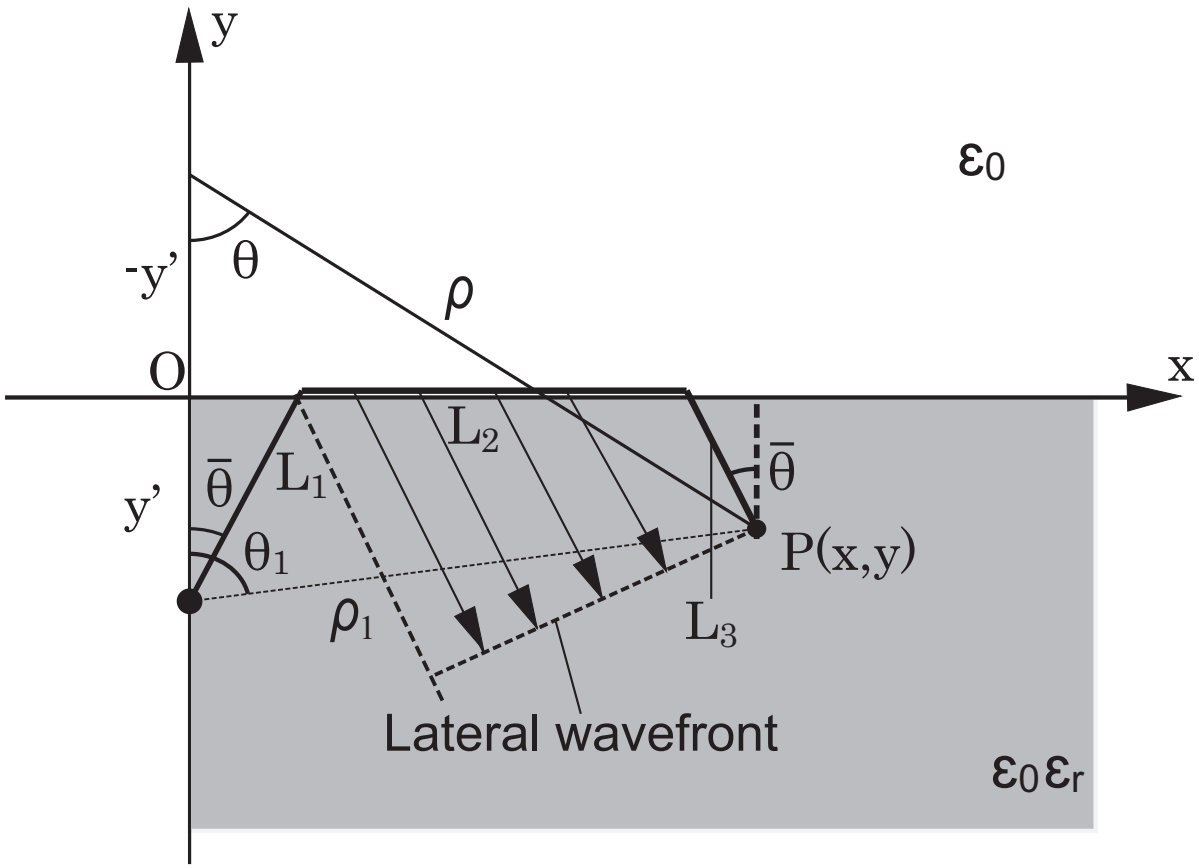

Figure A–1: Lateral wave.

A.4.1 TE polarization

For TE polarization, the radiation fields excited by the current source can be derived from the two-dimensional Green's functions, which satisfy:

$$\begin{aligned}\left(\nabla^2 + k_1^2\right) G_1(\boldsymbol{\rho}, \boldsymbol{\rho}') &= -\delta(\boldsymbol{\rho} - \boldsymbol{\rho}') \quad (y < 0) \\ \left(\nabla^2 + k_2^2\right) G_2(\boldsymbol{\rho}, \boldsymbol{\rho}') &= 0 \qquad\quad (y > 0),\end{aligned} \tag{A–50}$$

where $k_1 = \omega\sqrt{\mu\varepsilon_1}$ and $k_2 = \omega\sqrt{\mu\varepsilon_2}$ ($\varepsilon_1 = \varepsilon_0\varepsilon_r$, $\varepsilon_2 = \varepsilon_0$). Then the solution is given by: Subject to a radiation condition at infinity in both regions, and to the continuity requirements at $y = 0$:

$$G_1 = G_2, \qquad \frac{\partial G_1}{\partial y} = \frac{\partial G_2}{\partial y} \quad at \quad y = 0, \tag{A–51}$$

Then the solution is given by:

For $y < 0$ (media 1):

The radiation field can be found from Green's function G_1, which is given by:

$$G_1(\hat{\rho}, \hat{\rho}') = G_{f1}(\hat{\rho}, \hat{\rho}') + G_s(\hat{\rho}, \hat{\rho}'), \tag{A–52}$$

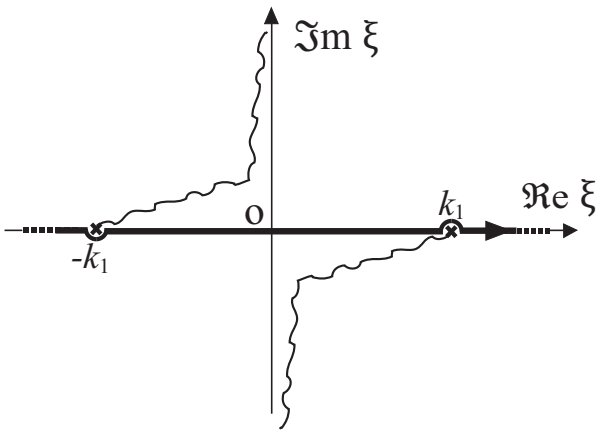

Figure A–2: Integration contours for G_{f1} integral in Eq.(A–53).

where G_{f1} is the two-dimensional free-space Green's function given by:

$$G_{f1}(x,y) = \frac{-j}{4\pi}\int_{-\infty}^{\infty} \frac{e^{-j\xi(x-x')-j\sqrt{k_1^2-\xi^2}|y-y'|}}{\sqrt{k_1^2-\xi^2}} d\xi \tag{A–53}$$

$G_s(\hat{\rho},\hat{\rho}')$ contains the interface effect and can be given by:

$$G_s(\hat{\rho},\hat{\rho}') = \frac{-j}{4\pi}\int_{-\infty}^{\infty} \frac{e^{-j\xi(x-x')+j\sqrt{k_1^2-\xi^2}(y+y')}}{\sqrt{k_1^2-\xi^2}} \Gamma(\xi) d\xi, \tag{A–54}$$

where

$$\Gamma(\xi) = \frac{\sqrt{k_1^2-\xi^2} - \sqrt{k_1^2 n-\xi^2}}{\sqrt{k_1^2-\xi^2} + \sqrt{k_1^2 n-\xi^2}} \tag{A–55}$$

with $n = \varepsilon_2/\varepsilon_1 = 1/\varepsilon_r$.

For $y > 0$ (media 2): The radiation field can be found from Green's function G_2:

$$G_2(\hat{\rho},\hat{\rho}') = \frac{-j}{4\pi}\int_{-\infty}^{\infty} \frac{e^{-j\xi(x-x')-j\sqrt{k_1^2 n-\xi^2}y+j\sqrt{k_1^2-\xi^2}y'}}{\sqrt{k_1^2-\xi^2}} \mathrm{T}(\xi) d\xi, \tag{A–56}$$

where $\mathrm{T}(\xi) = 1 + \Gamma(\xi)$. Now let us consider Green's functions in media 1 as follows:

1) Evaluation of $G_{f1}(\hat{\rho},\hat{\rho}')$:

$$G_{f1}(x,y) = \frac{-j}{4\pi}\int_{-\infty}^{\infty} \frac{e^{-j\xi(x-x')-j\sqrt{k_1^2-\xi^2}|y-y'|}}{\sqrt{k_1^2-\xi^2}} d\xi. \tag{A–57}$$

By using transformation $\xi = k_1 \sin w$ and coordinate system (ρ_1, θ_1) with $x-x' = \rho_1 \sin\theta_1$ and $|y-y'| = \rho_1 \cos\theta_1$, the integral can be rewritten as:

$$G_{f1} = \frac{-j}{4\pi}\int_{\bar{\mathrm{P}}} e^{-jk_1\rho_1\cos(w-\theta_1)} dw \tag{A–58}$$

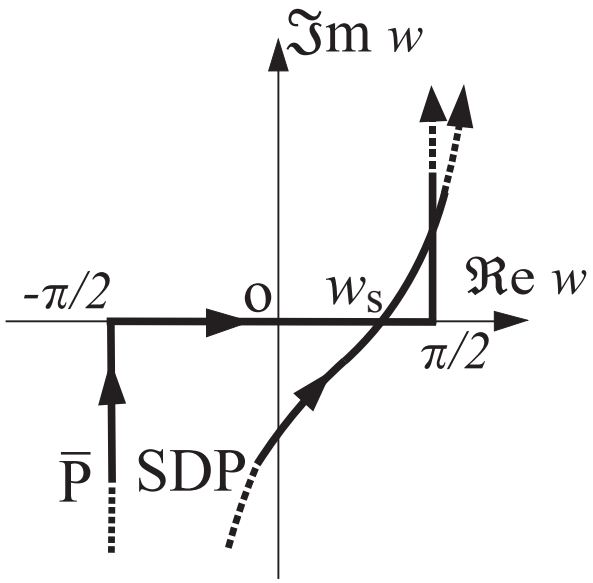

Figure A–3: Integration contours for G_{f1} integral in Eq.(A–58).

The integral in Eq.(A–58) has saddle point $w_s = \theta_1$. By saddle point technique, the integral in Eq.(A–58) can then be given by:

$$\begin{aligned} G_{f1} \approx & \frac{-j}{4\pi}\sqrt{\frac{-2\pi}{k_1\rho_1|\cos(w_s-\theta_1)|}}e^{-jk_1\rho_1\cos(w_s-\theta_1)-j\pi/4} \\ = & \frac{1}{\sqrt{8\pi k_1\rho_1}}e^{-jk_1\rho_1-j\pi/4} \end{aligned} \tag{A–59}$$

2) Evaluation of $G_s(\hat{\rho},\hat{\rho}')$:

$$G_s(\hat{\rho},\hat{\rho}') = \frac{-j}{4\pi}\int_{-\infty}^{\infty}\frac{e^{-j\xi(x-x')+j\sqrt{k_1^2-\xi^2}(y+y')}}{\sqrt{k_1^2-\xi^2}}\Gamma(\xi)d\xi. \tag{A–60}$$

Similarly, by using transformation $\xi = k_1\sin w$ and coordinate system $(\rho,\ \theta)$ with $x-x' = \rho\sin\theta$ and $y+y' = -\rho\cos\theta$, one has:

$$G_s(\hat{\rho},\hat{\rho}') = \frac{-j}{4\pi}\int_{\bar{\mathrm{P}}} e^{-jk_1\rho\cos(w-\theta)}\Gamma(k_1\sin w)dw, \tag{A–61}$$

where

$$\Gamma(k_1\sin w) = \frac{\cos w - \sqrt{n-\sin^2 w}}{\cos w + \sqrt{n-\sin^2 w}} \tag{A–62}$$

The integral in Eq.(A–61) has saddle point $w_s = \theta$ exists on the integration contour. And one may also have branch point $w_b = \mathrm{Arcsin}\sqrt{n} = \bar{\theta}$ exist on the positive imagine

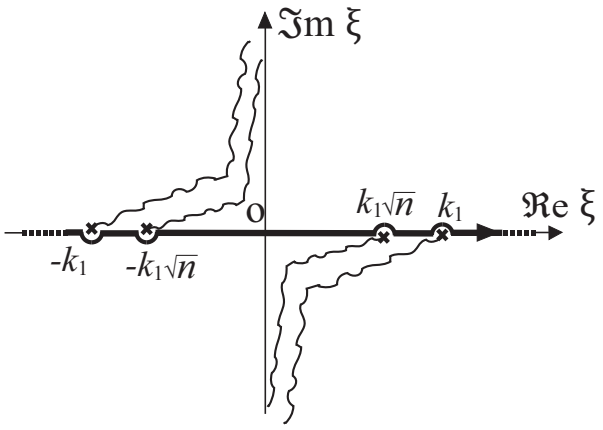

Figure A–4: Integration contours for G_s integral in Eq.(A–54).

domain. We may have the contribution from the branch point w_b when $w_s > w_b$ ($\theta > \bar{\theta}$) as in Fig. A–5. Then G_s can be given by:

$$G_s = G_{sd} + G_{sb}U(w_s - w_b) = G_{sd} + G_{sb}U(\theta - \bar{\theta}), \tag{A–63}$$

where G_{sd} is the contribution from the integral on the steepest-descent path P given by:

$$G_{sd} \approx \frac{\cos\theta - \sqrt{n - \sin^2\theta}}{\cos\theta + \sqrt{n - \sin^2\theta}} \frac{1}{\sqrt{8\pi k_1 \rho}} e^{-jk_1\rho - j\pi/4}, \tag{A–64}$$

and G_{sb} is the banch point contribution given by:

$$\begin{aligned} G_{sb} =& \frac{-j}{4\pi} \int_{\mathrm{P_b}} e^{-jk_1\rho\cos(w-\theta)} \Gamma(k_1 \sin w) dw \\ =& \frac{-j}{4\pi} \int_{\mathrm{P_b}} e^{-jk_1\rho\cos(w-\theta)} f(w) dw, \end{aligned} \tag{A–65}$$

where $f(w) = \Gamma(k_1 \sin w)$.

Now, let us consider the integral:

$$I_b = \int_{\mathrm{P_b}} f(w) e^{\Omega q(w)} dw \tag{A–66}$$

where

$$q(w) = -j\cos(w - \theta) \tag{A–67}$$

$$\Omega = k_1\rho, \tag{A–68}$$

and P_b is contour encircling the branch cut. In typical problem, $f(w)$ behaves like:

$$f(w) \cong a + b\sqrt{w - w_b}, \tag{A–69}$$

near w_b, where a and b are constants. Then we have:

$$\begin{aligned} & f'(w) = \frac{1}{2\sqrt{w - w_b}} b|_{w_b} \\ \text{as} \qquad & b = 2[\sqrt{w - w_b} f'(w)]_{w_b} \end{aligned} \tag{A–70}$$

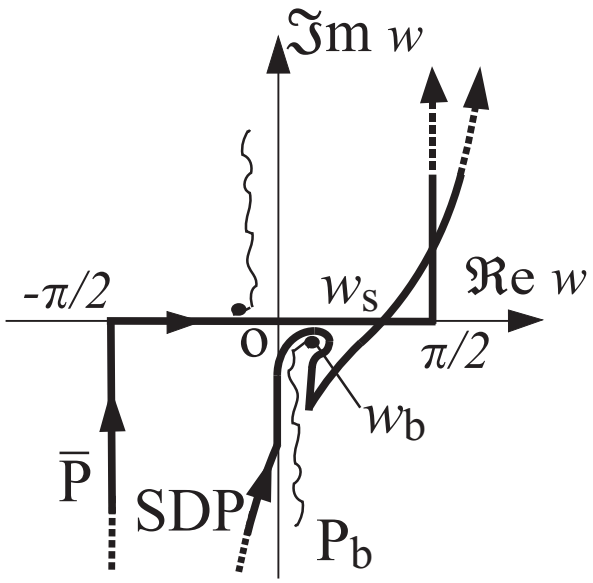

Figure A–5: Integration contours for G_s integral in Eq.(A–61).

We change variable to s ($s = 0$ when $w = w_b$) as:

$$\begin{aligned} & s^2 = q(w_b) - q(w) \\ \text{as} \quad & s^2 = -\frac{q(w) - q(w_b)}{w - w_b}(w - w_b) \\ \text{as} \quad & s^2 = -q'(w_b)(w - w_b) \\ \text{as} \quad & s = \sqrt{-q'(w_b)}\sqrt{(w - w_b)} \\ \text{as} \quad & \sqrt{(w - w_b)} = \frac{s}{\sqrt{-q'(w_b)}} \end{aligned} \tag{A–71}$$

and we have

$$\frac{dw}{ds} = \frac{2s}{-q'(w_b)} \tag{A–72}$$

so we have:

$$f(w) = a + \frac{bs}{\sqrt{-q'(w_b)}} \tag{A–73}$$

Then Eq.A–66 can be rewritten as:

$$\begin{aligned} I_b =& e^{\Omega q(w_b)} \int_{-\infty}^{\infty} f(w)\frac{dw}{ds}e^{-\Omega s^2}ds \\ =& e^{\Omega q(w_b)} \int_{-\infty}^{\infty} \left(\frac{2as}{-q'(w_b)} + \frac{2bs^2}{[-q'(w_b)]^{3/2}}\right)e^{-\Omega s^2}ds \\ =& e^{\Omega q(w_b)} \int_{-\infty}^{\infty} G(s)e^{-\Omega s^2}ds \end{aligned} \tag{A–74}$$

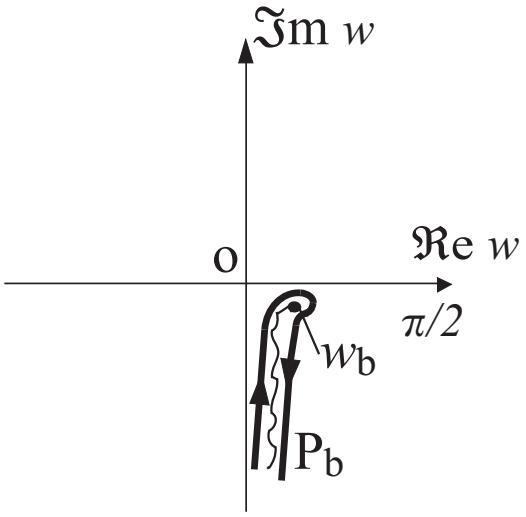

Figure A–6: Branch point contribution.

Since $G(s)$ is regular at $s = 0$, it can be expanded into a power series as:

$$G(s) = G(0) + G'(0)s + G''(0)\frac{s^2}{2!} + \cdots + G^m(0)\frac{s^m}{m!} + \cdots \tag{A–75}$$

I_b then can be written as:

$$I_b = e^{\Omega q(w_b)} \sum_{m=0}^{\infty} \frac{G^m(0)}{m!} I_m(\Omega), \tag{A–76}$$

where $I_m(\Omega) = 0$ can be evaluated in terms of the gamma function $\Gamma(x)$, in which $I_m(\Omega) = 0$ when m is odd, and

$$I_m(\Omega) = \int_{-\infty}^{\infty} s^m e^{-\Omega s^2} ds = \frac{\Gamma[(1+m)/2]}{\Omega^{(1+m)/2}} \tag{A–77}$$

when m is even. So, we have:

$$I_b = e^{\Omega q(w_b)} \frac{G''(0)}{2!} \frac{\Gamma(3/2)}{\Omega^{3/2}} \tag{A–78}$$

On the other hand $\Gamma(3/2) = \sqrt{\pi}/2$, so we have:

$$\begin{aligned} I_b =& e^{\Omega q(w_b)} \frac{\sqrt{\pi} 4b}{4[-q'(w_b)]^{3/2}} \frac{1}{\Omega^{3/2}} \\ =& e^{\Omega q(w_b)} \frac{b\sqrt{\pi}}{[-\Omega q'(w_b)]^{3/2}} \\ =& e^{\Omega q(w_b)} \frac{2\sqrt{\pi}}{[-\Omega q'(w_b)]^{3/2}} [\sqrt{w - w_b} f'(w)]|_{w_b} \\ =& \frac{2\sqrt{\pi}}{[\Omega |q'(w_b)|]^{3/2}} [\sqrt{w - w_b} f'(w)]|_{w_b} e^{\Omega q(w_b) - j\frac{3}{2}\arg[-q'(w_b)]} \end{aligned} \tag{A–79}$$

Then, one has the approximation of G_{sb} as

$$G_{sb} \approx \frac{-j}{4\pi} \frac{2\sqrt{\pi}}{[k_1 \rho \sin(\theta - w_b)]^{3/2}} \left[\sqrt{w - w_b} \frac{df(w)}{dw} \right]_{w_b} e^{-jk_1\rho\cos(w_b - \theta)} e^{j3\pi/4} \tag{A–80}$$

on the other hand, one has:

$$\frac{df(w)}{dw} = \frac{-2\sin w(n - \sin^2 w) + 2\sin w \cos^2 w}{\sqrt{n - \sin^2 w}\left(\cos w + \sqrt{n - \sin^2 w} \right)^2} \tag{A–81}$$

Then, one has

$$\begin{aligned}
\left[\sqrt{w - w_b} \frac{df(w)}{dw} \right]_{w_b} &= \lim_{w \to w_b} \left\{ \frac{\sqrt{w - w_b}}{\sqrt{n - \sin^2 w}} \frac{-2\sin w(n - \sin^2 w) + 2\sin w \cos^2 w}{\left(\cos w + \sqrt{n - \sin^2 w} \right)^2} \right\} \\
&= \frac{2\sin w_b \cos^2 w_b}{\cos^2 w_b} e^{-j\pi/2} \lim_{w \to w_b} \frac{\sqrt{w - w_b}}{\sqrt{\sin^2 w - \sin^2 w_b}} \\
&= 2\sin w_b e^{-j\pi/2} \sqrt{\frac{1}{\lim\limits_{w \to w_b} \dfrac{\sin^2 w - \sin^2 w_b}{w - w_b}}} \\
&= \frac{2\sin w_b e^{-j\pi/2}}{\sqrt{2\sin w_b \cos w_b}} = \frac{\sqrt{2}\sqrt{\sin w_b} e^{-j\pi/2}}{\sqrt{\cos w_b}} = \sqrt{2} e^{-j\pi/2} \left(\frac{n}{1 - n} \right)^{1/4}
\end{aligned} \tag{A–82}$$

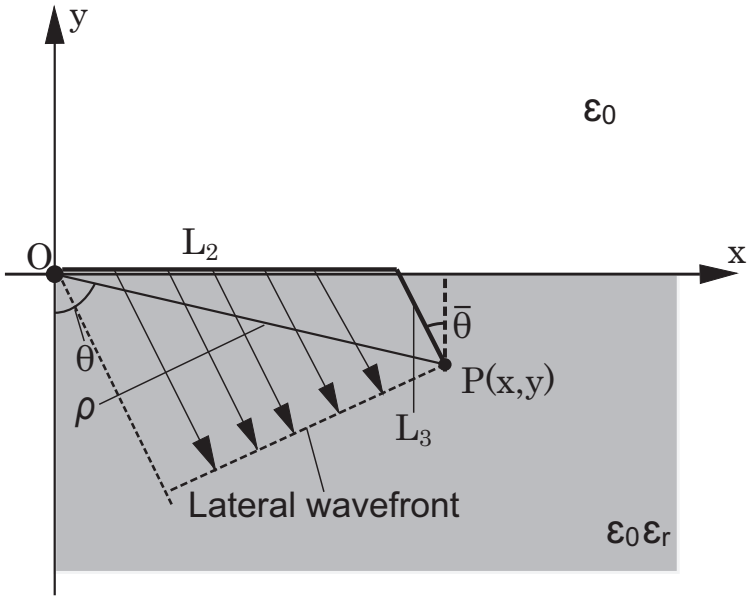

Figure A–7: Lateral wave when $y' = 0$.

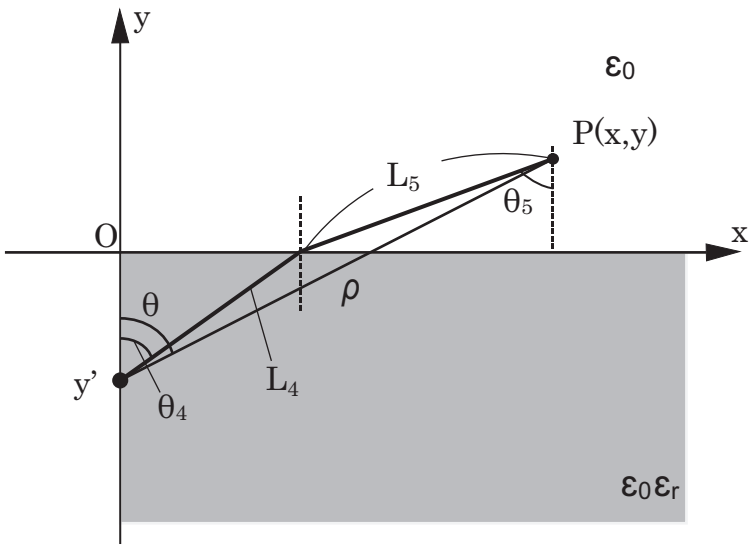

Figure A–8: Media 2.

Then, the lateral wave contribution from branch point can be written as:

$$\begin{aligned} G_{sb} \approx & \frac{-j}{4\pi} \frac{2\sqrt{\pi}}{\left[k_1\rho\sin(\theta-\bar{\theta})\right]^{3/2}} \sqrt{2} e^{-j\pi/2} \left(\frac{n}{1-n}\right)^{1/4} e^{-jk_1\rho\cos(\theta-\bar{\theta})} e^{j3\pi/4} \\ = & \frac{1}{\sqrt{2\pi}} \frac{e^{-jk_1\rho\cos(\theta-\bar{\theta})} e^{-j\pi/4}}{\left[k_1\rho\sin(\theta-\bar{\theta})\right]^{3/2}} \left(\frac{n}{1-n}\right)^{1/4} \\ = & \frac{1}{\sqrt{2\pi}} \frac{e^{-j(k_1L_1+k_2L_2+k_1L_3)} e^{-j\pi/4}}{\left[k_1L_2\right]^{3/2}} \frac{\sqrt{\sin\bar{\theta}}}{\cos^2\bar{\theta}} \\ = & \frac{1}{\sqrt{2\pi}} \frac{e^{-j(k_1L_1+k_2L_2+k_1L_3)} e^{-j\pi/4}}{\left[k_1L_2\right]^{3/2}} \frac{n^{1/4}}{1-n} \end{aligned} \tag{A–83}$$

where $\bar{\theta} = \arcsin\sqrt{n} = \arcsin\left(1/\sqrt{\varepsilon_r}\right)$

When the current source is located at the origin as in Fig. A–7, one has $L_1 = 0$, $\rho_1 = \rho$. Then, the contributions from G_{f1} and G_s can be written as

$$G_{f1} = \frac{1}{\sqrt{8\pi k_1\rho}} e^{-jk_1\rho - j\pi/4}, \tag{A–84}$$

$$G_s = \frac{\cos\theta - \sqrt{n-\sin^2\theta}}{\cos\theta + \sqrt{n-\sin^2\theta}} \frac{1}{\sqrt{8\pi k_1\rho}} e^{-jk_1\rho - j\pi/4} + G_{sb}U(\theta-\bar{\theta}), \tag{A–85}$$

$$\begin{aligned} G_{sb} = & \frac{1}{\sqrt{2\pi}} \frac{e^{-jk_1\rho\cos(\theta-\bar{\theta})} e^{-j\pi/4}}{\left[k_1\rho\sin(\theta-\bar{\theta})\right]^{3/2}} \left(\frac{n}{1-n}\right)^{1/4} \\ = & \frac{1}{\sqrt{2\pi}} \frac{e^{-j(k_1L_1+k_2L_2+k_1L_3)} e^{-j\pi/4}}{\left[k_1L_2\right]^{3/2}} \frac{n^{1/4}}{1-n}. \end{aligned} \tag{A–86}$$

3) Evaluation of $G_2(\hat{\rho}, \hat{\rho}')$:

One has:

$$G_2(\hat{\rho},\hat{\rho}') = \frac{-j}{4\pi}\int_{-\infty}^{\infty} \frac{e^{-j\xi(x-x')-j\sqrt{k_1^2 n-\xi^2}(-y)+j\sqrt{k_1^2-\xi^2}y'}}{\sqrt{k_1^2-\xi^2}} T(\xi)d\xi \tag{A–87}$$

By using transformation $\xi = k_1 \sin w$, we have:

$$\begin{aligned} G_2(\hat{\rho},\hat{\rho}') =& \frac{-j}{4\pi}\int_{-\infty}^{\infty} \frac{e^{-jk_1 \sin w(x-x')-jk_1\sqrt{n-\sin^2 w}(-y)+jk_1\cos wy'}}{k_1\cos w} T(k_1\sin w)k_1\cos w dw \\ =& \frac{-j}{4\pi}\int_{\bar{\mathrm{P}}} e^{-jk_1[\sin w(x-x')+\sqrt{n-\sin^2 w}(-y)-\cos wy']} T(k_1\sin w)dw \\ =& \frac{-j}{4\pi}\int_{\bar{\mathrm{P}}} e^{jk_1 q_2(w)} f_2(w)dw. \end{aligned} \tag{A–88}$$

where

$$q_2(w) = -\left[\sin w(x-x') + \sqrt{n-\sin^2 w}(-y) - \cos wy'\right] \tag{A–89}$$

$$f_2(w) = T(k_1\sin w) = \frac{2\cos w}{\cos w + \sqrt{n-\sin^2 w}} \tag{A–90}$$

The integral in Eq.(A–88) may have saddle points w_s satisfy:

$$q_2'(w_s) = 0 \tag{A–91}$$

Then, one has

$$\cos w_s(x-x') - (n-\sin^2 w_s)^{-1/2}\sin w_s\cos w_s(-y) + \sin w_s y' = 0 \tag{A–92}$$

On other hand, one has:

$$\begin{aligned} x - x' &= L_4\sin\theta_4 + L_5\sin\theta_5, \\ -y &= L_5\cos\theta_5, \\ y' &= -L_4\cos\theta_4. \end{aligned} \tag{A–93}$$

So, Eq.(A–92) can rewritten as:

$$\begin{aligned} & \cos w_s(L_4\sin\theta_4 + L_5\sin\theta_5) - (n-\sin^2 w_s)^{-1/2}\sin w_s\cos w_s L_5\cos\theta_5 - \sin w_s L_4\cos\theta_4 = 0 \\ \textit{or}\quad & L_4(\cos w_s\sin\theta_4 - \sin w_s\cos\theta_4) + L_5[\cos w_s\sin\theta_5 - (n-\sin^2 w_s)^{-1/2}\sin w_s\cos w_s\cos\theta_5] = 0 \end{aligned} \tag{A–94}$$

Eq.(A–94) satisfy $\forall L_4$ and L_5 when

$$\begin{aligned} & \cos w_s\sin\theta_4 = \sin w_s\cos\theta_4 \\ & \cos w_s\sin\theta_5 = (n-\sin^2 w_s)^{-1/2}\sin w_s\cos w_s\cos\theta_5 \\ \textit{or}\quad & \cos w_s\sin\theta_4 = \sin w_s\cos\theta_1 \\ & \frac{\cos w_s\sin\theta_4}{\sqrt{n-\sin^2\theta_4}} = \frac{\cos w_s\sin w_s}{\sqrt{n-\sin^2 w_s}} \end{aligned} \tag{A–95}$$

So we have $w_s = \theta_4 \pm 2m\pi$ ($m \in N$) and we choose the saddle point $w_s = \theta_4$ exists on the integration contour.

The integral in Eq.(A–88) also has a branch point $w_b = \arcsin\sqrt{n} = \bar{\theta}$. Because $w_s < w_b$ ($\theta_4 < \bar{\theta}$), we might not need the contribution from the branch point w_b.

So we have:

$$G_2 = G_{2s} \tag{A–96}$$

where G_{2s} is the contribution from the integral on the steepest-descent path P given by:

$$G_{2s} \approx \frac{-j}{4\pi}\sqrt{\frac{-2\pi}{k_1|q_2''(w_s)|}} f_2(w_s) e^{jk_1 q_2(w_s) - j\pi/4} \tag{A–97}$$

On other hand, we have:

$$q_2''(w_s) = \frac{\cos^2\theta_4}{\sin\theta_4}\left(\frac{L_4\sin\theta_4}{\cos^2\theta_4} + \frac{L_5\sin\theta_5}{\cos^2\theta_5}\right) \tag{A–98}$$

$$q_2(w_s) = -\left(L_4 + L_5\sqrt{n}\right) \tag{A–99}$$

then we have:

$$\begin{aligned} G_2 = G_{2s} \approx & \frac{-j}{4\pi}\sqrt{\frac{-2\pi}{k_1\frac{\cos^2\theta_4}{\sin\theta_4}\left(\frac{L_4\sin\theta_4}{\cos^2\theta_4} + \frac{L_5\sin\theta_5}{\cos^2\theta_5}\right)}} \frac{2\cos\theta_4}{\cos\theta_4 + \sqrt{n - \sin^2\theta_4}} e^{-jk_1(L_4 + L_5\sqrt{n}) - j\pi/4} \\ = & \frac{2e^{-jk_1(L_4 + L_5\sqrt{n}) - j\pi/4}}{\sqrt{8\pi k_1}} \frac{\sqrt{\sin\theta_4}}{\cos\theta_4 + \sqrt{n - \sin^2\theta_4}} \frac{1}{\sqrt{\frac{L_4\sin\theta_4}{\cos^2\theta_4} + \frac{L_5\sin\theta_5}{\cos^2\theta_5}}} \end{aligned} \tag{A–100}$$

When $w_s > w_b$ ($\theta_4 > \bar{\theta}$) G_{2b} is the banch point contribution given by:

$$G_{2b} \approx \frac{-j}{4\pi}\frac{2\sqrt{\pi}}{[k_1|jq_2'(w_b)|]^{3/2}}\left[\sqrt{w - w_b}\frac{df_2(w)}{dw}\right]_{w_b} e^{jk_1 q_2(w_b) + j\frac{3}{2}\arg[-jq_2'(w_s)]} \tag{A–101}$$

On the other hand, we have:

$$q_2'(w_b) = -\cos\bar{\theta} + (n - \sin^2\bar{\theta})^{-1/2}\sin\bar{\theta}\cos\bar{\theta}y - \sin\bar{\theta}y' \tag{A–102}$$

Because $\sin\bar{\theta} = \sqrt{n}$, $q_2'(w_b) \to \infty$. so we have $G_{2b} \to 0$

A.4.2 TM polarization

For the TM polarization, the radiation field excited by current source can also be derived from the two-dimensional Green's functions in Eqs.(A–53), (A–54) and (A–56) with the coefficients $\Gamma(\xi)$ and $\mathrm{T}(\xi)$ are replaced by

$$\bar{\Gamma}(\xi) = \frac{n\sqrt{k_1^2 - \xi^2} - \sqrt{k_1^2 n - \xi^2}}{n\sqrt{k_1^2 - \xi^2} + \sqrt{k_1^2 n - \xi^2}} \tag{A–103}$$

$$\bar{\mathrm{T}}(\xi) = 1 + \bar{\Gamma}(\xi) \tag{A–104}$$

Now let us consider Green's functions in media 1 as follows:

1) Evaluation of $G_{f1}(\hat{\rho},\hat{\rho}')$:

$$G_{f1}(x,y)=\frac{-j}{4\pi}\int_{-\infty}^{\infty}\frac{e^{-j\xi(x-x')-j\sqrt{k_1^2-\xi^2}|y-y'|}}{\sqrt{k_1^2-\xi^2}}d\xi. \tag{A–105}$$

By using transformation $\xi=k_1\sin w$ and coordinate system $(\rho_1,\,\theta_1)$ with $x-x'=\rho_1\sin\theta_1$ and $|y-y'|=\rho_1\cos\theta_1$, the integral can be rewritten as:

$$G_{f1}=\frac{-j}{4\pi}\int_{\bar{\mathrm{P}}}e^{-jk_1\rho_1\cos(w-\theta_1)}dw \tag{A–106}$$

The integral in Eq.(A–106) has saddle point $w_s=\theta_1$. By saddle point technique, the integral in Eq.(A–106) can then be given by:

$$\begin{aligned}G_{f1}\approx&\frac{-j}{4\pi}\sqrt{\frac{-2\pi}{k_1\rho_1|\cos(w_s-\theta_1)|}}e^{-jk_1\rho_1\cos(w_s-\theta_1)-j\pi/4}\\=&\frac{1}{\sqrt{8\pi k_1\rho_1}}e^{-jk_1\rho_1-j\pi/4}\end{aligned} \tag{A–107}$$

2) Evaluation of $G_s(\hat{\rho},\hat{\rho}')$:

$$G_s(\hat{\rho},\hat{\rho}')=\frac{-j}{4\pi}\int_{-\infty}^{\infty}\frac{e^{-j\xi(x-x')+j\sqrt{k_1^2-\xi^2}(y+y')}}{\sqrt{k_1^2-\xi^2}}\bar{\Gamma}(\xi)d\xi. \tag{A–108}$$

Similarly, by using transformation $\xi=k_1\sin w$ and coordinate system $(\rho,\,\theta)$ with $x-x'=\rho\sin\theta$ and $y+y'=-\rho\cos\theta$, one has:

$$G_s(\hat{\rho},\hat{\rho}')=\frac{-j}{4\pi}\int_{\bar{\mathrm{P}}}e^{-jk_1\rho\cos(w-\theta)}\bar{\Gamma}(k_1\sin w)dw, \tag{A–109}$$

where

$$\bar{\Gamma}(k_1\sin w)=\frac{n\cos w-\sqrt{n-\sin^2 w}}{n\cos w+\sqrt{n-\sin^2 w}} \tag{A–110}$$

The integral in Eq.(A–109) has saddle point $w_s=\theta$ exists on the integration contour. And one may also have branch point $w_b=\mathrm{Arcsin}\sqrt{n}=\bar{\theta}$ exist on the positive imagine domain. We may have the contribution from the branch point w_b when $w_s>w_b$ $(\theta>\bar{\theta})$ as in Fig. A–5. Then G_s can be given by:

$$G_s=G_{sd}+G_{sb}U(w_s-w_b)=G_{sd}+G_{sb}U(\theta-\bar{\theta}), \tag{A–111}$$

where G_{sd} is the contribution from the integral on the steepest-descent path P given by:

$$G_{sd}\approx\frac{n\cos\theta-\sqrt{n-\sin^2\theta}}{n\cos\theta+\sqrt{n-\sin^2\theta}}\frac{1}{\sqrt{8\pi k_1\rho}}e^{-jk_1\rho-j\pi/4}, \tag{A–112}$$

and G_{sb} is the banch point contribution given by:

$$\begin{aligned} G_{sb} =& \frac{-j}{4\pi}\int_{\mathrm{P_b}} e^{-jk_1\rho\cos(w-\theta)}\bar{\Gamma}(k_1\sin w)dw \\ =& \frac{-j}{4\pi}\int_{\mathrm{P_b}} e^{-jk_1\rho\cos(w-\theta)}f(w)dw, \end{aligned} \tag{A–113}$$

where $f(w)=\bar{\Gamma}(k_1\sin w)$. One has the approximation of G_{sb} as

$$G_{sb}\approx\frac{-j}{4\pi}\frac{2\sqrt{\pi}}{[k_1\rho\sin(\theta-w_b)]^{3/2}}\left[\sqrt{w-w_b}\frac{df(w)}{dw}\right]_{w_b} e^{-jk_1\rho\cos(w_b-\theta)}e^{j3\pi/4} \tag{A–114}$$

on the other hand, one has:

$$\frac{df(w)}{dw}=\frac{-2n\sin w(n-\sin^2 w)+2n\sin w\cos^2 w}{\sqrt{n-\sin^2 w}\left(n\cos w+\sqrt{n-\sin^2 w}\right)^2} \tag{A–115}$$

Then, one has

$$\begin{aligned} \rightarrow\left[\sqrt{w-w_b}\frac{df(w)}{dw}\right]_{w_b} =& \lim_{w\to w_b}\left\{\frac{\sqrt{w-w_b}}{\sqrt{n-\sin^2 w}}\frac{-2n\sin w(n-\sin^2 w)+2n\sin w\cos^2 w}{\left(n\cos w+\sqrt{n-\sin^2 w}\right)^2}\right\} \\ =& \frac{2n\sin w_b\cos^2 w_b}{n^2\cos^2 w_b}e^{-j\pi/2}\lim_{w\to w_b}\frac{\sqrt{w-w_b}}{\sqrt{\sin^2 w-\sin^2 w_b}} \\ =& \frac{2\sin w_b}{n}e^{-j\pi/2}\sqrt{\frac{1}{\lim\limits_{w\to w_b}\dfrac{\sin^2 w-\sin^2 w_b}{w-w_b}}} \\ =& \frac{2\sin w_b e^{-j\pi/2}}{n\sqrt{2\sin w_b\cos w_b}}=\frac{\sqrt{2}\sqrt{\sin w_b}e^{-j\pi/2}}{n\sqrt{\cos w_b}}=\frac{\sqrt{2}}{n}e^{-j\pi/2}\left(\frac{n}{1-n}\right)^{1/4} \end{aligned} \tag{A–116}$$

Then, the lateral wave contribution from branch point can be written as:

$$\begin{aligned} G_{sb}\approx& \frac{-j}{4\pi}\frac{2\sqrt{\pi}}{\left[k_1\rho\sin(\theta-\bar{\theta})\right]^{3/2}}\frac{\sqrt{2}}{n}e^{-j\pi/2}\left(\frac{n}{1-n}\right)^{1/4}e^{-jk_1\rho\cos(\theta-\bar{\theta})}e^{j3\pi/4} \\ =& \frac{1}{n\sqrt{2\pi}}\frac{e^{-jk_1\rho\cos(\theta-\bar{\theta})}e^{-j\pi/4}}{\left[k_1\rho\sin(\theta-\bar{\theta})\right]^{3/2}}\left(\frac{n}{1-n}\right)^{1/4} \\ =& \frac{1}{n\sqrt{2\pi}}\frac{e^{-j(k_1L_1+k_2L_2+k_1L_3)}e^{-j\pi/4}}{\left[k_1L_2\right]^{3/2}}\frac{\sqrt{\sin\bar{\theta}}}{\cos^2\bar{\theta}} \\ =& \frac{1}{n\sqrt{2\pi}}\frac{e^{-j(k_1L_1+k_2L_2+k_1L_3)}e^{-j\pi/4}}{\left[k_1L_2\right]^{3/2}}\frac{n^{1/4}}{1-n} \end{aligned} \tag{A–117}$$

where $\bar{\theta}=\arcsin\sqrt{n}=\arcsin\left(1/\sqrt{\varepsilon_r}\right)$

When the current source is located at the origin as in Fig. A–7, one has $L_1 = 0$, $\rho_1 = \rho$. Then, the contributions from G_{f1} and G_s can be written as

$$G_{f1} = \frac{1}{\sqrt{8\pi k_1 \rho}} e^{-jk_1\rho - j\pi/4}, \tag{A–118}$$

$$G_s = \frac{n\cos\theta - \sqrt{n - \sin^2\theta}}{n\cos\theta + \sqrt{n - \sin^2\theta}} \frac{1}{\sqrt{8\pi k_1\rho}} e^{-jk_1\rho - j\pi/4} + G_{sb}U(\theta - \bar{\theta}), \tag{A–119}$$

$$\begin{aligned} G_{sb} =& \frac{1}{n\sqrt{2\pi}} \frac{e^{-jk_1\rho\cos(\theta-\bar{\theta})} e^{-j\pi/4}}{\left[k_1\rho\sin(\theta-\bar{\theta})\right]^{3/2}} \left(\frac{n}{1-n}\right)^{1/4} \\ =& \frac{1}{n\sqrt{2\pi}} \frac{e^{-j(k_1L_1 + k_2L_2 + k_1L_3)} e^{-j\pi/4}}{\left[k_1L_2\right]^{3/2}} \frac{n^{1/4}}{1-n}. \end{aligned} \tag{A–120}$$

3) Evaluation of $G_2(\hat{\rho}, \hat{\rho}')$:

One has:

$$G_2(\hat{\rho}, \hat{\rho}') = \frac{-j}{4\pi} \int_{-\infty}^{\infty} \frac{e^{-j\xi(x-x') - j\sqrt{k_1^2 n - \xi^2}(-y) + j\sqrt{k_1^2 - \xi^2}y'}}{\sqrt{k_1^2 - \xi^2}} T(\xi) d\xi \tag{A–121}$$

By using transformation $\xi = k_1 \sin w$, we have:

$$\begin{aligned} G_2(\hat{\rho}, \hat{\rho}') =& \frac{-j}{4\pi} \int_{-\infty}^{\infty} \frac{e^{-jk_1\sin w(x-x') - jk_1\sqrt{n - \sin^2 w}(-y) + jk_1\cos wy'}}{k_1\cos w} T(k_1\sin w) k_1\cos w dw \\ =& \frac{-j}{4\pi} \int_{\bar{\mathrm{P}}} e^{-jk_1[\sin w(x-x') + \sqrt{n-\sin^2 w}(-y) - \cos wy']} T(k_1\sin w) dw \\ =& \frac{-j}{4\pi} \int_{\bar{\mathrm{P}}} e^{jk_1 q_2(w)} f_2(w) dw. \end{aligned} \tag{A–122}$$

where

$$q_2(w) = -\left[\sin w(x - x') + \sqrt{n - \sin^2 w}(-y) - \cos wy'\right] \tag{A–123}$$

$$f_2(w) = T(k_1\sin w) = \frac{2n\cos w}{n\cos w + \sqrt{n - \sin^2 w}} \tag{A–124}$$

The integral in Eq.(A–122) may have saddle points w_s satisfy:

$$q_2'(w_s) = 0 \tag{A–125}$$

Then, one has

$$\cos w_s(x - x') - (n - \sin^2 w_s)^{-1/2} \sin w_s \cos w_s(-y) + \sin w_s y' = 0 \tag{A–126}$$

On other hand, one has:

$$\begin{aligned} x - x' &= L_4\sin\theta_4 + L_5\sin\theta_5, \\ -y &= L_5\cos\theta_5, \\ y' &= -L_4\cos\theta_4. \end{aligned} \tag{A–127}$$

So, Eq.(A–126) can rewritten as:

$$\cos w_s(L_4\sin\theta_4+L_5\sin\theta_5)-(n-\sin^2 w_s)^{-1/2}\sin w_s\cos w_s L_5\cos\theta_5-\sin w_s L_4\cos\theta_4=0$$
$$or\quad L_4(\cos w_s\sin\theta_4-\sin w_s\cos\theta_4)+L_5[\cos w_s\sin\theta_5-(n-\sin^2 w_s)^{-1/2}\sin w_s\cos w_s\cos\theta_5]=0 \tag{A–128}$$

Eq.(A–128) satisfy $\forall L_4$ and L_5 when

$$\begin{aligned}&\cos w_s\sin\theta_4=\sin w_s\cos\theta_4\\&\cos w_s\sin\theta_5=(n-\sin^2 w_s)^{-1/2}\sin w_s\cos w_s\cos\theta_5\\or\quad&\cos w_s\sin\theta_4=\sin w_s\cos\theta_1\\&\frac{\cos w_s\sin\theta_4}{\sqrt{n-\sin^2\theta_4}}=\frac{\cos w_s\sin w_s}{\sqrt{n-\sin^2 w_s}}\end{aligned} \tag{A–129}$$

So we have $w_s=\theta_4\pm 2m\pi$ $(m\in N)$ and we choose the saddle point $w_s=\theta_4$ exists on the integration contour.

The integral in Eq.(A–122) also has a branch point $w_b=\arcsin\sqrt{n}=\bar{\theta}$. Because $w_s<w_b$ $(\theta_4<\bar{\theta})$, we might not need the contribution from the branch point w_b.

So we have:

$$G_2=G_{2s} \tag{A–130}$$

where G_{2s} is the contribution from the integral on the steepest-descent path P given by:

$$G_{2s}\approx\frac{-j}{4\pi}\sqrt{\frac{-2\pi}{k_1|q_2''(w_s)|}}f_2(w_s)e^{jk_1q_2(w_s)-j\pi/4} \tag{A–131}$$

On other hand, we have:

$$q_2''(w_s)=\frac{\cos^2\theta_4}{\sin\theta_4}\left(\frac{L_4\sin\theta_4}{\cos^2\theta_4}+\frac{L_5\sin\theta_5}{\cos^2\theta_5}\right) \tag{A–132}$$

$$q_2(w_s)=-(L_4+L_5\sqrt{n}) \tag{A–133}$$

then we have:

$$\begin{aligned}G_2=G_{2s}\approx&\frac{-j}{4\pi}\sqrt{\frac{-2\pi}{k_1\frac{\cos^2\theta_4}{\sin\theta_4}\left(\frac{L_4\sin\theta_4}{\cos^2\theta_4}+\frac{L_5\sin\theta_5}{\cos^2\theta_5}\right)}}\frac{2n\cos\theta_4}{n\cos\theta_4+\sqrt{n-\sin^2\theta_4}}e^{-jk_1(L_4+L_5\sqrt{n})-j\pi/4}\\=&\frac{2e^{-jk_1(L_4+L_5\sqrt{n})-j\pi/4}}{\sqrt{8\pi k_1}}\frac{n\sqrt{\sin\theta_4}}{n\cos\theta_4+\sqrt{n-\sin^2\theta_4}}\frac{1}{\sqrt{\frac{L_4\sin\theta_4}{\cos^2\theta_4}+\frac{L_5\sin\theta_5}{\cos^2\theta_5}}}\end{aligned} \tag{A–134}$$

When $w_s>w_b$ $(\theta_4>\bar{\theta})$ G_{2b} is the banch point contribution given by:

$$G_{2b}\approx\frac{-j}{4\pi}\frac{2\sqrt{\pi}}{[k_1|jq_2'(w_b)|]^{3/2}}\left[\sqrt{w-w_b}\frac{df_2(w)}{dw}\right]_{w_b}e^{jk_1q_2(w_b)+j\frac{3}{2}\arg[-jq_2'(w_s)]} \tag{A–135}$$

On the other hand, we have:

$$q_2'(w_b)=-\cos\bar{\theta}+(n-\sin^2\bar{\theta})^{-1/2}\sin\bar{\theta}\cos\bar{\theta}y-\sin\bar{\theta}y' \tag{A–136}$$

Because $\sin\bar{\theta}=\sqrt{n}$, $q_2'(w_b)\to\infty$. so we have $G_{2b}\to 0$

Acknowledgment

I really appreciate that MEXT and Chuo University always facilitate and support me to have a great opportunity to study in Japan. I would also like to express my deepest gratitude to Prof. Hiroshi Shirai for his enthusiastic support and dedicated guidance during my doctoral course. He has always been a kind and patient supervisor to me during these years. He has imparted to me a wealth of valuable knowledge and experience during my studies. His excellent standards of professionalism and ethics have helped me to always stay on the right way.

I would like to express special thank to Prof. Se-Yun Kim for providing numerical data and discussion. I would also like to thank to Prof. K. Kobayashi, Prof. M. Katori, and Prof. K. Goto for their helpful questions and comments during the defense session.

I would like to express special thanks to all members of Shirai Lab, especially to Mr. Khanh, Mr. Ngoc, Mr. Cuong, and Mr. Duc for their kind help during my research. I would also like to express my gratitude to my family and friends. Their attention and encouragement are a huge source of motivation for me to overcome challenges and finish my doctoral thesis.

References

[1] J. C. Maxwell, "On physical lines of force," *The London, Edinburgh, and Dublin Philosophical Magazine and Journal of Science*, vol. 21, no. 40, pp. 281–291, 1861.

[2] J. C. Maxwell, "A dynamical theory of the electromagnetic field," *Philosophical transactions of the Royal Society of London*, no. 155, pp. 459–512, 1865.

[3] J. B. Keller, "One hundred years of diffraction theory," *IEEE Trans. on Antennas and Propagation*, vol.AP-33, no.2, pp.123–126, 1985.

[4] J. H. Richmond, "Scattering by a dielectric cylinder of arbitrary cross section shape," *IEEE Trans. Antenna and Propagat.*, vol.AP-13, pp.334–341, 1965.

[5] H. Shirai and L. B. Felsen, "Wavefront and resonance analysis of scattering by a perfectly conducting flat strip," *IEEE Trans. Antenna and Propagat.*, vol. AP-15, pp. 662–668, 1967.

[6] A. Wexler, "Computation of electromagnetic fields," *IEEE transactions on Microwave Theory and Techniques*, 17(8), pp.416–439, 1969.

[7] A. Taflove and M. E. Brodwin, "Numerical solution of steady state electromagnetic scattering problems using the time-dependent Maxwell's equations," *IEEE Trans. Microwave Theory Tech.*, vol. 23, 623–630, 1975.

[8] D. K. Cheng, Fundamentals of Engineering Electromagnetics, Taylor & Francis Group, 1993.

[9] J. D. Jackson, Classical Electrodynamics, 3rd edn, Wiley, New York, 1998.

[10] J. A. Stratton, Electromagnetic Theory, John Wiley & Sons, vol.33, 2007.

[11] C. A. Brebbia, J. C. F. Telles and L. C. Wrobel, Boundary Element Techniques: Theory and Applications in Engineering, Springer Science & Business Media, 2012.

[12] M. Born and E. Wolf, Principles of Optics: Electromagnetic Theory of Propagation, Interference and Diffraction of Light, Elsevier, 2013.

[13] A. Kirsch and F. Hettlich, The Mathematical Theory of Time-Harmonic Maxwell's Equations, Applied Mathematical Sciences, vol. 190, 2015.

[14] J. J. Bowman, T. B. A. Senior and P. L. E. Uslenghi, Electromagnetic and acoustic scattering by simple shapes, North-Holland, Amsterdam, 1969.

[15] L. B. Felsen and N. Marcuvitz, Radiation and Scattering of Waves, Prentice-Hall, NJ, USA, 1973. (reissued from Wiley-IEEE Press, USA, 1994.)

[16] A. Taflove, Computational Electrodynamics: The Finite-Difference Time-Domain Method, Artech House, Boston, London, 1995.

[17] T. Uno, Electromagnetic Field and Antenna Analysis by FDTD Method, Corona Publ. Co., Japan, 1998 (in Japanese).

[18] P. K. Banerjee and R. Butterfield, Boundary Element Methods in Engineering Science, McGraw-Hill, London, 1981.

[19] M. M. Ney, "Method of Moments as Applied to Electromagnetic Problems," *IEEE Transactions on Microwave Theory and Techniques*, vol. 33, no. 10, pp.972–980, 1985.

[20] R. F. Harrington, "The method of moments in electromagnetics," *Journal of Electromagnetic waves and Applications*, 1(3), pp.181–200, 1987.

[21] R. F. Harrington, Field Computation by Moment Methods, Wiley-IEEE Press, 1993.

[22] F. M. Kahnert, "Numerical methods in electromagnetic scattering theory," *Journal of Quantitative Spectroscopy and Radiative Transfer*, 79, pp.775–824, 2003.

[23] J. A. Kong, L. Tsang, K. H. Ding and C. O. Ao, Scattering of Electromagnetic Waves: Numerical Simulations, John Wiley & Sons, 2004.

[24] J. W. Crispin and K. M. Siegel, Methods of Radar Cross Section Analysis, Academic Press, New York, 1968.

[25] G. T. Ruck, D. E. Barrick, W. P. Stuart, and C. K. Krickbaum, Radar Cross Section Handbook, G. T. Ruck ed., Plenum Press, NY, USA, 1970.

[26] L. Diaz and T. Milligam, Antenna Engineering Using Physical Optics, Artech House, Norwood, MA, USA, 1996.

[27] P. Ya. Ufimtsev, Theory of Edge Diffraction in Electromagnetics, Tech Science Press, Encino, CA, 2003.

[28] M. Kline and I. W. Kay, Electromagnetic Theory and Geometrical Optics, John Wiley & Sons, 1965.

[29] G. A. Deschamps, "Ray techniques in electromagnetics," *Proceedings of the IEEE*, 60(9), pp.1022–1035, 1972.

[30] S. W. Lee, "Electromagnetic reflection from a conducting surface: Geometrical optics solution," *IEEE Trans. on Antennas and Propagat.*, 23(2), pp.184–191, 1975.

[31] H. Shirai and L. B. Felsen, "Rays and modes for plane wave coupling into a large open-ended circular waveguide," *Wave Motion*, vol. 9, pp. 461–482, 1987.

[32] J. B. Keller, "Diffraction by an aperture," *J. Appl. Physics*, vol. 28, pp. 426–444, 1957. DOI: 10.1063/1.1722767

[33] J. B. Keller, "Geometrical theory of diffraction," *J. Opt. Soc. Am.*, vol. 52, pp. 116–130, Feb., 1962. DOI: 10.1364/JOSA.52.000116

[34] G. L. James, Geometrical Theory of Diffraction for Electromagnetic Waves, Peter Peregrinus Ltd, 1976.

[35] R. C. Hansen, ed., Geometrical Theory of Diffraction, IEEE Press, New York, 1981.

[36] H. Shirai, Geometrical Theory of Diffraction, Corona Publ. Co., Japan, 2015 (in Japanese).

[37] R. M. Lewis and J. Boersma, "Uniform asymptotic theory of edge diffraction," *J. Math. Phys.*, vol. 10, pp. 2291–2305, 1969. DOI: 10.1063/1.1664835

[38] D. S. Ahluwalia, "Uniform asymptotic theory of diffraction, by the edge of a three dimensional body," *SIAM J. Appl. Math.*, vol. 18, pp. 287–301, 1970. DOI: 10.1137/0118024

[39] R. G. Kouyoumjian and P. H. Pathak, "A uniform geometrical theory of diffraction for an edge in a perfectly conducting surface," *Proc. of IEEE*, vol. 62, pp. 1448–1461, 1974. DOI: 10.1109/PROC.1974.9651

[40] S. W. Lee and G. A. Deschamps, "A uniform asymptotic theory of electromagnetic diffraction by a curved wedge," *IEEE Trans. on Antennas and Propagat.*, vol. AP-24, pp. 25–34, 1976. DOI: 10.1109/TAP.1976.1141283

[41] D. A. McNamara, C. W. I. Pistorious and J. A. G. Malherbe, Introduction to The Uniform Geometrical Theory of Diffraction, Artech House, 1990.

[42] R. J. Luebbers, "A heuristic UTD slope diffraction coefficient for rough lossy wedges," *IEEE Trans. on Antennas and Propagat.*, vol. 37, no. 2, pp. 206–211, 1989. DOI: 10.1109/8.18707

[43] C. Huygens, Traite de la Lumiere, Leyeden, 1690. Translated into English by S. P. Thompson, London, 1912 and reprinted by the University of Chicago Press.

[44] S. A. Schelkunoff, "Some equivalence theorems of electromagnetics and their application to radiation problems," *Bell System Tech. J .*, vol. 15, no. 1, pp. 92–112, 1936. DOI: 10.1002/j.1538-7305.1936.tb00720.x

[45] S. R. Rengarajan and Y. Rahmat-Samii, "The field equivalence principle: illustration of the establishment of the non-intuitive null fields," *IEEE Trans. on Antennas and Propagat.*, vol. 42, no. 4, pp. 122–128, 2000. DOI: 10.1109/74.868058

[46] M. Ando, "Physical optics," Analysis Methods for Electromagnetic Wave Problems, Chap. 4, E. Yamashita ed., Artech House, Boston, USA, 1990.

[47] F. S. de Adana, I. G. Diego, O. G. Blanco, P. Lozano and M. F. Catedra, "Method based on physical optics for the computation of the radar cross section including diffraction and double effects of metallic and absorbing bodies modeled with parametric surface," *IEEE Trans. on Antennas and Propagat.*, vol. 52, no. 12, pp. 3295–3303, 2004.

[48] F. Weinmann, "Ray tracing with PO/PTD for RCS modeling of large complex objects," *IEEE Trans. on Antennas and Propagat.*, vol. 54, no. 6, pp. 1797–1806, 2006.

[49] N. Q. Ta and H. Shirai, "A field equivalence between physical optics and GO-based equivalent current methods for scattering from circular conducting cylinders," *IEICE Trans. on Electronics*, vol. E103-C, no. 9, pp. 382–387, 2020. DOI: 10.1587/transele.2019ECP5048

[50] N. Q. Ta and H. Shirai, "On the asymptotic evaluation of the physical optics approximation for plane wave scattering by circular conducting cylinders," *IEICE Trans. on Electronics*, vol. E105-C, no. 4, pp. 128–136, 2022. DOI: 10.1587/transele.2021REP0001

[51] D. M. Nguyen and H. Shirai, "A discussion on physical optics approximation for edge diffraction by a conducting wedge," *IEICE Trans. on Electronics*, vol. E105-C, no. 5, pp. 176–183, 2022. DOI: 10.1587/transele.2021ECP5031

[52] S. A. Schelkunoff, "Some equivalence theorems of electromagnetics and their application to radiation problems," *Bell Sys. Tech. J.*, no.15, pp. 92–112, 1936. DOI: 10.1002/j.1538-7305.1936.tb00720.x

[53] R. Harrington, Time Harmonic Electromagnetic Fields, McGraw-Hill Co., 1961. (reissued from Wiley-IEEE Press, USA, 2001.)

[54] C. A. Balanis, Advanced Engineering Electromagnetic, 2nd ed., Wiley, NJ, USA, 2012.

[55] H. N. Quang and H. Shirai, "A new interpretation of physical optics approximation from surface equivalence theorem," *IEICE Trans. on Electronics*, vol. E101-C, no. 8, pp. 664–670, 2018. DOI: 10.1587/transele.E101.C.664

[56] G. Gennarelli and G. Riccio, "A uniform asymptotic solution for the diffraction by a right-angled dielectric wedge," *IEEE Trans. on Antennas and Propagat.*, vol. 59, no. 3, pp. 898–903, 2011. DOI: 10.1109/TAP.2010.2103031

[57] M. Frongillo, G. Gennarelli and G. Riccio, "Plane wave diffraction by arbitrary-angled lossless wedges: high-frequency and time-domain solutions," *IEEE Trans. on Antennas and Propagat.*, vol. 66, no. 12, pp. 6646–6653, 2018. DOI: 10.1109/TAP.2018.2876602

[58] S. Y. Kim, J. W. Ra and S. Y. Shin, "Diffraction by an arbitrary-angled dielectric wedge: Part I – Physical optics approximation," *IEEE Trans. on Antennas and Propagat.*, vol. 39, no. 9, pp. 1272–1281, 1991. DOI: 10.1109/8.99035

[59] S. Y. Kim and J. W. Ra, "Diffraction by an arbitrary-angled dielectric wedge: Part II – Correction to physical optics solution," *IEEE Trans. on Antennas and Propagat.*, vol. 39, no. 9, pp. 1282–1292, 1991. DOI: 10.1109/8.99036

[60] S. Y. Kim, "Hidden rays of diffraction," *IEEE Trans. on Antennas and Propagat.*, vol. 55, no. 3, pp. 892–906, 2007. DOI: 10.1109/TAP.2007.891859

[61] S. Y. Kim, "Hidden rays on the shadow boundaries of penetrable wedges," *Proc. of 2013 International Symposium on Electromagnetic Theory*, pp. 778–781, 2013. DOI: 10.34385/proc.30.23PM3F-02

[62] J. Meixner, "The behavior of electromagnetic fields at edges," *IEEE Trans. on Antennas and Propagat.*, vol. 20, no. 4, pp. 442–446, 1972. DOI: 10.1109/TAP.1972.1140243

List of Publications

Journal Papers

[1] D. M. Nguyen and H. Shirai, "A discussion on physical optics approximation for edge diffraction by a conducting wedge," *IEICE Trans. on Electronics*, vol. E105-C, no. 5, pp. 176–183, May 2022.

[2] D. M. Nguyen, H. Shirai and S. Y. Kim, "An Extension of Physical Optics Approximation for Dielectric Wedge Diffraction for a TM-Polarized Plane Wave," *IEICE Trans. on Electronics*, vol. E107-C, no. 5, May 2024.

International Conference Papers

[1] D. M. Nguyen, H. Shirai and S. Y. Kim, "Uniform Asymptotic Solution for Dielectric Wedge Diffraction Based on Equivalent Currents," *Proc. of XXXIV General Assembly and Scientific Symposium of the International Union of Radio Science (URSI GASS 2021)*, CDROM, Rome, Italy, 2021.

[2] D. M. Nguyen, H. Shirai and S. Y. Kim, "New Formulation of Physical Optics Approximation for Edge Diffraction by Dielectric Wedges," *Proc. of 2022 International Conference on Electromagnetics in Advanced Applications (ICEAA 2022)*, p. 66, Cape Town, South Africa, 2022.

[3] D. M. Nguyen, H. Shirai and S. Y. Kim, "Uniform Asymptotic Solution for Edge Diffraction of H-Polarized Electromagnetic Plane Wave by Dielectric Wedges," *Proc. of URSI International Symposium on Electromagnetic Theory 2023 (URSI EMTS 2023)*, Vancouver, BC, Canada, 2023.

[4] D. M. Nguyen, H. Shirai and S. Y. Kim, "Extended Physical Optics Approximation for Edge Diffraction by Dielectric Wedges," *Proc. of 24th edition of the International Conference on Electromagnetics in Advanced Applications (ICEAA 2023)*, p. 49, Venice, Italy, 2023.

Domestic Conference Papers

[1] D. M. Nguyen and H. Shirai, "Uniform Asymptotic Solution For Conducting Wedge Diffraction Based On Physical Optics Current," *Proc. of 2020 IEICE General Conference*, C-1-1, CDROM, Hiroshima, Japan, 2020.

[2] D. M. Nguyen and H. Shirai, "Diffraction of E-Polarized EM Plane Wave by Dielectric Wedges," *Proc. of 2024 IEICE General Conference*, C-1-17, Hiroshima, Japan, 2024.